Study of sequence dependent *in-situ* peptide cyclization and its applications as biomolecules

A dissertation submitted to the Indian Institute of Technology Guwahati in partial fulfillment for the degree of

Doctor of Philosophy

By:

Nibedita Ghosh

Roll No 146152007

Centre for the Environment

Indian Institute of Technology Guwahati

Guwahati, Assam-781039,

India

Dedicated

To

My little angel, Auroni

You are my sunshine. You inspire me to be the greatest version of myself.

Indian Institute of Technology Guwahati

Centre for the Environment

STATEMENT

I hereby declare that the matter embodied in this thesis entitled "**Study of sequence dependent *in-situ* peptide cyclization and its applications as biomolecules**" under the supervision of Dr. Lal Mohan Kundu is a bona fide research work carried out by me, except where due references were made. Whole or any part of the work has not been submitted before in order to qualify for any other academic degree at this or any other institution.

20th January 2021

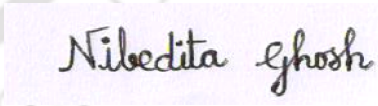

Nibedita Ghosh

Indian Institute of Technology Guwahati

Certificate

Indian Institute of Technology Guwahati

Centre for the Environment

CERTIFICATE

This is to certify that **Nibedita Ghosh** has been working under my supervision since December 2014 as a regular registered Ph. D. student. I am forwarding her thesis entitled "**Study of sequence dependent *in-situ* peptide cyclization and its applications as biomolecules**" for being submitted for the Ph. D. degree from this institute. I certify that she has fulfilled all the requirements according to the rules of this institute regarding the investigations embodied in her thesis and this work has not been submitted elsewhere for a degree.

20th January 2021

Dr. Lal Mohan Kundu
Thesis Supervisor
Department of Chemistry
Centre for the Environment
Indian Institute of Technology Guwahati

Prof. A. B. Kunnumakkara
Thesis Co-Supervisor
Department of Bioscience and Bioengineering
Centre for the Environment
Indian Institute of Technology Guwahati

Synopsis

The thesis entitled, "Study of sequence dependent *in-situ* peptide cyclization and its applications as biomolecules" is divided into five main chapters. The abstracts of the main chapters are described below.

Chapter 1: Introduction

The peptides are gaining escalating recognition due to its progress in the area of biotechnology and bioengineering. Peptides are used for several research purposes including cancer diagnosis and treatment, production of antibodies, antibiotic drug development, drug delivery systems, vaccine design, epitope mapping, cell-penetrating peptides as molecular carries, etc. A considerable number of selected peptides and peptide hormones are used as *in vivo* probes for targeted molecular imaging. Robust strategies for the design of receptor-specific small peptides have been developed from the recent advancement in combinatorial peptide chemistry and phage display technology.

To release covalently attached biomolecules in a controlled manner, we want to establish a peptide cyclization method at the physiological condition. This method may be a new direction to design peptide-drug conjugates where no external stimuli will be needed to release the drug. On the other hand, aspartimide formation is an undesirable side product in Fmoc based solid-phase peptide synthesis. Aspartimide results from the nucleophilic attack of nitrogen (of C-terminus amide of Asp) on the side chain carbonyl group (of the Asp) with release of alcohol as the leaving group. Sometimes side chain acid functional group is protected by different ester group to make the release of alcohol a facile process in basic condition. Using this concept, we want to attach Trp and Serotonine covalently with the side-chain carbonyl group of Asp. In basic condition, N→N acyl migration and O→N acyl migration is expected to happen to release bioactive molecules through aspartimide formation. So, it may be a potent technique to release bioactive molecules at the physiological condition.

In the biological systems, Protein folding, unfolding, and misfolding are commonly occurring process.[1] Functionally active folded proteins are called the native state of the protein. Due to protein misfolding, native monomers form the early pre-fibrillar oligomers in the nucleation phase. Later these type of oligomers is elongated with the

other monomers in the growth phase which further forms mature amyloid fibril in the saturation phase.[2] Amyloids are insoluble protein aggregates with highly ordered β-sheet conformations that differ from its native states conformation. Misfolding and aggregation of the amyloid β (Aβ) peptide into fibrillar aggregates is a cause of Alzheimer's disease (AD) which is a progressive neurodegenerative disorder and the most common form of dementia.[3] Aβ peptide found in amyloid deposits is produced at the plasma membrane and after coming out in extracellular space gets deposited as senile plaques with β-sheet.[4] Various strategies are being developed for the treatment of Alzheimer's disease though there is no cure available till date. One of the possible approaches is to inhibit or disrupt the aggregation of a Aβ peptide using peptide-based molecules. Peptides are considered as highly selective, efficient and relatively safe. Tjernberg, in 1996, first introduced a short peptide fragment KLVFF which is part of Aβ peptide sequence itself and known as core sequence responsible for initiation of self-aggregation, as a potent inhibitor of Aβ aggregation in vitro.[5] Soto and coworkers reported another peptide-based molecule LPFFD as 'β- sheet breaker peptide' which showed a promising result to inhibit Aβ peptide aggregation and dissolution of preformed fibrils.[6] Getting inspired by the Tjernberg's work and Soto's work, we focussed on the hydrophobic region (K_{16}LVFFA_{21}) of Aβ to develop breaker peptides.

Aim of the work:

Peptides are early leading for the realistic design to deliver bioactive molecules as they can provide target specificity, potency, resistance towards chemical or enzymatic hydrolysis and longer resident times for more effective duration of action to improve biological efficacy and minimize side effects. We are broadly interested in the design and synthesis of *in situ* peptide cyclization using side chain modified peptides at the physiological condition without the need for any external reagent. The concept of peptide cyclization between two side chains of a modified tripeptide containing covalently attached small molecule through an ester bond and the cyclization due to aspartimide formation can be applied as controlled release of bioactive molecules from peptide-based moiety beside hydrolysis occurring chemically or enzymatically.

Inhibition and disruption of amyloid is a promising therapeutic approach against AD and related disorders. Our goal is to develop potent inhibitors by *in situ* side chain peptide self-cyclization as a β-sheet breaker strategy.

Chapter 2: *In-situ* peptide self-cyclization for controlled release of small bioactive molecules

Delivery of small bioactive molecules including therapeutic agents to targeted cells in a controlled way is extremely important in the modern-day therapeutics. A simple, highly efficient and green procedure for the release of small bioactive molecules in a site-specific manner is established here *via* peptide cyclization, at the physiological condition without using any external reagents. Bioactive molecules, as well as other organic leaving groups (having primary or secondary alcohol as a functional group), were conjugated to a short peptide RXE sequence (X= P/ A/ G). The peptide was designed to undergo cyclization under physiological condition and releases the covalently attached bioactive molecule, in a controlled manner. *In vitro* studies were performed in detail, with optimized physiological parameters, to understand the kinetics of bioactive molecule release as well as the mechanism of cyclization. The mechanism of action was investigated by HPLC and ESI-Mass spectrometry. The conformational changes, due to cyclization of the peptide, was monitored by CD spectra. The present concept of effective and target-directed drug delivery *via* peptide cyclization could be a potential drug delivery technique.

From HPLC kinetics, the release progression (%) of Peptide1-3 was compared quantitatively. It was noticed that the leaving group (bioactive molecule) was released in a more controlled way in the case of Peptide3 having Glycine compare to Peptide1 having Proline (commonly used as the bent unit) and Peptide2 having Alanine (used to force side chain of its N- and C-terminus amino acid to be in the same direction) as the bridging unit. Considering the formation of cyclized product from its mother compound as a controlled release parameter, the rate of reactivity of Peptide3 concerning release system was found to be higher than Peptide1-2 at any point of the kinetics. Peptide3 released the bioactive molecule (having primary alcohol as a functional group, benzyl alcohol for the general example) almost 75% after 36h of incubation in PBS (pH 7.4) at 37 ^{o}C, following the saturation point thereafter and the quantities are 85% after 72h, and 98% after 120h.

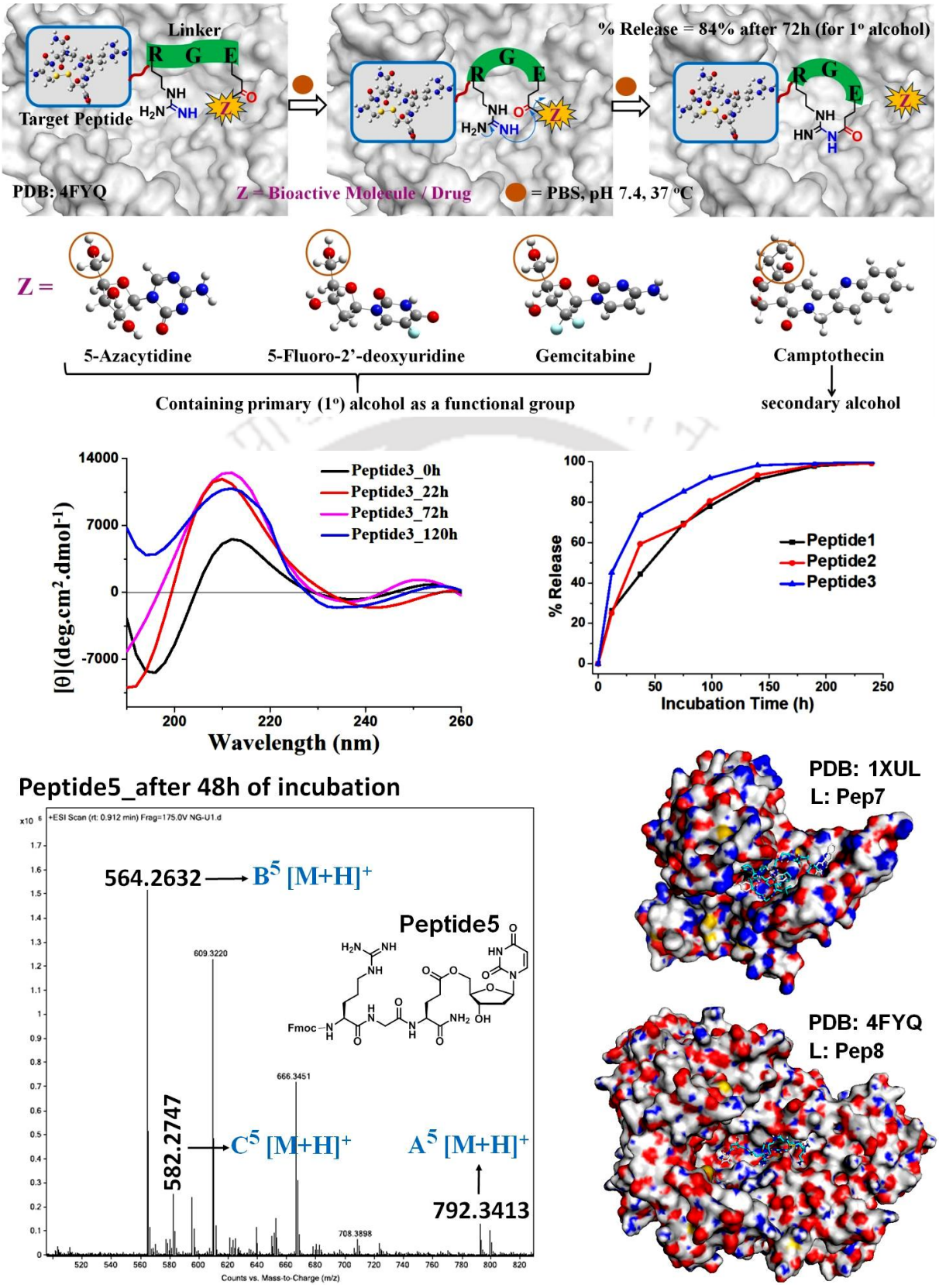

Figure 1. Schematic diagram of the peptide-based targeted delivery system, and release of small molecules including therapeutic agents by various kinetics assays.

After finding the Peptide3 as the best delivery system *in vitro* among Peptide1-4, for the defined purpose we have designed and synthesized Peptide5 in-which 2'-deoxyuridine (building block and alike structure of various drugs; for example 5-Fluoro-2'-deoxyuridine, Gemcitabine, 5-Azacytidine, etc.) was attached with the side chain of Glutamic acid. We have also checked the release studies of 2'-deoxyuridine and Camptothecin from Peptide5 and Peptide6 respectively *in vitro*. The result obtained from ESI-MS spectra clearly indicates the formation of a cyclic peptide as expected confirms the controlled release process.

Chapter 3: *In situ* side chain peptide cyclization as a breaker strategy against the amyloid aggregating peptide

Accumulation and deposition of misfolded Amyloid β (Aβ) outside the nerve cells are one of the culprits for Alzheimer's disease (AD). Till the date, one of the promising therapeutic strategies for AD is to block the early steps involved in the aggregation of Aβ. After investigating peptide-based breaking strategies, we developed breaker peptides derived from the original Aβ sequences. Inspired from the Tjernberg's and Soto's work, we have focussed and replaced Val-18 (of Aβ) by side chain modified Glu(OBn) to generate adequate bent unit through *in-situ* peptide cyclization to break the β-sheet structure of Aβ. The formation of Amyloid in the form of fibril and the mechanism of aggregation was characterized by various biophysical tools; e.g., ThT-assay, TEM, Congo-Red birefringence study, and the conformation changes during aggregation process were characterized by CD and FTIR. Results suggest that designed breaker peptides may be useful to inhibit and disrupt not only Aβ peptide but related aggregated peptides also.

It was found that the fluorescence intensity of $A\beta_{1-40}$ peptide was increased with time in the absence of BPs and became static after four days. But in the presence of one-fold and five-fold molar excess of BPs, a significant decrease in fluorescence signal of $A\beta_{1-40}$ peptide was observed probably due to the formation of *in situ* side chain peptide cyclization. From the results, the dose-dependent inhibiting capability of BPs was confirmed, and five-fold BP3 have shown the best result among all.

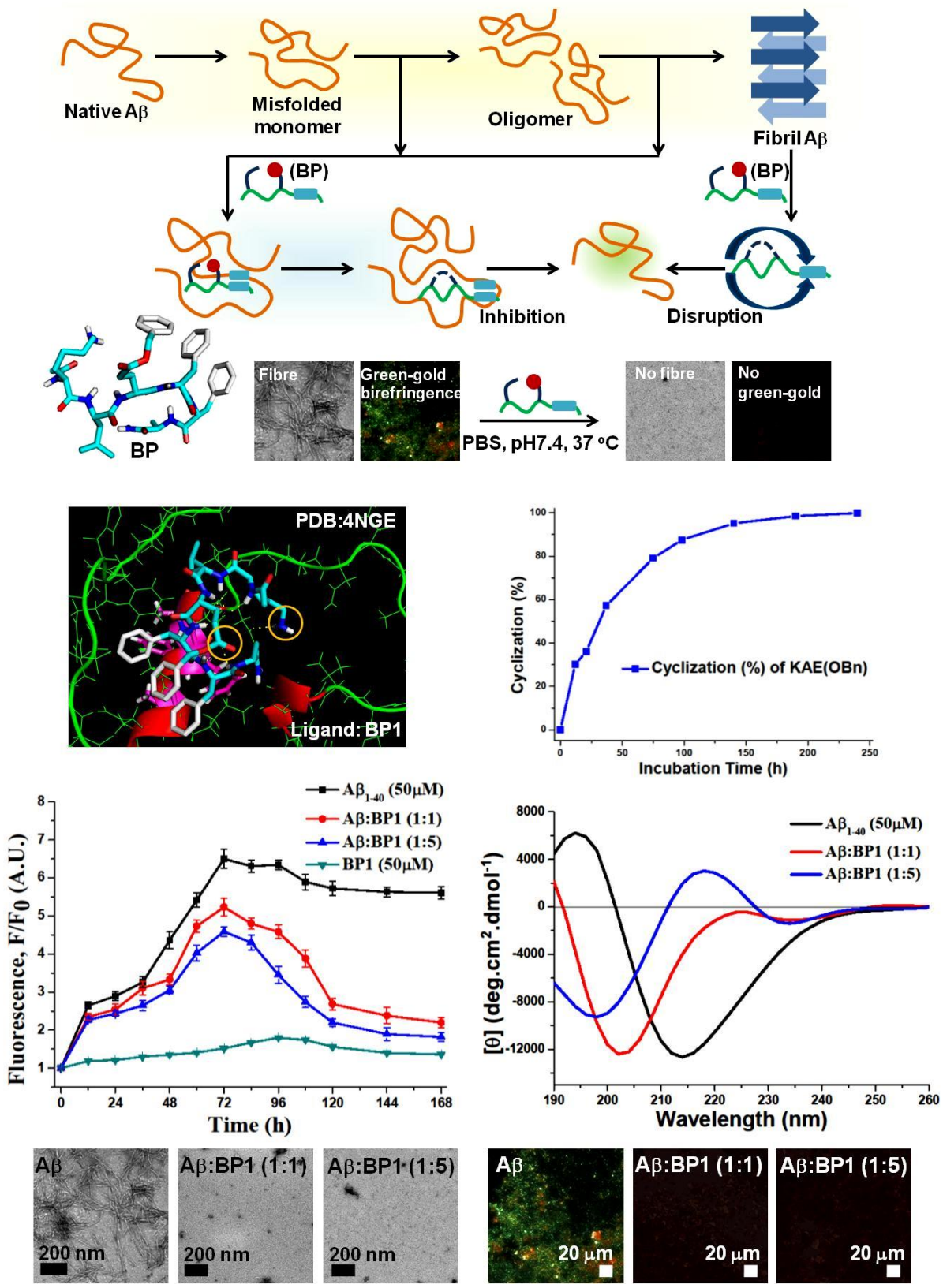

Figure 2. Concept of the work, and various biophysical studies to observe the kinetics of amyloid accumulation of $A\beta_{1\text{-}40}$ in the absence and presence of BP1 at the physiological condition.

From CD spectroscopy, the β-sheet structure of $A\beta_{1-40}$ peptide was confirmed, but in the presence of BPs, a mixture of a predominantly random coil and β-turn structure was obtained in most of the cases. The same results were noticed in FTIR spectra also. It was observed that the $A\beta_{1-40}$ peptide alone exhibited clear fibrillar structure when viewed under TEM after seven days of incubation. But BPs of different molar ratios along with $A\beta_{1-40}$ peptide exhibited no such characteristic fibrillar assembly when viewed under TEM at the same time. Clear green gold birefringence was observed in case of $A\beta_{1-40}$ alone under cross-polarized light, but no such birefringence was noticed when incubated along with BPs.

Chapter 4: Cyclic di-peptide via dual O→N acyl migration inhibited protein-aggregation

An increasing number of human diseases seem to be associated with protein aggregation, which directly contributes to or modulates the associated pathology. Certain protein aggregation diseases affect the central nervous system, and in these neurodegenerative diseases the pathological proteins may accumulate within the nucleus (for example in Huntington's disease), extracellularly (in prion diseases), or both intracellularly and extracellularly (for example, tau and amyloid-β in Alzheimer's disease). In the generalized purpose, we have taken the core sequence of amyloid-β (responsible for its aggregation) as the aggregating peptide (AP). Among various therapeutic approaches such as diminishing the monomeric precursor protein, inhibiting aggregation, or blocking aggregation-induced cellular toxicity pathways, we focussed on the inhibition of protein aggregation (the product of misfolded proteins). The "O→N acyl migration" concept was used to form *in situ* cyclic peptide, and thus the generation of a bent unit may act as a potent inhibitor. The kinetics of aggregation was characterized by various biophysical tools (ThT-assay, TEM, CD, and FTIR). Results implied that the designed inhibiting peptides (IP) might be valuable to inhibit all the related aggregated peptides.

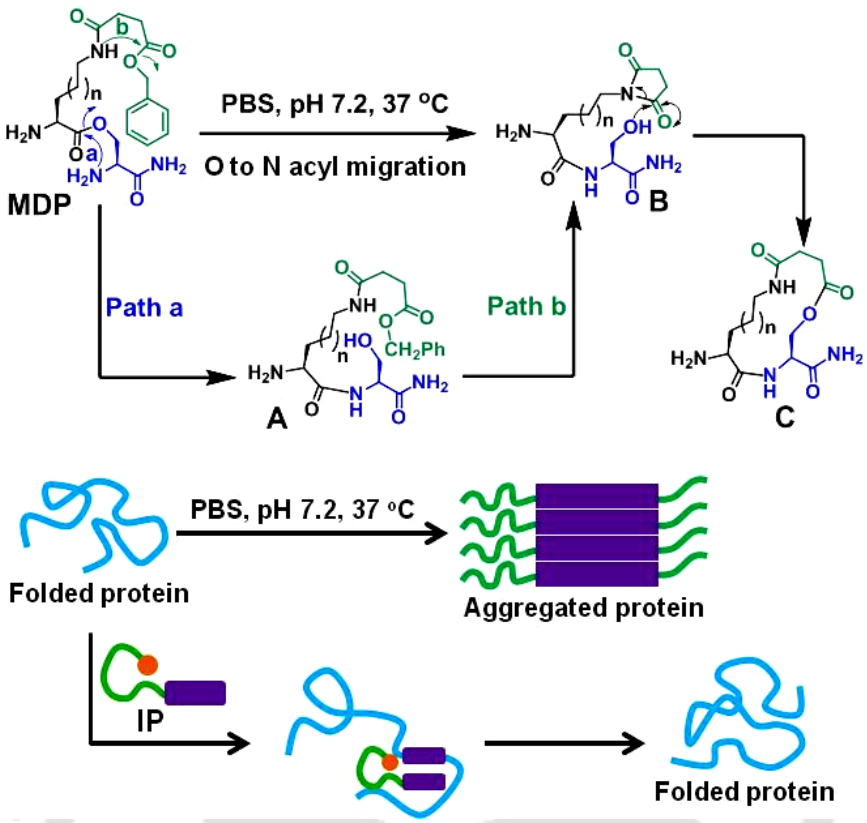

Figure 3. Schematic diagram of the inhibition of aggregated protein.

The inhibition mechanism involves the dual "O→N acyl migration" of a side-chain modified dipeptide, followed by the nucleophilic attack of Ser to the carbonyl group of succinamide unit to form a cyclic dipeptide finally. All the biophysical studies were carried out in PBS of pH 7.2 at 37 °C. The fluorescence intensity of the aggregating peptide alone increased gradually with time, but decreased significantly in the presence of different fold molar excess of IPs. From CD and FTIR spectra, it was observed that the β-sheet conformation of AP converted to the non β-sheet structure in the presence of IPs. IPs also inhibited the fibrillar structure of AP and the change in morphologies was studied by TEM.

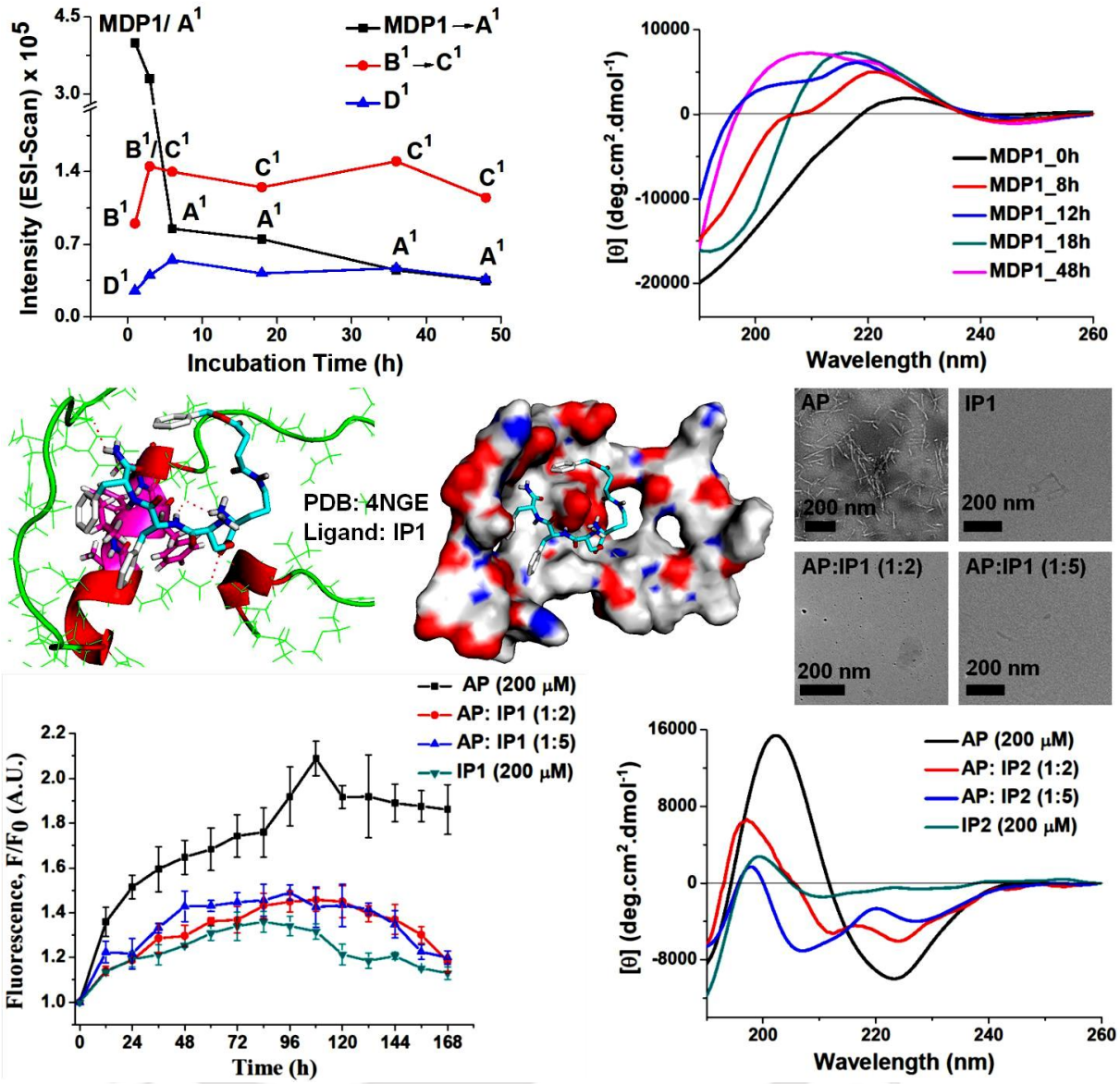

Figure 4. Various biophysical studies to get proof of principle, and to monitor the kinetics of protein-aggregation in the absence and presence of IP.

Chapter 5: N→N and O→N acyl migration towards the release of bioactive molecules

Peptide sequence containing aspartic acid (Asp) tends to form a five-membered ring which is well-known as aspartimide formation in peptide chemistry, could be a useful tool to release drug or bioactive molecules. Hence we have designed and synthesized Asp containing peptides having bioactive molecules at its side chain. In this context, we used amine group (for N→N acyl migration) and hydroxyl group (reported, for O→N acyl

migration) as the functional group to attach with Asp. Various kinetics assay (ESI-Mass, CD, TEM, etc.) was performed to get proof of principle of our hypothesis. From ESI-Mass spectra, we determined the intermediate and products. From TEM images, it was noticed that a well-organized (partially aggregated) structure (due to π-π interaction in-between Trp and Fmoc gr.) of Peptide 1 converted to an amorphous structure due to releasing Trp.

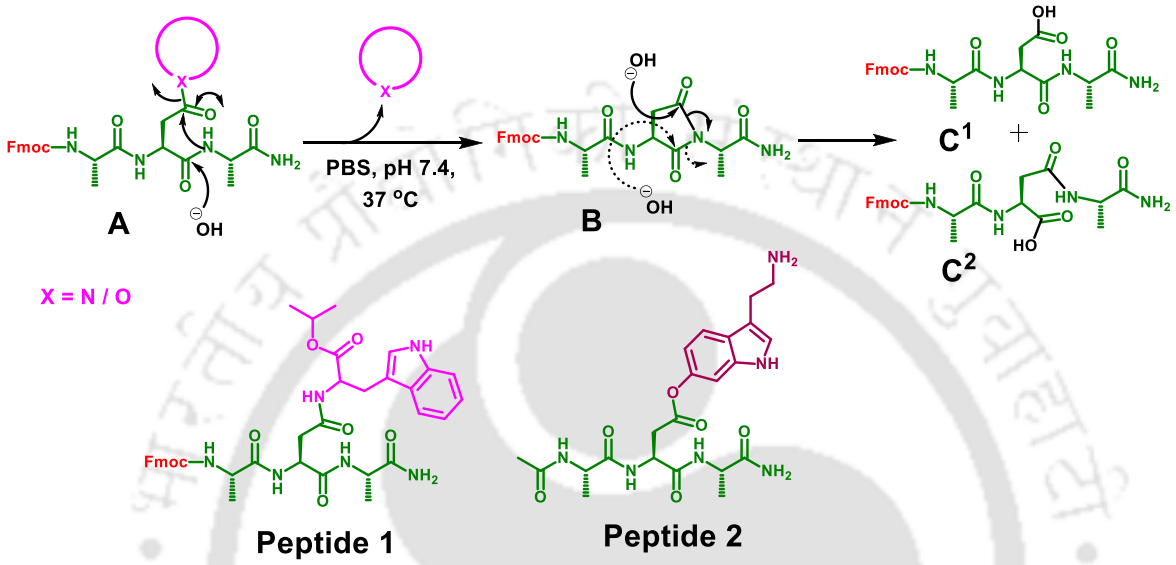

Figure 5. A plausible mechanism of releasing bioactive molecule from the designed peptide moiety.

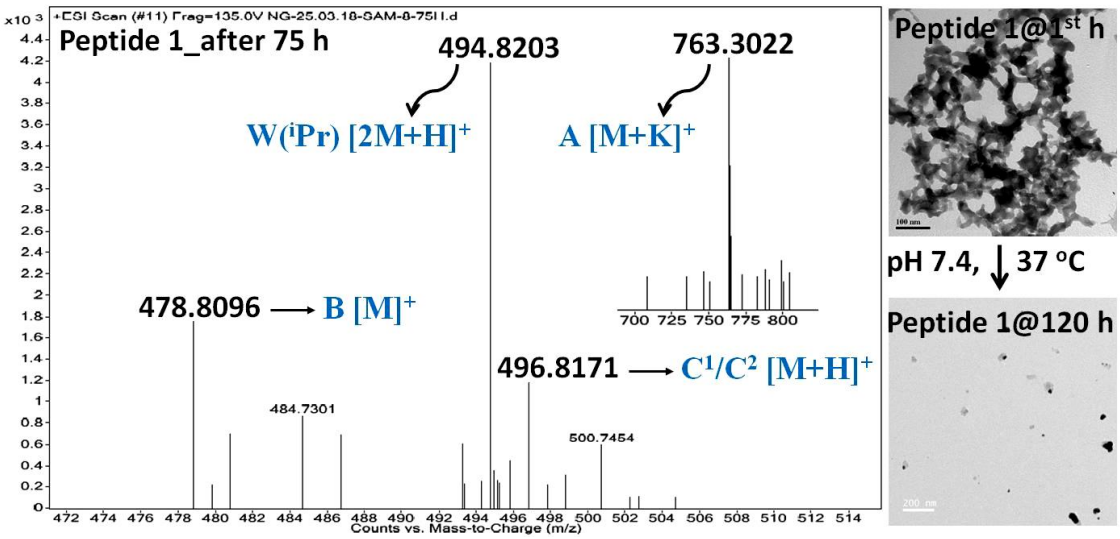

Figure 6. Various biophysical results related to releasing bioactive molecule from the designed molecule.

Conclusion:

The work presented in this thesis mainly centred on the design and synthesize of side chain modified peptides which can form cyclic peptide *in situ* at the physiological condition *in-vitro*. Further, we have applied the cyclization concept to release bioactive molecules and also to inhibit the protein aggregation. In the second chapter, a quick conversion of a smartly designed linear tri-peptide (RXE, X= P/ A/ G) into the cyclic one has been demonstrated to release the bioactive molecules in a controlled manner *in-vitro*. In the third and fourth chapters, we have introduced *in situ* side chain peptide cyclization as a β-sheet breaker strategy, and this is a promising therapeutic approach against AD and related disorders. In the fifth chapter, inspiring from the concept of aspartimide formation; N→N and **O→N** acyl migration were applied to release the bioactive molecules *in-vitro*.

Scope of the works:

The proof of the concept is obtained for the biological problems that we have addressed in this thesis, but a more comprehensive investigation is necessary for extension of the concept. For example strategically designed linear tripeptides were synthesized for *in situ* self-conversion into cyclic peptides under physiological conditions with application of selective release and delivery of small molecules in a controlled manner. But we need to examine the toxic nature (cytotoxicity) of side chain modified peptides against various cell lines. We are also interested to replace Bzl (benzyl) group, 2'-deoxyuridine and Camptothecin with other small drugs containing primary and secondary alcohol and to check the release of covalently attached drugs. Then the present concept of peptide self-cyclization leading to a bond cleavage could be a potential approach for delivering drugs in targeted and controlled way.

After examining the toxic nature (cytotoxicity) of our breaker peptides and inhibiting peptides against various cell lines, number of equivalents required (dose dependent studies), our concept of *in situ* cyclic peptide as a β-sheet breaker strategy can be useful for the development of therapeutics against Alzheimer's disease. This concept can be further explored to inhibit aggregation of neurodegenerative diseases (such as Parkinson's

disease, Huntington's disease, etc.) and on other aggregating peptides like IAPP known to cause diabetes type II.

References:

[1] F. Chiti, C. M. Dobson, *Annu. Rev. Biochem*. **2006**, 75, 333−366.

[2] K. E. Marshall, *et al*. *Biochemistry* **2011**, 50, 2061–2071.

[3] D. J. Selkoe, *Physiol. Rev*. **2001**, 81, 741−766.

[4] D. J. Selkoe, *J. Neuropathol. Exp. Neurol*. **1994**, 53, 438−447.

[5] L. O. Tjernberg, *et al*. *J. Biol. Chem.* **1996**, 271, 8545−8548.

[6] C. Soto, *et al*. *Nat. Med*. **1998**, 4, 822-826.

Table of contents

Chapter 2. In-situ peptide self-cyclization for controlled release of small bioactive molecule

---

Acknowledgements

At the outset, with the deepest sense of gratitude, I would like to express my sincere thanks to my supervisor, Dr. Lal Mohan Kundu for his boundless patience in supporting me, imparting immense knowledge and advising in my research work. His observations and continuous guidance with all the useful discussions helped me to establish the overall direction of the research and to move forward with investigation in depth. I am also thankful to him for giving me the freedom to pursue my own interests in his lab, encouraging me towards diligent perseverance and I find myself privileged to have worked under his kind guidance.

I also would like to thank my co-supervisor Prof. Ajaikumar B. Kunnumakkara for his guidance, enthusiastic encouragement and useful critiques of my research work.

My sincerest gratitude goes to my Chairperson Prof. Bhubaneswar Mandal for his inspiring encouragement, care and moral support. I am indeed fortunate to have him as my project guide also. I would like to acknowledge my other doctoral committee members, Prof. Bishnupada Mandal, Prof. Gopal Das for their valuable suggestions and advice.

I want to thank MHRD, Government of India, for financial support through GATE, and IIT Guwahati for providing necessary facilities. I am thankful to the Centre for the Environment, Department of Chemistry, Central Instruments Facility, lab technicians and all the non-teaching staff of the Centre for the Environment for their help during my Ph.D. tenure.

I must thank my former and present labmates for their constant cooperation, support and creating the pleasant environment in the laboratory. My special thanks

to Milan for TEM analysis, Dr. Tanmay for birefringence studies. I also would like to thank all of my Ph.D. batchmates (December 2014) for the wonderful time I had spent with them. Also, my sincere thanks to my seniors, juniors and friends as my stay in IIT Guwahati was made pleasant by them.

I cannot express enough words of gratitude to my dear friend Dr. Tanmay Mondal for introducing me with solid-phase peptide synthesis during my project time, encouraging me, sharing his knowledge and guiding me throughout my research. Without his continuous support and tremendous help in my studies, this task would have been difficult to achieve.

I extend my sincere thanks to all of my hard working teachers for their teaching, invaluable motivation, suggestions, and advice for academic as well as for progress of life. I also would like to thank my school and college friends for their constant unfailing support, encouragement, and all the help they extended from time to time whenever required.

Most importantly, my loving, caring family is my pillar of strength. I am thankful to my mother, father, husband, uncle, mother-in-law, father-in-law for their love, good wishes and endless moral support, especially at difficult times. My Ph.D. endeavors would not have been completed without their inspiration and blessings. I express my sincere gratitude to my beloved parents for loving me unconditionally, motivating me, supporting me always. I am forever indebted to my beloved husband, Dr. Arindam Das for instilling a vision for higher education in me and inspiring me to achieve it. He taught me about dreams and how to catch them. His unwavering support and encouragement gave me the strength at the challenging time. Finally, I

would not have been able to endure the stress of my thesis writing without my little baby, Auroni who kept me entertained.

I would like to thank all others who are associated with my work either directly or indirectly in completion of my research successfully.

Nibedita Ghosh

Abbreviations

Aβ	**A**myloid **b**eta
Abs	**Abs**orbance
Ac_2O	**Ac**etic anhydride
AD	**A**lzheimer's **d**isease
APP	**A**myloid **p**recursor **p**rotein
AU	**A**rbitrary **u**nit
Boc	*tert*-**b**utyl**o**xy**c**arbonyl
BOP	**B**enzotriazol-1-yl**o**xy tris(dimethylamino) **p**hosphonium hexafluorophosphate
Bzl	**B**en**z**y**l**
CD	**C**ircular **d**ichroism
CPT	**C**amptothecin
CR	**C**ongo **r**ed
DBU	1,8-**D**iaza**b**icyclo[5.4.0]**u**ndec-7-ene
DCM	**D**i**c**hloro**m**ethane
DFT	**D**ensity **f**unctional **t**heory
DIPEA	**Di**iso**p**ropyl**e**thyl **a**mine
DMF	N, N **d**i**m**ethyl **f**ormamide
DMPC	1,2-**Di**m**y**ristoyl-sn-glycero-3-**p**hospho**c**holine
DPPC	1,2-**Di**p**i**palmitoyl-*sn*-glycero-3-**p**hospho**c**holine
dU	**D**eoxy**u**ridine
ESI MS	**E**lectro**s**pray **i**onization **m**ass **s**pectrometry
Et_2O	Di**et**hyl ether
5-FdUrd	5-fluoro-2'-deoxyuridine
Fmoc	9-**F**luorenyl**m**eth**o**xy**c**arbonyl

FTIR	**F**ourier **t**ransformation **i**nfra **r**ed spectroscopy
GM1	**M**onosialotetrahexosyl**g**anglioside
GnRH	**G**o**n**adotropin-**r**eleasing **h**ormone
HEPES	*N*-2-**h**ydroxy**e**thyl **p**iperazine-*N*-2-**e**thane **s**ulphonic acid
HFIP	1,1,1,3,3,3-**h**exa**f**luoro-**2**-**p**ropanol
HOBt	1-**h**ydr**o**xy **b**enzo**t**riazole
HPLC	**H**igh **p**ressure **l**iquid **c**hromatography
iPr	**I**so**pr**opyl
KBr	Potassium **br**omide
LC-MS	**L**iquid **c**hromatography **m**ass **s**pectrometry
LHRH	**L**uteinizing **H**ormone **R**eleasing **H**ormone
LUV	**L**arge **u**nilamellar **v**esicles
mAβ	**M**odified **Aβ**
mL	**m**illi **l**iter
mM	**m**illi **m**ol
nm	**N**ano**m**etre
µM	**m**icro **m**ol
MW	**M**olecular **w**eight
NC	**N**egative **c**ontrol
NFT	**N**eurofibrillary **t**angles
NMI	***N***-**m**ethyl **i**midazole
NRP-1	**N**europilin-1
Pbf	2,2,4,6,7-**P**entamethyldihydro**b**enzo**f**uran-5-sulfonyl
PBS	**P**hosphate **b**uffer **s**olution
PDB	**P**rotein **d**ata **b**ank
PDCs	**P**eptide-**d**rug **c**onjugate**s**
RP	**R**everse **p**hase

SPPS	**S**olid **p**hase **p**eptide **s**ynthesis
Tau	**T**aurine
tBu	***t**ert*-**bu**tyl
TEM	**T**ransmission **e**lectron **m**icroscopy
TFA	**Tri**fluoroacetic **a**cid
ThT	**Th**ioflavin **T**
Trt	**Trit**yl
UV	**U**ltra**v**iolet
ZnBr2	Zinc bromide

Amino Acids:

Ala	A	Alanine
Arg	R	Arganine
Asn	N	Asparagine
Asp	D	Aspartic acid
Cys	C	Cysteine
Gln	Q	Glutamine
Glu	E	Glutamic acid
Gly	G	Glycine
His	H	Histidine
Ile	I	Isoleucine
Leu	L	Leucine
Lys	K	Lysine
Met	M	Methionine

Phe	F	Phenylalanine
Pro	P	Proline
Pyl	O	Pyrrolysine
Sec	U	Selenocysteine
Ser	S	Serine
Thr	T	Threonine
Trp	W	Tryptophan
Tyr	Y	Tyrosine
Val	V	Valine
Orn	O	Ornithine

Chapter 1: Introduction and Objectives

1.1. Introduction:

This thesis was developed on the concept of *in situ* peptide cyclization under physiological conditions without the need for any external reagent and its application as the release of covalently attached bioactive molecules and inhibitors for aggregating peptides. Here, in this introductory chapter, a brief discussion on the background and fundamental topics related to peptide-based drugs and drug delivery system, peptide cyclization, protein misfolding and related diseases such as AD, recent advances in treatment for AD, the instruments used to prove our hypothesis are provided.

1.2. Amino acids:[1,2,3]

Amino acids are the compounds that form the building blocks of proteins. Each amino acid consists of a central carbon atom referred to as the Cα atom, an amino group (NH_2), a carboxyl group (-COOH), and a side chain (-R). The R-group represents the side chain that varies from one amino acid to another to make each amino acid unique in nature.

Twenty different kinds of amino acids, along with some unusual amino acids, are found in biological systems. Pyrrolysine, Selenocysteine are two newly added amino acids. All amino acids, except glycine (R = H) are chiral and exist in D and L forms. But all the amino acids in the biological system exists in the L-configuration. When dissolved in water, amino acids exist as dipolar ions called "zwitterion" in solution. As it can act as an acid (proton donor) or a base (proton acceptor), they are called ampholytes.

The properties, reactivity, and hydrogen bonding ability of each amino acid are mainly dictated by the side chains, which vary in size, shape, charge. Glycine, alanine, methionine, valine, leucine, isoleucine, proline are aliphatic in nature. Glycine is the smallest amino acid. Valine, leucine, and isoleucine are considerably hydrophobic in nature. Phenylalanine, tryptophan, and tyrosine contain an aromatic side chain. These aromatic amino acids are specifically absorbed in 280 nm, which form the basis of quantitative estimation of protein by ultraviolet (UV) method. Phenylalanine is highly hydrophobic, which is found buried within globular proteins. Tyrosine can play an important catalytic role in the active site of some enzymes when reversible phosphorylation of –OH group in some enzymes occurs to regulate metabolic pathways. Lysine, arginine, and histidine are considered basic hydrophilic since they contain basic side chain groups that will have a positive charge at pH 7.4, whereas aspartic acid and glutamic acid are acidic hydrophilic since they contain acidic side chain groups that will have a negative charge at pH 7.4. Asparagine and glutamine are amide of two acidic amino acids- aspartic and glutamic acid. Methionine and cysteine are sulfur-containing amino acids. Cysteine forms an intermolecular disulfide bond (called cystine) with another cysteine of the polypeptide chain. These disulfide bonds are the only covalent bond besides peptide bond in the protein, which is important in the formation and maintenance of the tertiary (folded) structure in many proteins. Serine and Threonine both have hydroxyl group-containing side chains which form a hydrogen bond to water or to other groups on neighbouring macromolecules and play an important role in enzymes that regulate phosphorylation and energy metabolism. Proline is an imine with its secondary nitrogen atom has cyclic structure leads to bending of the protein chain. It restricts the geometry of the backbone chain in any protein where it is present.

1.3. Peptides:[2]

A peptide bond is simply the amide linkage (Figure 1.1) formed by the condensation reaction between the amino group of one amino acid and a carboxylic acid group of another after the loss of a water molecule. By this procedure, a repeating unit is obtained, which is the main chain or the backbone of the peptide where side chains lying outside.

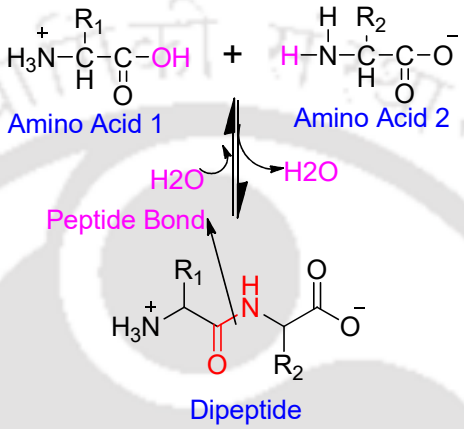

Figure 1.1. Schematic diagram of the peptide-bond formation.

Due to electron delocalization (Figure 1.2) between the carbonyl group and the amino group (-CO-NH), C=N gets a partial double bond character, which keeps these four atoms planar. The planarity and rigidity of the peptide bond are accounted for by the fact that free rotation cannot occur around double bonds and the restricted rotations about C=N resist hydrolysis also. Carbonyl oxygen being a suitable hydrogen bond acceptor and NH good hydrogen donor (except proline) makes hydrogen bonding possible for peptide backbone. This hydrogen bonding between the polypeptide backbones gives stability to the protein structure. Peptide bond exists in two different geometric forms: trans and cis. Though the peptide bond is planar, it undergoes very little rotation or twisting between N-Cα and C-Cα, which gives flexibility to the peptide chain.

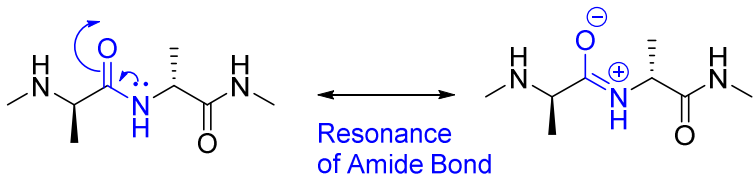

Figure 1.2. Resonance of an amide bond in a peptide.

Peptides, the small biological molecules, act as hormones, antibiotics, enzyme substrates, and inhibitors, regulate a wide range of physiological processes, operate interactions with numerous biological targets, thereby providing a vast opportunity for biotechnological applications as both therapeutic and diagnostic agents. In the past 15 years, an increasing number of peptides that are used as active pharmaceutical ingredients and have gained attention from academia to the pharmaceutical industry.

A number of unique properties make some peptides highly potent drugs and some drug carriers. Synthetic peptides and peptide-based molecular architectures offer plenty of opportunities due to their enormous variation in chemical structures and functional groups, biocompatibility, biodegradability, aqueous processability, resemblance to protein, unique molecular recognition properties, and tuneable chemical properties under mild condition. Many peptides being highly selective agonists or antagonists of different receptors involving human diseases, can bind specifically to their in vivo targets with great potency of action. High target specificity makes peptide drug candidates more potential with minimum side-effects. Some peptides can penetrate different barriers present in cells and tissues due to their physical, chemical, and biological properties. In various disease states, those functional peptides are served as effective drug carriers to overcome the extracellular and intracellular barriers. Generally having a short half-life, peptides do not accumulate in tissues which minimize the risk of complications from their metabolites. As degradation products of peptides are only amino acids, so low systematic toxicity is expected.

Versatility in molecular design, combined with potent biological roles in mediating different intercellular and cellular events, has triggered application of peptides and peptide-based materials in drug discovery, drug delivery, tissue engineering, vaccines, regenerative medicine, and molecular imaging technologies.

There are many disadvantages to the practical application of peptides as a drug. Due to low stability against proteolysis and quick renal clearance, many peptides suffer from *in vivo* short half-life. Another drawback is the low transport rates of peptides across biological barriers, which makes poor peptide candidates for oral delivery. Some peptides have poor solubility. Many peptide agonists show non-selective receptor binding.

To overcome these issues, researchers have developed many strategies based on formulations and chemical modification of peptides to provide a more efficient uptake across the biological barrier and increase metabolic stability. It includes peptide cyclization to increase stability, N-methylation to increase membrane permeability and stability, incorporation of unnatural amino acids like D- and β-amino acids to increase specificity and stability, the addition of polyethylene glycol for reduced clearance, assorting structural constraints (e.g., disulfide bonds), side-chain functionality-modifying strategies.

1.4. Peptide-based drugs and drug delivery system:

As protein-protein interaction executes many fundamental cellular functions, it is served as prime drug targets. Smaller size, the balance of conformational rigidity, and flexibility have made peptides suitable candidates as a targeting moiety with satisfactory binding affinity and specificity for cancer diagnosis and treatment. Besides this, peptides that mimic natural peptide hormones have therapeutic opportunities, such as synthetic human insulin for diabetic patients. To disrupt protein-protein interaction, target or inhibit intracellular molecules like receptor tyrosine kinase, peptides have entered as drug candidates in

pharmaceutical industries. After penetrating the cell membrane, effective recognization of targetable disease-associated protein-protein interaction and optimization of peptide drug binding characteristics with minimal toxicity have turned peptide therapeutics into a centre of attention, which help nearly 20 new peptide-based drugs into clinical trials annually. More than 400 peptide drugs are under global clinical developments already. To date, over 60 peptides have been approved and administrated worldwide. Some popular peptide drugs are liraglutide (Victoza) for metabolic disease, glucagon-like peptide 1 (GLP-1), leuprolide (Lupron), gosarelin (Zoladex) and somatostatin analogs, octreotide, lanreotide, etc.

For the targeted delivery and controlled release of therapeutic agents, different types of materials such as liposomes, micelles, hydrogels, polymeric nanoparticles, dendrimer, peptides are used as drug delivery vehicles.[4,5,6,7,8,9,10,11] With varying sizes, architectures, surfaces physicochemical properties, and targeting strategies, these drug delivery vehicles have been developed to reduce adverse side effects of drugs. As the development of a new drug molecule is highly expensive and time-consuming, delivering an existing drug molecule with the help of a novel drug delivery system instead of its conventional form is now a concerning research topic. It can significantly improve patient compliance, increase the efficacy and safety of the drug. It can decrease toxicity and side effects by releasing the drug at a specific site at a specific rate.

To transport sufficient drugs to the target site minimizing exposure to healthy tissues, covalent modification of the drug with some small moiety (prodrug strategy) is another strategy besides encapsulating the drug and transporting it through delivery vehicles. In the prodrug strategy,[12,13,14,15,16,17,18,19] physicochemical properties can be tailored by means of changing the structure of the carrier group, and the active drug is released by hydrolytic cleavage either chemically or by enzymatically in a non-toxic manner. Peptide-drug

conjugates (PDCs)[20] are prodrugs in which a drug is covalently attached with a specific peptide sequence via a cleavable linker. Due to biocompatibility, chemical diversity, and resemblance to proteins, PDCs are continuously gaining attention.

A simple PDC consists of a cytotoxic agent (drug), a navigating/targeting moiety, and a biodegradable linker that binds these two components. In PDCs, different categories of linkers are used, which vary on their length, stability, release mechanism, functional groups, hydrophilicity/hydrophobicity, etc. Linkers are designed to bear an enzyme-hydrolyzable unit like a carboxylic ester bond (succinyl deriving from succinic acid and glutaryl deriving from glutaric acid).or an amide bond, which can be cleaved by esterases and amidases respectively, some are degradable peptide linkers (cathepsin B) specific to certain enzymes. Stimuli-responsive linkers are designed to be cleaved when they sense specific stimuli like slightly acidic pH, increased levels of reducing agents, or in the presence of external stimuli like ultrasound, temperature, irradiation. Linkers with. imine, oxime, hydrazone, orthoester, acetal, vinyl ether, and polyketal bonds are known to undergo hydrolysis at acidic cellular compartments of cancer cells to release the active drugs. Disulfide linkers are cleaved by reducing agents like cysteine and glutathione present in malignant cells in high concentrations. The self-immolative or self-destructive spacers/linkers are now gaining attention as another rapidly emerging category in PDC linkers. *Para*-amino benzyl alcohol is a representative example of this category where active drug is released after simultaneous cascade reactions following the 1,6-elimination reaction mechanism.

Many synthetic peptides have been devised for diagnosis and therapy of human cancers on the basis of their targeting ability towards specific receptors overexpressed on cancer cell surface or cell membrane penetration capacity. Chemical modifications of amino acid chains have been done to improve the biological activity, stability, and efficacies of peptide

analogues currently employed as anticancer drugs or as molecular imaging tracers, and the results are promising. Facile preparation of many different PDCs is possible due to the diversity of amino acid combinations that can control the sequence to maintain the overall conjugate hydrophobicity and ionization; both of these influence the bioavailability in vitro and in vivo. The utilization of peptides allows for the incorporation of a great degree of functionality into PDCs. The amino acid sequence can be chosen to control the physicochemical properties of the conjugate and to allow for active targeting. Since PDCs are prepared from amino acids and generally have short peptide lengths, they should not elicit undesired immunogenic responses. Also, PDCs are biodegradable.[21,22,23]

Peptide-drug conjugates (PDCs) are an emerging class of prodrugs where the short peptide is combined with one or more drug molecules through a biodegradable linker. Amino acid sequence controls the physicochemical properties of the conjugate, allow active targeting of a particular receptor on the tumor cell surface; hence peptides incorporate a great degree of functionality into PDCs. Moreover, the diversity of amino acid control over the sequence helps in tuning the overall conjugate hydrophobicity and ionization, both influence bioavailability *in vitro* and *in vivo*.

1.4.1. Water-soluble PDCs:

Conjugating a drug to a hydrophilic peptide can alleviate solubility problems providing the opportunity for the inclusion of greater functionality.

1.4.1.1. Integrin targeted peptide-drug conjugates: Between a drug or delivery vehicle and a cell, the first point of interaction occurs at the exterior surface; any abnormally expressed receptors in diseased tissues present there may be a focal point for targeted delivery. For specific targeting to a particular cell type, a great diversity of targeting groups

can be integrated into the PDC design. Integrins are widely used receptors. The αvβ3 integrin targets the Arg-Gly-Asp (RGD) motif. It is reported doxorubicin, paclitaxel, camptothecin[24,25,26,27,28] conjugated to integrin-targeting peptides through amide or ester bond to exhibit enhanced *in vivo* tumor growth and metastasis inhibition efficacy over free drug having less toxicity.

1.4.1.2. Guanidinium-rich peptide-drug conjugates: Some functional peptides, due to their physical, chemical, and biological properties, can bind and penetrate barriers present in cells and tissues. These peptides serve as effective drug carriers as in the various diseased states. They overcome the extracellular and intracellular barriers, including the blood-brain barrier, gastrointestinal tract, tumor microenvironment. To enhance the internalization capacity through the non-polar cell membrane, researchers have developed drugs having a suitable hydrophilic- hydrophobic balance. Arginine-rich Tat49-57 peptide, a basic domain from HIV-1 Tat protein, was taken for rapid cellular uptake. Heptamer of arginine, a polycationic cell-penetrating peptide conjugated with a drug is a valuable tool for tumor-targeted drug delivery.[29,30]

1.4.1.3. Theranostic peptide-drug conjugates: Incorporating aggregation-induced emission fluorogenic (AIEgens) into peptide-drug conjugates offer superior photostability, high signal-to-noise ratio, low background interference during monitoring how and when the *in vitro* drugs are released. For tracking drug activation in targeted cells, Platinum-based prodrug functionalized with αvβ3 integrin targeting peptide cRGD, AIEgen tetraphenylsilole (TPS) based probe and caspase-enzyme-specific sequence-based linker Asp-Glu-Val-Asp (DEVD) peptide is reported.[31] Glutathione- the responsive selective release of Pt(II) species occurs to induce apoptosis in the cell, leading to an increased

expression of caspases result in activation of TPS-DEVD probe to get intracellular light-up imaging. Another method to monitor drug activation is attaching a quencher. It eliminates any fluorescence emission from a fluorescent drug. Restoration of the drug's fluorescence occurs upon drug-quencher separation, and an observable signal is produced. Lock et al. reported enzyme-specific doxorubicin drug beacon[32], which was covalently conjugated to a black hole quencher and octaarginine, a cell-penetrating peptide through a lysine junction. Cathepsin B sensitive enzyme-cleavable tetrapeptide Gly-Ple-Leu-Gly (-GFLG-) was incorporated between doxorubicin and quencher to release the drug.

1.4.1.4. Self-assembling peptide-drug conjugates: The hydrophobic drugs of low-molecular-weight combined with hydrophilic peptide increases overall amphiphilicity, which has a tendency of self-aggregation in an aqueous environment. Nanostructured nature of self-assembling peptide-conjugates has a local, topical, systemic mode of administration, and physicochemical properties can be tuned, altering the surface chemistry.

Supramolecular hydrogels are formed in an aqueous solution when low-molecular-weight gelators assemble through non-covalent interaction. Several factors like pH, ionic strength, temperature changes trigger the hydrogel formation. Peptide-based hydrogelators are gaining attention in biomedical applications for controlled drug release and intracellular imaging.[33,34,35]

In nanostructure-based strategy, covalent modification of drugs form discrete nanostructures and remain soluble without further hierarchical assembly. These PDCs are termed as drug amphiphiles where one or more drugs are conjugated with the cleavable linker and rationally designed peptide.[36],[37],[38],[39] In the conjugates, the functionally active unit is a peptide which modulates drug amphiphiles into discrete, stable, well-defined

supramolecular nanostructures in an aqueous solution. Variation of drug content leads to the change in morphologies of the nanostructure.

1.4.2. Peptides as carriers for tumor targeting and penetration:

There is an immense variety of linear and cyclic peptides; some are cell-specific, some bind to certain receptors promoting their internalization; have been exploited as carriers or targeting moiety for the successful delivery of a drug to cancer cells.

1.4.2.1. Arginine-glycine-aspartic acid (RGD): This tripeptide motif is applied as a peptide carrier as it is .known to be recognized by over ten integrins. Various proteins like fibronectin, prothrombin, fibrinogen, tenascin, and other glycoproteins contain this motif.[40,41] Integrin αvβ3, known as vitronectin receptor, is another important integrin regarding cell proliferation, invasion, and angiogenesis and is overexpressed on tumor cells, a suitable target for anti-angiogenic therapy. CDCRGDCFC , a cyclic peptide[42,43,44] containing the RGD motif, has been used for the formulation of PDCs due to its high levels of expression in cancer cells. A 9-amino acid cyclic peptide iRGD (CRGDKGPDC) having tumor tissue penetration activity can bind to αVβ3 and αVβ5 integrins initially that are overexpressed in tumor endothelial cells. During proteolytical cleavage, the peptide is cleaved to eventually expose the cryptic RXXK/R motif located at the C-terminus (CendR motif, C-End Rule), binds to neuropilin-1 (NRP-1), resulting in tissue and cell penetration.[45]

1.4.2.2. Gonadotropin-releasing hormone (GnRH): GnRH[46] hormone, pGlu-His-Trp-Ser-Tyr-Gly-Leu-Arg-Pro-Gly-NH2 is synthesized and released from GnRH neurons within the hypothalamus. It is also known as luteinizing hormone-releasing hormone (LHRH), responsible for the secretion of follicle-stimulating hormone (FSH) and luteinizing hormone (LH) from the anterior pituitary gland. GnRH selectively binds to its

receptor (GnRH-R), a seven-transmembrane G-protein-coupled receptor. specific human cancer cells (mostly ovarian, prostate, lung, and breast) overexpress GnRH-R with respect to normal tissues, so GnRH peptide analogs are applied as tumor homing peptides.[47,48]

1.4.2.3. Somatostatin (SST):[49,50,51,52] It is a neuropeptide that exists in two distinct active forms: somatostatin-14 (SST-14) and somatostatin-28 (SST-28). Both forms exhibit biological activity through high-affinity membrane receptors (somatostatin receptor 1–5; SSTR1–5) that are distributed throughout the human body in the nervous, pituitary, kidney, lung tissues, and immune cells. As SSTRs are overexpressed in various neuroendocrine malignant tumors (pancreatic, pituitary, prostate, lung carcinoids, osteosarcoma, etc.) and another non-neuroendocrine malignant tumor (breast, colorectal, ovarian, cervical, etc.), these receptors can be targeted for selective delivery of a cytotoxic agent to the tumor sites. Some analogs of somatostatin are cyclic peptides named octreotide (*d*-Phe-*c*[Cys-Phe-*d*-Trp-Lys-Thr-Cys]-Thr-ol), lanreotide (*d*-2Nal-*c*[Cys-Tyr-*d*-Trp-Lys-Val-Cys]-Thr-NH2), and vapreotide (*d*-Phe-*c*[Cys-Tyr-*d*-Trp Lys-Val-Cys]-Trp-NH2), which bind to the most frequently overexpressed subtype 2 receptor (SSTR2).

1.4.2.4. Epidermal growth factor (EGF): Epidermal growth factor receptor (EGFR) is a transmembrane protein which belongs to the ErbB family of receptor tyrosine kinases and consist of four cell surface receptors. Peptides like YHWYGYTPQNVI,[53] CMYIEALDKYAC,[54] LTVSPWY,[55] YWPSVTL,[56] etc. have been used to bind the EGFR with high affinity and selectivity.

1.4.2.5. Angiopep-2: A 19-mer peptide named angiopep-2 (TFFYGGSRGKRNNFKTEEY) has the ability to cross the blood-brain barrier (BBB), formed by the endothelial cells of the brain. This peptide can target low-density lipoprotein

receptor-related protein-1 (LRP-1) on the surface of brain cells and cross the BBB via receptor-mediated transcytosis. [57]

1.5. Cyclic peptides:

Cyclic peptides are polypeptide chains formed by amide bonds in a circular sequence. Nature itself is the source of many cyclic peptides, and several of them have been synthesized in the laboratory. Naturally occurring cyclic peptides isolating from plants,[58] mammals,[59] bacteria,[60,61,62] sponges,[63] fungi,[64,65] algae[66,67] have antibacterial, antifungal, anticancer, antiviral, and other biological activities so can be used as therapeutic agents and biochemical tools. Some cyclic peptides have excellent potential as therapeutics, such as antibiotics vancomycin, daptomycin and polymyxin B, the immunosuppressant cyclosporine, the hormone analogues oxytocin, vasopressin, octreotide.[68,69] Due to reduced conformational flexibility, cyclic peptides have better biological activity, cell permeability, oral bioavailability, low toxicity, good binding affinity, and target selectivity with lower immunogenicity compared with their linear counterparts.[70,71] The rigid structure of cyclic peptides decreases the entropy term of the Gibbs free energy, which helps the molecules to bind to receptors with high affinity.[72,73] Confining a peptide into a cyclic structure lacks both amino and carboxyl termini, facilitating resistance to hydrolysis by exopeptidases, and this less flexible structure resists endopeptidases also.[74] Cyclic mimetics force the molecule to stay in an ordered secondary structure; off-target side effects are prevented, leading to harmless metabolic products.

1.5.1. Synthetic approaches for peptide cyclization:[75,76,77]

Cyclic peptides have commonly being prepared using different chemical synthesis strategies either entirely in the solution phase or linear peptides in the solid-phase, followed by releasing linear chain from the solid support and cyclization step in the solution phase. The backbone constraint approaches are considered crucial in the lead optimization process during peptide cyclization to enhance drug-like properties, to stabilize peptide sequences into a specific secondary structure that are involved in the molecular recognition process by the target.

To minimize unwanted intermolecular processes like oligo- and polymerizations, the peptide cyclization in solution is performed under high dilution. The suitable orthogonal monomeric building blocks facile the ring closure on a solid support using standard coupling reagents. Different strategies have been designed to perform cyclization on the solid support, each of which requires a different type of linker. In the coupling achievement, the solid-support plays a critical role, which involves the incorporation of mechanical strength, good swelling capacity in solvents, and accessibility to the active sites of the polymer by the reagents. The solid-support may be linked to the *C*-terminus of the peptide through a 'safety catch linker' or an activated linker for tethering carboxylic acids to support. Alternatively, the solid support may be attached to the peptide through a side chain or through an amide bond nitrogen. The synthetic process begins on an insoluble and activated solid support, through covalent binding to the C or N-terminal of one amino acid. The peptide chain grows due to the activation of the carboxyl group and coupling to a protected amino acid. Polymer-supported synthesis is faster than liquid-phase procedures because of experimental simplicity, facility of selective separation of excess reagents and by-products from the growing and insoluble peptide through simple washing and filtration rather than liquid-liquid extraction and chromatographic purification. The Nα protected

amino acid residues in combination with Fmoc/tBu synthetic methodology is an efficient and attractive strategy where final deprotection occurs under mildly acidic conditions.

1.5.2. Types of Cyclization:[78,79,80,81]

Cyclic peptides can be classified into two major categories:

(1) homodetic cyclic peptides where ring formation occurs to form the amide linkage between an amino and carboxylic acid functional group.

(2) heterodetic. cyclic peptides where any other linkages such as lactone, ether, thioether, and, most commonly, the disulfide bridge are used to connect the amino acids.

Depending on functional groups, the peptide can be cyclized in different ways. The final ring-closing reaction is lactamization, lactonization, the disulfide bridge formation.

Intramolecular cyclizations (Figure 1.3) that peptides can undergo can be split into three categories:

A. Classical routes

Head-to-tail cyclization (homodetic): Between the N-terminus amino group and the C-terminus carboxyl group, the peptide bond is formed.[82]

When the peptide bond is formed due to head-to-tail cyclization and the ring is usually strengthened by three disulfide bonds, it is called Cyclotides.[83,84]

Side chain-to-one of the termini cyclization: Between the N- or C- terminus and the side chain functional group of amino acids, this type bond is formed due to head-to-side chain and side chain-to-tail (heterodetic) cyclization.[85]

Side-chain-to-side-chain cyclization: The bond formation occurs between two side chains of amino acids (homodetic and heterodetic).[86]

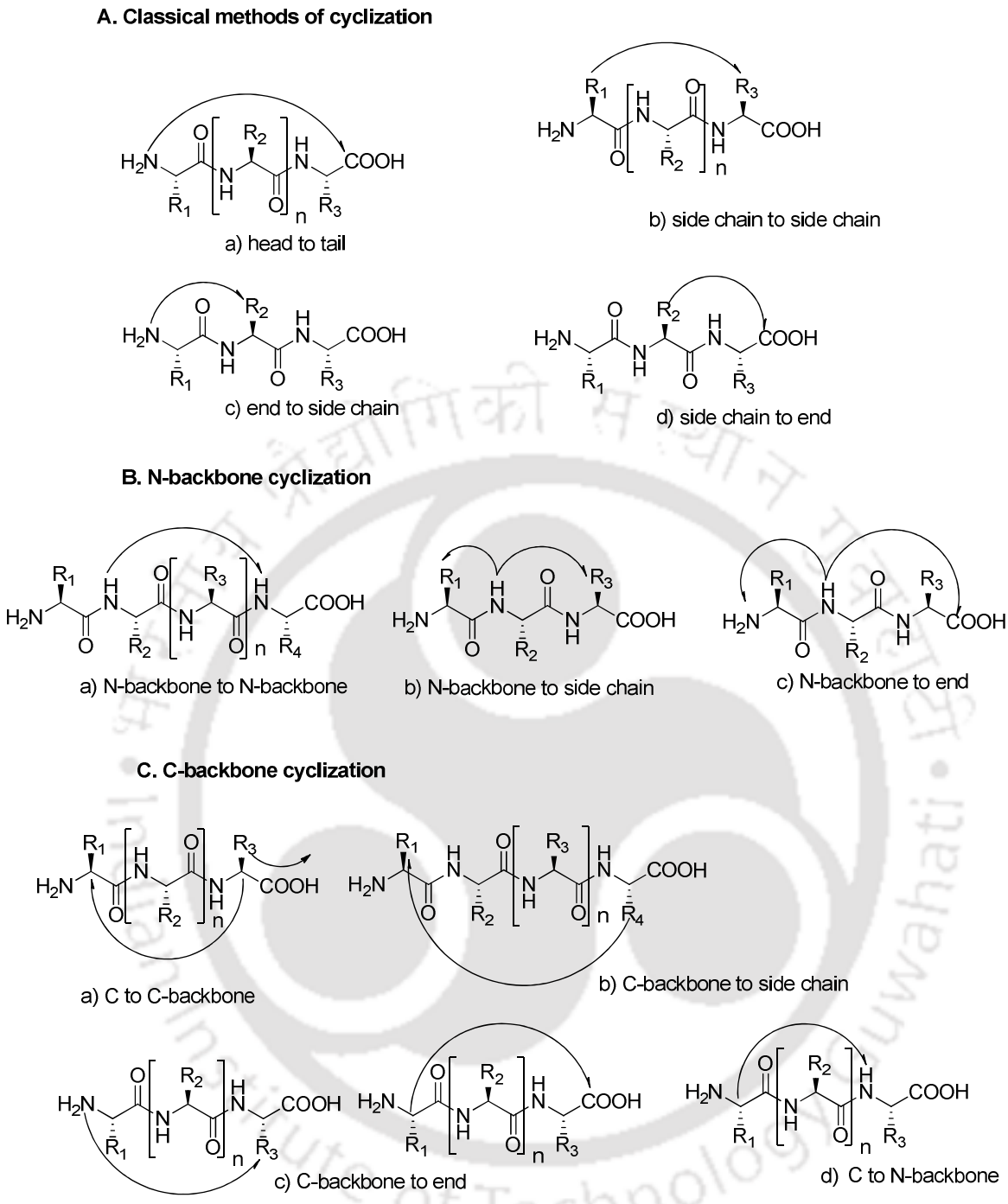

Figure 1.3. Intramolecular peptide-cyclization.

B. *N*-backbone cyclization

C. *C*-backbone cyclization

The concept of backbone cyclization was introduced to stabilize the bioactive peptide conformation keeping unaffected its functional groups.

The disulfide bond forms between two thiol groups from cysteine, and the thioether bond formation occurs between the side chain thiol group of cysteine and the α-carbon atom of amino acid.[87,88]

1.6. Aspartimide formation: unwanted cyclization in peptide chemistry[89,90,91,92,93]

This side reaction occurs in the Fmoc based synthesis of peptides containing aspartic acid. Aspartimide (Figure 1.4) can be generated spontaneously during the synthesis of Asp containing peptides in the presence of a base like piperidine or DBU during the Fmoc cleavage step. The nucleophilic attack occurs from the amide nitrogen of the preceding residue to the β-functional group in the side chain of aspartic acid, which is generally masked as an ester, here acting as a leaving group. Under the certain strongly acidic condition, aspartimide formation is also noticed in some cases in Boc based SPPS.

Aspartimide formation depends on a) nature of neighbouring amino acid residue located at the C-terminus of the aspartic acid, b) side-chain ester group.

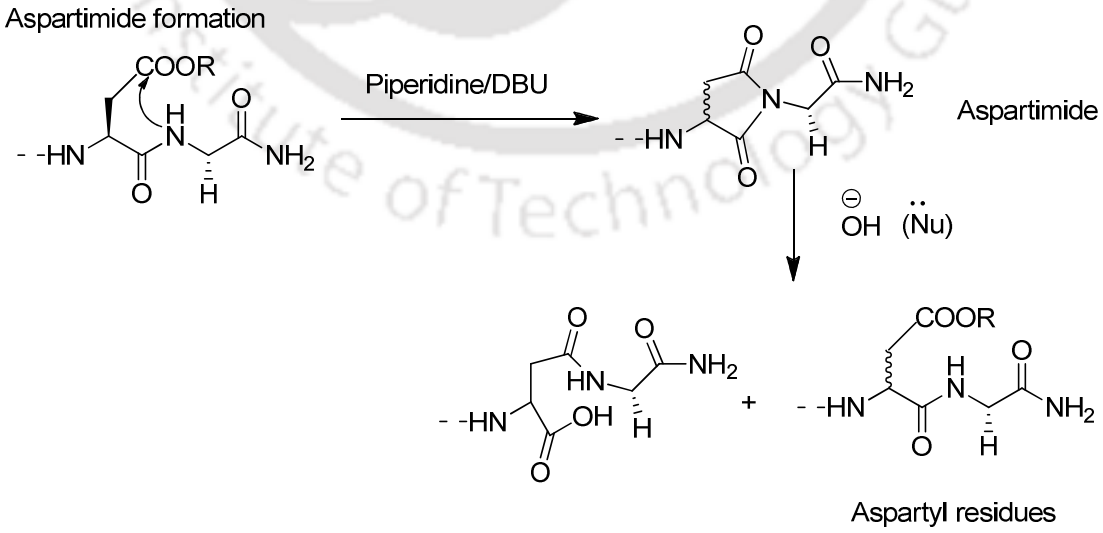

Figure 1.4. Formation of the aspartimide in aspartic acid containing peptide.

1.7. Cyclization-activated Prodrugs[94]

Activation of prodrugs *via* a cyclization pathway has been capturing the attention of medicinal chemists as this approach allows fine-tuning of the rate of drug release when the functional groups involved in ring closure are chosen appropriately and stereoelectronic constraints in the course of the cyclization step. To develop intramolecular-activated prodrugs, many strategies have been exploited, such as i) the cyclization reaction is used to release the active drug as the cyclization product, ii) the cyclization involves the release of parent drug as a leaving group and (iii) the cyclization is preceded by an enzymatic reaction where nucleophile is generated internally.

Release of drug from prodrug due to intramolecular activation or cyclization-elimination strategies are based on the attack of nitrogen (acidic amide or basic amine) or oxygen (hydroxyl, carboxylate) nucleophiles over a carbonyl moiety.

1.7.1. When an active drug is a leaving group in the cyclization-elimination reaction:

Hemiesters of aliphatic dicarboxylic acids have been developed as cyclization-activated prodrugs of phenols and were released *via* intramolecular cyclization (Figure 1.5) which occurred due to an attack of the carboxylate on the ester bond.[95]

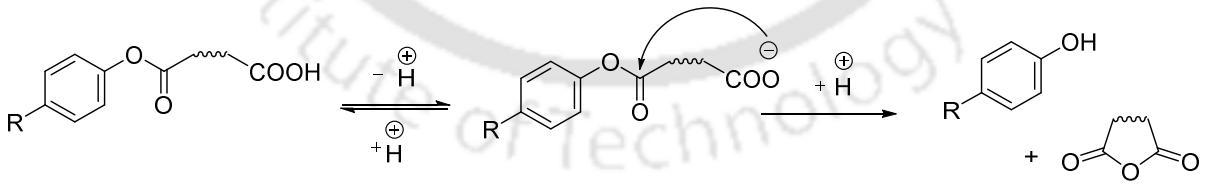

Figure 1.5. Intramolecular activation of phenol prodrugs using carboxylate nucleophiles.

To promote intramolecular prodrug activation, acidic amides supply (Figure 1.6) nucleophilic nitrogen.[96]

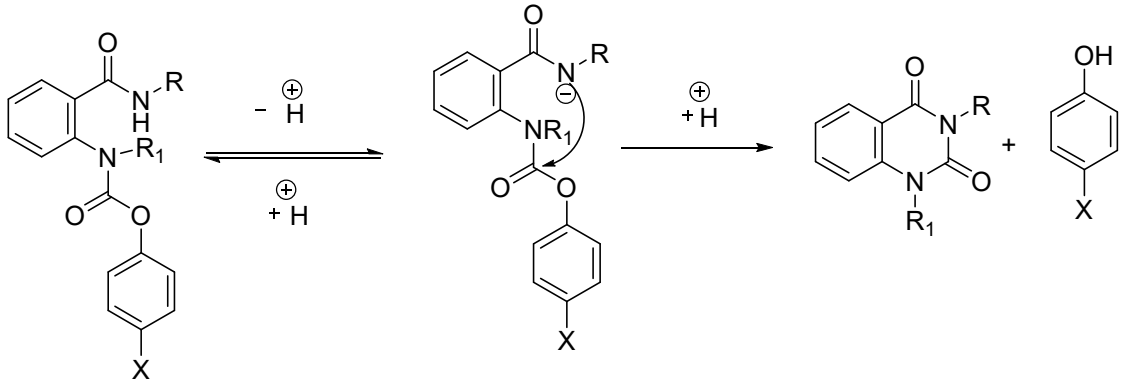

Figure 1.6. Cyclization activated phenyl carbamate prodrugs of phenols.

Water-soluble prodrugs of HIV-1 protease inhibitors, KNI-727 were designed to release the parent drug through intramolecular cyclization-elimination (Figure 1.7) by an acidic amide nucleophile.[97,98]

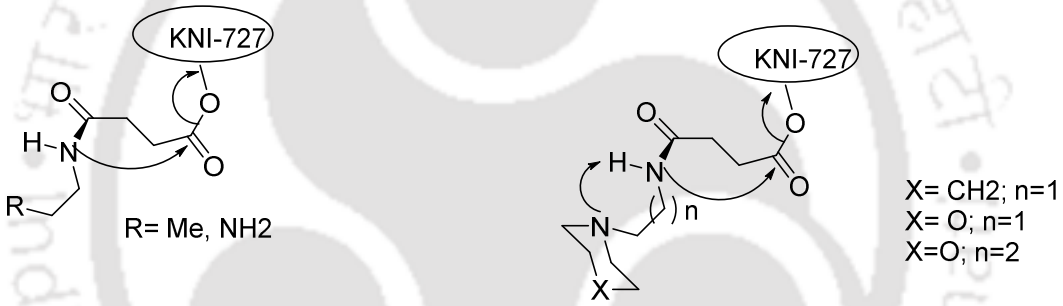

Figure 1.7. Intramolecular cyclization-elimination reaction of water-soluble prodrugs of KNI-727.

Carriers containing a terminal nucleophilic amino group can release drug through amino-mediated intramolecular cyclization result in cleavage of the drug-carrier bond. For such purposes, peptides have also been used as carriers to provide the basic amino group. Aminocarbamate prodrugs of 4-hydroxyanisole can release the parent compound by intramolecular cyclization (Figure 1.8) of the carrier moieties, leaving imidazolidin-2-ones.[99]

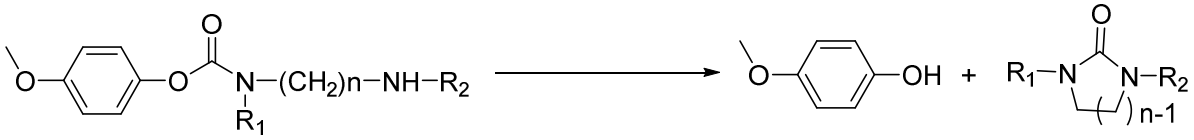

Figure 1.8. Intramolecular decomposition of 4-hydroxyanisole carbamates (n=2,3).

1.7.2. Peptide-based prodrug activation via diketopiperazines (DKP) formation

Linking linear dipeptide carriers to a drug, a prodrug can be designed which may undergo a chemical cyclization-elimination process by intramolecular aminolysis of the dipeptide moiety to a DKP (Figure 1.9) resulting in simultaneous departure of the drug moiety as a leaving group.[100,101,102,103,104,105,106]

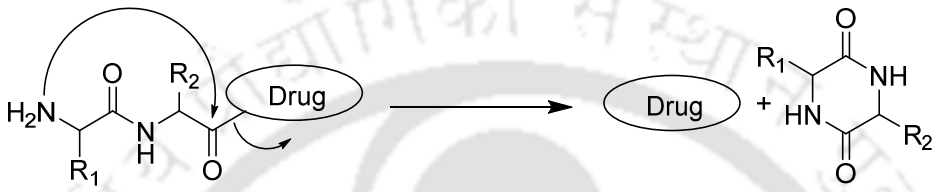

Figure 1.9. Prodrug activation via DKP formation.

1.8. Proteins:[107,108,109]

Proteins are the most important class of bio-macromolecules in the living system consisting of one or more polypeptide chains. These polypeptide chains usually contain more than 50 amino acids. In every aspect of cellular life, proteins are involved. Proteins function to transport ions and molecules from one organ to another, organize DNA, catalyze chemical reactions, regulate cellular and physiological activities, respond to stimuli, provide structure to cells. Proteins are also served as hormones, growth factors, neurotransmitters.

1.8.1. Structures of proteins:

Proteins are described according to their four levels of structure.

a) Primary Structure: It tells about the simple amino acid sequence of a protein. The primary structure is held together by covalent linkage or peptide bond.

b). Secondary Structure: It involves a specific geometry of the polypeptide backbone where the backbone atoms are stabilized by hydrogen bonds. Frequently occurring substructures in a polypeptide that are either coiled or folded in patterns is the concern of secondary structure.

α-helix: The α-helix is a right-handed helical coil where the peptide planes are roughly parallel with the helix axis, the side chain of the amino acids point outward from the helix axis. The helix is stabilized by hydrogen bonding between the carbonyl group of each first nth amino acid of the chain to the NH group of the (n+4)th amino acid in the sequence. The α-helices have 3.6 amino acid residues per turn within a fixed pitch of 5.4A˚, and the separation of residues along the helix axis is 1.5˚.

β-sheet: It consists of several β-strands, stretched segments of the polypeptide chain which are connected by an extensive network of hydrogen bonds between N-H groups of one strand and C=O groups in the adjacent strands. Two types of alignments of the β-strands are possible depending on the nature of the hydrogen bond pattern. When adjacent β-strands in a β-sheet run in the same direction, it is called parallel β-sheet, and for the opposite direction, it is called antiparallel β-sheet. The distance between adjacent amino acids along a β-strand is almost nearly 3.5 A˚. Higher levels of β-sheets association form protein aggregates and insoluble amyloid fibrils which are responsible for generating many human diseases like Alzheimer's disease, Parkinson's disease, etc.

β turn or β bend: It is nearly 180˚ fold or turns by polypeptide chain involving four consecutive amino acids. Here the CO group of the nth residue is hydrogen-bonded to the NH group of the (n+3)th residue but the remaining two residues present at the middle do not participate in any kind of interactions.

Omega loop: When a polypeptide chain consists of 6 to 16 residues, it forms a loop to get the compact and rigid structure.

c) Tertiary Structure: It refers to the overall folded native structure of a single polypeptide or protein in three dimensional (3D) space. Distinct amino acids are brought closer in the chain are further linked by ionic, hydrophobic, van der Waals forces of interaction, hydrogen bonding, and disulfide bonds. Polar and charged amino acids are located on the surface, whereas hydrophobic amino acids are buried inside the core of the protein.

d) Quaternary Structure: If a protein is composed of two or more subunits, each subunit being a monomer, i.e., one polypeptide chain, then their overall organization of multimeric functional proteins is referred to as the quaternary structure of a protein. This structure is stabilized by non-covalent interactions as well as disulfide linkages.

1.8.2. Protein folding and misfolding:[110,111]

In the ribosome, as a linear sequence of amino acids, polypeptide chains are synthesized which is organized into a space-filling, compact, characteristic, and functional three-dimensional structure via a physicochemical process known as protein folding. The amino acid sequence of a particular protein and its natural solvent environment are the governing factors for folding and the resulting native structure of the protein. Covalent interaction like disulfide bonds and non-covalent interactions like Vander Waals interaction, hydrogen bonds, electrostatic and hydrophobic interaction among the amino acid residues stabilize the energetically stable and biologically active native state of the protein. This native form is thermodynamically and kinetically stable. The hydrogen bonding between CO and NH groups within the same polypeptide chain, and the hydrogen bonding between the next neighbouring strand cause certain folding patterns known as α-helix and β-sheet respectively. These stable folding patterns make up the secondary structure of a protein. In

a globular protein, the internal core is formed by hydrophobic amino acid residues, where the surface is formed by the charged and polar side chain of amino acids. If protein molecules were not to acquire or preserve the native conformation, it would not function, rather give rise to the misfolded or partially unfolded state of the protein called protein misfolding that acts as an intermediate of the aggregation pathway. This state of change in conformation resulted from the misfolding of the secondary structure of the protein leads to various diseases like Alzheimer's disease, Parkinson's disease. The exact cause of protein misfolding is unknown, but some factors like pH, ionic strength, genetics, and mutations are believed to be involved during the process of misfolding.

1.9. Amyloids:

Amyloids are insoluble ordered fibrillar protein aggregates having a diameter of 3-10 nm and of indefinite length, resulting from the nonspecific amalgamation of the misfolded proteins. The common structural unit of all the amyloid fibrillar structure is a cross β-sheet motif where β-sheets are hydrogen-bonded along the length of the fibrils, and β-strands run perpendicular to the longitudinal axis of fibrils.

From the growing evidence, it is generally agreed that amyloid fibril formation is a nucleation-dependent process following a sigmoidal profile where three consecutive phases are noticed, (a) nucleation or lag phase, (b) growth phase, and (c) saturation phase.

At first, in the nucleation phase, protein monomers are arranged to come closer to form the nuclei, which are the early pre-fibrillar oligomers. These are elongated with the other monomers in the growth phase and later forms mature fibrils in the saturation phase. In this phase, the rate of monomer elongation is equal to the rate of monomer dissociation as the free monomers and the monomers incorporated into fibrils remain in equilibrium. Under

certain biophysical conditions, conformational alterations lead to the formation of a partially folded metastable state, which facilitates intermolecular interactions and finally forms oligomeric species. During oligomeric species formation, the secondary structural element β-sheet content increases. During the folding process, the intermediates which are generated contain surface-exposed hydrophobic amino acid residues are more prone to interact with other such molecules to give protein aggregates. For characterizing amyloid formation, different biophysical techniques are used, such as UV-vis spectroscopy, Fluorescence spectroscopy, Circular dichroism spectroscopy, FTIR measurement, Transmission electron microscopy. These fibrils can be prepared in vitro, and there are three criteria to define a protein aggregate as an amyloid fibril, which are green birefringence upon staining with Congo Red, β-sheet secondary structure, and fibrillar morphology. Abnormal association of the misfolded proteins leads to toxicity to the biological system. Amyloid deposition is associated with more than 30 human degenerative diseases, known as "amyloidoses", and this includes Alzheimer's disease, Parkinson's disease, Huntington's disease, type-2 diabetes, *etc*. Some amyloid-forming proteins or peptides and related diseases are shown in the Table 1.1.

Table 1.1. List of amyloidoses and associated peptide:

Disease	**Aggregating peptide/protein**	**Number of residues**
Alzheimer's disease	Amyloid _	40 or 42
Parkinson's disease	Synuclein	140
Huntington's disease	Huntingtin with poly Q expansion	3144
Diabetes type-2	Amylin	37
Creutzfeldt-Jacob disease	Prion protein	253

1.10. Alzheimer's disease (AD)[112,113]

AD is a devastating neurodegenerative disorder of the central nervous system and the most common form of dementia (estimated ~50-60% of all cases), which manifests as progressive cognitive decline, behavioral and physical disability, memory impairment in the elderly people that eventually leads to death.

Gradual memory loss, problems with language and communications, confusion, disorientation to time and place, loss of good judgment, problems with abstract thinking and recognition, rapid mood swings, changes in personality and behaviour, progressive impairment of activities of daily living are the symptoms associated with AD.

German psychiatrist and neuroanatomist Alois Alzheimer, a pioneer in linking symptoms to microscopic brain changes, describes the haunting case of Auguste D., a female patient who was admitted for paranoia, had progressive sleep and memory disturbance, aggression, confusion, and other worsening psychological changes until her death 5 years later. In her brain at autopsy, he saw dramatic shrinkage and abnormal deposits in and around nerve cells which Dr. Alzheimer reported as "A peculiar severe disease process of the cerebral cortex". A German psychiatrist Emil Kraepelin, who worked with Dr. Alzheimer first names "Alzheimer's Disease" in the eighth edition of his book Psychiatrie in 1910.

As the global population ages, AD impacts a greater percentage of people. Currently 50 million people worldwide are affected by AD or another type of dementia, with prevalence growing steadily. The 2019 Alzheimer's Disease Facts and Figures report reveal that one in 10 Americans aged 65 or older is suffering from AD. At present, over 5.8 million Americans are suffering from AD, and the total number of people with AD in the United States could touch 16 million by 2050. Reports from the World Health Organization

indicate that the total number of people with dementia is projected to reach 82 million in 2030 and 152 million in 2050.

The two main histopathological criteria for AD are the presence of extracellular deposits of dense fibrillar aggregates of amyloid-β (Aβ) peptides (Figure 1.10) called senile plaques (SP), and intraneuronal twisted strands of hyperphosphorylated tau (ptau) proteins called neurofibrillary tangles (NFT). AD-afflicted brains exhibit traits such as an overall decrease in size due to loss of neurons and synapses in the cerebral cortex, a reduction in glucose uptake, impaired energy metabolism, altered calcium, iron, zinc, copper homeostasis, oxidized biomolecules reminiscent of oxidative stress.

1.11. Amyloid β (Aβ) peptide:[114,115,116,117,118]

Aβ peptides, the main component of senile plaques, are derived from the proteolytic cleavage of amyloid precursor protein (APP). APP is a type I membrane glycoprotein with one transmembrane domain (TMD) and made up of 695 to 770 amino acids with three splice variants APP695, APP751, and APP770. APP695 is the most abundant form found in the brain and is produced mainly by neurons. The N-terminal domain resides in the extracellular space, whereas the C-terminal domain resides in the cytoplasm. APP can be processed via two alternative pathways: amyloidogenic and nonamyloidogenic, leading to different outcomes. In the nonamyloidogenic route, APP is cleaved between Lys687 and Leu688 (APP770 numbering) by a multidomain zinc metalloenzyme α-secretase, results in the release of the soluble N-terminal fragment. Then within the TMD of APP, γ-secretase cleaves the remaining membrane-bound fragment at either position Val711/Ile712 or Ala713/Thr714 to produce Aβ(17–40) or Aβ(17–42). The amyloidogenic processing of APP involves the initial cleavage of APP between Met671 and Asp672 performed by a copper metalloprotein β-secretase to release the soluble fragment. The remaining

membrane-bound C-terminal fragment is then cleaved by γ-secretase to generate amyloidogenic peptides Aβ(1-40) (~90%) and Aβ(1–42) (~10%) having a tendency to form oligomers and fibrils.

The primary sequence of Aβ is given below,

H_2N-D_1AEFRHDSGYEVHHQK**LVFFA**EDVGSNK**GAIIGLMVGGVV**$_{40}$**IA**$_{42}$-COOH.

The peptide sequence is bipolar, where N-terminus is hydrophilic, and the C-terminus is hydrophobic. The central hydrophobic residues (Aβ17-21, LVFFA) known as the core hydrophobic region, probably due to the presence of aromatic amino acids, are also believed to be essential for Aβ aggregation. The hydrophobic C-terminus facilitates the interaction of Aβ with membranes resulting in possible enhancement of Aβ aggregation.

Aβ fibril formation is thought to proceed via a nucleated growth mechanism that is initiated by a lag phase during which nuclei is formed, and followed by an elongation phase in which protofibrils grow, culminating in mature fibril formation which remain in equilibrium with monomer units.

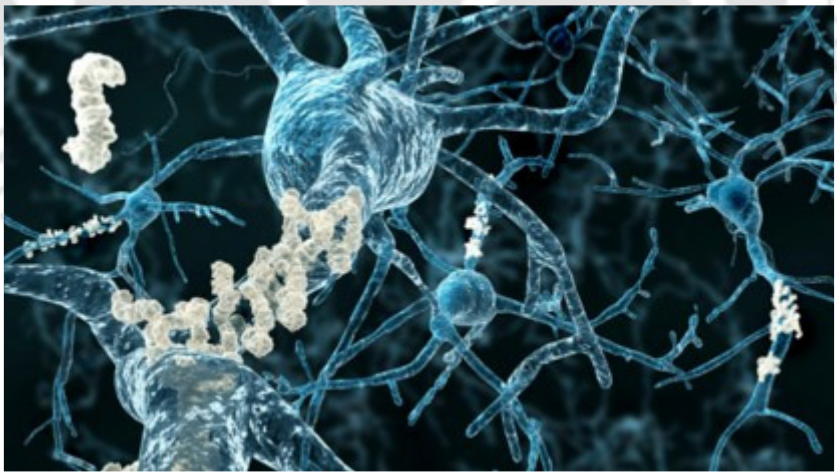

Figure 1.10. Deposition of Aβ aggregates outside neurons [Courtesy: https://www.medicalnewstoday.com/articles/313412.php]

Both monomeric peptides, Aβ(1−40) and Aβ(1−42) exist as mostly unfolded random coil conformation along with some α-helical and β-sheet content. Aβ monomers aggregate into various types of assemblies like oligomers, protofibrils, and amyloid fibrils. Amyloid oligomers are soluble, but fibrils are larger and insoluble, further assemble into amyloid plaques. Aggregated Aβ forms have inherent β-sheet structures determined by solid-state nuclear magnetic resonance spectroscopy. Aß fibrils adopt a cross-ß structure in which ß-strand segments from aggregating peptides run perpendicular to the direction of fibril elongation. Plaques of aggregated Aβ are enriched in more aggregation-prone Aβ(1−42) relative to Aβ(1−40), possibly due to the additional two hydrophobic C terminal residues for which Aβ(1−42) is thought to be more amyloidogenic and neurotoxic. As the oligomers could impair synapse plasticity and function, recent evidence indicates that Aβ oligomers are the more toxic.

1.12. Recent advances in treatment for AD:[119,120]

In the last 30 years, despite the major scientific and clinical advances made in AD research, the currently available treatments are all symptomatic.[121] They lessen the symptoms of the disease by acting on different levels of the neuropathological process, which only improves the patient's quality of life, but none of them is capable of slowing the rapid, fatal progression of the disease. To date, only a total of five drugs have been approved for treating AD.[122] Among them, three drugs are Donepezil, rivastigmine, and galantamine, belong to the acetylcholinesterase inhibitors group are used to increase cholinergic

transmission by means of inhibiting acetylcholinesterase in the synaptic cleft; which could increase the cognitive capacity of AD patients somewhat.[123] Another one is Memantine, an N-methyl-D-aspartate receptor antagonist that can reduce excitotoxicity by blocking that ionotropic receptor, as the excitatory neurotransmitter glutamate levels are pathologically high in AD.[124,125] Namzaric, a combination of two drugs, donepezil and memantine is used to reduce the levels of both acetylcholine and glutamate. None of these approved drugs has a real curative effect; they are only a palliative medicine to treat patients in moderate stages of AD, but their effectiveness decreases over time. In order to slow or stop disease progression, current research remains focused on exploring new treatments and therapeutic strategies.[126]

1.12.1. Therapeutic strategies used in developing disease-modifying treatments (DMTs) for AD

Alzheimer's disease is histopathologically characterized by extraneuronal Aβ deposits; hence Aβ-based therapeutic approaches for the treatment remains of paramount importance.

Anti-amyloid DMTs have focused on three major mechanisms of action:

(1) **Reduction of Amyloid-β production:** As the amyloidogenic pathway is promoted after the sequential cleavage of APP by β-secretase and γ-secretase, the inhibition of these

enzymes has been considered as a major therapeutic target.[127,128] Flurizan™, identified as γ secretase inhibitor, is a selective Aβ42-lowering agent. The α-secretase cleaves within the Aβ peptide sequence region of APP results in the decreased full length of Aβ production. So the development of α-secretase activators or α-secretase mimetics has been found interesting in current research as a treatment strategy for AD.

(2) Reduction of Aβ-plaque burden:

i) Peptide-based molecular strategies to inhibit aggregation of Aβ:[129] The formation of amyloid fibrils by Aβ can be hampered in the presence of short synthetic peptides homologous to the central hydrophobic region of Aβ1-42 (residues 17-21) are called β-sheet breaker peptides (BSBp). Peptide inhibitors are usually derived from or contain a self-recognition segment Aβ (16–20) after suitable modifications. In 1996, the proof of principle was provided when Tjernberg et al. identified Aβ (16–20) or KLVFF as a minimum self-recognition sequence of Aβ40 and also found that Aβ (15–20) or QKLVFF suppressed Aβ 40 fibrillogenesis.[130,131] Amyloid core sequences are intrinsically highly amyloidogenic with poor solubility. In the same year, Soto et al. reported KLVFF-derived pentapeptide LPFFD (*i*Aβ5p), where proline residue owing very low β sheet propensity, acts as the "β-sheet Breaker".[132,133] Being nonamyloidogenic and able to inhibit Aβ fibrillogenesis both *in vitro* and in a rat model *in vivo,* this one is the earliest peptide leads for anti-amyloid drugs.

Doig, Meredith, Findeis, and Giralt groups reported N-methylated analogues of Aβ self-recognition segments as inhibitors because N-methylation of amide bonds restricts peptide conformation and the ability to propagate β sheets, improves peptide solubility and proteolytic resistance, increase the ability to cross the blood-brain barrier, exhibit higher

stability. To increase the resistance to proteolysis, several conformationally restricted α/β-hybrid peptides have been reported replacing the proline residue of *i*Aβ5p with synthetic non-proteinogenic amino acids like azetidin-2 carboxylic acid and its 3-phenyl derivative, β-proline, β-sulfonylproline, and anthranilic acid. Kiesling, Murphy, and co-workers designed KLVFFKKKK and KLVFFEEEE, oligo-Lys or -Glu tags as potent inhibitors by linking KLVFF to"disruptive elements".[134] An aspartyl derivative containing dipeptide BSBp is identified, which is able to undergo a chemical transformation under physiological conditions to generate a kink into the peptide backbone *in situ* as the breaker element.

ii) Metal ions homeostasis approach:[135,136] Abnormal accumulation or dyshomeostasis of metal ions such as iron, copper, and zinc and/ or aluminum within senile plaques exacerbates Aβ-mediated oxidative damage and acts as a catalyst for Aβ aggregation.[137] Therefore a rational therapeutic approach is chelation therapies aimed at disrupting aberrant interactions between Aβ and metals for preventing AD pathogenesis. PBT2, a second-generation 8-OH quinoline metal protein–attenuating compound that affects the Cu^{2+}-mediated and Zn^{2}+-mediated toxic oligomerization of Aβ, is currently in Phase IIa clinical trials.

iii) Small molecule-based approach:[138,139] Some small molecules being able to inhibit the formation and elongation of Aβ fibrils and also to destabilize Aβ fibrils *in vitro*, has increasingly gained attention as a potential therapeutic approach. Several polyphenols, including epigallocatechin-3-gallate (EGCG), curcumin, resveratrol, oleuropein being a rich source for a variety of different structural backbones with antioxidant, anti-inflammatory properties, metal chelating capacities, have progressed to clinical trials for AD treatment. 3-amino-1-propane sulfonic acid (3-APS, Alzhemed, tramiprosate) has

reached a phase II trial as an Aβ aggregation inhibitor but not the potential to stop cognitive dysfunction. A small compound, scylloinositol, has shown its ability to stabilize oligomeric aggregates of Aβ and inhibit Aβ toxicity in the murine hippocampus, is under clinical trial.

(3) Promoting the removal of amyloid deposits and aggregates: To promote the clearance of existing amyloid aggregates and deposits is another potential treatment option. It can be achieved by i) activating the enzymes that degrade amyloid plaques, ii) modulation of A*β* transport between the brain and the peripheral circulation, iii) immunotherapy strategy, which is divided into active and passive immunization. Immunotherapy strategy is based on stimulation of the host immune system to recognize and attack Aβ or produces antibodies to enhance the clearance of Aβ oligomers or plaques. Active immunotherapy (vaccination) approaches raise polyclonal antibodies against a therapeutic composed of an Aβ sequence-derived antigen and adjuvant by utilizing the capability of the immune system. A passive immunotherapy approach is used to treat a patient by intravenous administration of monoclonal antibodies with known antigen-binding capacities. CAD 106, designed by Novartis, the first second-generation vaccine, recently completed phase II clinical trials. Currently, anti-Aβ antibodies such as solanezumab, gantenerumab, crenezumab, intravenous immune globulin having the binding ability with soluble Aβ result in cognitive performance improvement, are in clinical trials.

Another pathogenic factor in AD is neurofibrillary tangles caused by hyperphosphorylated tau; hence the tau protein is also an important biological target for therapies. The inhibition of tau protein oligomerization and aggregation, tau phosphorylation, microtubule stabilization, enhancement of tau degradation as well as tau immunotherapy are the therapeutic approaches for the treatment of AD.

1.13. Biophysical methods used for the studies:

1.13.1. Electrospray ionization mass spectrometry (ESI-MS):[140]

ESI-MS has emerged as an important analytical technique that can provide both qualitative (structure) and quantitative (molecular mass or concentration) information when analyte molecules such as proteins, peptides, and other biological macromolecules are converted to ions. Ionization source, a mass analyzer, and a detector are the three basic components of the ESI-mass spectrometer. Using electrical energy, the transfer of ionic species from solution into the gas phase by ESI involves three steps: (1) dispersal of a fine spray of charged droplets from the high-voltage capillary tip, (2) solvent evaporation from the charged droplet followed by droplet disintegration into much smaller droplets and (3) ion ejection from the highly charged droplets.

The mass analyzer takes different types of ions from the ion beam, separates them based on their mass-to-charge ratio (m/z value), then the ions are passed to the detector systems to measure their concentration, and the relative abundance of ion signals against the m/z ratios are displayed graphically called a mass spectrum.

Mass of the synthesized peptides, the mass of various peptide fragments obtained during kinetics study were analyzed using Agilent-Q-TOF 6500 instrument (ESI +ve mode) equipped with Mass hunter work station software.

1.13.2. High-Performance Liquid Chromatography (HPLC):[141]

HPLC is a chromatographic technique to separate a mixture of compounds. It is an important analytical method to identify, quantify, and purify the individual components of the mixture. In this technique, a pump creates high pressure to move the mobile phase

(solvent which carries the analyte) carrying the components of the mixture through the stationary phase (the substance on which adsorption of the analyte takes place). Sample components displaying stronger interactions with the stationary phase travel more slowly through the column than components with weaker interactions. There are two types of HPLC based on the mode of separation: Normal phase chromatography (stationary phase is polar and the mobile phase is non-polar) and Reverse phase chromatography (stationary phase is non-polar and the mobile phase is polar).

Crude peptides after dissolving in CH_3CN/H_2O mixture was purified by RP-HPLC (reverse phase-high performance liquid chromatography) on Waters 600E using a C18-μ Bondapak semi-preparative column. To confirm the purity of the peptides, Waters 600E analytical HPLC system was used where the Ascentis C18 analytical column was used. The kinetics study of the designed peptide was done using a Waters 600E analytical HPLC system also.

1.13.3. Circular dichroism (CD)[142,143,144,145]

CD is one of the most routine techniques to examine the secondary structure of protein/peptide in a solution. The main principle involved in the CD is the differential absorption of right-handed and left-handed circularly polarized light as a function of wavelength exhibited by optically active molecules. The resulting component shows elliptical polarization, which is reported in terms of ellipticity (θ) in degrees. The different types of secondary structures of a protein (helix, sheet, or turn) and peptide bond usually give characteristic CD spectra in the far UV region (180-250 nm). The peptide bond generally absorbs at 220 nm and 190 nm due to $n\rightarrow\pi^*$ and $\pi\rightarrow\pi^*$ electronic transitions, respectively.

The CD spectra were recorded on a JASCO (Model J-1500) instrument. From Spectra Manager, Observed ellipticity (mDeg) was obtained, which was converted to mean residue molar ellipticity using the following equation:

$[\theta]$ (deg. cm^2 .$dmol^{-1}$) = Ellipticity (mdeg). 10^6 / Pathlength (mm). [Protein] (μM). N

1.13.4. Transmission Electron Microscopy (TEM):[146,147]

TEM is a widely used qualitative technique for morphological analysis. The presence of fibrillar structure under TEM is another characteristic property of amyloid formation of the aggregating peptide. In this technique, a cathode-ray source emits and accelerates a high-voltage electron beam through which incident light is transmitted and interacts with a thin, electron-transparent specimen, and transformed into elastically or inelastically scattered electrons to produce the inner structure of the specimen, which is recorded by the in-built camera. The thin film of peptide sample was prepared over the carbon-coated copper grid and stained with a negative staining agent like uranyl acetate as this staining helps to enhance the contrast of images, to reduce image noise, to improve the resolution of the image when viewed under low voltage conditions at 200 kV

To perform TEM analysis JEOL instrument (Model: JEM 2100) was used.

1.13.5. Fourier transformation infrared (FTIR) spectroscopy:[148]

As most of the molecules, except homonuclear diatomic molecules, show IR absorption, so infrared radiation is used to excite the vibrational modes of the molecule of interest due to a net dipole change in IR spectroscopy. FTIR spectroscopy is extensively used due to its high signal to noise ratio, fast data acquisition, and reliable digital subtraction.

Protein misfolding and amyloidogenesis is related to changes in secondary structures. Vibrational spectroscopy such as infrared is highly sensitive to the secondary structure of

proteins, which makes them a qualitative technique to detect the presence of the secondary structure of a protein and a peptide. The amide I band, arising primarily from the C=O stretching vibration, is used to assign secondary structure, which occurs in the region between 1600 cm^{-1} and 1700 cm^{-1}. The amide I vibration is affected very little by the nature of the side chain and mostly depends on the secondary structure of the backbone. Being the amide I band most sensitive spectral region to protein secondary structures of α helix, β sheet, turn, and disordered conformations, one can differentiate between different secondary structures from the amide I band.

The presence of a peak near 1645 cm^{-1} is indicative of random coil, 1655 cm^{-1} of α helix, and 1620–1640 cm^{-1} of β sheet conformation of peptides or proteins. The amide I band of the aggregated amyloid β sheet is generally in the range of 1610–1630 cm^{-1}, probably being in a more hydrophobic environment and formation of stronger hydrogen bonding. More ordered fibres absorb at around 1620 cm^{-1} whereas more disordered fibres at 1635 cm^{-1} approximately due to stronger coupling. If amyloid fibrils composed of parallel or antiparallel β sheets, antiparallel β sheets exhibit an additional weaker high frequency compare to parallel β sheets, amide I transition occurs at approximately 1670–1690 cm^{-1}

1.13.6. Thioflavin T (ThT) fluorescence assay:[149,150,151]

Thioflavin T(ThT), a small molecule that gives strong fluorescence upon binding to amyloids, is a commonly used probe to monitor *in vitro* amyloid fibril formation. ThT is a quantitative technique to monitor the formation of amyloid with time. The fluorescence intensity of an aggregated peptide solution increases when the amount of fibrils present in the solution increases. On the other hand, a decrease in intensity indicates the inhibition of fibrillar assembly. So the kinetics of amyloid formation and its inhibition on the addition of inhibitor can be monitored by the ThT assay method.

This benzothiazole fluorescent dye is weakly fluorescent in water with excitation and emission maxima at 350 and 440 nm, respectively. Upon binding to fibrils and other β-rich peptide self-assemblies, ThT gives a strong fluorescence signal as excitation and emission maxima shift to a higher wavelength at 435 to 490 nm, respectively. The rotational immobilization of the central C–C bond connecting the benzothiazole and aniline rings is considered for the fluorescence enhancement upon binding to amyloid. It is a normally accepted fact that ThT dye binds to the side chain networks along the long axis of amyloid fibrils. An aromatic hydrophobic groove spanning across four consecutive β-strands represents a minimal ThT binding site on amyloid fibril surfaces. So grooves which are formed by aromatic hydrophobic residues on amyloid fibril surfaces may be recognition source for amyloid dyes. For ThT fluorescence assay, Fluoromax-4, Horiba instrument was used.

1.13.7. Congo red-stained birefringence study:[152,153,154,155]

An amyloidosis is a group of diseases in which various types of misfolded proteins get deposited in tissues as fibrils. A specific characteristic property of amyloid fibrils is dye-binding, which is used as a diagnostic test on polarization microscopy. This qualitative technique helps in monitoring the formation of amyloid. Only mature fibrils and amyloid form of Aβ show green-gold birefringence under cross-polarized light after staining with Congo red. During the examination of Congo red-stained section by polarization microscopy, specifically when two polarizing filters termed the polarizer and analyzer are inserted into the optical path below, and above the section, various colors can be observed depending on the degree of rotation of filter. These filters convert ordinary, unpolarized light into linearly polarized light that travels in one plane only. When the polarizer and analyzer are accurately crossed, the background is dark, and birefringent materials appear

bright. Congo red-stained amyloid is only reported to show "green birefringence" under these conditions.

Commercially available Congo red was dissolved in 80 % aqueous ethanol to prepare a saturated solution. Then a saturated sodium chloride solution was added into the saturated Congo red solution, and after filtration, Congo red solution was obtained.

For analysis, the required amount of peptide solution was taken from the stock and placed over a glass slide, followed by saturated Congo red solution. The excess solution should be removed using blotting paper. After drying the sample at room temperature, it was kept in desiccators. Birefringence analyses were performed on Leica ICC50 HD polarizable microscope.

1.13.8. Large unilamellar vesicles (LUVs) leakage study:[156,157,158]

A key pathological marker of Alzheimer's disease is the formation of extracellular plaques surrounded by dead and damaged neurons in the brain. Due to misfolding and aggregation, *β*-amyloid peptides adopt antiparallel *β*-sheet conformation, which is the most abundant component in the core of the plaques. Several studies reported that the primary target of amyloid peptides is the cell membrane of neurons. Due to aggregation of Aβ peptide, important physical and biological properties of membranes are altered, causing membrane barrier disruption, lipid regulation in cells, and variations in lipid composition, particularly the presence of raft domains can affect the amyloid toxicity in cells. Common components of lipid rafts are cholesterol, sphingomyelin, and gangliosides which are reported having increased interactions with Aβ peptide.

The amyloid fibril formation occurs via transient oligomers that eventually go on to more stable fibrillar structures. The intermediate smaller soluble oligomers of Aβ have been

found to be the more toxic species than the monomers or fully formed insoluble amyloid fibrils because soluble oligomers form pores in the cell membrane by interacting strongly with lipid membrane resulting in membrane disruption.

Lipid membranes are gaining attention as a potentially vital factor in disease propagation. To study *in vitro* peptide-induced membrane leakage, artificial synthetic large unilamellar lipid vesicles (LUV) are often employed as a model membrane system. This method involves the preparation of lipid vesicles loaded with fluorophore like carboxyfluorescein at a self-quenching concentration and are incubated together with membrane disrupting peptide. When the externally added peptide forms relatively large pores (≥1 nm in diameter), leakage of self-quenched fluorescent molecules occurs from LUV. It is detected as a time-dependent increase in fluorescence emission intensity due to fluorescence dequenching upon release of the fluorescent molecules.

1.14. Molecular docking studies:[159,160]

In drug designing and discovery, molecular docking, structure-based virtual screening, molecular dynamics are structure-based drug design methods with a wide range of applications in the analysis of binding energetics, molecular interactions, and induced conformational changes like molecular recognition events. Molecular docking is a well-established computational technique to predict the intermolecular interactions that stabilize the ligand-receptor complex, to find the best binding orientation and conformation of small-molecule ligands to their protein target binding site with overall minimum energy with a substantial degree of accuracy.

AutoDock Vina, an open-source program, has been designed and implemented by Dr. Oleg Trott (2010) in the Molecular Graphics Lab (MGL) at The Scripps Research Institute for

drug designing and discovery, molecular docking, and virtual screening. It offers multi-core capability with high performance and accuracy. Vina uses the PDBQT molecular structure file format used by AutoDock for its input and output. PDBQT files can be generated and viewed using MGL Tools.

For the synthesized compounds, a molecular docking study was performed using AutoDock Vina version 1.1.2 software. Different protein crystal structures were retrieved from the Protein Data Bank.

1.15. Peptide synthesis overview:

Many natural peptides have therapeutic applications as hormones, neuropeptides, and antibiotics are difficult to isolate from nature in sufficient quantities. The chemical synthesis of peptides has solved the problem by increasing production. The peptides can be synthesized in three ways: in a solution medium, on a solid support, combining solid and solution phase synthesis.

In 1901, Fischer and Fourneau first reported dipeptide Gly-Gly which was produced by hydrolysis of 2, 5-diketopiperzaine in acid-catalyzed conditions.[161,162] M. Bergmann and L. Zervas introduced a removable amino-protecting carbobenzoxy (Cbz) group for peptide synthesis in 1932. J. C. Sheehan, G. P. Hess[163] and H. G. Khorana[164] developed carbodiimide based coupling strategy in 1955 to form peptide bonds. du Vigneaud was awarded the Nobel Prize[165] for developing an active hormone, the octapeptide Oxytocin in solution phase applying early “classical” strategies by combining blocking/deblocking the N-terminus of amino acid followed by activation and coupling with C-terminal amino acid. Utilization of an insoluble polystyrene-based solid polymeric support (resin) to link the nascent peptide chain is the most conspicuous breakthrough invention by R. B.

Merrifield[166] in early 1963. Solid-phase peptide synthesis (SPPS) then started from the C to N terminus using Cbz as an α-amino-protecting group, *N,N'*-dicyclohexylcarbodiimide (DCC) as a coupling reagent, and peptide cleavage from the support by saponification or using HBr. From the 1960s through the 1980s, after extensive research by Merrifield Boc-based SPPS[167] was fine-tuned, which ultimately led to the Nobel Prize in 1984. In 1970, Carpino introduced the 9-fluorenylmethoxycarbonyl (Fmoc) group for Nα protection,[168] which requires moderate base piperidine for removal. This Fmoc-based strategy utilized *t*-butyl (*t*Bu)-based side-chain protection, which is labile in the presence of trifluoroacetic acid (TFA), and hydroxymethylphenoxy-based linkers for the synthesis of peptide sequences to the resin, making it an "orthogonal" synthesis.

Choosing the right solid support, linker (between the solid support and the synthesized peptide) to provide control and flexibility of the synthetic process, *t*-Boc/Bzl and Fmoc/*t*Bu protecting groups strategies, coupling methodology, and appropriate cleavage conditions, purification by reverse-phase HPLC have made SPPS a powerful tool for the advancement of peptide-based research.

1.16. Reagents and solvents:

Rink amide MBHA resin (Loading 0.5 mmol/g), all Fmoc (N- terminus protected) amino acids, N,N-Diisopropylethylamine (DIPEA), Thioflavin T (ThT), Congo red, potassium bromide (KBr), were purchased from Sigma-Aldrich (India), Dimethylformamide (extra pure grade), dichloromethane (extra pure grade), and acetonitrile of HPLC grade were obtained from Merck (India). Acetic anhydride (synthesis grade), N-methyl imidazole (extra pure), Trifluoroacetic acid (TFA) of extra pure grade were purchased from SRL (India). Milli-Q water at 18.2 Ω was used. BOP [(Benzotriazole-1-yloxy) tris (dimethylamino) phosphonium hexafluorophosphate], Diethyl ether were obtained from

Spectrochem Pvt. Ltd.(India). 2'-Deoxyuridine, Camptothecin, Serotonin hydrochloride, Zinc bromide anhydrous were bought from AlfaAesar. All the solvents were purchased from Merck (India). All the chemicals were used directly as received.

1.17. Objective of the thesis:

In this thesis, our main objective is to design and synthesis of peptide based moiety for *in situ* peptide cyclization using side chain modified peptides at the physiological condition without the need for any external reagent with application of selective release and delivery of small molecules in a controlled manner. Beside this, we have used this concept of side chain peptide self-cyclization as a β-sheet breaker strategy. We have chosen peptide based approach considering it effective as well as safe approach being very selective, target specific and less toxic.

In the second chapter of this thesis, we have shown our interest in the design and synthesis of *in situ* peptide cyclization to release covalently attached biomolecules from a peptide conjugate in a control way at the physiological condition without any external stimuli.

Inspired by the Tjernberg's work and Soto's work on AD, we have tried to develop a therapeutic agent against AD by designing breaker peptides based on the core hydrophobic segment of Aβ ($K_{16}LVFFA_{21}$), which is described in the third chapter of this thesis.

In the fourth chapter of this thesis, we have made a strategy to inhibit protein aggregation (responsible for several diseases) by generating an *in situ* bent unit via dual O →N acyl migration at nearly physiological condition.

In the fifth chapter of this thesis, we have attached bio-active molecules (having alcohol or amine as the functional group) at the side-chain of aspartic acid, biomolecules were released due to aspartimide formation (in the terms of O →N and N →N acyl migration) *in vitro*.

1.18. References:

[1] Russell, P. J. *iGenetics: A Molecular Approach,* 3rd ed. Pearson Education, **2010**.

[2] Berg, J. M.; Tymoczko, J. L.; Stryer, L. Protein Structure and Function, *Biochemistry*, 5th edition. W H Freeman: New York, **2002**.

[3] Eaton, L.; Rogers, K. The Building Blocks of Life: Examining Basic Chemical Molecules, 1st ed., Britannica Digital Learning: New York, **2018**, p. 5.

[4] Senapati, S.; Mahanta, A. K.; Kumar, S. *Sig. Transduct. Target Ther.* **2018**, *3*, 7.

[5]. Langer, R. *Nature* **1998**, *392*, 5–10.

[6] Torchilin, V. P. *Nat Rev Drug Discov*. **2014**, *13*, 813–827.

[7] Brannon-Peppas, L.; Blanchette, J. O. *Adv Drug Deliv Rev*. **2012**, *64*, 206–212.

[8] Torchilin, V.P. *Nat Rev Drug Discov*. **2005**, *4*, 145–160.

[9] Mura, S.; Nicolas, J.; Couvreur, P. *Nat Mater*. **2013**, *12*, 991–1003.

[10] Lin, R.; Cheetham, A. G.; Zhang, P.; Lin, Y. A.; Cui, H. *Chem Commun*. **2013**, *49*, 4968–4970.

[11] Kaneda, Y. *Adv Drug Deliv Rev*. **2000**, *43(2-3)*, 197–205.

[12] Kratz, F. *J Control Release* **2008**, *132*(3), 171–183.

[13] Chari, R. V.; Miller, M. L.; Widdison, W. C. *Angew Chem Int Ed*. **2014**, *53(15)*, 3796–3827.

[14] Su, H.; Koo, J. M.; Cui, H. *J Control Release* **2015**, *219*, 383–395.

[15] Duncan, R. *Nat Rev Cancer* **2006**, *6*, 688–701.

[16] Khandare, J.; Minko, T. *Prog Polym Sci*. **2006**, *31*, 359–397.

[17] Schrama, D.; Reisfeld, R. A.; Becker, J. C. *Nat Rev Drug Discov*. **2006**, *5(2)*, 147–159.

[18] MacEwan, S. R.; Chilkoti, A. *Biopolymers* **2010**, *94(1)*, 60–77.

[19] MacKay, J. A.; Chen, M.; McDaniel, J. R.; Liu, W.; Simnick, A. J.; Chilkoti, A. *Nature materials* **2009**, *8(12)*, 993–999.

[20] Wang, Y.; Cheetham, A. G.; Angacian, G.; Su, H.; Xie, L.; Cui, H. *Adv. Drug Delivery Rev*. **2017**, 110–111, 112–126.

[21] Urry, D. W.; Parker, T. M.; Reid, M. C.; Gowda, D. C. J *Bioact Compat Polym*. **1991**, *6*, 263–282.

[22] Shamji, M. F.; Betre, H.; Kraus, V. B.; Chen, J.; Chilkoti, A.; Pichika, R.; Masuda, K.; Setton, L. A. *Arthritis Rheum*. **2007**, *56*, 3650–3661.

[23] Hu, Y.; Lin, R.; Zhang, P.; Fern, J.; Cheetham, A. G.; Patel, K.; Schulman, R.; Kan, C.; Cui, H. *ACS Nano*, **2016**, *10*, 880–888.

[24] Arap, W.; Pasqualini, R.; Ruoslahti, E. *Science*, **1998**, *279*, 377–380.

[25] Chen, X.; Plasencia, C.; Hou, Y.; Neamati, N. *J Med Chem*. **2005**, *48*, 1098–1106.

[26] Choi, K. Y.; Swierczewska, M.; Lee, S.; Chen, X. *Theranostics*. **2012**, *2*, 156–178.

[27] Dal Pozzo, A. *et al. Bioorg Med Chem*. **2010**, *18*, 64–72.

[28] Dal Pozzo, A. *et al. Bioconjugate Chem*. **2010**, *21(11)*, 1956–1967.

[29] Rothbard, J. B.; Jessop, T. C.; Lewis, R. S.; Murray, B. A.; Wender, P. A. *J Am Chem Soc*. **2004**, *126*, 9506–9507.

[30] Wender, P. A.; Mitchell, D. J.; Pattabiraman, K.; Pelkey, E. T.; Steinman, L.; Rothbard, J. B. *Proc Natl Acad Sci USA*, **2000**, *97*, 13003–13008.

[31] Yuan, Y.; Kwok, R. T.; Tang, B. Z.; Liu, B. *J Am Chem Soc*. **2014**, *136*, 2546–2554.

[32] Lock, L. L.; Tang, Z.; Keith, D.; Reyes, C.; Cui, H. *ACS Macro Lett*. **2015**, *4*, 552–555.

[33] George, M.; Weiss, R. G. *Acc Chem Res*. **2006**, *39*, 489–497.

[34] Terech, P.; Weiss, R. G. *Chem Rev*. **1997**, *97*, 3133–3160.

[35] Carter, J. M.; Qian, Y.; Foster, J. C.; Matson, J. B. *Chemical Communications* **2015**, *51*, 13131–13134.

[36] Chen, Z.; Zhang, P.; Cheetham, A. G.; Moon, J. H.; Moxley, J. W.; Jr, Lin, Y. A.; Cui, H. *J Control Release* **2014**, 191, 123–130.

[37] Lock, L. L.; Reyes, C. D.; Zhang, P.; Cui, H. *J Am Chem Soc*. **2016**, *138*, 3533–3540.

[38] Kang, M.; Zhang, P.; Cui, H.; Loverde, S. M. *Macromolecules*, **2016**, *49*, 994–1001.

[39] Su, H.; Zhang, P.; Cheetham, A. G.; Koo, J. M.; Lin, R.; Masood, A.; Schiapparelli, P.; Quiñones-Hinojosa, A.; Cui, H. *Theranostics* **2016**, *6*, 1065–1074.

[40] Pierschbacher, M. D.; Ruoslahti, E. *Nature* **1984**, *309,* 30–33.

[41] Plow, E. F.; Haas, T. A.; Zhang, L.; Loftus, J.; Smith, J. W. *J. Biol. Chem.* **2000**, *275*, 21785–21788.

[42] Chen, K.; Chen, X. *Theranostics* **2011**, *1*, 189–200.

[43] Burkhart, D. J.; Kalet, B. T.; Coleman, M. P.; Post, G. C.; Koch, T. H. *Mol. Cancer Ther.* **2004**, *3*, 1593–1604.

[44] Gilad, Y.; Noy, E.; Senderowitz, H.; Albeck, A.; Firer, M. A.; Gellerman, G. *Pept. Sci.* **2016**, *106*, 160–171.

[45] Teesalu, T.; Sugahara, K. N.; Ruoslahti, E. *Front. Oncol.* **2013**, *3*, 216.

[46] Baba, Y.; Matsuo, H.; Schally, A. V. *Biochem. Biophys. Res. Commun.* **1971**, *44*, 459–463.

[47] Limonta, P.; Marelli, M. M.; Mai, S.; Motta, M.; Martini, L.; Moretti, R. M. *Endocr. Rev.* **2012**, *33*, 784–811.

[48] Cheung, L. W. T.; Yung, S.; Chan, T. M.; Leung, P. C. K.; Wong, A. S. T. *Mol. Ther.* **2013**, *21*, 78–90.

[49] Keskin, O.; Yalcin, S. *OncoTargets Ther.* **2013**, *6*, 471–483.

[50] Lahlou, H.; Guillermet, J.; Hortala, M.; Vernejoul, F.; Pyronnet, S.; Bousquet, C.; Susini, C. *Ann. N. Y. Acad. Sci.* **2004**, *1014*, 121–131.

[51] Sun, L. C.; Coy, D. H. *Curr. Drug Delivery* **2011**, *8(1)*, 2–10

[52] Modlin, I. M.; Pavel, M.; Kidd, M.; Gustafsson, B. I. *Aliment. Pharmacol. Ther.* **2010**, *31*, 169–188.

[53] Li, Z.; Zhao, R.; Wu, X.; Sun, Y.; Yao, M.; Li, J.; Xu, Y.; Gu, J. *FASEB J.* **2005**, *19*, 1978–1985.

[54] Ai, S.; Jia, T.; Ai, W.; Duan, J.; Liu, Y.; Chen, J.; Liu, X.; Yang, F.; Tian, Y.; Huang, Z. *Br. J. Pharmacol.* **2013**, *168*, 1719–1735.

[55] Orbán, E.; Manea, M.; Marquadt, A.; Bánóczi, Z.; Csık, G.; Fellinger, E.; Bősze, S.; Hudecz, F. *Bioconjugate Chem.* **2011**, *22*, 2154–2165.

[56] Wang, X. F.; Birringer, M.; Dong, L. F.; Veprek, P.; Low, P.; Swettenham, E.; Stantic, M.; Yuan, L. H.; Zobalova, R.; Wu, K.; Ledvina, M.; Ralph, S. J.; Neuzil, J. *Cancer Res.* **2007**, *67*, 3337–3344.

[57] Bertrand, Y.; Currie, J. C.; Demeule, M.; Régina, A.; Ché, C.; Abulrob, A.; Fatehi, D.; Sartelet, H.; Gabathuler, R.; Castaigne, J. P.; Stanimirovic, D.; Béliveau, R. *J. Cell. Mol. Med.* **2010**, *14*, 2827–2839.

[58] Tan, N. H.; Zhou, J. *Plant cyclopeptides*. *Chem. Rev.* **2006**, *106*, 840–895.

[59] Falanga, A.; Nigro, E.; De biasi, M.G.; Daniele, A.; Morelli, G.; Galdiero, S.; Scudiero, O. *Molecules* **2017**, *22*, 1217.

[60] Liu, J.; Zhu, X.; Kim, S. J.; Zhang, W. *Nat. Prod. Rep*. **2016**, *33*, 1146–1165.

[61] Abdalla, M. A. *Nat. Prod. Res*. **2017**, *31*, 1014–1021.

[62] Abdalla, M. A.; Matasyoh, J. C. *Nat. Prod. Bioprospect*. **2014**, *4*, 257–270.

[63] Andavan, G. S. B.; Lemmens-Gruber, R. *Drugs* **2010**, *8*, 810–834.

[64] Taevernier, L.; Wynendaele, E.; De Vreese, L.; Burvenich, C.; De Spiegeleer, B. J. *Environ. Sci. Health Part C* **2016**, *34*, 114–135.

[65] Abdalla, M. A. J. *Nat. Med*. **2016**, *70*, 708–720.

[66] Blunt, J.W.; Copp, B. R.; Keyzers, R. A.; Munro, M. H. G.; Prinsep, M. R. *Marine natural products. Nat. Prod. Rep*. **2016**, *33*, 382–431.

[67] Zhang, P.; Li, X.; Wang, B. G. *Planta Med*. **2016**, *82*, 832–842.

[68] Craik, D. J.; Fairlie, D. P.; Liras, S.; Price, D. *Chem. Biol. Drug* **2013**, *81*, 136–147.

[69] Driggers, E. M.; Hale, S. P.; Lee, J.; Terrett, N. K. *Nat. Rev. Drug Discov*. **2008**, *7*, 608–624.

[70] Zorzi, A.; Deyle, K.; Heinis, C. *Curr. Opin. Chem. Biol.* **2017**, *38*, 24–29.

[71] Kang, H. K.; Choi, M. C.; Seo, C. H.; Park, Y. *Int. J. Mol. Sci*. **2018**, *19*, 919.

[72] Edman, P. *Annu. Rev. Biochem.* **1959**, *28*, 69–96.

[73] Horton, D. A.; Bourne, G. T.; Smythe, M. L. *J. Comput. Aided Mol. Des*. **2002**, *16*, 415–430.

[74] Joo, S. H. *Biomol. Ther. (Seol.)* **2012**, *20*, 19–26.

[75] du Vigneaud, V.; Ressler, C.; Swan, J. M.; Roberts, C. W.; Katsoyannis, P. G.; Gordon, S. *J Am Chem Soc*, **1953**, *75*, 4879– 4880.

[76] Erickson B. W; Merrifield R. B. *In The Proteins*, 3rd ed.; Neurath, H.; Hill, R. L.; Boeda, C. L., *Eds.; Academic: New York*, **1976**, *2*, 255–527.

[77] (a) Barlos, K.; Gatos, D.; Koutsogianni, S.; Sch€afer, W.; Stavropoulos, G.; Wenqing, Y. *Tetrahedron Lett* **1991**, *32*, 471–474; (b) Rink, H. *Tetrahedron Lett* **1987**, *28*, 3787–3790; (c) Tjoeng F. S.; Heavner G. A. *Tetrahedron Lett* **1982**, *23*, 4439– 4442; (d) Wang, S. S. *J Am Chem Soc* **1973**, *95*, 1328–1333.

[78] Gilon, C.; Halle, D.; Chorev, M.; Selinger, Z.; Byk, G. *Biopolymers* **1991**, *31*,745-750.

[79] Al-Obeidi, F.; Castrucci, A. M. L.; Hadley, M. E.; Hruby, V. J. *J. Med. Chem.* **1989**, *32*, 2555-2561.

[80] Charpentier, B.; Dor, A.; Roy, P.; England, P.; Pham, H.; Durieux, C.; Roques, B. P. *J. Med. Chem.* **1989**, *32*, 1184-1190.

[81] Reissmann, S.; Imhof, D. *Curr. Med. Chem.* **2004**, *11*, 2823-2844.

[82] (a) Satoh, T.; Li, S.; Friedman, T. M.; Wiaderkiewicz, R.; Korngold, R.; Huang, Z. *Biochem Biophys Res Commun* **1996**, 460 Tapeinou *et al*. *224*, 438–443; (b) Deber, C. M.; Madison, V.; Blout, E. R. *Acc Chem Res* **1976**, *9*, 106–113.

[83] Craik, D. J.; Daly, N. L.; Bond, T.; Waine, C. *J Mol Biol*, **1999**, *294*, 1327–1336.

[84] Craik, D. J.; Swedberg, J. E.; Mylne, J. S.; Cemazar, M. *Expert Opin Drug Discov* **2012**, *7*, 179–194.

[85] Shibata, K.; Suzawa, T.; Soga, S.; Mizukami, T.; Yamada, K.; Hanai, N.; Yamasaki, M. *Bioorg Med Chem Lett* **2003**, *13*, 2583–2586.

[86] Piserchio, A.; Salinas, G. D.; Li, T.; Marshall, J.; Spaller, M. R.; Mierke, D. F. *Chem Biol* **2004**, *11*, 469–473.

[87] Hahn, M.; Winkler, D.; Welfle, K.; Misselwitz, R.; Welfle, H.; Wessner, H.; Zahn, G.; Scholz, C.; Seifert, M.; Harkins, R.; Schneider-Mergener, J.; Hohne, W. *J Mol Biol*, **2001**, *314*, 279– 295.

[88] Akamatsu, M.; Roller, P. P.; Chen, L.; Zhang, Z. Y.; Ye, B.; Burke, T. R., *Jr. Bioorg Med Chem* **1997**, *5*, 157–163.

[89] Nicolas, E.; Pedroso, E.; Giralt, E. *Tetrahedron. Lett.* **1989**, *30*, 497-500.

[90] Dolling, R.; Beyermann, M.; Haenel, J.; Kernchen, F.; Krause, E.; Franke, P.; Brudel, M.; Bienert, M. *J. Chem. Soc. Chem. Commun.,* **1994**,*7*, 853-854.

[91] Tam, J. P.; Yang, Y.; Sweeney, W. V.; Schneider, K.; Thornqvist, S.; Chait, B. T. *Tetrahedron Lett*. **1994**, *35*, 9689-9692.

[92] Tam, J.; Riemen, M.; Merrifield, R. *Peptide Res*. **1988**, *1*, 6-18.

[93] Mergler, M.; Dick, F.; Sax, B.; Weiler, P.; Vorherr, T. *J. Peptide Sci.* **2003**, *9*, 36-46.

[94] Gomes, P.; Vale, N.; Moreira, R. *Molecules* **2007**, *12(11)*, 2484-2506

[95] Fredholt, K.; Mork, N.; Begtrup, M. *Int. J. Pharm.* **1995**, *123*, 209-216.

[96] Thomsen, K. F.; Bundgaard, H. *Int. J. Pharm.* **1993**, *91*, 39-49.

[97] Matsumoto, H.; Sohma, Y.; Kimura, T.; Hayashi, Y.; Kiso, Y. *Bioorg. Med. Chem. Lett.* **2001**, *11*, 605-609.

[98] Sohma, Y.; Hayashi, Y.; Ito, T.; Matsumoto, H.; Kimura, T.; Kiso, Y. *J. Med. Chem.* **2003**, *46*, 4124-4135.

[99] Saari, W. S.; Schwering, J. E.; Lyle, P. A.; Smith, S. J.; Engelhardt, E. L. *J. Med. Chem.* **1990**, *33*, 97-101.

[100] Davies, J. S. *J. Peptide Sci.* **2003**, *9*, 471 501.

[101] Bray, A. M.; Maeji, N. J.; Valerio, R. M.; Campbell, R. A.; Geysen, H. M. *J. Org. Chem.* **1991**, *56*, 6659-6666.

[102] Capasso, S.; Vergara, A.; Mozzarella, I. *J. Am. Chem. Soc.* **1998**, *120*, 1990-1995.

[103] Besada, P.; Mamedova, L.; Thomas, C. J.; Costanzi, S.; Jacobson, K. A. *Org. Biomol. Chem.* **2005**, *3(10)*, 2016–2025.

[104] Moyroud, J.; Gelin, J.; Chêne, A.; Mortier, J. *Tetrahedron* **1996**, *52*, 8525-8534.

[105] Szardenings, A. K.; Burkoth, T. S.; *Tetrahedron* **1997**, *53*, 6573-6593.

[106] Sollis, S. L. *J. Org. Chem.* **2005**, *70*, 4735-4740.

[107] Andersen, N. H. *J. Am. Chem. Soc.***2001**, *123,* 12933-12934

[108] Shirley, Bret A. *Protein Stability and Folding, Theory and Practice*, *Methods in Molecular Biology*, **1995**, *40*, 1064-3745.

[109] Pauling, L.; Corey, R. B.; Branson, H. R. *Proc. Nat. Acad. Sci. USA*, **1951**, *37*, 205-211.

[110] Lewis, P. N.; Momany, F. A.; Scheraga, H. A. *Proc. Nat. Acad. Sci. USA*, **1971**, *68*, 2293-2297.

[111] Chiti, F.; Dobson, C. M. *Annu. Rev. Biochem.* **2006**, *75*, 333-366.

[112] Alzheimer, A. *Alg. Z. Psychiatry,* **1907,** *64*, 146-148.

[113] Selkoe, D. J. *Physiol. Rev*.**2001**, *81*, 741-766.

[114] Lesne, S.; Koh, M. T.; Kotilinek, L.; Kayed, R.; Glabe, C.G.; Yang, A.; Gallagher, M.; Ashe, K. H. *Nature* **2006**, *440*, 352–357.

[115] Lue, L.; Kuo, Y.; Roher, A. E.; Brachova, L.; Shen, Y.; Sue, L.; Beach, T.; Kurth, J. H.; Rydel, R. E.; Rogers, J. *Am. J. Pathol*., **1999**, *155*, 853–862.

[116] Naslund, J.; Haroutunian, V.; Mohs, R.; Davis, K.L.; Davies, P.; Greengard, P.; Buxbaum, J. D. *J. Am. Med. Ass*.**2000**, *283*, 1571–1577.

[117] Harper, J. D.; Lansbury, P.T. *Jr. Annu. Rev. Biochem*. **1997**, *66*, 385-407.

[118] Butterfield, D. A.; Kanski, J. *Mech. Aging. Dev*.**2001**, *122*, 945-62.

[119] Yoon, S. S.; Jo, S. A. *Biomolecules & therapeutics* **2012**, *20(3)*, 245-255.

[120] Lannfelt, L *et al*. *Journal of internal medicine* **2014**, *275(3)*, 284-295.

[121] Folch J, Ettcheto M, Petrov D, *et al*. *Neurologia*. **2018**, *33(1)*, 47-58.

[122] Galimberti, D.; Scarpini, E. *Ther Adv Neurol Disord*. **2011**, *4(4)*, 203-216.

[123] Grossberg, G. T. *Curr Ther Res Clin Exp*. **2003**, *64(4)*, 216-235.

[124] Wang, R.; Reddy, P. H. *Journal of Alzheimer's disease* **2017**, *57(4)*, 1041-1048.

[125] Koola, M. M. *et al*. *Journal of geriatric care and research* **2018**, *5*(*2*), 57-67.

[126] Cummings, J.; Fox, N. *The journal of prevention of Alzheimer's disease* **2017**, *4*(2), 109–115.

[127] Tomita, T. *Expert Rev Neurother*. **2009**, *9(5)*, 661-679

[128] MacLeod, R.; Hillert, E.; Cameron, R. T.; Baillie, G. S.; *Future science OA*. **2015**, *1(3)*, FSO11

[129] Armiento, V.; Spanopoulou, A.; Kapurniotu, A. *Angew. Chem. Int. Ed.* **2019**, *59*, 3372–3384

[130] Tjernberg, L. O.; Näslund, J.; Lindqvist, F.; Johansson, J.; Karlström, A. R.; Thyberg, J.; Terenius, L.; Nordstedt, C. *J Biol Chem*. **1996**, *271(15)*, 8545-8548.

[131] Tjernberg, L. O.; Lilliehöök, C.; Callaway, D. J. *et al*. *J Biol Chem* **1997**; *272(28)*, 17894. *J Biol Chem*. **1997**, *272(19)*, 12601-12605.

[132] Soto, C.; Kindy, M. S.; Baumann, M. *Biochem Biophys Res Commun*. **1996**, *226(3)*, 672-680

[133] Soto, C.; Sigurdsson, E. M.; Morelli, L.; Kumar, R. A.; Castaño, E. M.; Frangione, B. *Nat Med*. **1998,** *4(7)*, 822-826.

[134] Lowe, T. L.; Strzelec, A.; Kiessling, L. L.; Murphy, R. M. *Biochemistry*. **2001**; *40(26)*, 7882-7889.

[135] Barnham, K. J.; Bush, A. I. *Current Opinion in Chemical Biology,* **2008**, *12*, 222–228.

[136] Zatta, P.; Drago, D.; Bolognin, S.; Sensi, S. L. *Trends in Pharmacological Sciences,* **2009**, *30*, 346–355.

[137] Campbell, A. *Journal of Alzheimers Diseases,* **2006**, *10*, 165–172.

[138] Fu, Z.; Aucoin, D.; Ahmed, M.; Ziliox, M.; Van Nostrand, W. E.; Smith, S. O. *Biochemistry* **2014,** *53 (50)*, 7893-7903

[139] Nie, Q.; Du, X. G.; Geng, M. Y. *Acta Pharmacologica Sinica*. **2011,** *32(5)*, 545-551.

[140] Ho, C. S.; Lam, C. W.; Chan, M. H. *et al*. *Clin Biochem Rev*. **2003**, *24(1)*, 3-12.

[141] Coskun, O. *North Clin Istanb*. **2016**; *3(2)*, 156-160.

[142] Kelly, S. M.; Jess, T. J.; Price, N. C. *Biochim. Biophysica. Acta*. **2005**, *1751*, 119-139.

[143] Manavalan, P.; Johnson, W. C. *Nature* **1983**, *305*, 831-832.

[144] Correa, D. H. A.; Ramos, C. H. I. *African J. Biochemistry Research* **2009**, *3*, 164-173.

[145] Greenfield, N. J. *Nat. Protoc.* **2006**, *1*, 2876-90.

[146] Serpell, L. C. *Biochim. Biophys. Acta*. **2000**, *1502*, 16-30.

[147] Merz, P. A.; Wisniewski, H. M.; Somerville, R. A.; Bobin, S. A.; Masters, C. L.; Iqbal, K. *Acta. Neuropathol*. **1983**, *60*, 113-124.

[148] Nilsson, M. R. *Methods* **2004**, *34*, 151-160.

[149] Jameson, L. P., Smith, N. W., Dzyuba, S. *Acs Chem. Neurosci*. **2012**, *3*, 807-819.

[150] Levine, H. *Protein Sci*. **1993**, *2*, 404-410

[151] Levine, H. *Methods in Enzymology*, **1999**, *309*, 274-284.

[152] Sipe, J. D.; Benson, M. D.; Buxbaum, J. N. *et.al*. *Amyloid*, **2016**, *23*, 209-213.

[153] Howie, A. J.; Owen-Casey, M. P. *Amyloid*, **2010**, *17*, 109-117.

[154] .Westermark, P.; Benson, M. D.; Buxbaum, J. N.; Cohen, A. S.; Frangione, B.; Ikeda, S. I.; Masters, C. L.; Merlini, G.; Saraiva, M. J.; Sipe, J. D. *Amyloid,* **2005**, *12*, 1-4.

[155] Dobson, C. M. *Philos. Trans. R. Soc. Land*. **2001**, *356*, 133-145.

[156] Kristensen, K.; Henriksen, J. R.; Andresen, T. L. *Biochim. Biophys. Acta Biomembr*., **2014**, *1838 (12)*, 2994-3002

[157] Ladokhin, A. S.; Wimley, W. C.; White, S. H. *Biophys. J.* **1995**, *69(5)*, 1964-1971.

[158] Lindberg, D. J.; Wesén, E.; Björkeroth, J.; Rocha, S.; Esbjörner, E. K. *Biochim. Biophys. Acta Biomembr.* **2017,** *1859(10)*, 1921-1929.

[159] Ferreira, L. G.; Dos Santos, R. N.; Oliva, G.; Andricopulo, A. D. *Molecules* **2015**, *20(7)*, 13384-13421.

[160] Trott, O.; Olson, A. J. *J. Comput Chem,* **2010***, 31(2)*, 455–461.

[161] Baeriswyl, V.; Rapley, H.; Pollaro, L.; Stace, C.; Teufel, D.; Walker, E.; Chen, S.; Winter, G.; Tite, J.; Heinis, C. *Chem. Med. Chem.* **2012**, *7(7)*, 1173–1176.

[162] Barlos, K.; Chatzi, O.; Gatos, D.; Stavropoulos, G. *Int. J. Pept. Protein Res.* **1991**, *37(6)*, 513–520.

[163] Góngora-Benítez, M.; Tulla-Puche, J.; Albericio, F. *Chemical reviews.* **2014**, *114(2)*, 901–926.

[164] Berg, J. M.; Tymoczko, J. L.; Stryer, L. *W H Freeman: New York*, **2002**.

[165] Baslé, E.; Joubert, N.; Pucheault, M. *Chem. Biol.* **2010**, *17(3)*, 213–227.

[166] Blackwell, H. E.; Grubbs, R. H. *Angew. Chem. Int. Ed.* **1998**, *37(23)*, 3281–3284.

[167] Bois-Choussy, M.; Cristau, P.; Zhu, J. *Angew. Chem. Int. Ed.* **2003**, *42*, 4238-4241.

[168] Carbonnelle, A. C.; Zhu, J. *Org. Lett.* **2000**, *2 (22)*, 3477–3480.

Chapter 2: *In-situ* peptide self-cyclization for controlled release of small bioactive molecules

2.1. Introduction:

Peptide cyclization is generally performed using a chemical linker or with an external reagent. Currently a number of methodologies have been developed for peptide cyclization, including chemoselective backbone cyclization and *in situ* activation of specific amino acid residues.[1,2,3] Here we are broadly interested in the design and synthesis of *in situ* peptide cyclization using side chain modified peptides.[4,5,6] Peptide sequences can be modulated and tuned finely due to chemical diversity of amino acids and possibility to incorporate building blocks after chemical modifications on the peptide backbone and/or side chain during peptide synthesis.[7] So at first, attention is given to the tailored covalent conjugation of bioactive molecule with side chain of a hydrophilic amino acid. The linear peptides were designed to undergo self-cyclization under physiological condition without using any external reagent along with release of bioactive molecule as leaving group. This unique concept can be applied as controlled release of bioactive molecules from peptide-based moiety beside hydrolysis occurring chemically or enzymatically and bio imaging from peptide-based cargos. Before designing the desired peptides for controlled release, we have focussed on a few specific peptide moieties as described in the literature. Neuropilin-1 (NRP-1) is a cell-surface receptor that plays a crucial role in angiogenesis, vascular permeability, and the development of the nervous system. Peptides with an N-terminal

Arginine especially peptides with the four-residue consensus sequence RXXR, bind to NRP-1 on the target cell cause cellular internalization and vascular leakage.[8,9]

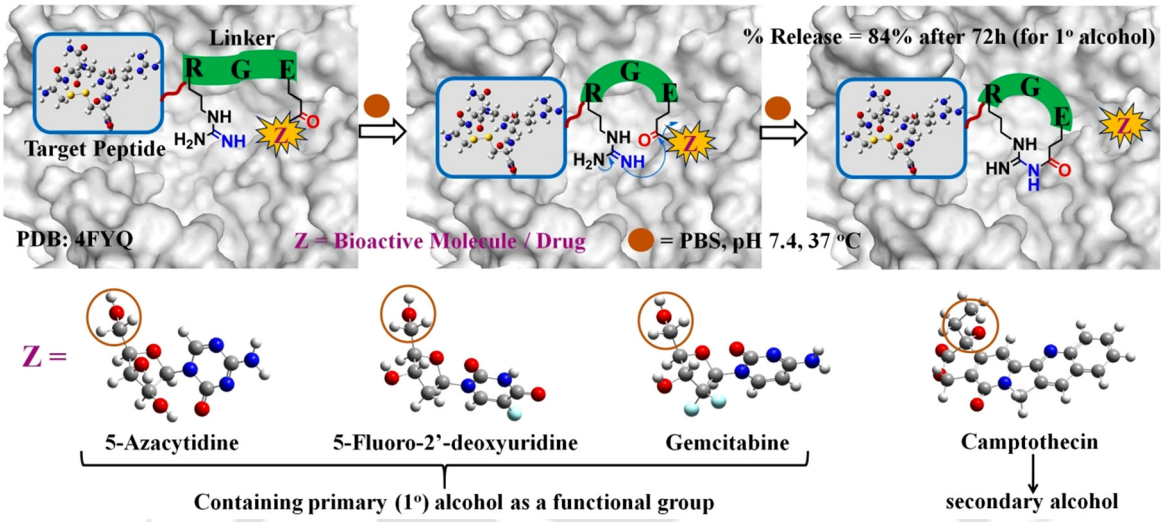

Figure 2.1. Schematic diagram of the peptide-based controlled delivery system.

2.2. Design of the peptides:

From the literature survey, it is evident that many strategies have been and are being developed for controlled delivery systems. In this work, we have focussed on the peptide-based delivery system to release bioactive molecule by *in-situ* peptide self-cyclization without the need for any external reagent in a controlled way to decrease the toxicity and side effects of therapeutic agents. Inspiring from the four-residue consensus sequence RXXR, we have designed a variety of tri-peptides having Glutamic acid to attach bioactive molecules through covalent bonding. A series of tri-peptide (Peptide1-3, Table 2.1) was designed, having Arginine at the N-terminus and Glutamic acid conjugated with bioactive molecule at the C-terminus, with a variation of Proline/ Alanine/ Glycine as a bridging amino acid to find out the best possibility for the desired nucleophilic attack by the side

chain nucleophilic centre of Arginine to the side chain electrophilic centre of carbonyl group of Glutamic acid. We have also prepared a negative control peptide (Peptide4, Table 2.1) having Alanine replacing Arginine to show the release of a bioactive molecule through hydrolysis method only.

Table 2.1. List of the designed peptides:

Sl. No.	Name of the Peptides	Peptide Sequence	Functional Activity
1.	Peptide1	Ac-RPE(OBn)-NH_2	peptide cyclization
2.	Peptide2	Ac-RAE(OBn)-NH_2	peptide cyclization
3.	Peptide3	Ac-RGE(OBn)-NH_2	peptide cyclization
4.	Peptide4	Ac-APE(OBn)-NH_2	negative control
5	Peptide5	Fmoc-RGE(2'-deoxyuridine)-NH_2	peptide cyclization
6	Peptide6	Ac-RPGGE(Camptothecin)-NH_2	peptide cyclization
7	Peptide7	p-Glu-HWSYGLRPGGE(Camptothecin)-NH_2	peptide cyclization

2.2.1. Structure of the designed and synthesized peptides:

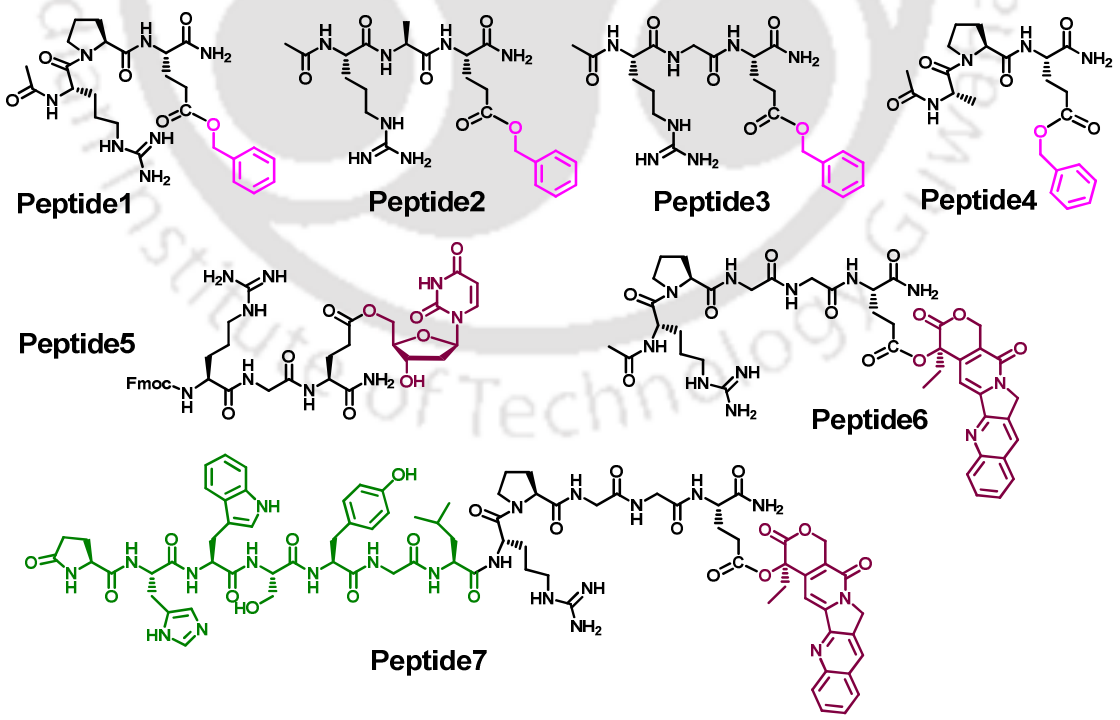

Figure 2.2. Chemical structure of the designed peptides.

Designing tripeptides with N-terminus Arginine and C-terminus Glutamic acid with covalently attached bioactive molecules, we aim to establish another mechanism where the release of bioactive molecules occurs through nucleophilic attack via peptide cyclization and this mechanism occurs beside hydrolysis but in a more controlled manner.

2.2.2. Protocol of solid phase peptide synthesis:

All the designed peptides were synthesized by following the standard Fmoc/tBu solid-phase peptide synthesis (SPPS) (Figure 2.3) method. [10] 100 mg of Rink amide MBHA resin (loading 0.5mmol/g) was taken in a 5 ml frit-fitted plastic syringe. The resin was swelled with DCM solvent first and then with DMF solvent. Fmoc group which was attached to the resin was cleaved with 20% piperidine in DMF, and the resin was then washed with DMF. After that, in DMF solvent, 2.5 equivalent of Fmoc amino acid, 3.0 equivalent of BOP (coupling reagent), and 5.5 equivalent of DIPEA (base) were dissolved and were taken in a syringe. The syringe was kept in rotation for coupling. After a certain time, the reaction mixture in the syringe was washed with DMF. This process was repeated to reach the end of the peptide sequence. At last, the reaction mixture was washed by DCM. When the synthesis of the peptide sequence was complete, it was acetylated (capping) with a mixture of 2 equivalent of acetic anhydride, two equivalent of N-methyl imidazole in DCM. Finally, cocktail cleavage was done with 2 ml of TFA: DCM (8.5:1.5) for 3h (or 5h where necessary) to cleave the C-terminus of the peptide from the resin. After completion, the mixture was precipitated by cold diethyl ether to get the crude peptide.

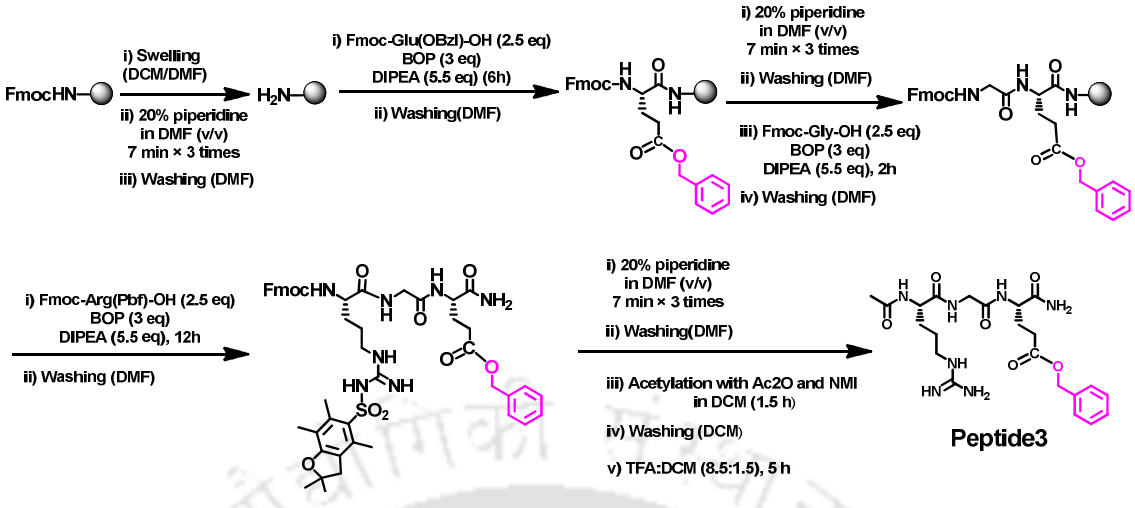

Figure 2.3. Schematic diagram of the synthesis of Peptide3.

Peptide1-4 were synthesized according to the described protocol with the variation of coupling reaction time only. When bridging amino acid was Pro in Peptide1, coupling reaction time was 12h, and for Ala in Peptide2, it was 3h. For negative control Peptide4, second coupling i.e. coupling of Pro with Glu took 12 h, and next coupling between Pro and Ala took 3h. In case of Peptide6, during cocktail cleavage in TFA: DCM, tert butyl group of -Glu(OtBu)-OH was cleaved along with the cleavage of C-terminus of the peptide from the resin. The side-chain modification of glutamic acid unit was carried out in solution phase by coupling reaction of the crude peptide Ac-(RPGGE)-NH_2 with two equivalent of camptothecin, two equivalent of BOP (coupling reagent) and five equivalent of DIPEA (base) in DCM and DMF solvent mixture for 35h.

2.2.3. Purification of the synthesized peptides:

Crude peptides were dissolved in CH_3CN/H_2O mixture to purify by RP-HPLC using a C18-μ Bondapak column at a flow rate of 4 ml/ min. Binary solvent system [solvent A (0.1 % TFA in H_2O) and solvent B (0.1 % TFA in CH_3CN)], UV detector with dual detection at

214 and 254 nm were used during purification. A total run time of 20 min. was set for purification with gradient 5-100 % CH_3CN for 18 min followed by 100% CH_3CN till 20 min.

The purity of the peptides was confirmed by analytical HPLC system using Ascentis C18 analytical column, flow rate of 1 ml/min, linear gradient of 5-100% CH_3CN over 18 min in a total run time of 20 min selecting dual-wavelength at 214 nm and 254 nm. ESI-Mass of the purified peptide samples were analyzed also.

2.3. Proof of the hypothesis:

To prove our hypothesis, three different types of kinetic studies (HPLC, ESI-MS, and CD) were performed with designed small peptides *in vitro*. All the biophysical studies were performed in PBS at pH 7.4 and 37 ^oC to maintain similarity with the physiological condition. After analysing all the results, the plausible mechanism was drawn in Figure 2.4, which coincide exactly with our hypothesis as described during the design of the peptides.

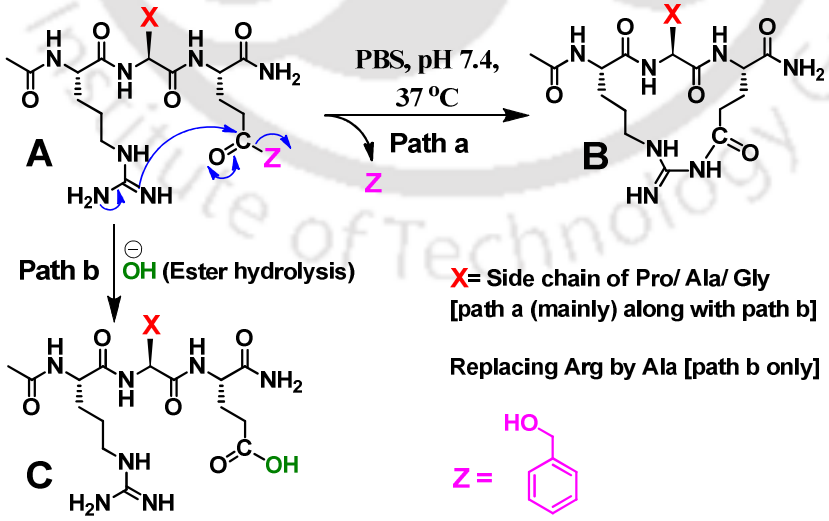

Figure 2.4. A plausible mechanism of controlled release of primary (mainly) and secondary alcohol.

2.3.1. Sample preparation:

To obtain a clear solution, the sample was dissolved in a required amount of PBS (50 mM, pH 7.4) followed by sonication and vortex. Then the total solution was divided into different vials, equally maintaining a final concentration of 500 µM.

Samples were taken in Eppendorf tubes, kept in an incubator at 37 ºC to perform various kinetic studies *in vitro*. For kinetic studies, the required amount of aliquots were collected from vials at different time intervals. The stock solutions were sonicated and vortexed for 1 min before collecting the sample.

2.3.2. HPLC and ESI-MS kinetics of the Peptide1:

For the study, binary solvent system [solvent A (0.1 % TFA in H2O) and solvent B (0.1 % TFA in CH3CN)] were used and dual-wavelength at 214 nm and 254 nm were selected in the UV detector. Using an Ascentis C18 analytical column with a flow rate of 0.9 ml/min and a linear gradient of 5-100% CH_3CN over 0-18 min in a total run time of 20 min kinetic study was performed. 20 µL sample of 500 µM concentration was injected in HPLC at different time intervals.

Rate of formation of the cyclic product was studied using HPLC (Figure 2.5). At the 1st h, the major peak was observed at retention time (t_R) 12.1min corresponding to the pure Peptide1 (A^1, identified from the ESI-MS spectrum). After that, a new peak appeared at t_R 13.3min corresponding to the cyclic product (B^1, identified from the ESI-MS spectrum). The peak corresponding to A^1 was transformed into that of B^1 gradually with increase in time, clearly indicating its controlled nature concerning the release system. Also, the

stability of Peptide1 was confirmed from the peak found in the HPLC chromatogram even after 98h of incubation at the physiological condition.

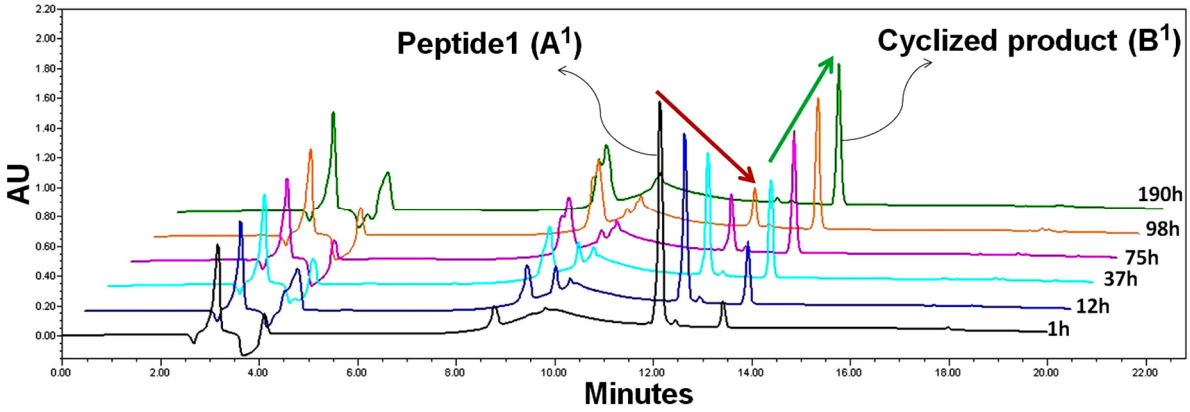

Figure 2.5. HPLC kinetics of Peptide1 (500 µM) at the physiological condition.

2.3.3. ESI-MS kinetics study of Peptide1:

Mass of the peptide samples were analyzed in ESI positive mode. Samples that were taken for kinetic studies were quenched with 20% HCl, diluted with HPLC grade CH_3CN and Mili-Q water and filtered through 0.2-micron filter paper before analysis.

In ESI-MS spectra (Figure 2.6-2.8), only one major peak was noticed for Peptide1 (A^1) at the 1st hr. After nearly 4h, a new peak was appeared for the cyclic product (B^1) along with the uncontrolled hydrolysed product (C^1), and this was continued till the end.

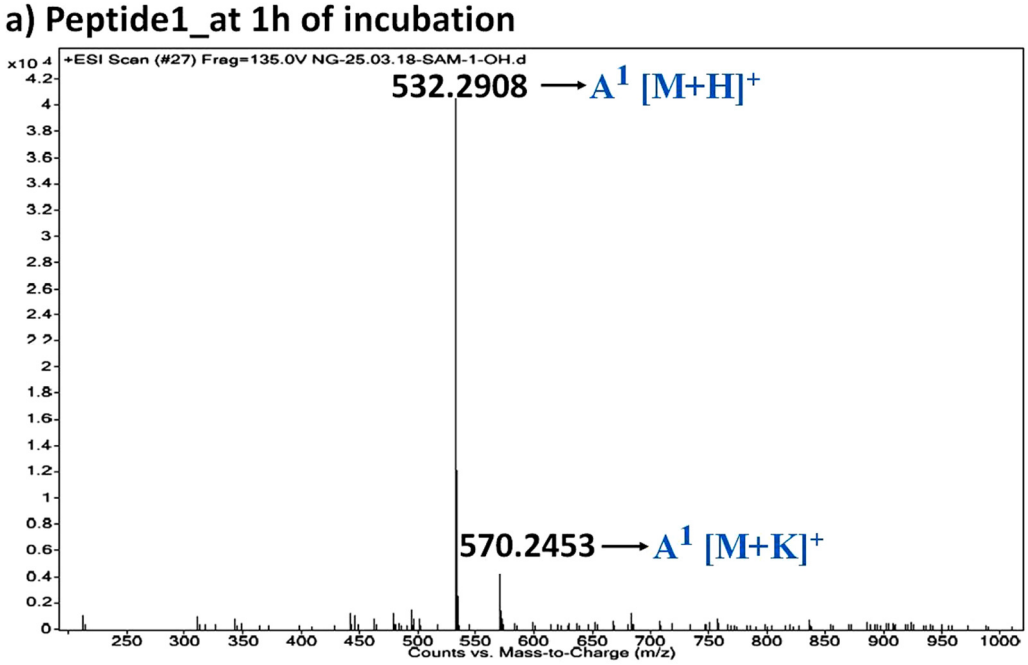

Figure 2.6. ESI-MS spectrum of Peptide1 at 1st h of incubation.

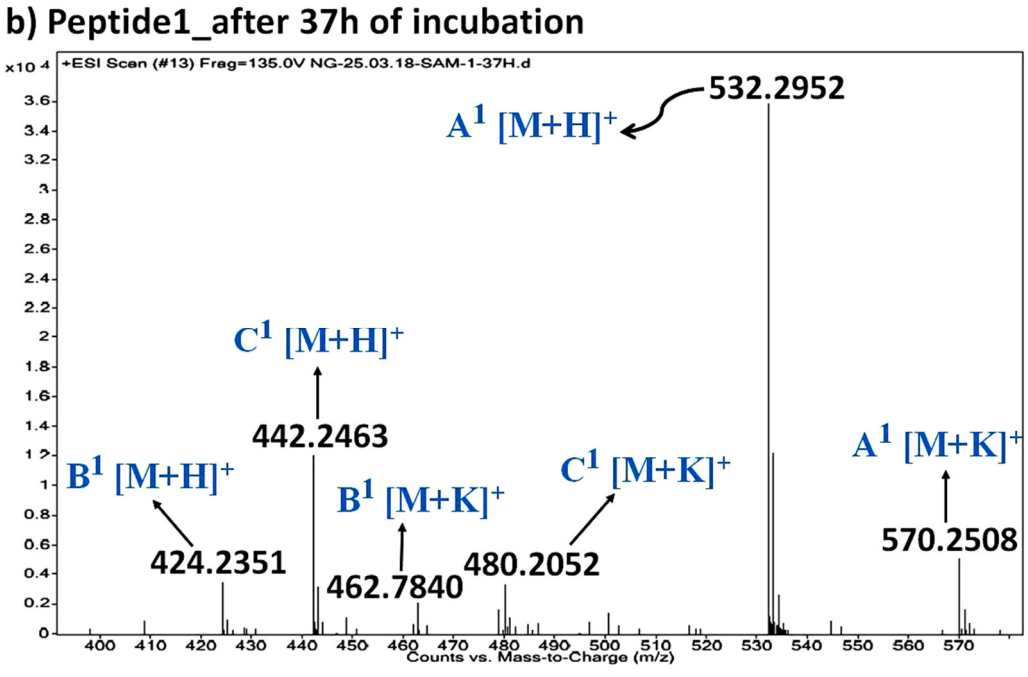

Figure 2.7. ESI-MS spectrum of Peptide1 after 37 h of incubation.

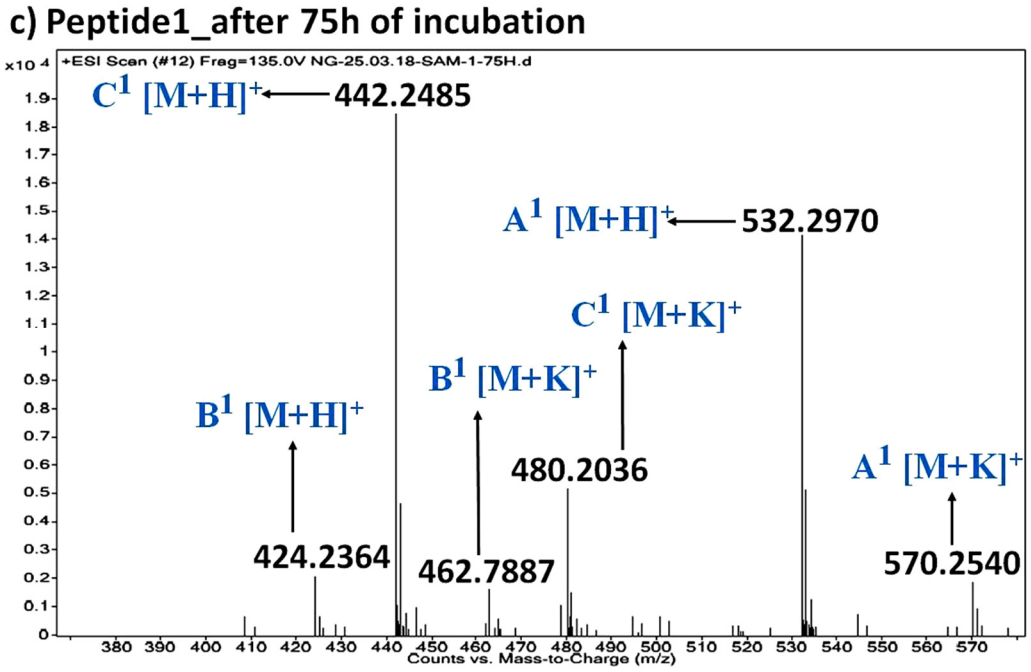

Figure 2.8. ESI-MS spectrum of Peptide1 after 75 h of incubation.

2.3.4. CD spectra of the Peptide1:

The presence of secondary structure within a peptide or protein can be determined from the CD spectrum in the far-UV region (190-250 nm).[11] CD Spectroscopy was used to monitor changes in secondary structure and to define the conformational state of the designed peptides in a time-dependent manner.[12]

At first incubated samples were treated with 0.1% trifluoroacetic acid to quench any further reaction and were stored at -20 °C For CD spectroscopy, the samples were diluted with PBS buffer solutions to obtain a final concentration of 100 µM. 200 µL of the sample was taken in a cuvette (Model SPC-001) having a pathlength of 1 mm. Samples were measured twice and spectra was recorded from 190 nm to 260 nm. Then observed ellipticity (mDeg) [obtained from Spectra Manager] was converted to mean residue molar ellipticity.

In the case of Peptide1 (Figure 2.9), at the 1st h of incubation, a spectrum was found with two negative bands at 209 nm and 228 nm and one positive band at 195 nm which is assigned to α-helix conformation. After 22h of incubation, a mixture of turn, random coil and α-helix conformation was obtained of the peptide, where turn structure predominated. A positive band around 200 nm and 208 nm was observed after 72h and 120h of incubation respectively indicating the turn structure of Peptide1 which confirmed the formation of cyclic compound.

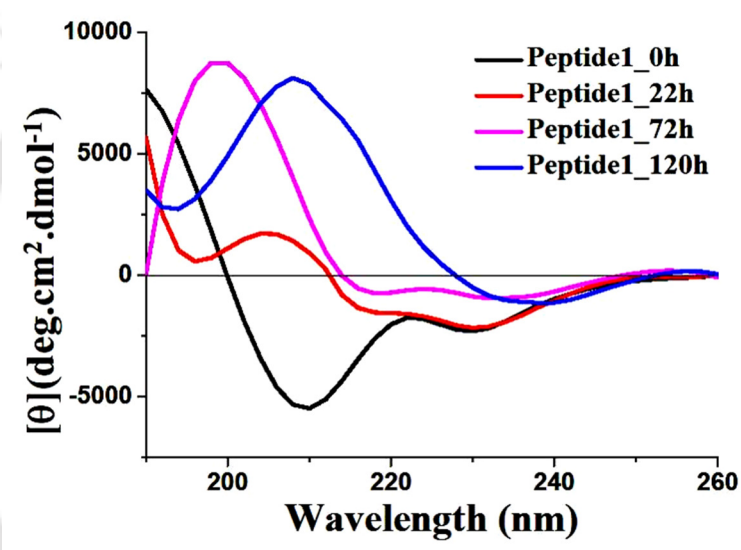

Figure 2.9. Time dependent CD spectra of Peptide1 at physiological condition.

2.3.5. HPLC and ESI-MS kinetics study of Peptide2:

From the HPLC kinetics of Peptide2 (Figure 2.10), it was observed that A^2 (t_R 11.9min) converted to B^2 (t_R 13.4min) gradually with time alike Peptide1. One major peak was observed at t_R 11.9min corresponding to the pure Peptide2 (A^2, identified from the ESI-MS spectrum) at the 1st hour. Slowly after a few hours, a new peak was emerged at t_R 13.4min which corresponds to the cyclic product (B^2, identified from the ESI-MS spectrum). The peak corresponding to A^2 was transformed into that of B^2 gradually with increase in time, indicating controlled nature of the release system of Peptide2. After 98h of incubation the peak of Peptide2 was found in the HPLC chromatogram which confirmed the stability of the compound at the physiological condition.

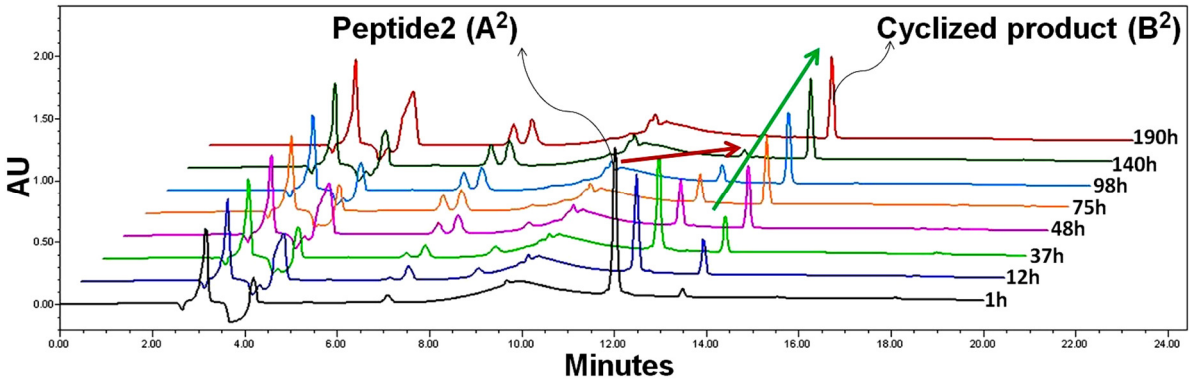

Figure 2.10. HPLC kinetics of Peptide2 (500 µM) at physiological condition.

2.3.6. ESI-MS kinetics study of Peptide2:

In ESI-MS spectra (Figure 2.11-2.13), the similar conversion of A^2 into B^2, along with C^2 was observed. Only one major peak was noticed for Peptide2 (A^2) at the 1st hr. After around 6h, emergence of a new peak was found for the cyclic product (B^2) along with the uncontrolled hydrolysed product (C^2), which was continued till the end.

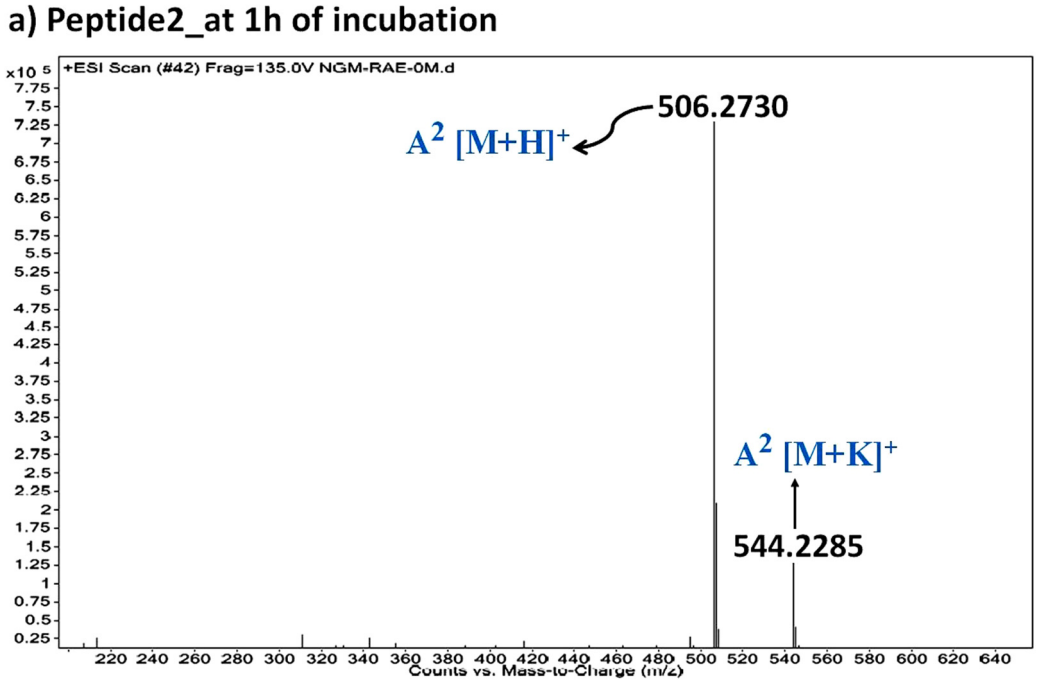

Figure 2.11. ESI-MS spectrum of Peptide1 at 1st h of incubation.

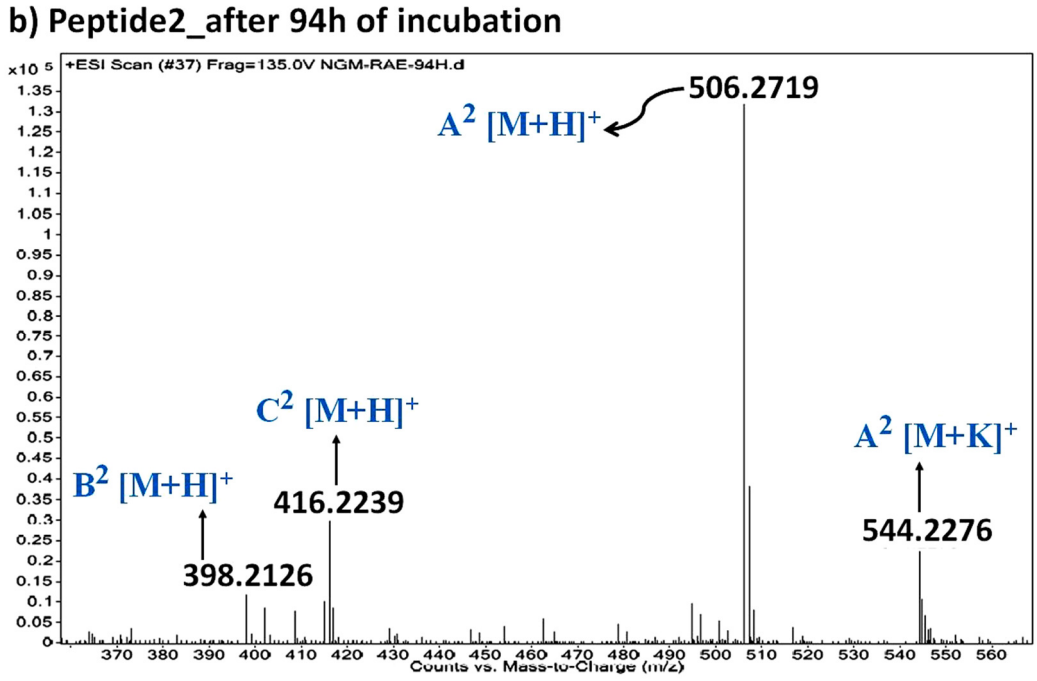

Figure 2.12. ESI-MS spectrum of Peptide2 after 94 h of incubation.

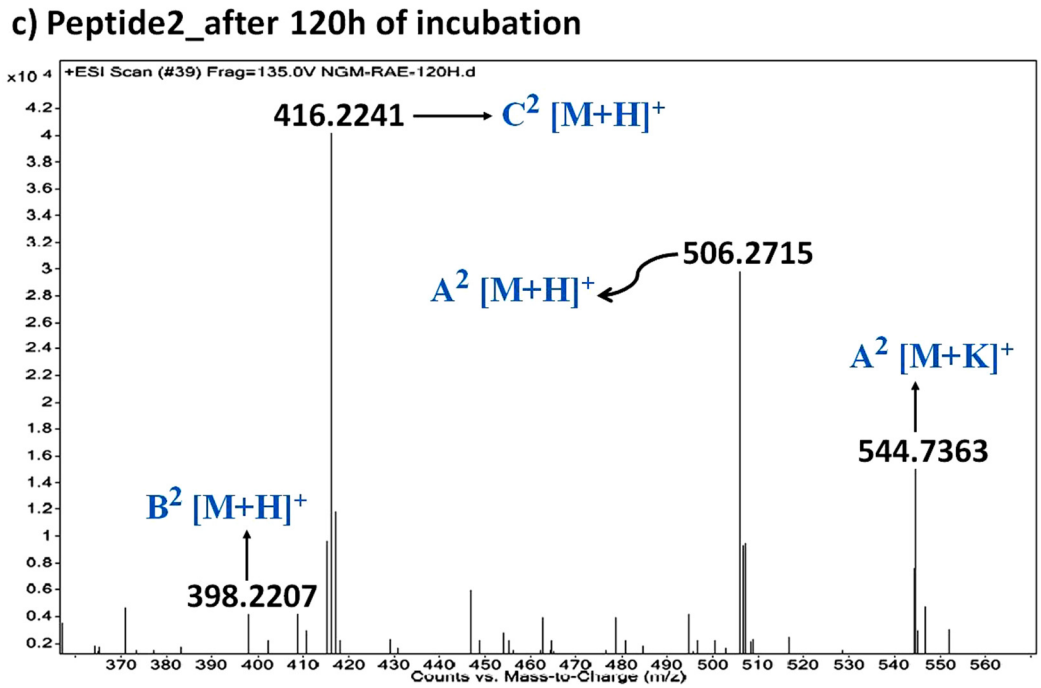

Figure 2.13. ESI-MS spectrum of Peptide2 after 120 h of incubation.

2.3.7. CD kinetics study of Peptide2:

A time-dependent conversion of a random coil (a negative band around 198 nm) into turn structure (a positive band around 215 nm) was also observed in the CD kinetics of Peptide2 (Figure 2.14). Hence the formation of the cyclic peptide and controlled release study was justified.

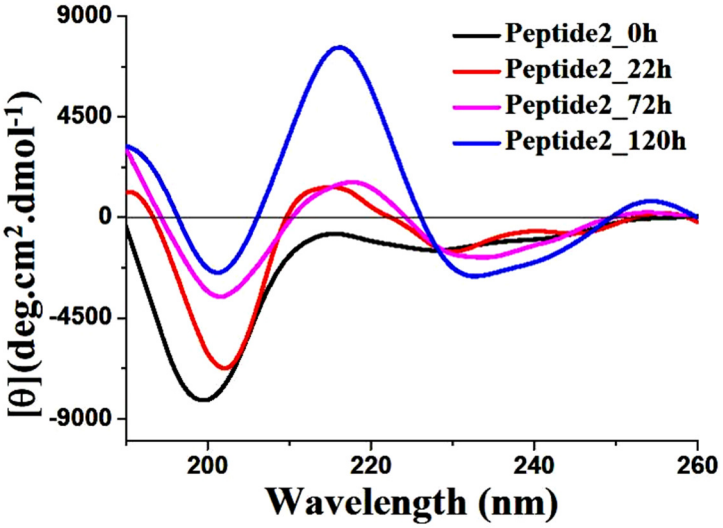

Figure 2.14. Time dependent CD spectra of Peptide2 at physiological condition.

2.3.8. HPLC kinetics study of Peptide3:

A similar kind of chromatogram of the HPLC kinetics (Figure 2.15) like Peptide1 and Peptide2 was obtained in the case of Peptide3 (A^3), but the conversion of A^3 (t_R 12.1min) into B^3 (t_R 13.5min) was faster than former cases. At the 1st h, the observed major peak at t_R 12.1min was assigned to the pure Peptide3 (A^3, identified from the ESI-MS spectrum). Then a new peak eluting after the pure peptide at t_R 13.5min was confirmed as the cyclic product (B^3, identified from the ESI-MS spectrum). The peak corresponding to A^3 was slowly transformed into that of B^3 with increase in time. This result clearly indicates the controlled release of the benzyl alcohol. The peak corresponding to pure Peptide3 was found in the HPLC chromatogram even after 75h of incubation confirmed the stability of the Peptide3 at the physiological condition.

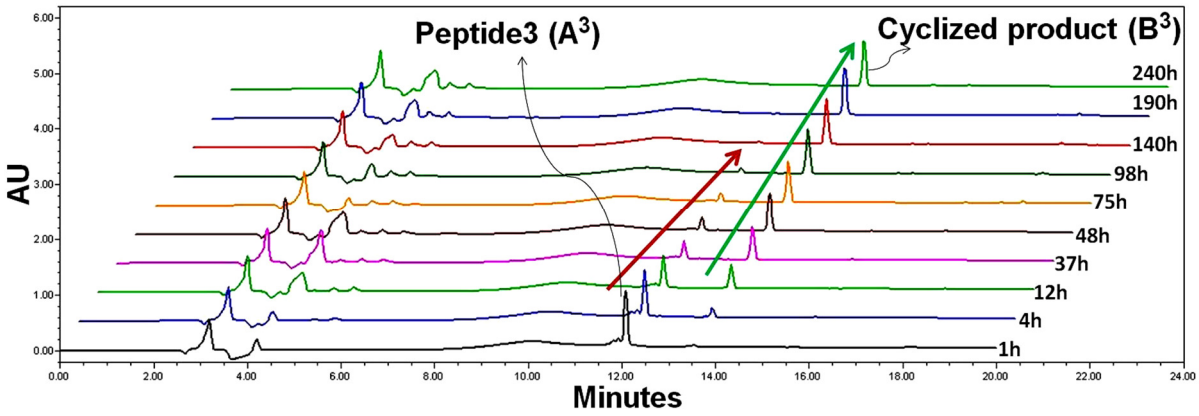

Figure 2.15. HPLC kinetics of Peptide3 (500 µM) at physiological condition.

2.3.9. ESI-MS kinetics study of Peptide3:

The result obtained from ESI-MS spectra (Figure 2.16-2.18) also agrees with the HPLC kinetics. Only one major peak for Peptide3 (A^3) was found at the 1st hr. Slowly after 4h, the formation of a new peak was noticed corresponding to the cyclic product (B^3). Beside this, another peak was observed simultaneously for the uncontrolled hydrolysed product (C^3) and these two peaks was found till the end.

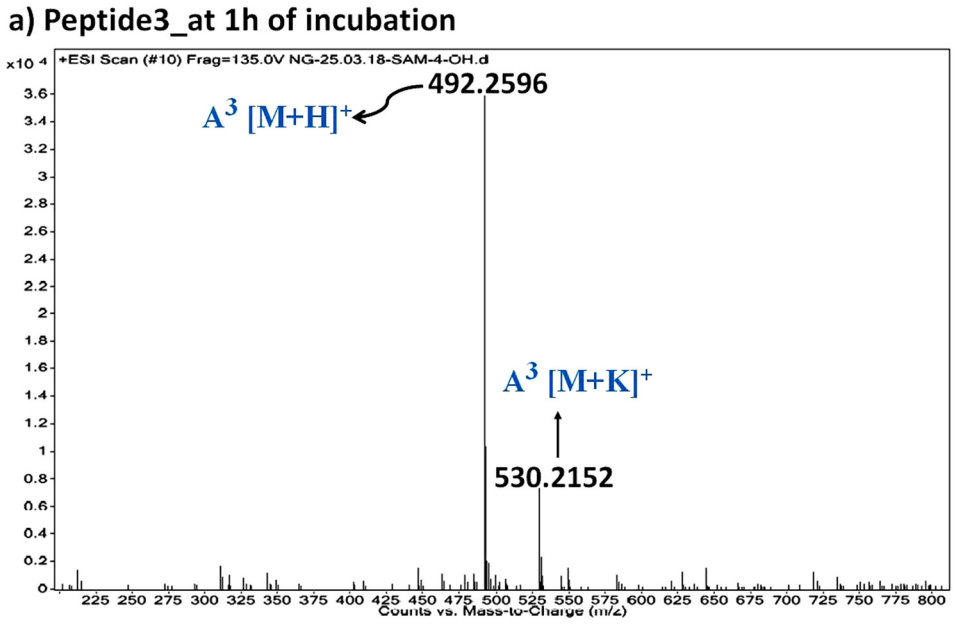

Figure 2.16. ESI-MS spectrum of Peptide3 at 1st h of incubation.

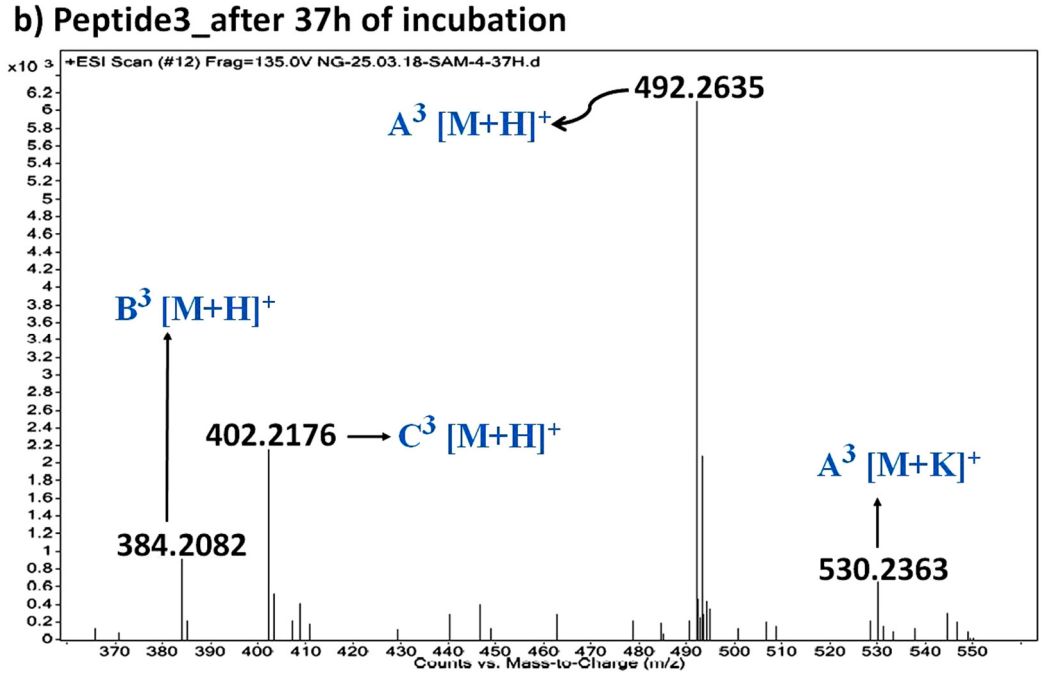

Figure 2.17. ESI-MS spectrum of Peptide3 after 37 h of incubation.

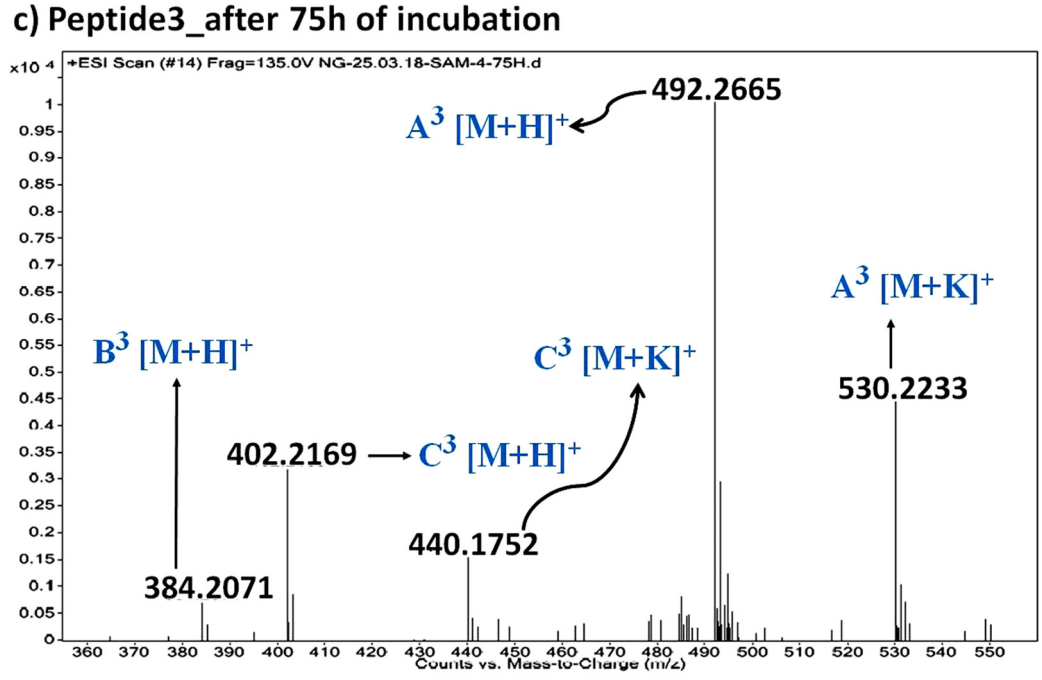

Figure 2.18. ESI-MS spectrum of Peptide3 after 75 h of incubation.

2.3.10. CD kinetics study of Peptide3:

In CD spectra (Figure 2.19), conversion of the turn structure (a positive band of higher intensity at around 212 nm) from predominantly random-coil structure (a negative band around 195 nm) of Peptide3 with the progression of time simply indicates the formation of a cyclic product.

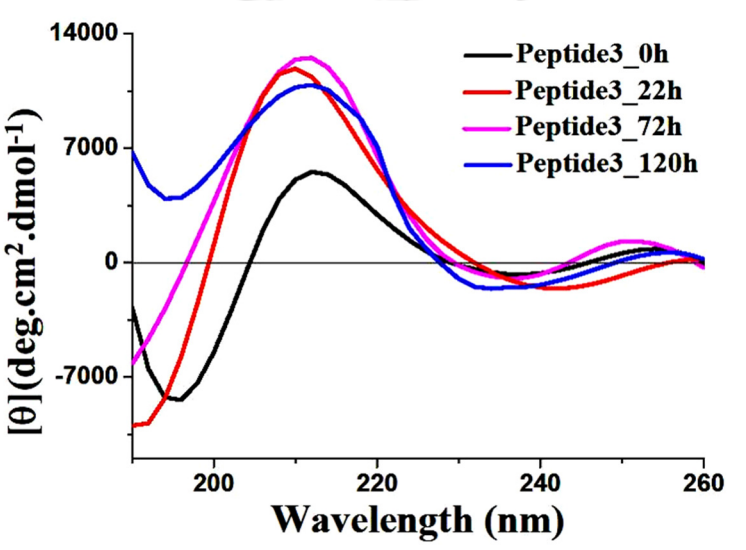

Figure 2.19. Time dependent CD spectra of Peptide3 at physiological condition.

2.3.11. Comparison of the % release of bioactive molecules:

From HPLC kinetics, the release progression (%) of Peptide1-3 was compared quantitatively. It was noticed that the leaving group (bioactive molecule) was released in a more controlled way in the case of Peptide3 (Figure 2.20) having Glycine compare to Peptide1 having Proline (commonly used as the bent unit) and Peptide2 having Alanine (used to force side chain of its N- and C-terminus amino acid to be in the same direction) as the bridging unit. Considering the formation of cyclised product from its mother compound as a controlled release parameter, the rate of reactivity of Peptide3 concerning release system was found to be higher than Peptide1-2 at any point of the kinetics (Figure

2.20). Peptide3 released the bioactive molecule (having primary alcohol as a functional group, benzyl alcohol for the general example) almost 75% after 36h of incubation in PBS (pH 7.4) at 37 ^{o}C, following the saturation point thereafter and the quantities are 85% after 72h, and 98% after 120h.

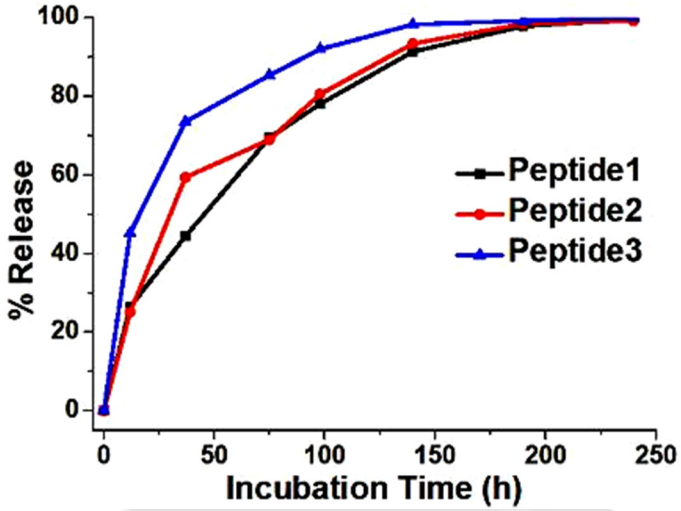

Figure 2.20. Comparison of % release of bioactive molecules for Peptide1-3.

2.3.12. HPLC kinetics study of Peptide4 (negative control):

The Peptide4 (A^4) released benzyl alcohol (C^4) at the physiological condition, but not in a controlled way (Figure 2.21-2.22). More importantly, it (A^4) was present in the solution in a major amount even after 190h of incubation. A conversion of A^4 (t_R 13.5min) into C^4 (t_R 4.0min) was observed without formation of the cyclic product.

a) Peptide4_after 6h of incubation

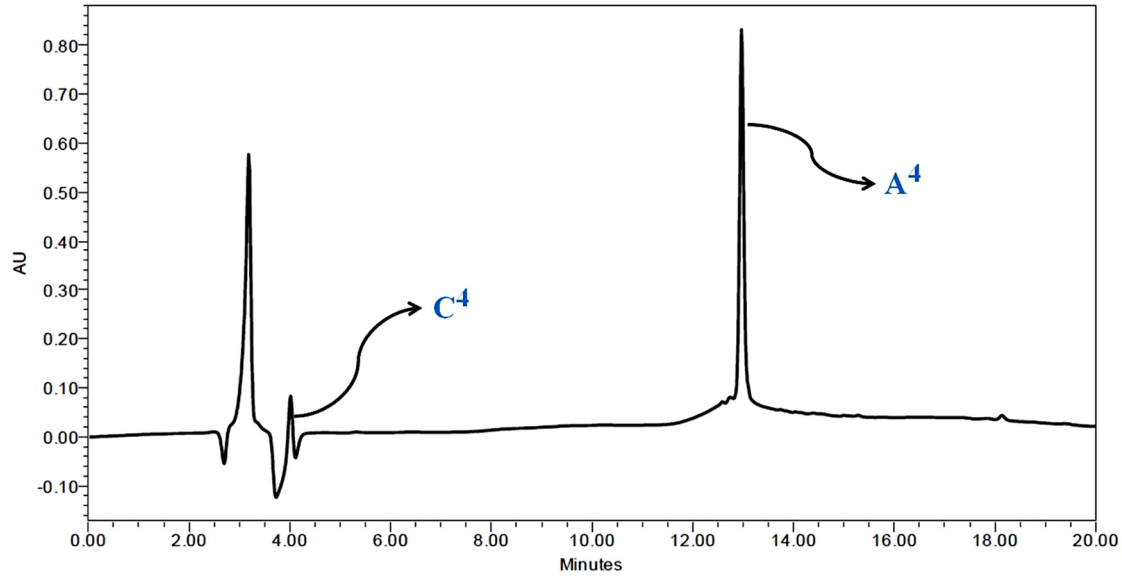

Figure 2.21. HPLC profile picture of Peptide4 after 6 h of incubation.

b) Peptide4_after 190h of incubation

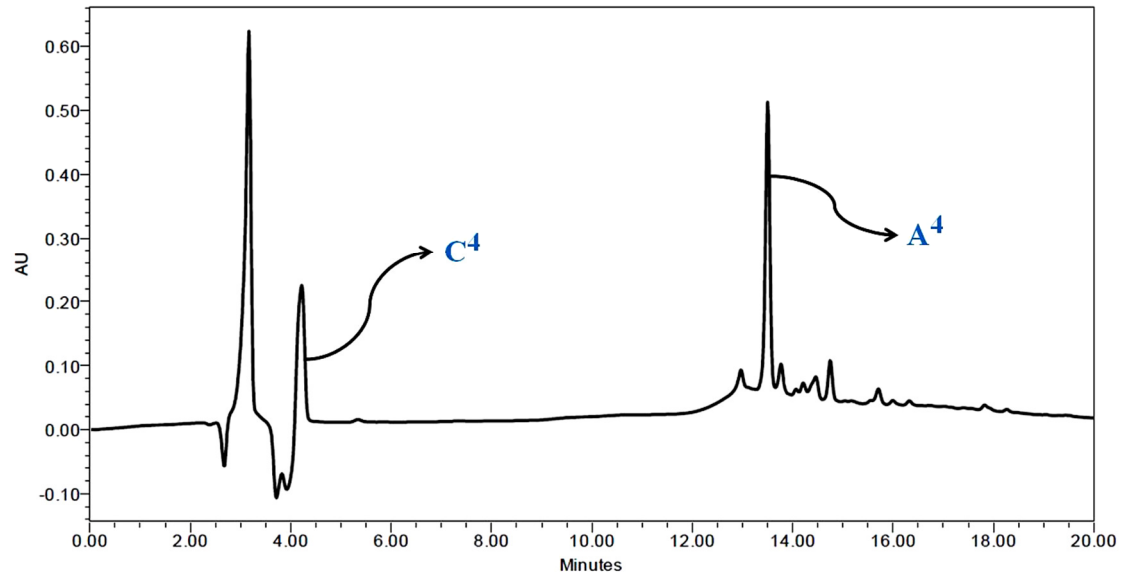

Figure 2.22. HPLC profile picture of Peptide4 after 190 h of incubation.

2.3.13. ESI-MS kinetics study of Peptide4 (negative control):

Peptide4 (A^4) also released benzyl alcohol (C^4) at the physiological condition, but not in a controlled way and more importantly it (A^4) was present in the solution in a major amount even after 190h of incubation (ESI-MS spectra, Figure 2.23-2.24)

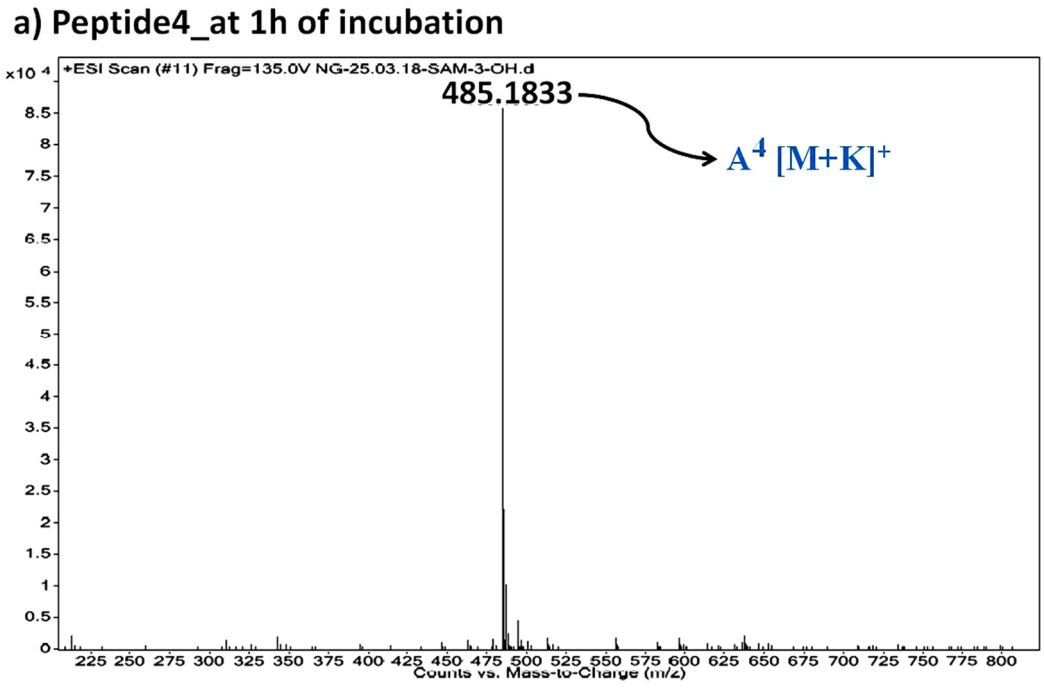

Figure 2.23. ESI-MS spectrum of Peptide4 at 1st h of incubation.

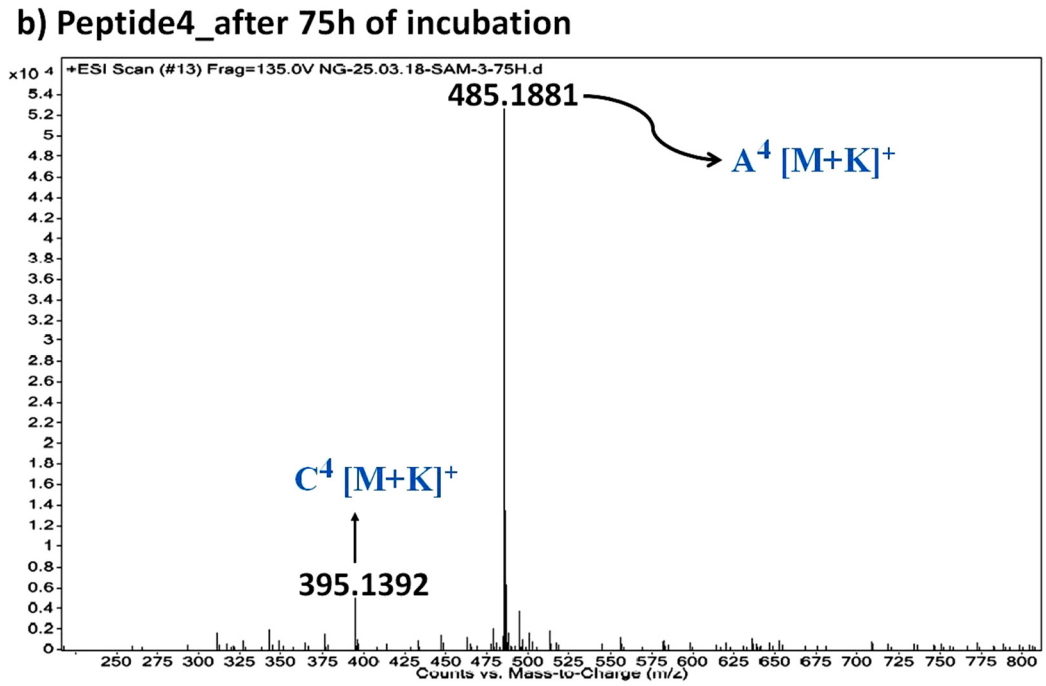

Figure 2.24. ESI-MS spectrum of Peptide4 after 75 h of incubation.

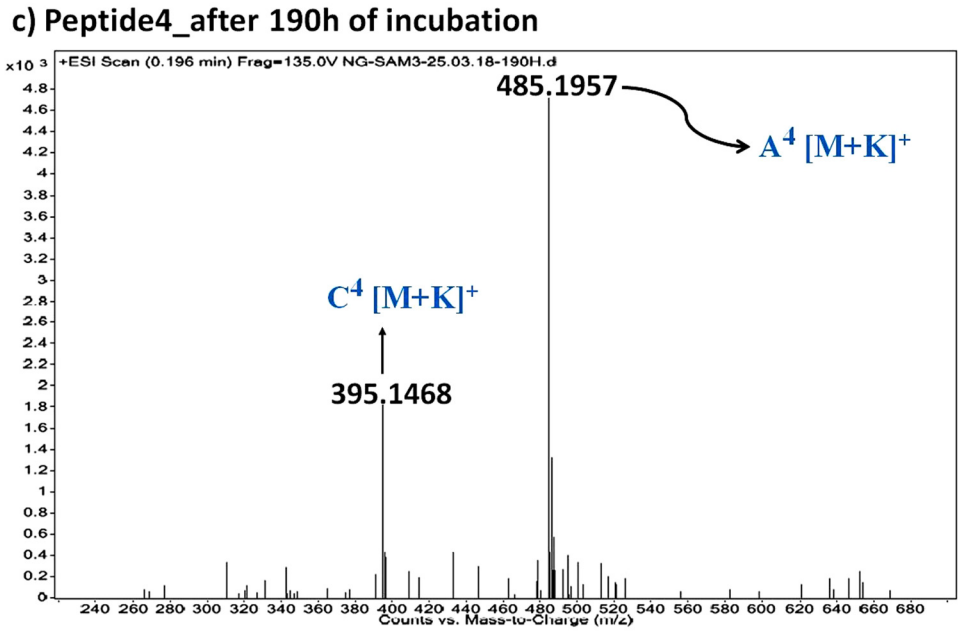

Figure 2.25. ESI-MS spectrum of Peptide4 after 190 h of incubation.

2.3.14. CD kinetics study of Peptide4:

In CD spectra (Figure 2.26), the random coil structure (a negative band around 200 nm) of A^4 remained unaltered throughout the kinetics.

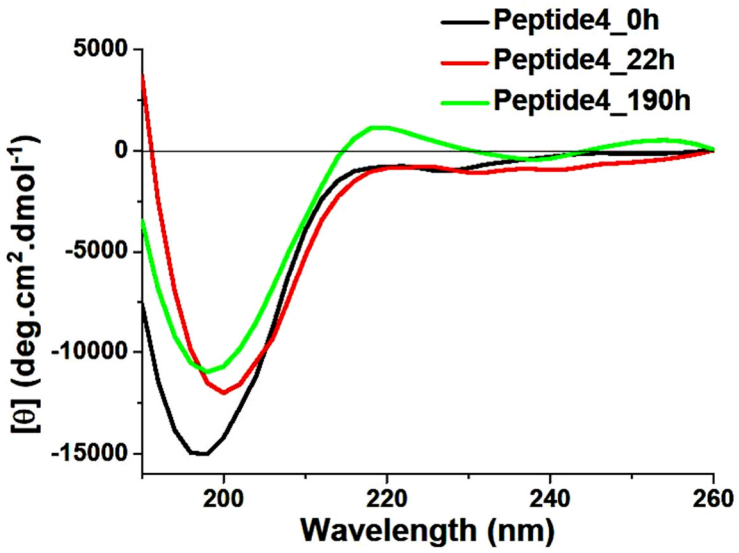

Figure 2.26. Time dependent CD spectra of Peptide4 at physiological condition.

2.4. Logic behind the design of Peptide5:

After finding the Peptide3 as the best delivery system *in-vitro* among Peptide1-4, for the defined purpose Peptide5 (Table 1) was designed and synthesized in which 2'-deoxyuridine (building block and alike structure of various drugs; for example 5-Fluoro-2'-deoxyuridine, Gemcitabine, 5-Azacytidine, etc.) was attached with the side chain of Glutamic acid.

2.4.1. Synthesis procedure of Peptide5 in solid phase:

Peptide5 was synthesized by following standard Fmoc/tBu solid-phase peptide synthesis (SPPS) method. In case of a side-chain modification of the Glutamic acid, first ^{t}Bu group of Glutamic acid was cleaved with $ZnBr_2$/DCM (as described in the protocol)[13] on the resin.

Then with the de-protected Glutamic acid, coupling reaction was carried out in solid-phase with the required amount of bioactive molecules (having primary alcohol as a functional group), BOP (coupling reagent) and DIPEA (base) in DMF and DCM solvent mixture.

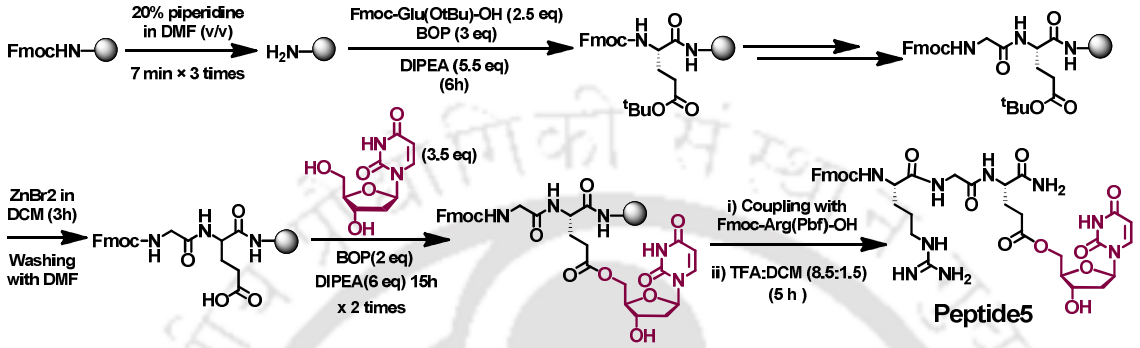

Figure 2.27. Synthesis procedure of the Peptide5 (in solid phase) as a representative example.

2.4.2. ESI-MS kinetics study of Peptide5:

The release studies of 2'-deoxyuridine from Peptide5 *in-vitro*. was also checked. The result obtained from ESI-MS spectra (Figure 2.28-2.29) clearly indicate the formation of a cyclic peptide as expected confirms the controlled release process.

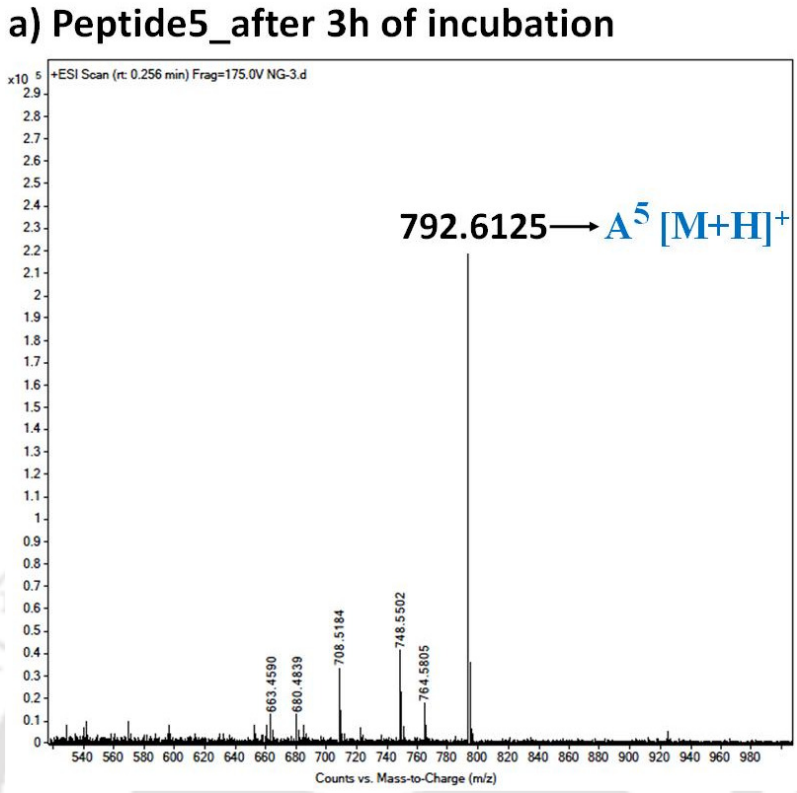

Figure 2.28. ESI-MS spectrum of Peptide5 after 3 h of incubation.

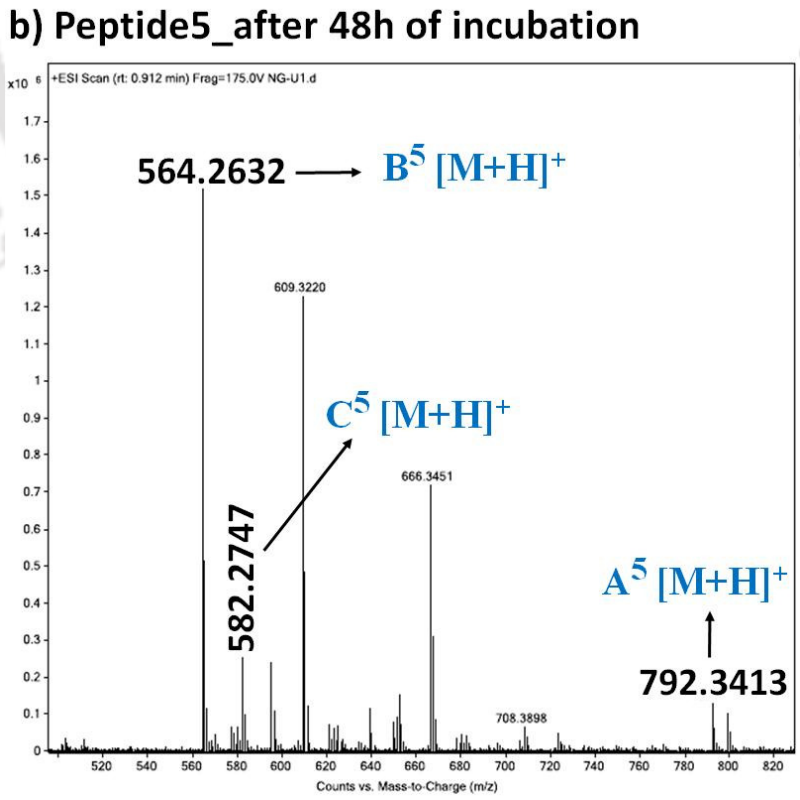

Figure 2.29. ESI-MS spectrum of Peptide5 after 48 h of incubation.

2.5. Logic behind the design of Peptide6-7:

As the release of secondary alcohol is comparatively easier than that of primary alcohol, RPGGE was designed in place of RGE to control the release system and the particular sequence was derived from Gonadotropin-releasing hormone in-short GnRH.[14] GnRH (pGlu-His-Trp-Ser-Tyr-Gly-Leu-Arg-Pro-Gly-NH_2) is also known as luteinizing hormone-releasing hormone (LHRH).[14] GnRH peptide analogs constituting tumor homing peptides for malignant tissues can selectively bind to its receptor GnRH-R and overexpress on cancer cell (mostly ovarian, prostate, lung and breast) surface.[14] Therefore, covalent attachment of a cytotoxic agent with this peptide may be a potent tumor-targeting PDCs. An apoptosis-inducing agent camptothecin conjugated with poly(ethylene glycol) carrier which is covalently attached with targeting moiety LHRH is reported as drug delivery system.[15] So Peptide6-7 (Table 1) were also designed and synthesized after adding modified -GE- to the C-terminus of GnRH structure.

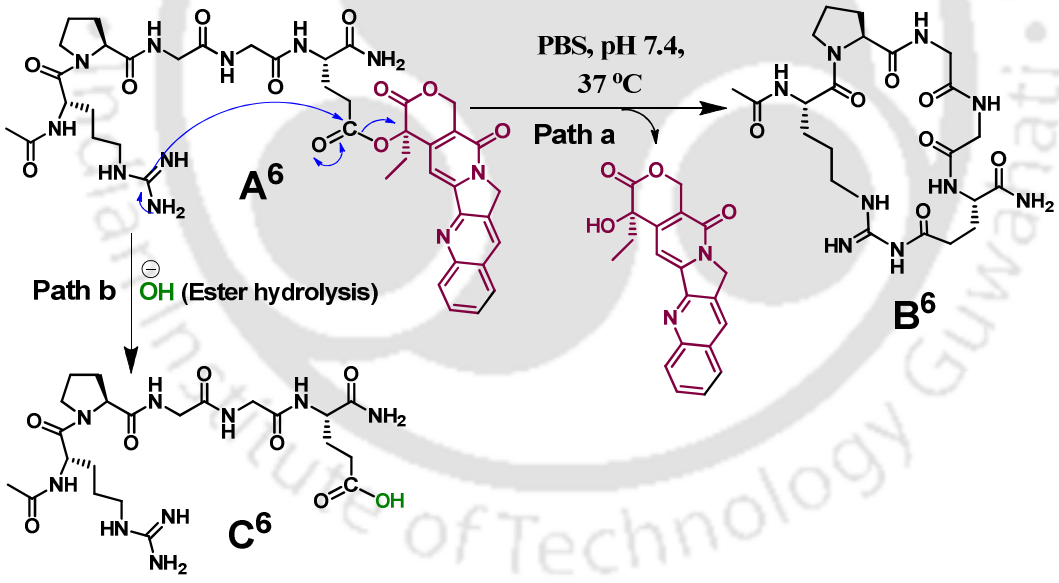

Figure 2.30. Plausible mechanism of the release system of Camptothecin from Peptide6.

The release studies of Camptothecin from Peptide6 *in-vitro*. was also checked. The result obtained from ESI-MS spectra (Figure 2.31) clearly indicate the formation of a cyclic peptide as expected confirms the controlled release process.

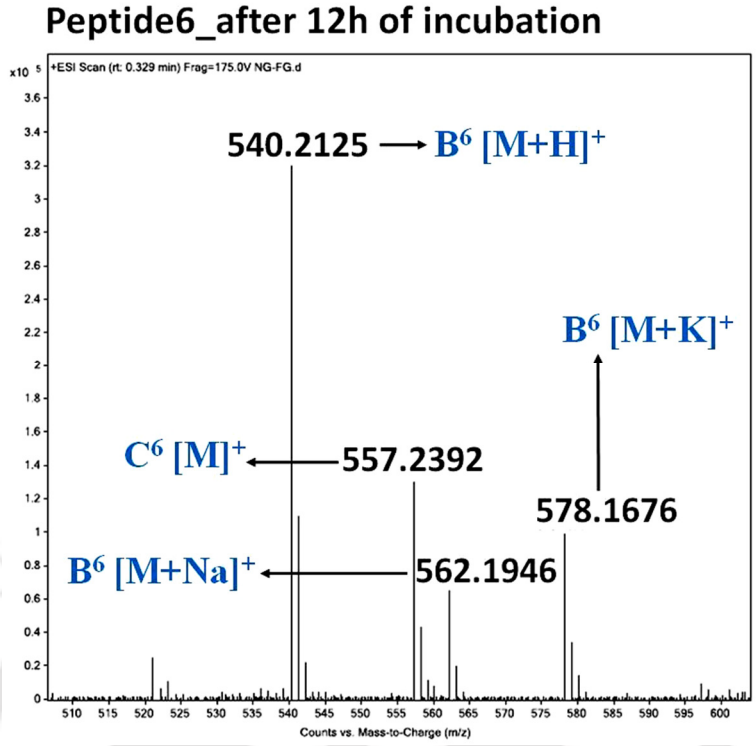

Figure 2.31. ESI-MS spectrum of Peptide6 after 12 h of incubation.

2.6. Molecular docking studies:

Molecular docking studies were performed to check whether the designed peptides after attaching with both drug molecule and the target peptide are liable to fit in the corresponding binding pocket. Camptothecin, 5-fluoro-2'-deoxyuridine, gemcitabine, 5-azacytidine drugs have been used in our designed peptides.

Gemcitabine is clinically used as a first-line treatment for pancreatic cancer and other cancers. To minimize adverse effects and maximize therapeutic efficacy, a dipeptide monoester prodrug of gemcitabine is reported to improve drug delivery to the tumor site.[16] 5-fluoro-2'-deoxyuridine (5-FdUrd), a cytotoxic anticancer drug is used for the treatment of metastatic cancers. A synthesis of tumor-homing cyclic peptide CNGRC conjugated with 5-FdUrd by succinate and glutarate linkers is reported.[17] 5-azacytidine is an established nucleoside drug used for the treatment of myelo-dysplastic syndrome. For the clinical management of acute myeloid leukemia, this drug has also been used successfully. Delivery

of 5-Azacytidine by elaidic acid esterification is reported to increases therapeutic drug efficacy.[18]

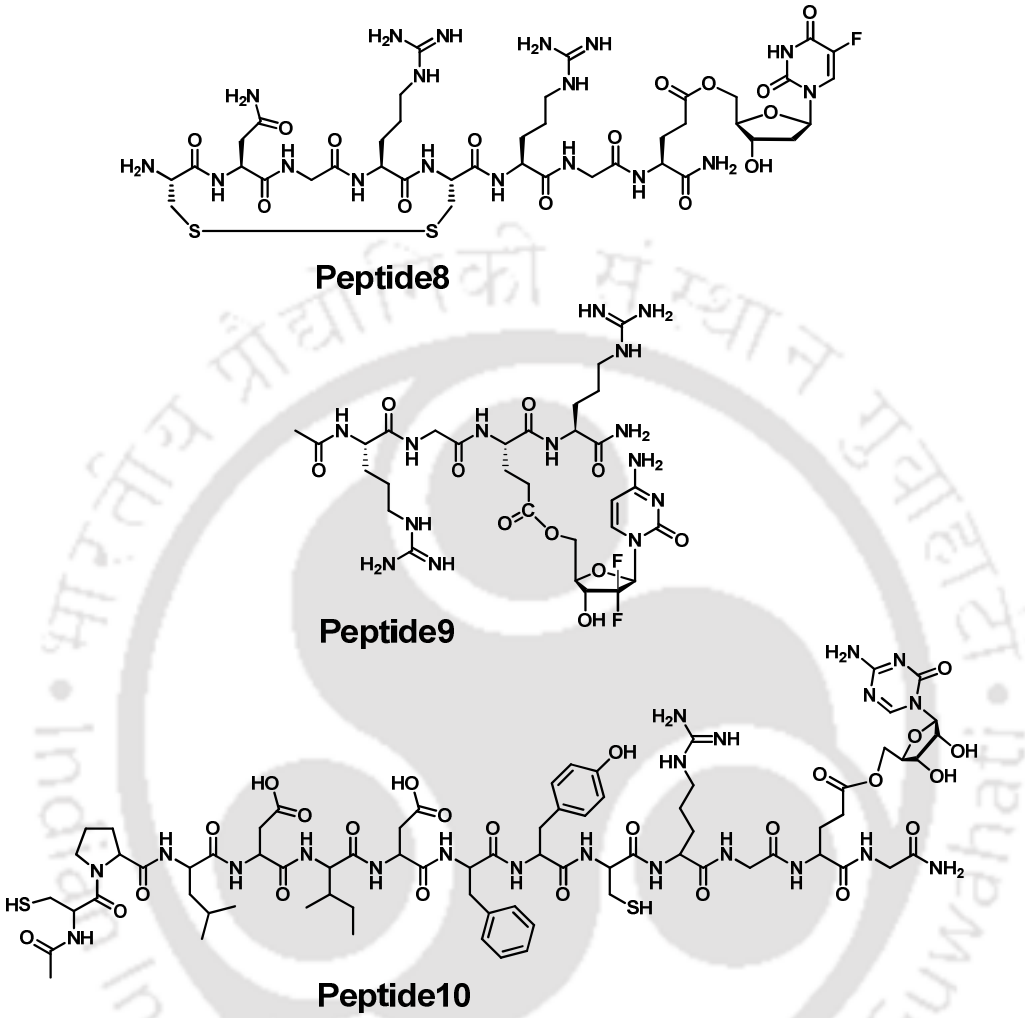

Figure 2.32. Chemical structure of the peptides designed for molecular docking.

Next, molecular docking studies were performed as described in the literature[19] [20] with Peptide7-10 (Table 2.1, and Figure 2.32). Lutropin [PDB: 1XUL], Human aminopeptidase N (CD13) [PDB: 4FYQ], Neuropilin-1 [PDB: 2ORZ], and AML1-ETO Nervy Domain [PDB: 2KYG] have been used for docking studies. Proteins were prepared using AutoDock 4.2 MGL Tools version 1.5.6 software package. To avoid errors, water molecules were removed; polar hydrogen atoms were added to the protein; Gasteiger charges of the

macromolecule were added and thus PDBQT format for proteins were generated and saved. Ligands were converted in PDB format after minimizing energy using OpenBabel version 2.4.1 software and the PDB file was modified by addition of Gasteiger charges. PDBQT format of the ligands were generated. It coordinates files including atomic partial charges and atom types. To assign the fixable and non-bonded rotation of molecules torsion angles were calculated. Grid parameters was calculated with Auto Grid version 4.2 and grid file was customized for ligands to find the best possible binding site of the protein molecule with lowest binding energy and higher binding affinity within the short range of volume. Blind docking experiments of ligands with respective proteins were performed after adjusting grid volume, grid spacing, and centre. When docking was completed, the output file was created as ligand_out.pdbqt format containing binding affinity (in kcal/mol) and RMSD lower bound, RMSD upper bound. PyMOL version 1.7.4.5 software was used to view the docking results. The docking calculation generated ten poses among which the best pose was selected on the basis of interaction between the ligand and the protein.

After performing docking, it was very clear that all the designed peptides bind very well and fitted properly in the related binding pocket (Figure 2.33-2.36) having a negative binding affinity.

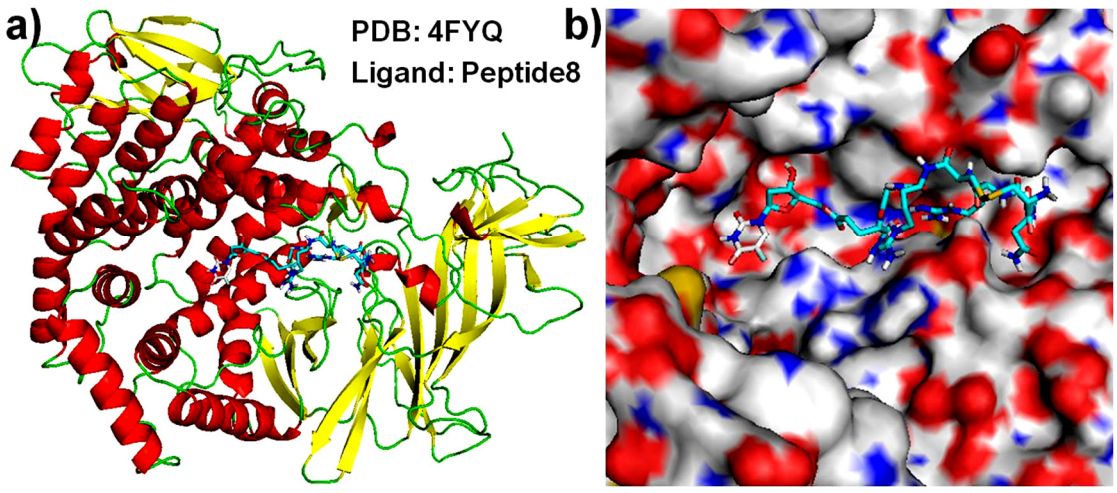

Figure 2.33. Molecular Docking images of peptide8 into protein (PDB ID: 4FYQ). Structures are shown as cartoon (a) and surface representation (b). The surface of protein is coloured according to the charges of the atoms where negatively and positively charged zones are represented in red and blue, respectively.

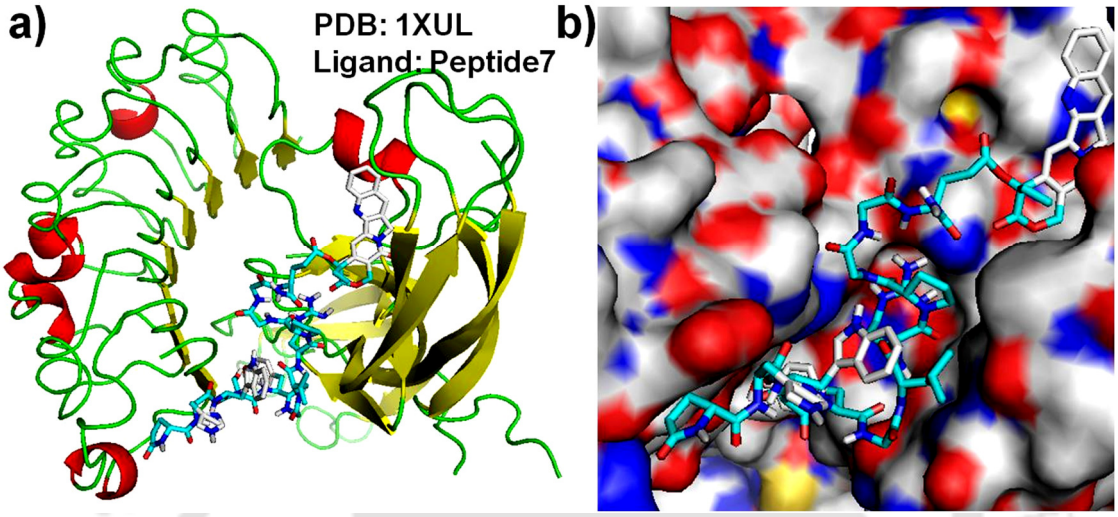

Figure 2.34. Molecular Docking images of peptide7 into protein (PDB ID: 1XUL). Structures are shown as cartoon (a) and surface representation (b). The surface of protein is coloured according to the charges of the atoms where negatively and positively charged zones are represented in red and blue, respectively.

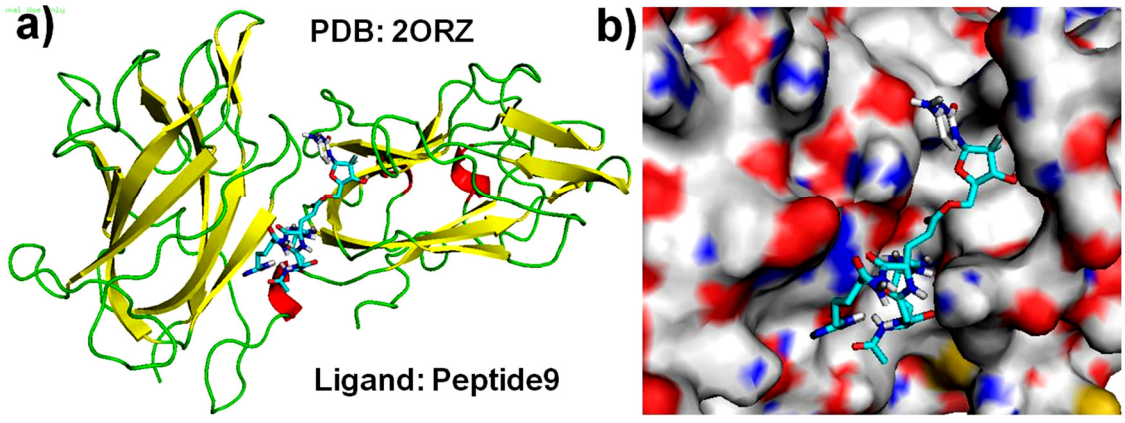

Figure 2.35. Molecular Docking images of peptide9 into protein (PDB ID: 2ORZ). Structures are shown as cartoon (a) and surface representation (b). The surface of protein is coloured according to the charges of the atoms where negatively and positively charged zones are represented in red and blue, respectively.

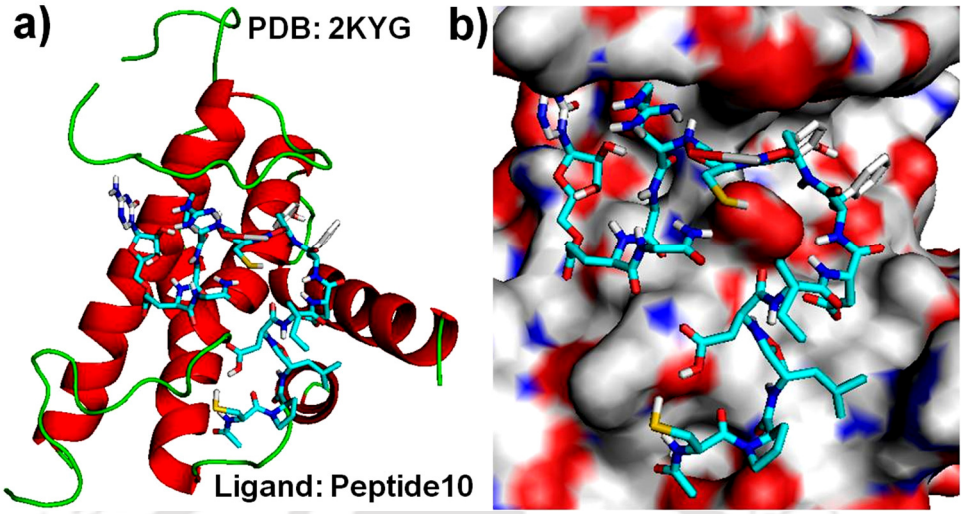

Figure 2.36. Molecular Docking images of peptide10 into protein (PDB ID: 2KYG). Structures are shown as cartoon (a) and surface representation (b). The surface of protein is coloured according to the charges of the atoms where negatively and positively charged zones are represented in red and blue, respectively.

2.7. Conclusions:

The growing attention in peptide-based drugs and the drug delivery system in medicinal research offer many opportunities for the development of linear and cyclic peptides with variation of sequences and amino acid residues. In this work, linear tripeptides (RXE, X= Pro/ Ala/ Gly) were designed and synthesized for *in situ* self-conversion into cyclic peptides under physiological conditions without the need for any external reagent. The methodology was further applied for selective release and delivery of small molecules in a controlled manner. The cyclization step was considered as the critical parameter, and RGE peptide was found to be the best sequence for such side chain to side chain peptide cyclization. The mechanism of cyclization reaction and release kinetics of the bioactive molecules were determined by HPLC, ESI-MS, and CD measurements. The synthesized, water-soluble peptides being capable of undergoing self-stimulated cyclization leading to a bond cleavage for the release of covalently attached bioactive compounds, could be a potential approach for delivering therapeutic agents.

2.8. Characterization data of the Peptides:

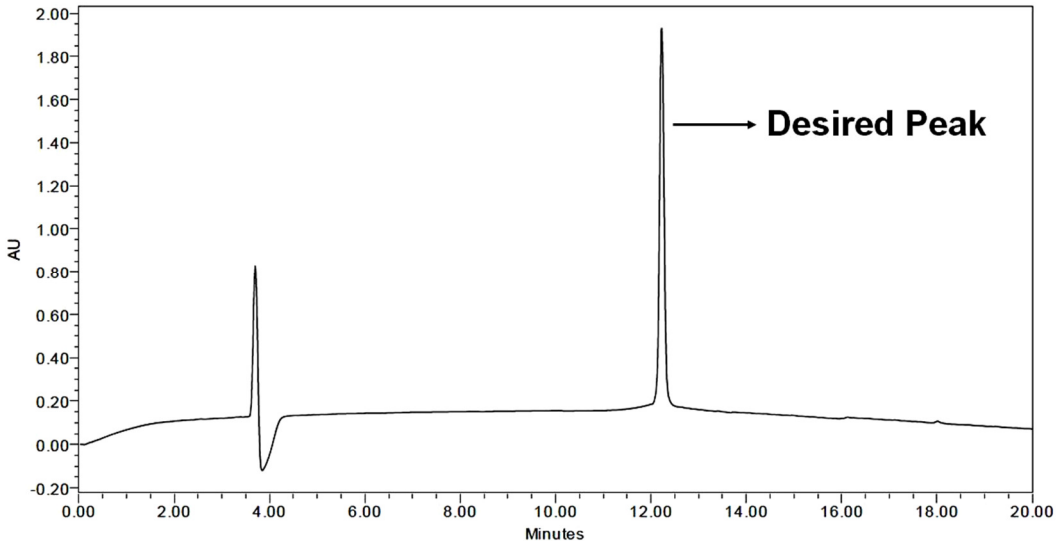

Figure 2.37. HPLC profile picture of the purified Peptide1.

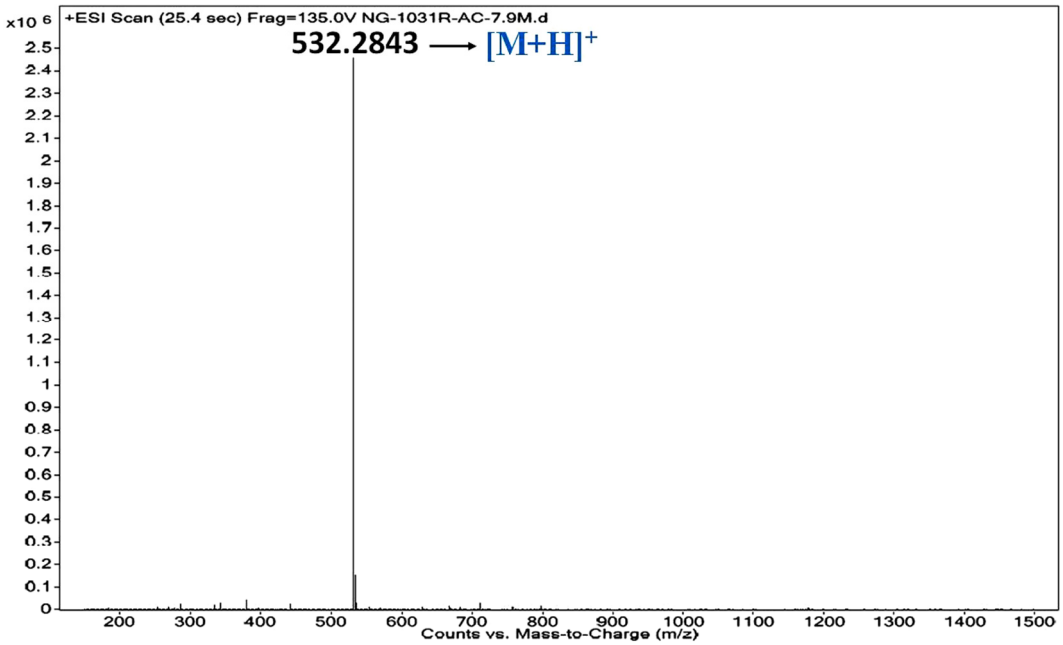

Figure 2.38. ESI-Mass spectrum of the Peptide1. Calculated m/z for $C_{25}H_{37}N_7O_6$ $[M+H]^+$ is 532.2884, observed 532.2843.

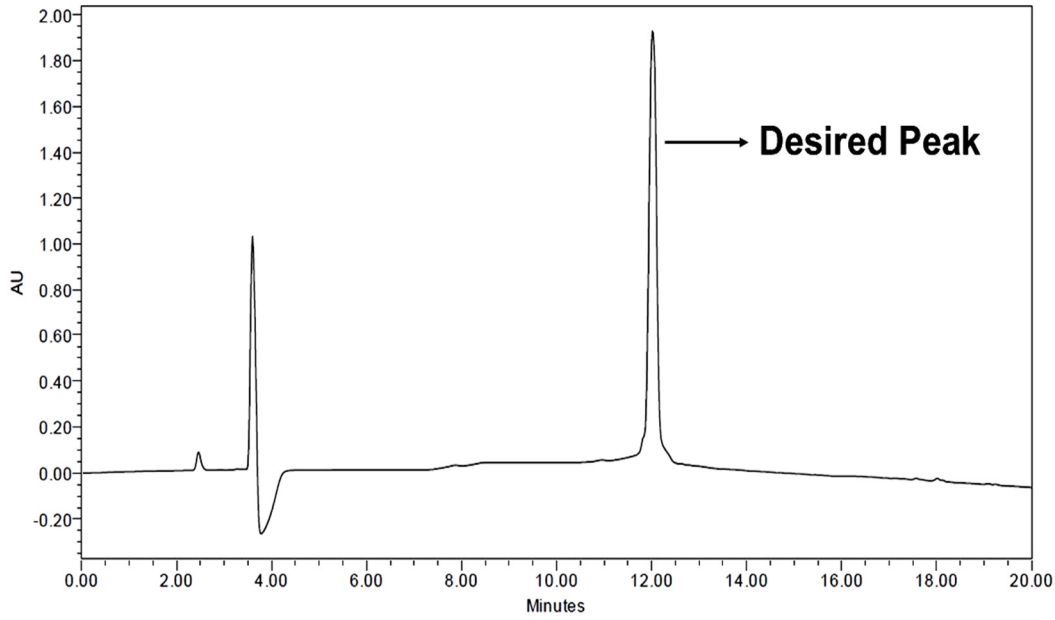

Figure 2.39. HPLC profile picture of the purified Peptide2.

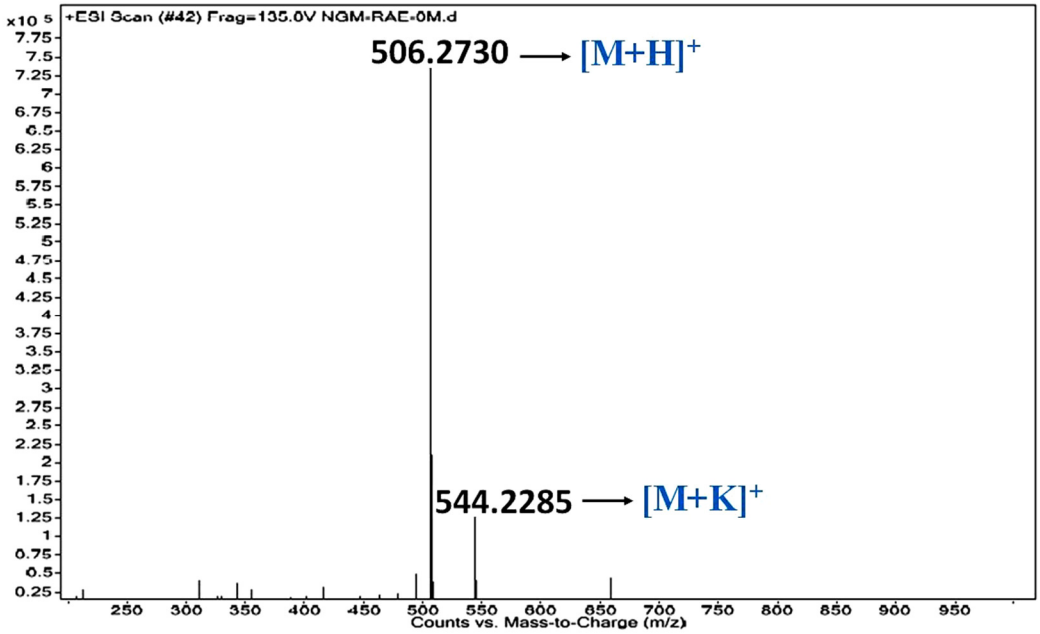

Figure 2.40. ESI-Mass spectrum of the Peptide2. Calculated m/z for $C_{23}H_{35}N_7O_6$ $[M+H]^+$ is 506.2649, observed 506.2730.

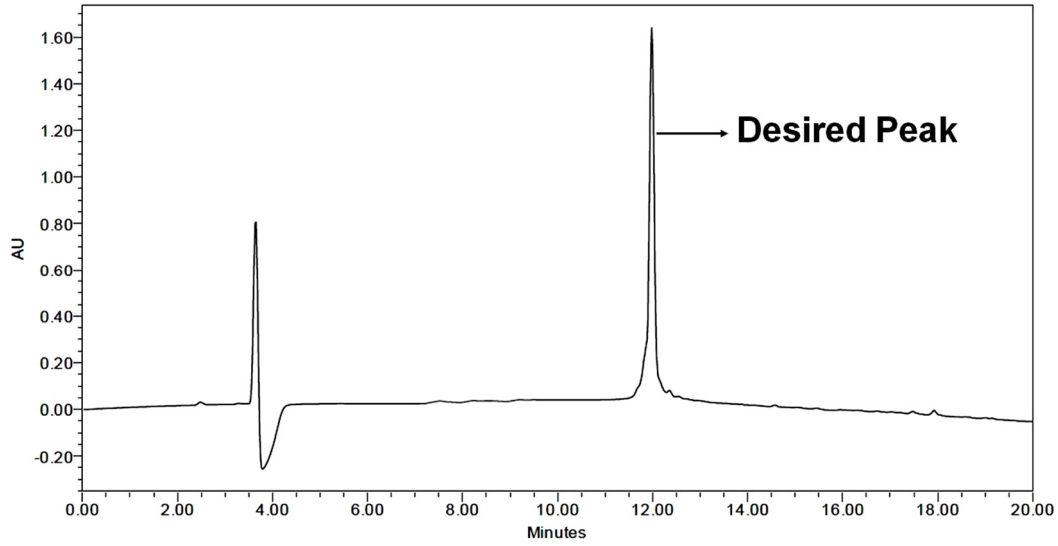

Figure 2.41. HPLC profile picture of the purified Peptide3.

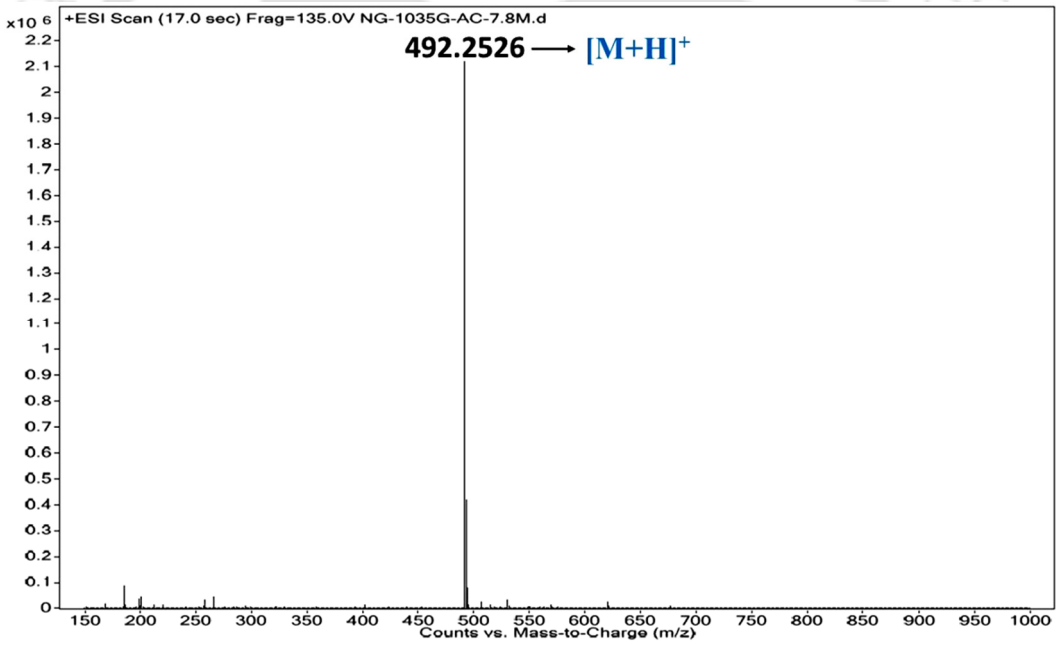

Figure 2.42. ESI-Mass spectrum of the Peptide3. Calculated m/z for $C_{22}H_{33}N_7O_6$ $[M+H]^+$ is 492.2571, observed 492.2526.

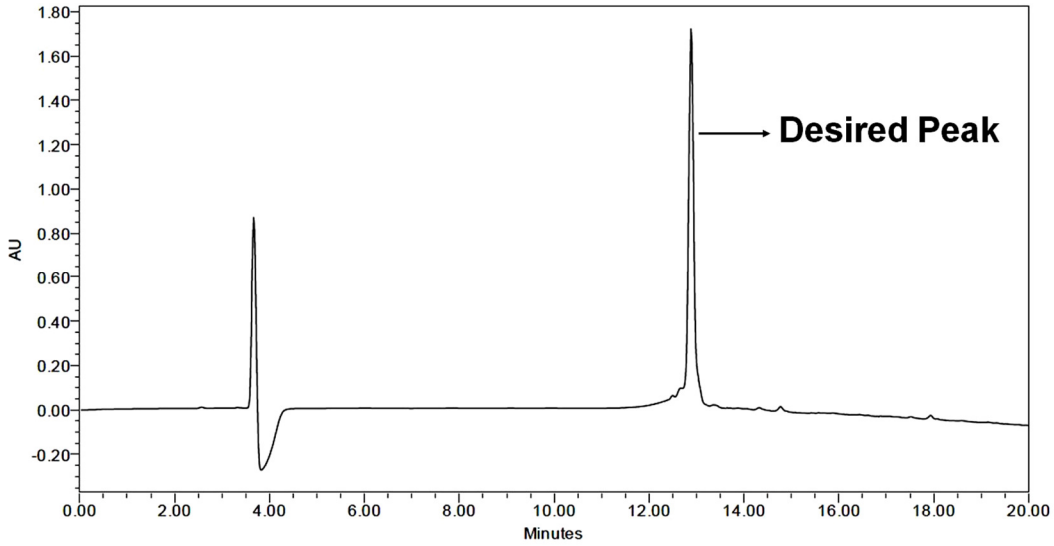

Figure 2.43. HPLC profile picture of the purified Peptide4.

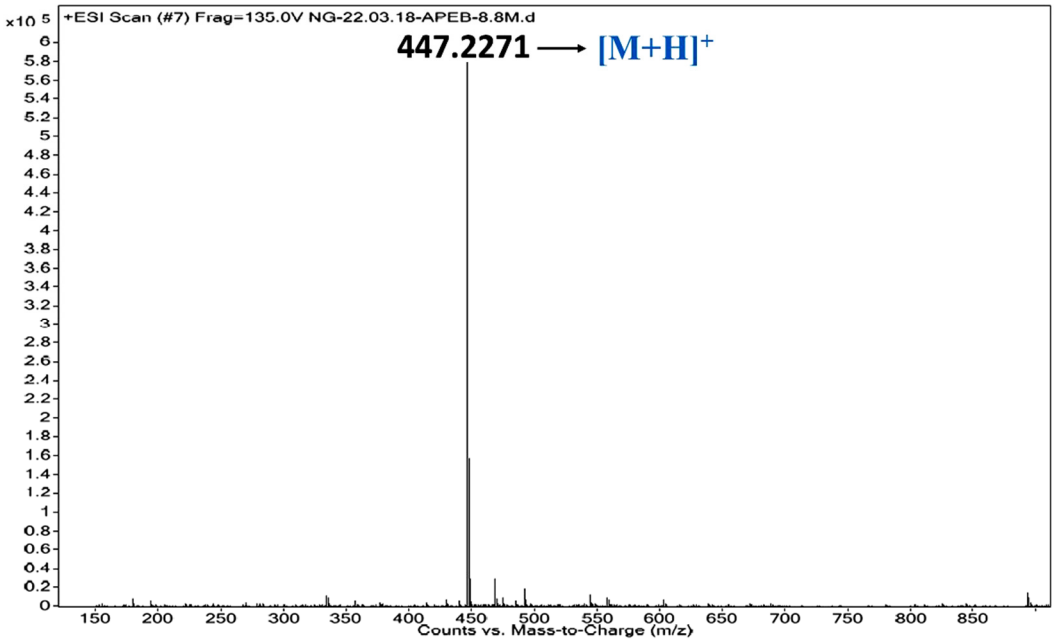

Figure 2.44. ESI-Mass spectrum of the Peptide4. Calculated m/z for $C_{22}H_{30}N_4O_6$ $[M+H]^+$ is 447.2244, observed 447.2271.

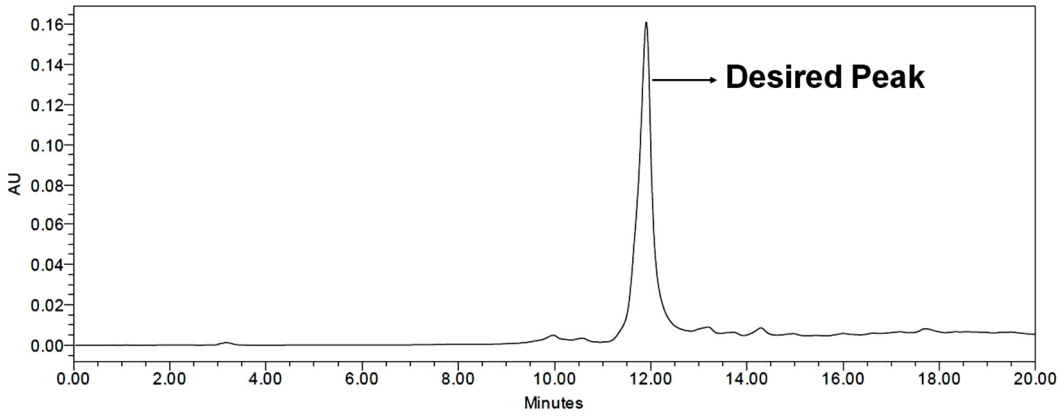

Figure 2.45. HPLC profile picture of the purified Peptide5.

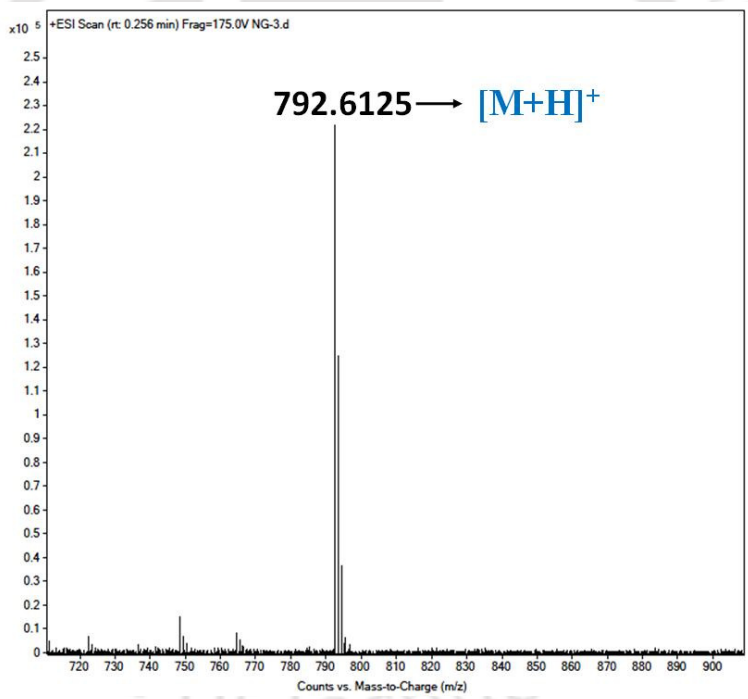

Figure 2.46. ESI-Mass spectrum of the Peptide5. Calculated m/z for $C_{37}H_{45}N_9O_{11}$ $[M+H]^+$ is 792.3239, observed 792.6125.

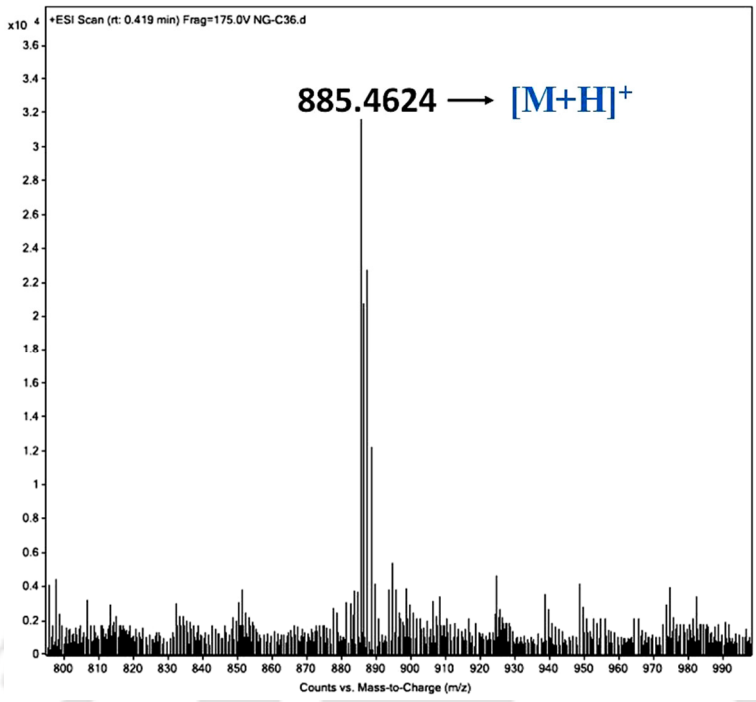

Figure 2.47. ESI-Mass spectrum of the Peptide6. Calculated m/z for $C_{42}H_{51}N_{11}O_{11}$ $[M+H]^+$ is 885.3770, observed 885.4624.

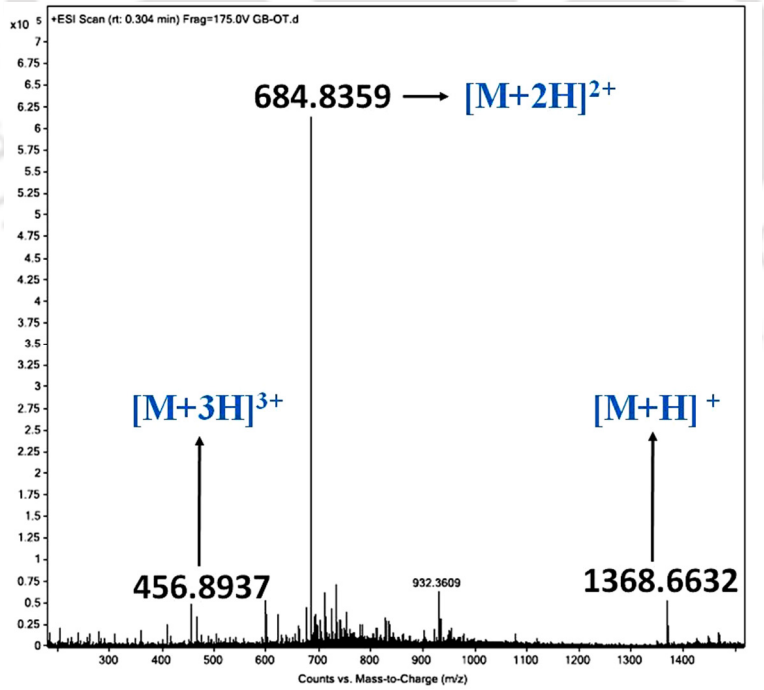

Figure 2.48. ESI-Mass spectrum of crude Peptide7 before attaching the Camptothecin. Calculated m/z for $C_{62}H_{85}N_{19}O_{17}$ $[M+H]^+$ is 1368.6449, observed 1368.6632.

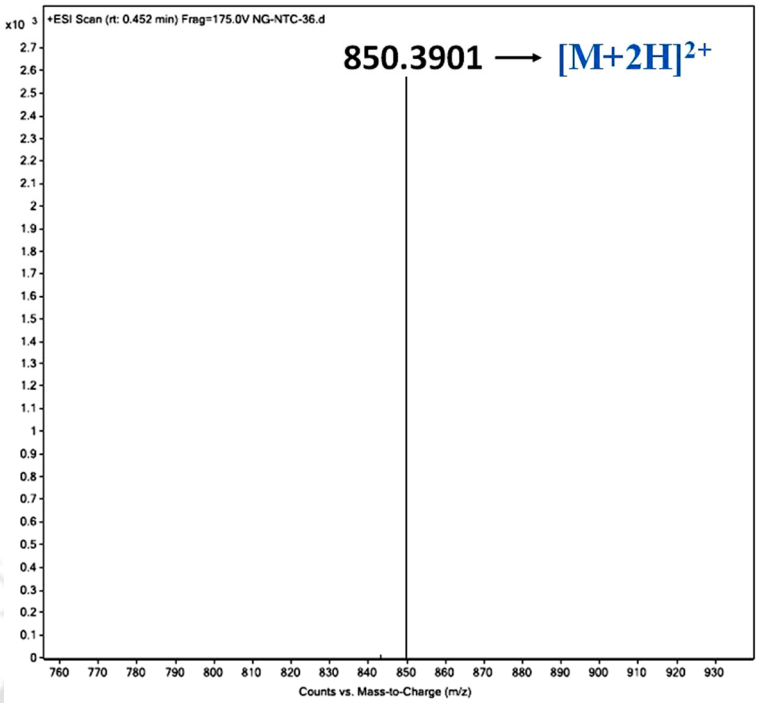

Figure 2.49. ESI-Mass spectrum of the Peptide7. Calculated m/z for $C_{82}H_{99}N_{21}O_{20}$ $[M+2H]^{2+}$ is 850.3961, observed 850.3901.

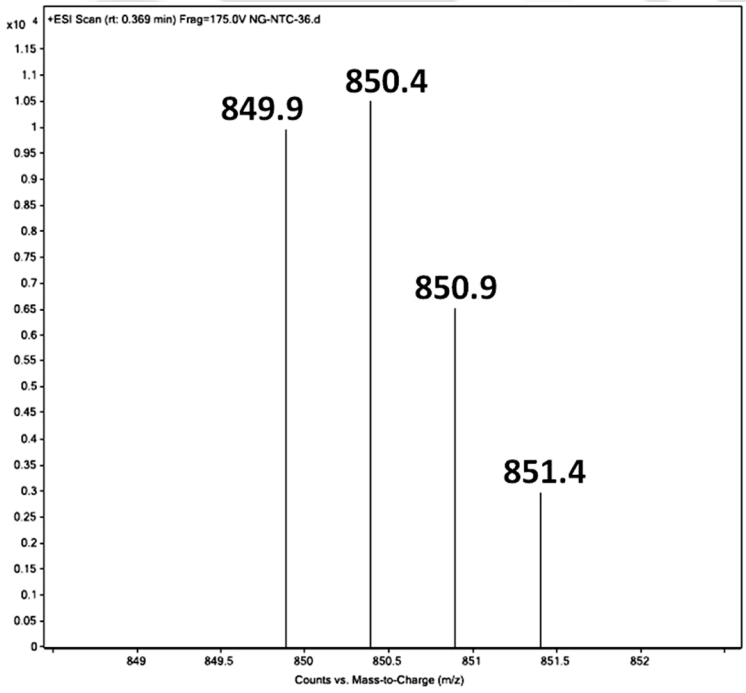

Figure 2.50. Expanded ESI-Mass spectrum of the Peptide7. The difference of 0.5 in ESI-MS values confirm the m/z as $[M+2H]^{2+}$ form.

2.9. References:

[1] Schmidt, U.; Langner, J. *J. Pept. Res*. **1997**, *49*, 67-73.

[2] Galibert, M.; Renaudet, O.; Dumy, P.; Boturyn, D. *Angew. Chem. Int. Ed*. **2011**, *50*, 1901-1904.

[3] Y. Zhang, Q. Zhang, C. Wong, X. Li, *J. Am. Chem. Soc*. **2019**, *141*, 12274-12279.

[4] Tavassoli, A.; Benkovic, S. J. *Nat. Protoc*. **2007**, *2*, 1126-1133.

[5] Hackenberger, C. P. R.; Schwarzer, D. *Angew. Chem*. **2008**, *120*, 10182-10228.

[6] Kent, S. B. H. *Chem. Soc. Rev*., **2009**, *38*, 338-351.

[7] Gilon, C.; Mang, C.; Lohorf, E.; Friedler, A.; Kessler, H. *Thieme* **2004**, *E 22b*, Ch. 6.8.

[8] Teesalu, T.; Sugahara, K. N.; Kotamraju, V. R.; Ruoslahtia, E. *Proc Natl Acad Sci U S A*. **2009**, *106*, 16157-16162.

[9] Haspel, N.; Zanuy, D.; Nussinov, R.; Teesalu, T.; Ruoslahti, E.; Aleman, C. *Biochemistry* **2011**, *50*, 1755-1762.

[10] Coin, I.; Beyermann, M.; Bienert, M. *Nat. Protoc.* **2007**, *2*, 3247-3256.

[11] Martin, S. R.; Schilstra, M. J. *Methods Cell Biol.* **2008**, *84*, 263–293.

[12] Clarke, D. T. *Methods Mol Biol.* **2011**, *752*, 59–72.

[13] Kaul, R.; Brouillette, Y.; Sajjadi, Z.; Hansford, K. A.; Lubell, W. D. *J. Org. Chem*. **2004**, *69*, 6131-6133.

[14] Baba, Y.; Matsuo, H.; Schally, A. V. *Biochem. Biophys. Res. Commun.* **1971**, *44*, 459–463.

[15] Dharap, S. S.; Wang, Y.; Chandna, P. *et al. Proc Natl Acad Sci U S A.* **2005**, *102*(36), 12962–12967.

[16] Tsume, Y.; Drelich, A. J.; Smith, D. E.; Amidon, G. L. *Molecules* **2017**, *22*(8), 1322.

[17] Zhang, Z.; Hatta, H.; Tanabe, K.; Nishimoto, S. *Pharmaceutical research*, **2005**, *22(3)*, 381–389.

[18] Brueckner, B.; Rius, M.; Markelova, M. R. *et al. Mol Cancer Ther*. **2010**, *9(5)*, 1256-1264.

[19] Mondal, T.; Mandal, B. *ChemComm.* **2019**, *55*, 4933-4936.

[20] Trott, O.; Olson, A. J. *J. Comput. Chem.* **2010**, *31*, 455-461.

Chapter 3: *In-situ* side chain peptide cyclization as a breaker strategy against the amyloid aggregating peptide

3.1. Introduction:

Misfolding and aberrant aggregation of amyloid β (Aβ) peptides form amyloid fibrils which is believed to be the root cause of Alzheimer's disease (AD), a progressive and devastating neurodegenerative disorder of the central nervous system.[1-2] The transformation from the natively folded state of Aβ peptide into highly ordered β-sheet rich aggregates occurs through nucleation dependent pathway.[3] Inhibition of Aβ aggregation by using small molecule drugs is an attractive therapeutic strategy as this appears to be the early step in the pathogenic process of amyloidosis.[4-5] Besides the traditional small molecule drugs, therapeutic peptides are also gaining attention for drug discovery due to their high biological activity associated with high specificity and low toxicity.

To block Aβ aggregation and amyloid formation, a wide range of Aβ binding peptides were reported to date for therapeutic purposes, and some of those are "β-sheet breaker peptides".[6-7] "β-sheet breaker peptides" contain a sequence similarity to the region of the protein involved in the abnormal folding for recognition purposes but prevent β-sheet stacking of amyloid fibrils by interfering with the intermolecular backbone hydrogen bonds needed to form the structure which hampers further elongation of β-sheet fibril structures. In 1996, Tjernberg *et al.* reported that a short Aβ fragment 'KLVFF', (Aβ16-20) is the core

sequence responsible for the initiation of self-aggregation, can bind full-length Aβ where Lys16, Leu17, and Phe20 are crucial for binding and act as a potent inhibitor of Aβ (1-40) aggregation *in vitro*.[8] It is considered as a starting point for modified peptide aggregation inhibitors. Later, Soto and co-workers introduced another peptide-based molecule 'LPFFD', a 'β-sheet breaker peptide', termed as iAβ5 along with a recognition motif to inhibit Aβ peptide aggregation and dissolution of preformed amyloid fibrils of Aβ.[9] Here, an inherently rigid proline residue was inserted as a breaker element in place of valine to generate a kink in the peptide sequence and alanine was substituted by aspartic acid to improve the peptide solubility.

After that, various potential breaker peptides containing breaker elements like *N*-methylated amino acids,[10] α-Aminoisobutyric acid (Aib),[7] and Dehydrophenylalanine were reported to disrupt amyloid aggregates. However, with these breaker peptides containing preinstalled disrupting elements, e.g., kink (for proline and Aib) or *N*-methylated amino acids may prevent proper alignment and recognition with the existing aggregating Aβ peptide because of conformational mismatch. If the recognition of the β-breaker peptide with the aggregating peptide is not proper enough, breaking efficiency will be decreased.

In this chapter, we have developed a concept of a linear peptide without any kink in the sequence initially which is anticipated to get aligned with Aβ peptide in a better manner. Later, to inhibit fibrillization and to disrupt the preformed fibrillar assembly of Aβ peptide, our designed peptides will form an *in situ* turn structured β-breaker element via peptide cyclization at the physiological condition.

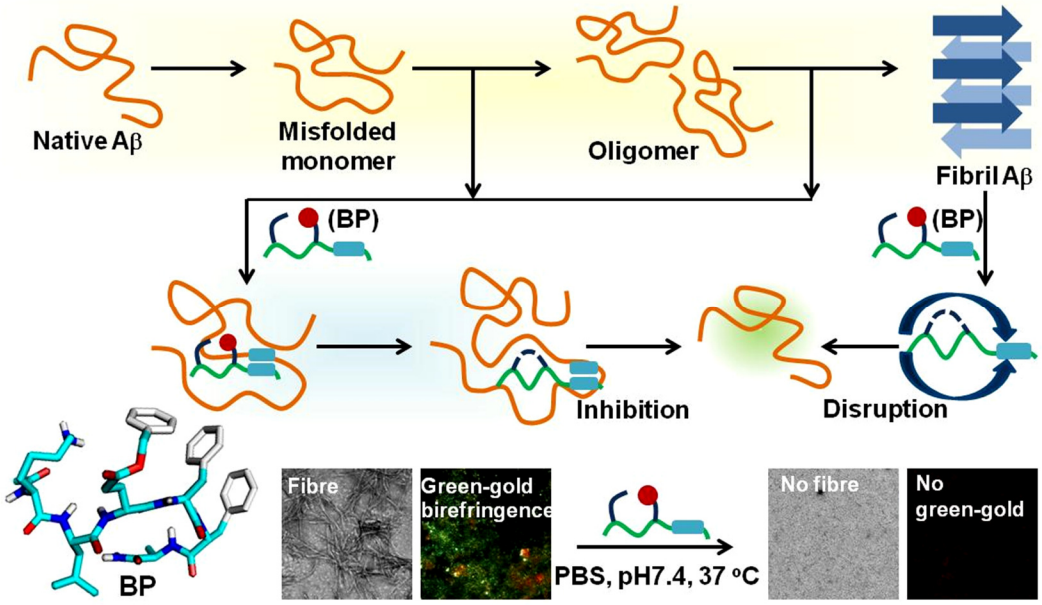

Figure 3.1. Schematic diagram of the breaking strategy.

3.2. Results and Discussions:

3.2.1. Design of the Model Peptides (MPs):

From the above discussions, it is believed that aggregation of the protein Amyloid-β in the brain is responsible for Alzheimer's disease. So, we have planned to inhibit as well as disrupt the β-sheet structure of Aβ by the concept of turn generating unit, and for that purpose, we have designed and synthesized a series of side chain modified tripeptide MP1-MP3.

The MPs were designed, having Lysine at the N-terminus and Glutamic acid covalently attached (by side chain) with good leaving group (Benzyl alcohol in the generalised purpose) at the C-terminus, with a variation of leucine/ Alanine/ Glycine (keeping in mind the hydrophobic region of Aβ peptide) to find out the best possibility for the desired nucleophilic attack by the side chain nucleophilic centre of Lysine to the side chain

electrophilic centre of carbonyl group of Glutamic acid. This concept may be useful to produce stable *in-situ* bent-unit at physiological condition without using any external reagents.

Table 3.1. List of the designed peptides:

Sl. No.	Name of the Peptides (Short Name)	Peptide Sequence	Functional Activity
1.	Model Peptide1 (MP1)	Ac-KLE(OBn)-NH_2	peptide cyclization
2.	Model Peptide2 (MP2)	Ac-KAE(OBn)-NH_2	peptide cyclization
3.	Model Peptide3 (MP3)	Ac-KGE(OBn)-NH_2	peptide cyclization
4.	Breaker Peptide1 (BP1)	Ac-KLE(OBn)FFA-NH_2	β-sheet breaker
5	Breaker Peptide2 (BP2)	Ac-KAE(OBn)FFA-NH_2	β-sheet breaker
6	Breaker Peptide3 (BP3)	Ac-KGE(OBn)FFA-NH_2	β-sheet breaker

3.2.1.1. Synthesis and purification procedure of the designed peptides:

Our designed peptides were synthesized following the standard Fmoc/^{t}Bu solid-phase peptide synthesis (SPPS) method (Figure 3.2) starting each with 100 mg of Rink amide MBHA resin (loading 0.5mmol/g) taken in 5 ml frit-fitted plastic syringe. Fmoc protected amino acids were sequentially coupled on the resin using BOP coupling reagent and DIPEA base at room temperature.

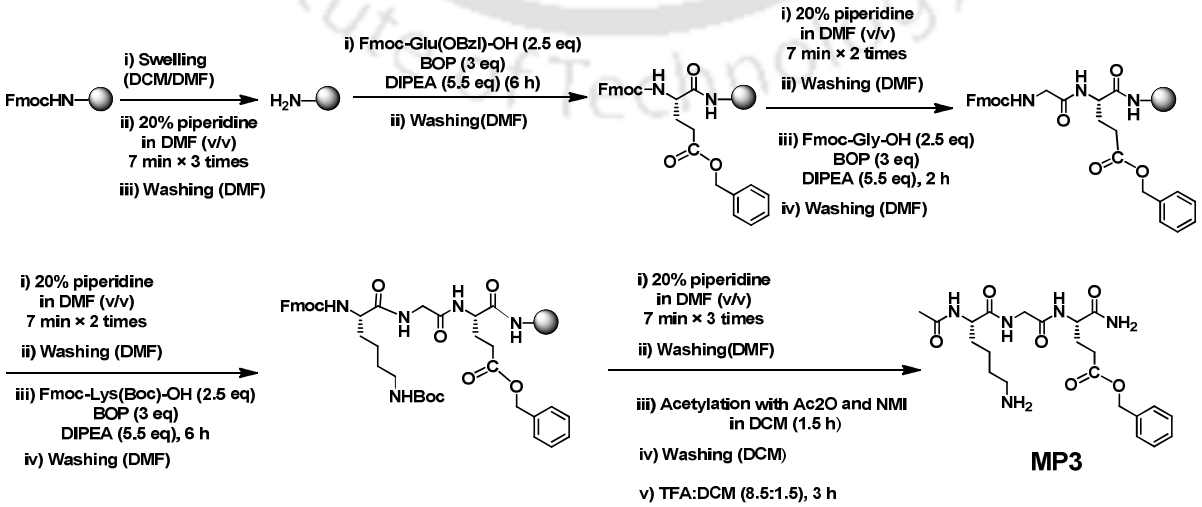

Figure 3.2. The procedure of peptide synthesis in solid phase.

Peptide MP1 and MP2 were synthesized following the above method with only variation of coupling reaction time. When bridging amino acid was Leu in peptide MP1, coupling reaction time was 8h, and for Ala in peptide MP2, it was 3h.

Crude peptides were precipitated in cold diethyl ether, centrifuged and washed with ether, then dissolved in CH_3CN/H_2O mixture. For purification by Semi-preparative HPLC, a C18-reversed-phase column where binary solvent system [solvent A (0.1 % TFA in H_2O) and solvent B (0.1 % TFA in CH_3CN)], UV detector with dual detection at 214 and 254 nm, total run time of 20 min. (gradient 5-100 % CH_3CN for 18 min followed by 100% CH_3CN till 20 min.) with a flow rate of 4 mL/ min were used. Then samples were lyophilized.

The purity of the peptides was confirmed by analytical HPLC system where C18 reversed-phase column with linear gradient of 5-100% CH_3CN over 18 minutes in a total run time of 20 min selecting dual-wavelength at 214 nm and 254 nm with flow rate of 1 ml/min. were used. Mass spectrometry of the purified peptide samples were performed using positive polarity electrospray ionization (+ESI).

3.2.2. Plausible mechanism of the side-chain cyclization:

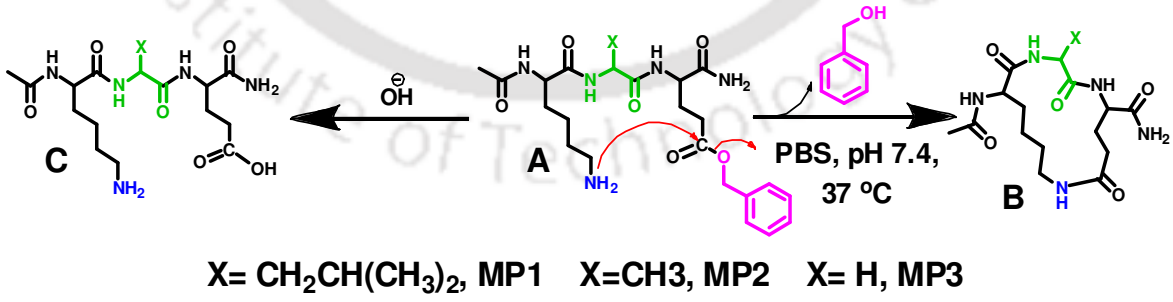

Figure 3.3. Plausible mechanism of side-chain cyclization of the model peptides.

3.2.3. Proof of hypothesis of the side chain cyclization:

To establish our hypothesis, ESI-MS kinetic studies were performed with designed MPs *in vitro*. For MP2 peptide, HPLC kinetic study and CD kinetic study beside ESI-MS kinetic study were also performed. All the biophysical studies were carried out in PBS at pH 7.4 and 37 °C. After analysing all the results, the plausible mechanism (Figure 3.3) was drawn, which goes with our hypothesis.

3.2.3.1. Sample preparation:

Each lyophilised sample was dissolved in a required amount of PBS (50 mM, pH 7.4) followed by sonication and vortex to obtain a clear solution. Then the total solution was divided into different Eppendorf tubes, equally maintaining a final concentration of 500 µM and kept in an incubator at 37 ºC to perform the kinetic studies *in vitro*. ESI-MS kinetic study was performed to get proof of cyclic peptide formation. For kinetic studies, the required amount of aliquots were collected from Eppendorf tubes at different time intervals. Before the sample collection, the stock solutions were sonicated and vortexed for 1 min each.

3.2.3.2. ESI-MS kinetics of MP1 at the physiological condition:

Samples taken for kinetic studies were quenched with 20% HCl, diluted with HPLC grade CH_3CN and Mili-Q water and filtered through 0.2-micron filter paper and were analyzed in ESI positive mode.

In ESI-MS spectra (Figure 3.4-3.7), only one major peak for MP1 (A^1) was noticed initially, but with the progression of time, another two peaks were found, the cyclic product (B^1) and the uncontrolled hydrolysed product (C^1) along with A^1.

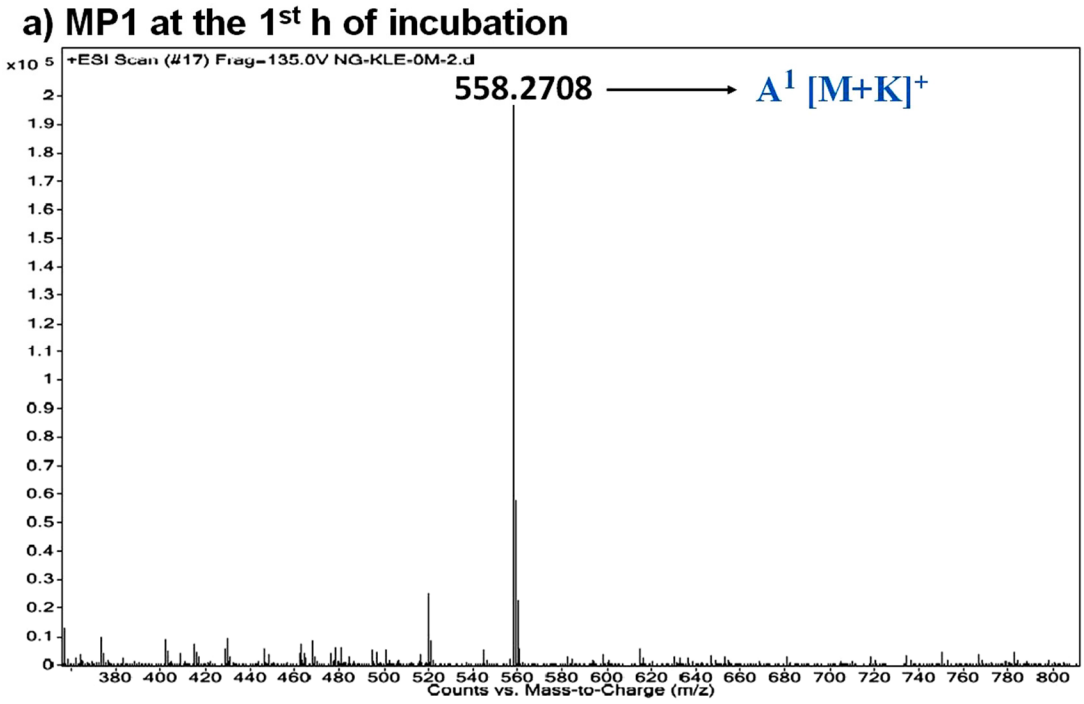

Figure 3.4. ESI-MS spectrum of MP1 at the 1st h of incubation at PBS, pH 7.4, 37 °C.

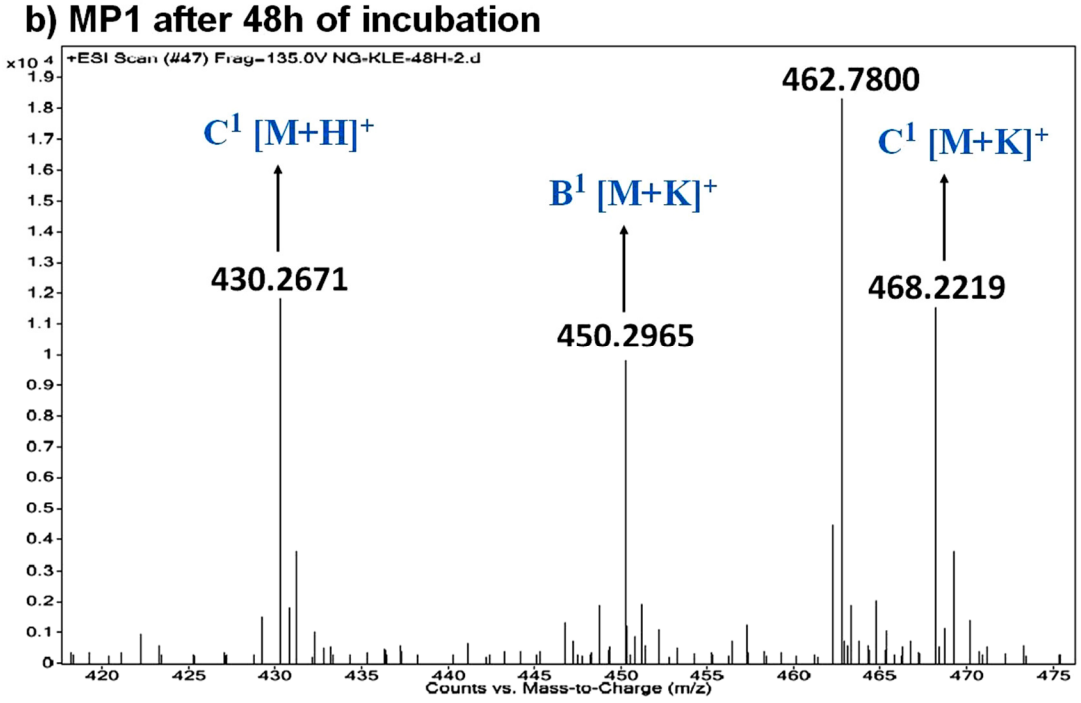

Figure 3.5. ESI-MS spectrum of MP1 after 48 h of incubation at PBS, pH 7.4, 37 °C.

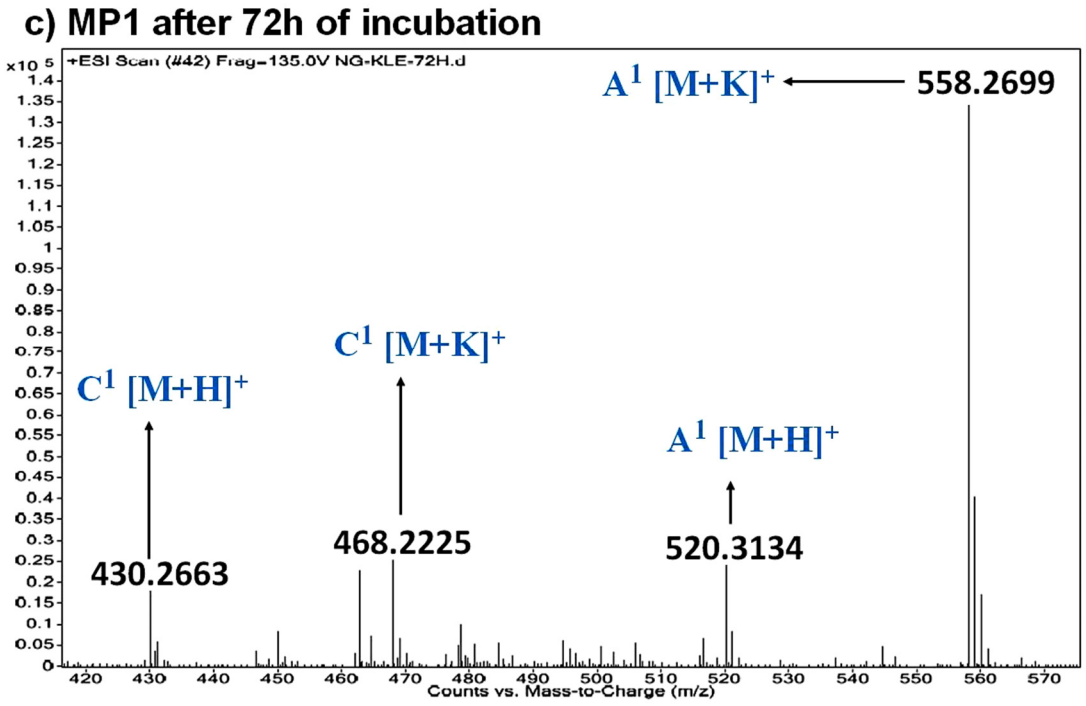

Figure 3.6. ESI-MS spectrum of MP1 after 72 h of incubation at PBS, pH 7.4, 37 °C.

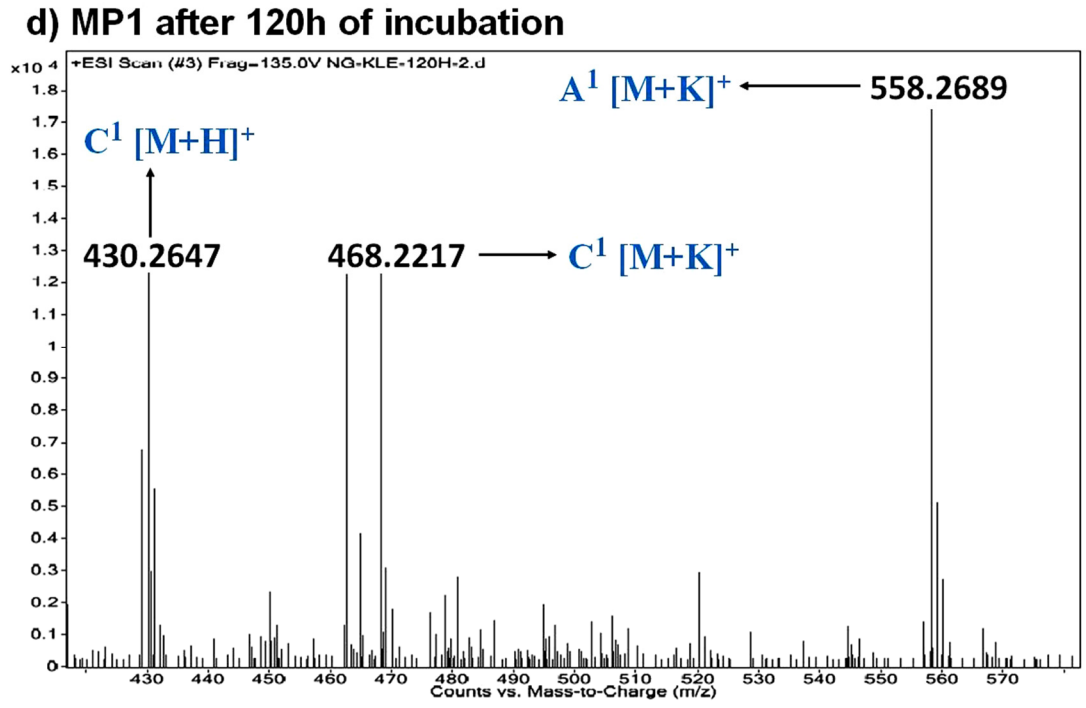

Figure 3.7. ESI-MS spectrum of MP1 after 120 h of incubation at PBS, pH 7.4, 37 °C.

3.2.3.3. ESI-MS kinetics of the side-chain cyclization of MP2:

In ESI-MS spectra (Figure 3.8-3.10), only one major peak was observed for MP2 (A^2) initially, but with the progression of time, a new peak was found for the cyclic product (B^2) along with the uncontrolled hydrolysed product (C^2).

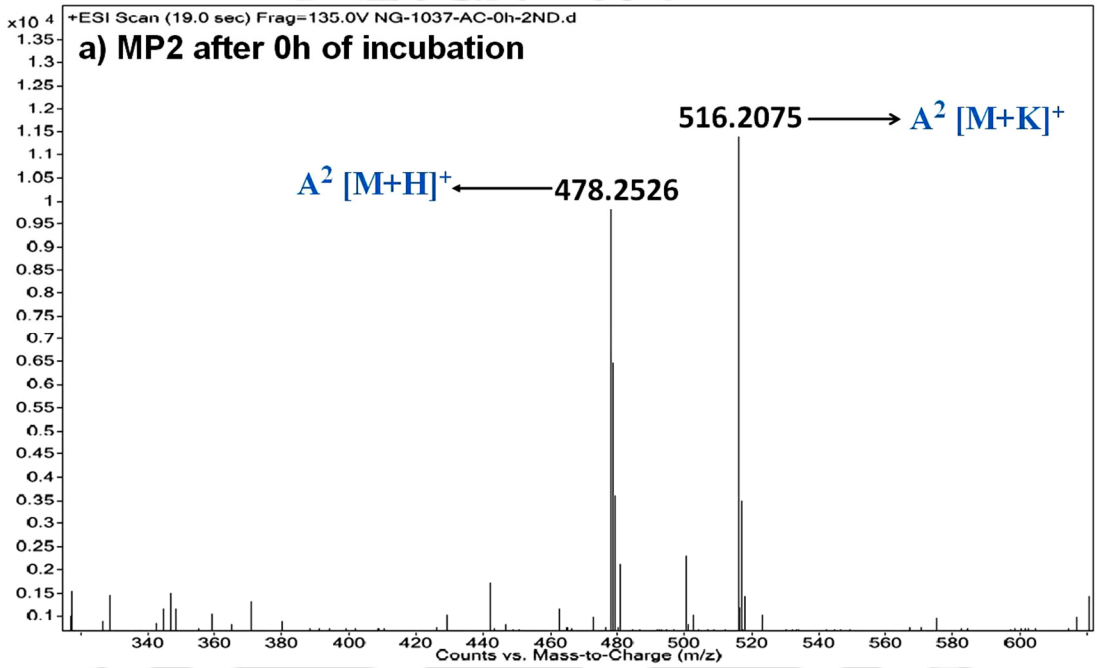

Figure 3.8. ESI-MS spectrum of MP2 at the 1st h of incubation at PBS, pH 7.4, 37 °C.

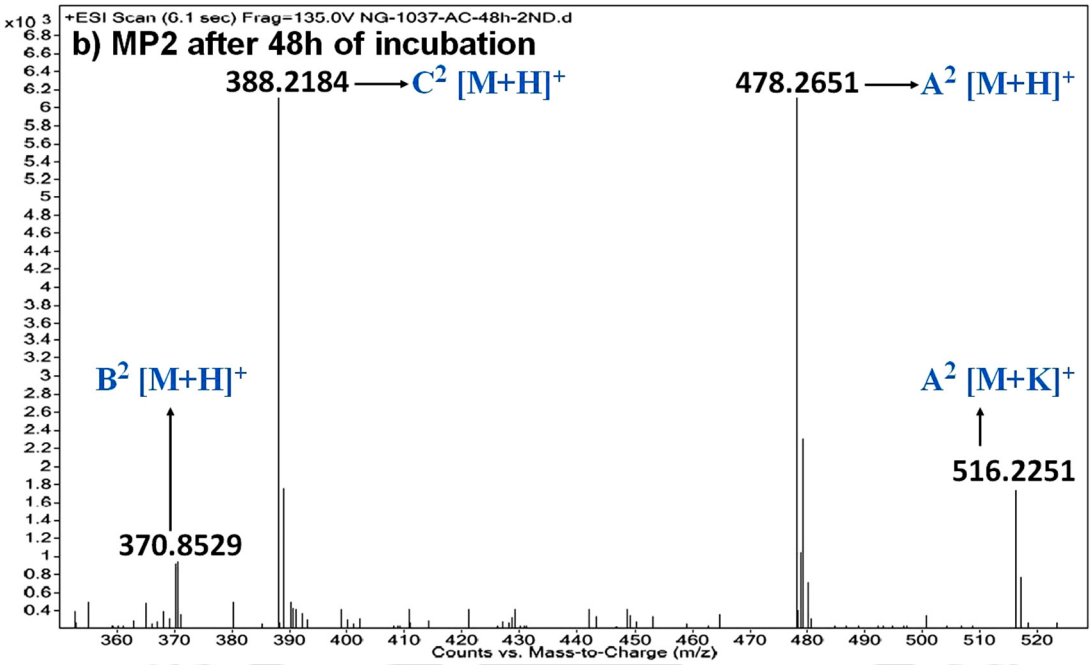

Figure 3.9. Detection of an *in-situ* cyclic product obtained from MP2 by ESI-MS after 48h.

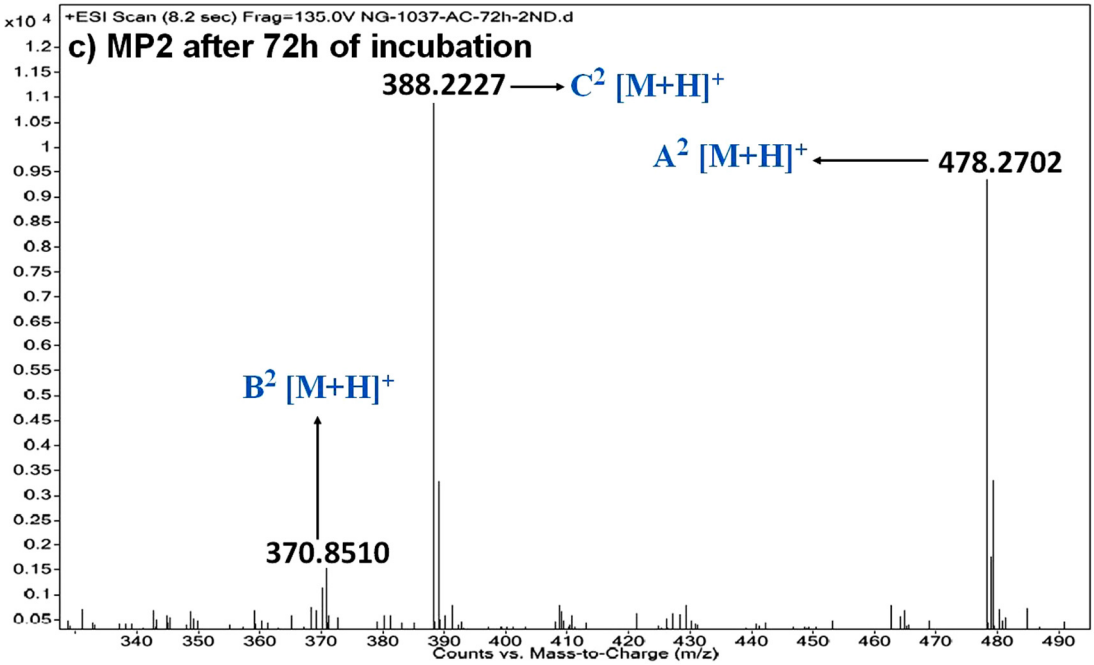

Figure 3.10. Detection of an *in-situ* cyclic product obtained from MP2 by ESI-MS after 72h.

3.2.3.4. ESI-MS kinetics of the side-chain cyclization of MP3 at the physiological condition:

In ESI-MS spectra (Figure 3.11-3.14), at the 1st h of incubation, a major peak for MP3 (A^3) was found along with its cyclic product (B^3). But with the progression of time, the cyclic product (B^3) appeared as the major peak (in terms of intensity).

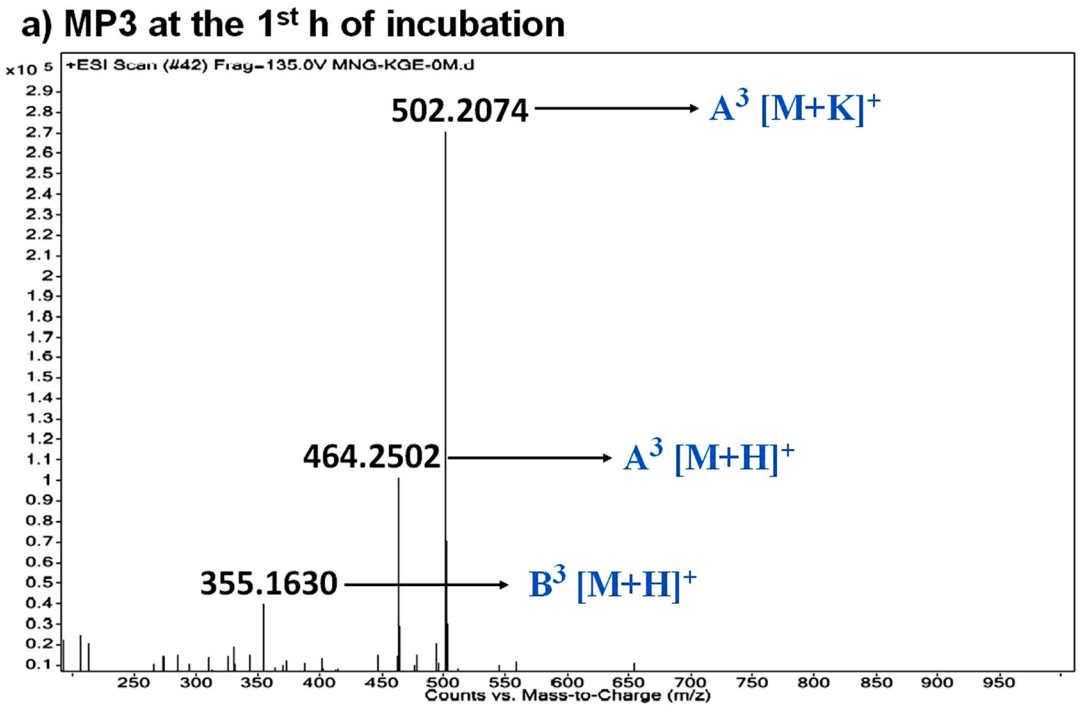

Figure 3.11. ESI-MS spectrum of MP3 at the 1st h of incubation at PBS, pH 7.4, 37 °C.

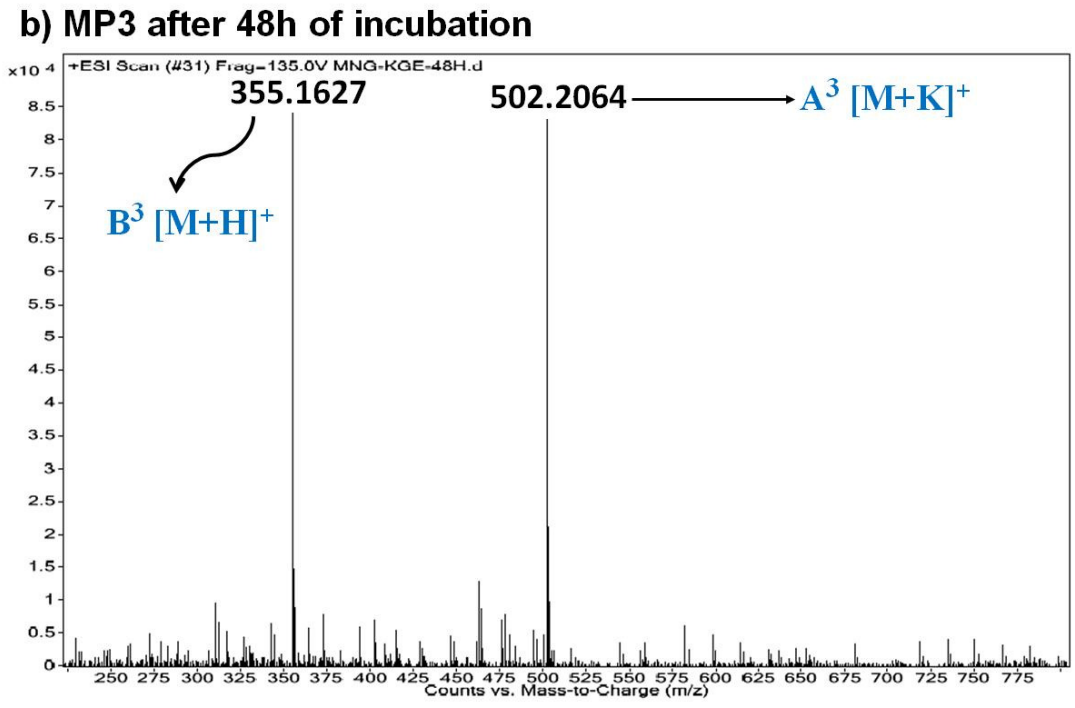

Figure 3.12. Detection of an *in-situ* cyclic product obtained from MP3 by ESI-MS after 48h.

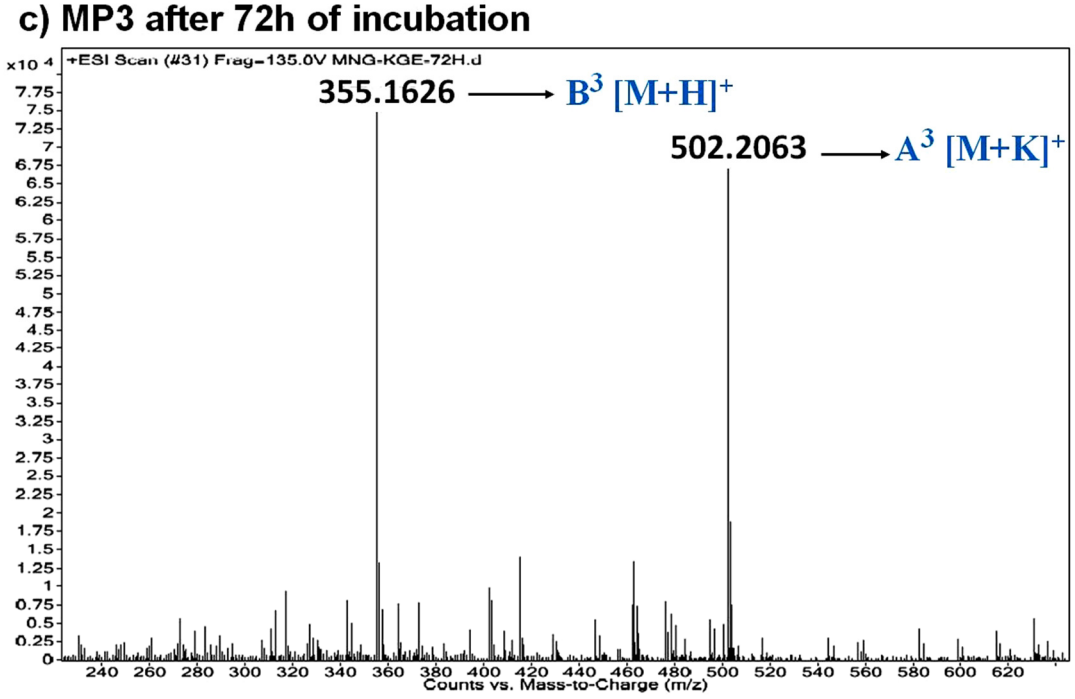

Figure 3.13. Detection of an *in-situ* cyclic product obtained from MP3 by ESI-MS after 72h.

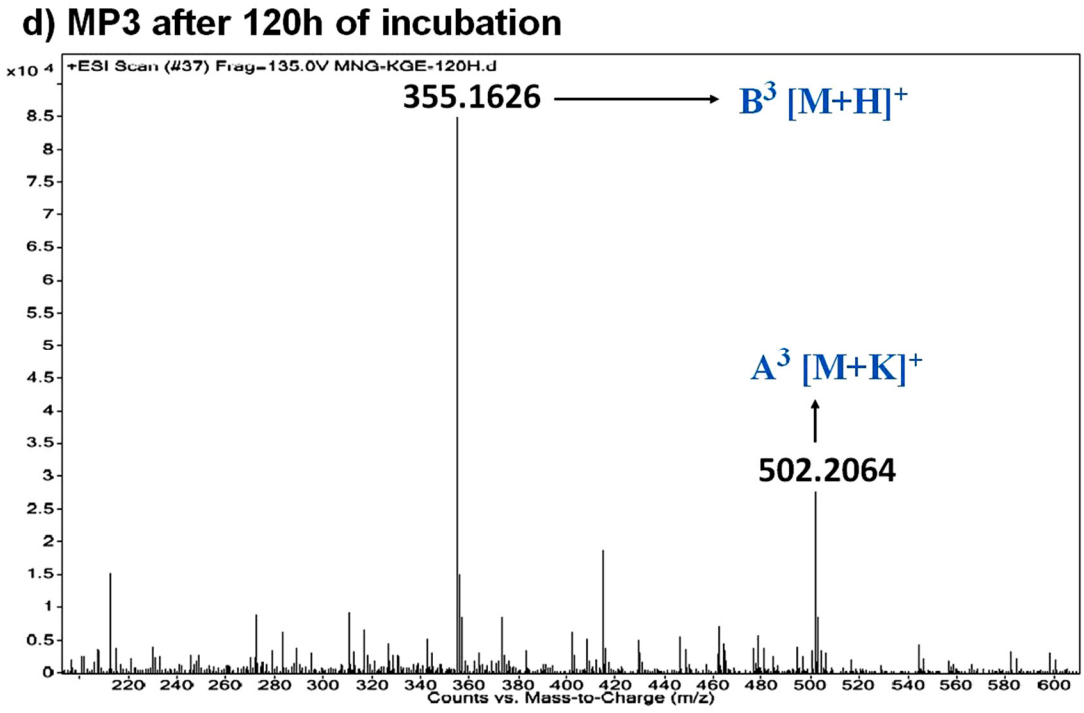

Figure 3.14. Detection of an *in-situ* cyclic product obtained from MP3 by ESI-MS after 120h.

3.2.3.5. HPLC kinetics of the side chain cyclization:

For the study, an Ascentis C18 analytical column was used with binary solvent system [solvent A (0.1 % TFA in H2O) and solvent B (0.1 % TFA in CH3CN)], dual-wavelength at 214 nm and 254 nm in the UV detector was selected. With a flow rate of 0.9 ml/min and a linear gradient of 5-100% CH_3CN over 0-18 min in a total run time of 20 min kinetic study was performed. 20 µL sample of 500 µM was injected in analytical HPLC at different time intervals.

The rate of formation of the cyclic product (the desired bent-unit) was studied using HPLC. The results of the MP2 were described here as a representative example. The peak (Figure 3.15) corresponding to A (retention time [t_R] 12.1min, identified from the ESI-MS spectrum) was transformed into that of B (newly appeared, t_R 13.5min) gradually with an increase in time, clearly indicating its controlled nature concerning the release system.

Also, the stability of MP2 was confirmed from the peak found in the HPLC chromatogram even after 98h of incubation at the physiological condition.

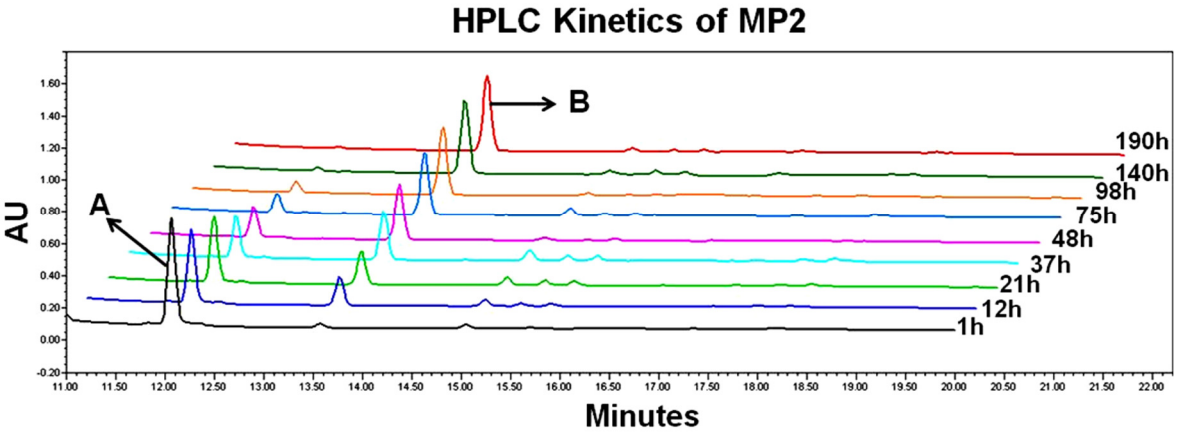

Figure 3.15. HPLC kinetics of side-chain cyclization of MP2 at physiological condition.

3.2.3.6. CD kinetics of the side chain cyclization:

For CD spectroscopy, incubated samples taken from stock were treated with 0.1% trifluoroacetic acid to quench any further reaction and were stored at -20 °C. Then the samples were diluted with PBS buffer solutions to obtain a final concentration of 100 µM. 200 µL of the sample was taken in a cuvette having a pathlength of 1 mm. and were measured twice, spectra was recorded from 190 nm to 260 nm. The observed ellipticity (mDeg) [obtained from Spectra Manager] was converted to mean residue molar ellipticity.

The results of MP2 were described here as a representative example. Time-dependent CD kinetics (Figure 3.16) was performed to monitor the conformational changes and predominantly the turn structure (a positive band at 200 nm) was found in the final solution. All the results confirmed the formation of the *in-situ* cyclic compound.

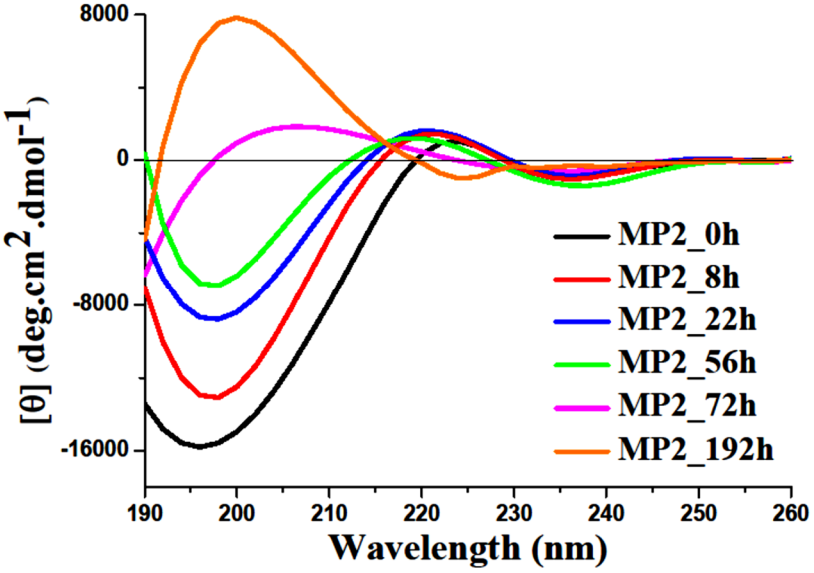

Figure 3.16. The time-dependent CD spectra of MP2 at PBS, pH 7.4, 37 °C.

3.2.3.7. Rate of the cyclic product formation of MP2:

From HPLC kinetics, the formation of cyclised product (after releasing benzyl alcohol from the starting material MP2) was determined quantitatively. MP2 released the benzyl alcohol (Figure 3.17) almost 56% after 36h of incubation in PBS (pH 7.4) at 37 ºC, following the saturation point thereafter and the quantities are 79% after 72h, and 88% after 100h.

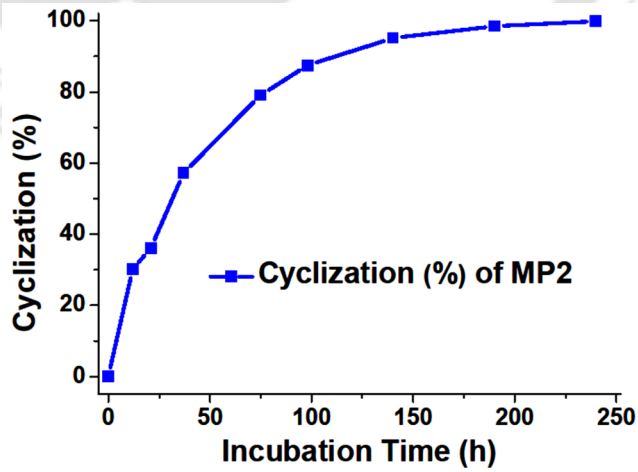

Figure 3.17. Rate of formation of cyclic product (% of cyclization) of MP2 at the physiological condition.

3.2.4. Design of the Breaker Peptides (BPs):

Inspired by Tjernberg's work[8] and Soto's work[9], we focussed on the hydrophobic region ($K_{16}LVFFA_{21}$) of Amyloid-β to develop breaker peptides (BPs). After getting proof of the principle of side chain cyclization, we used the modified KXE unit in the hydrophobic region to design (Figure 3.18) BP1-BP3 to inhibit as well as disrupt the aggregation of Aβ peptide.

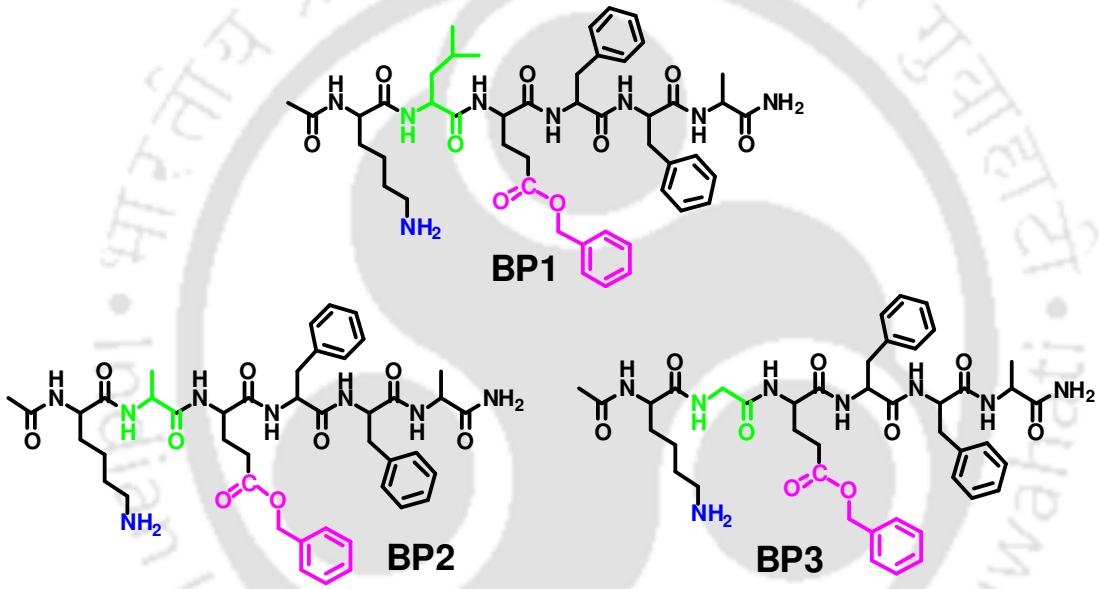

Figure 3.18. Chemical structure of the breaker peptides.

Here, the synthesis procedure of BP2 (Figure 3.19) has been described. BP1 and BP3 were synthesized using the same protocol with a variation of coupling reaction time such as for bridging amino acid Leu in BP1 time was 4h, and 2h for Gly in BP3.

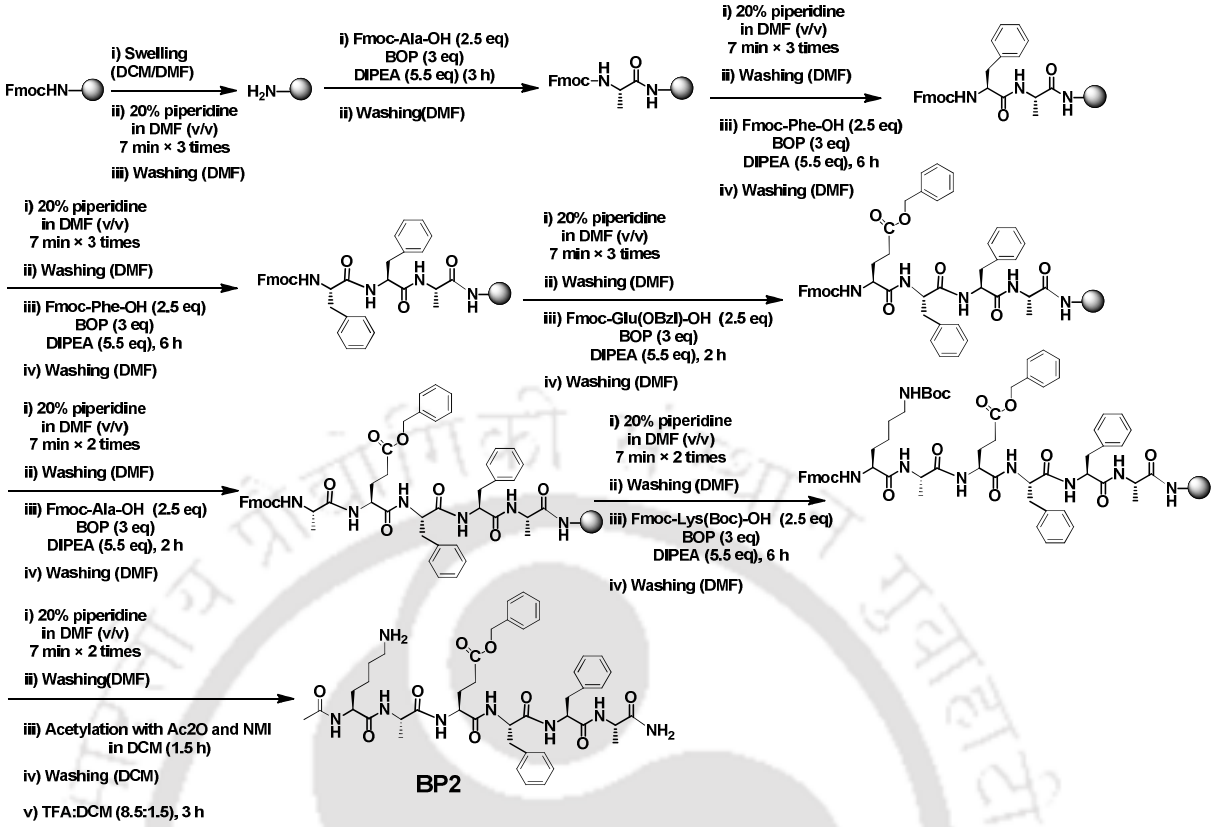

Figure 3.19. The procedure of peptide synthesis in solid phase.

3.2.5. Molecular docking studies:

Docking studies (Figure 3.20-3.21) have been performed with the designed peptides (BP1, BP2 and BP3) using AutoDock Vina version 1.1.2 software (as described in the literature)[11,12,13] to check whether the designed BPs are liable to fit in the Aβ binding pocket. The segment of helical and fibril $A\beta_{1\text{-}40}$ have been used after extracting from RCSB protein data bank (PDB ID: 4NGE and 2M4J respectively) for docking studies. For protein preparation AutoDock 4.2 MGL Tools version 1.5.6 software package was used where removing all water molecules, assigning polar hydrogens for correct geometry optimization and calculation of partial charges, calculating Gasteiger charges to protein structures, the prepared file was saved in PDBQT format. OpenBabel version 2.4.1 software was used to convert ligand in PDB format after minimizing energy and the PDB file was modified by

combining with non-polar hydrogens, addition of Gasteiger charges and rotable bonds, then converted to the PDBQT format of the ligand which contains three-dimensional Cartesian coordinates of each ligand atom. The fixable and non-bonded rotation of molecules were assigned after calculating torsion angles. Auto Grid version 4.2 was used for the preparation of the grid map using a grid box. Ligands were docked individually to the receptor helical $A\beta_{1-40}$ peptide (PDB ID: 4NGE) with grid coordinates (grid centre) and grid boxes of certain sizes for each receptor. The grid size was set at 60×60×60 (x, y, and z) points, and the grid centre was designated at x, y, and z dimensions of 3.130, -3.283, -17.750 respectively, with a grid spacing of 1.000 Å. Ligands were also docked with fibril $A\beta_{1-40}$ peptide (PDB ID: 2M4J). For that, grid size was set to 68×100×60 (x, y, and z) points with grid spacing of 0.803Å and grid centre was designated at dimensions (x, y, and z): 3.646, -20.424, 101.725. Both the protein and ligands were considered as rigid during the docking procedure. The output file was generated as ligand_out.pdbqt format which contains ligand-binding affinity predicted as negative Gibbs free energy (ΔG) scores (in kcal/mol) and root-mean-square deviation (RMSD) lower bound, RMSD upper bound. The pose with lowest energy of binding or binding affinity was extracted, aligned with receptor structure for analysis and post-docking analyses were visualized using PyMOL version 1.7.4.5 software. From molecular docking studies, it was observed that designed BPs docked with the hydrophobic region as expected and fitted properly in the related binding pocket having a negative binding affinity. Notably, the possibility of turn generation was clearly viewed from the structure of ligand after performing docking.

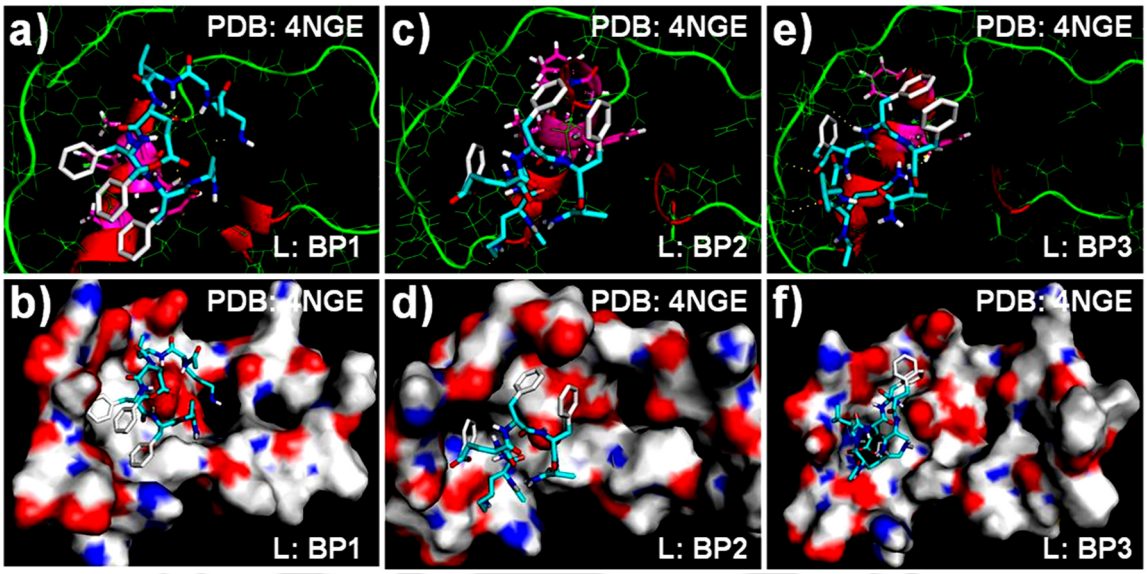

Figure 3.20. Molecular docking images of BP1 (a, b), BP2 (c, d), and BP3 (e, f) into helical Aβ$_{1-40}$ (PDB ID 4NGE) reveals that BPs binds very well with binding affinity -6.1 kcal/mol, -6.3 kcal/mol and -5.5 kcal/mol respectively. Structures are shown as line and cartoon representation (for a, c, e), and surface representation (for b, d, f). The surface of Aβ$_{1-40}$ is coloured according to the charges of the atoms where negatively and positively charged zones are represented in red and blue, respectively.

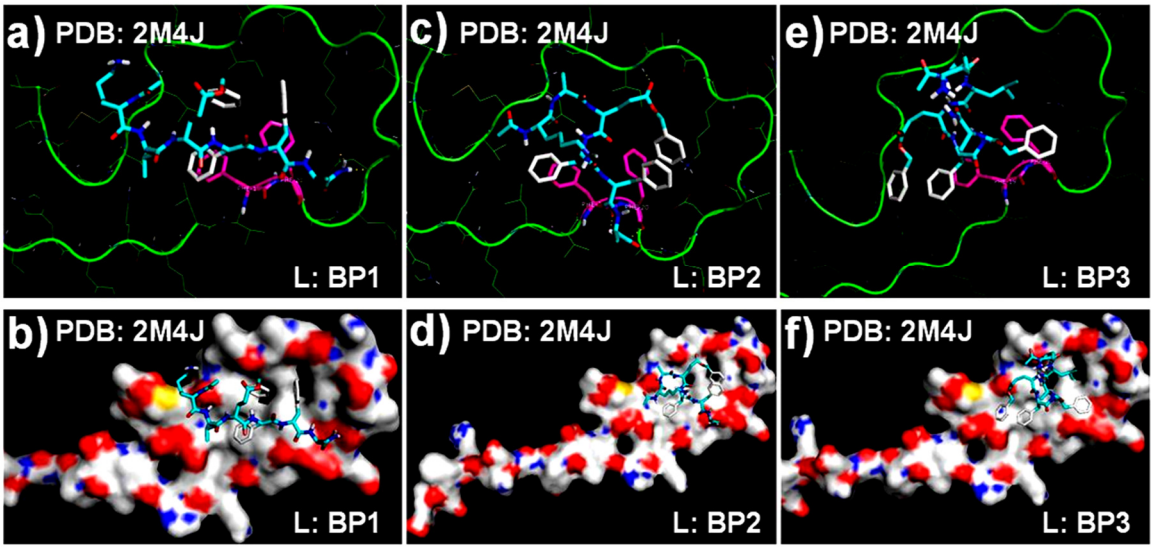

Figure 3.21. Molecular docking images of BP1 (a, b), BP2 (c, d), and BP3 (e, f) into sheet form of Aβ$_{1-40}$ (PDB ID 2M4J) reveals that BPs binds very well with binding affinity -5.6 kcal/mol, -5.3 kcal/mol, and -4.3 kcal/mol respectively. Structures are shown as line and cartoon representation (for a, c, e), and surface representation (for b, d, f). The surface of Aβ$_{1-40}$ is coloured according to the charges of the atoms where negatively and positively charged zones are represented in red and blue, respectively.

3.2.6. Non-aggregating and non-amyloidogenic property of the BPs:

It was essential to check the non-aggregating and non-amyloidogenic properties of the designed BPs before its application for the inhibition of aggregation against aggregating peptides. The non-amyloidogenicity of the BPs were studied using various biophysical tools.[11-12,14] At first, the BPs were dissolved in phosphate buffer solution (PBS, 50 mM, pH 7.4) to make the concentration of the stock solution ~0.25 mM. Then the stock solutions of the BPs were incubated on a water bath at 37 °C for seven days.

3.2.6.1. Thioflavin T (ThT) Fluorescence assay:

ThT-Fluorescence assay is a commonly used quantitative technique to monitor the amyloid fibril formation over time. The fluorescence intensity peak of an aggregating peptide solution is directly proportional to the amount of fibrils formed in a given set of conditions and decrement in fluorescence peak intensity indicates inhibition of fibrillar assembly. The kinetics of amyloid formation and its inhibition on the addition of inhibitor can be monitored easily by the ThT assay.[11-12,14]

From the result of ThT assay (Figure 3.22), initially, a slight time-dependent increase of the fluorescence intensity was observed due to the presence of the hydrophobic segment, but later the fluorescence intensity was suppressed significantly due to the cyclization. In the case of BP1 initial increment was comparatively higher than others due to the presence of rigid Leu which may cause a lower rate of cyclization. Above mentioned results indicate that the BPs are non-aggregating peptide as expected.

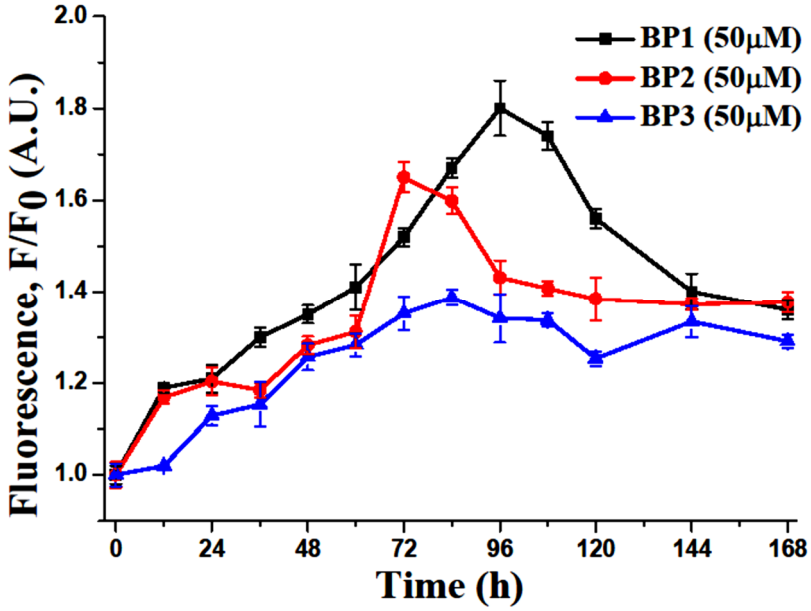

Figure 3.22. Th.T. fluorescence assay of BP1 (black), BP2 (red), and BP3 (blue). Error bars represent the standard deviation of measurements from at-least three replicate solutions. All the peptide solutions were incubated in PBS pH 7.4 (50 mM) at 37 °C.

3.2.6.2. Circular Dichroism (CD) and Fourier transformation infrared (FT-IR) spectra:

CD is another used spectroscopic technique to measure the secondary structural changes of amyloid fibrils in a solution. Using CD signal of one negative band at 220 nm and one positive band at 195 nm, the growth of β-sheet conformation can be characterized. This technique is also useful to compare the structural changes occurring during aggregation. Peptide bond absorbs at 220 nm and 190 nm due to n → π* and π → π* transitions respectively.[11-12,14]

FT-IR is also a useful technique to detect the growth of the β-sheet structure during fibril formation. The β-sheet structure corresponds to the bands that arise in the region of 1625-1640 cm^{-1} and bands that arise in between 1640-1660 cm^{-1} indicate random coil or α-helix conformation of peptides or proteins.[11-12,14]

After seven days, the conformational changes were studied using CD and FT-IR. In CD spectra (Figure 3.23), for all the BPs, a negative band at ~200 nm and a positive band at ~218 nm were observed indicating a mixture of a random coil and β-turn conformation of the BPs. Similarly, in FT-IR spectra (Figure 3.24), the amide I band at 1641 cm^{-1} was observed. These results clearly indicated non-β-sheet conformations of the peptides.

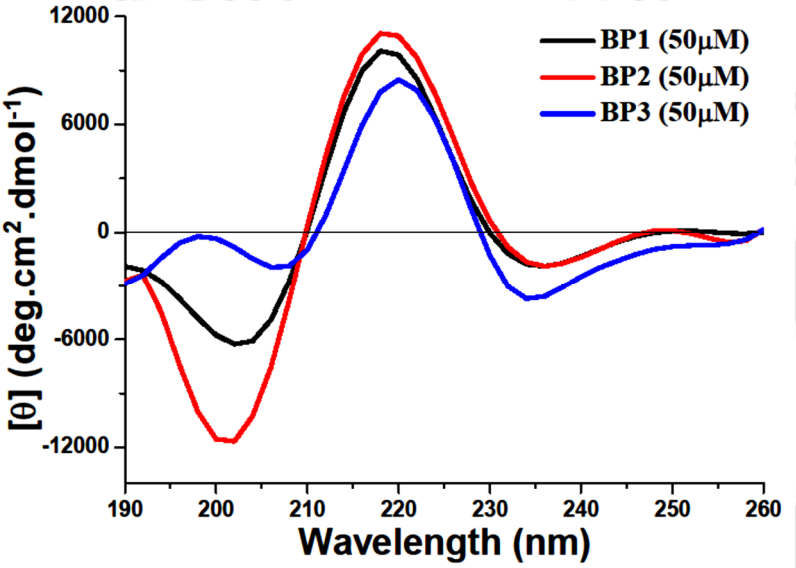

Figure 3.23. CD spectra of BP1 (black), BP2 (red), and BP3 (blue). All the peptide solutions were incubated in PBS pH 7.4 (50 mM) at 37 °C.

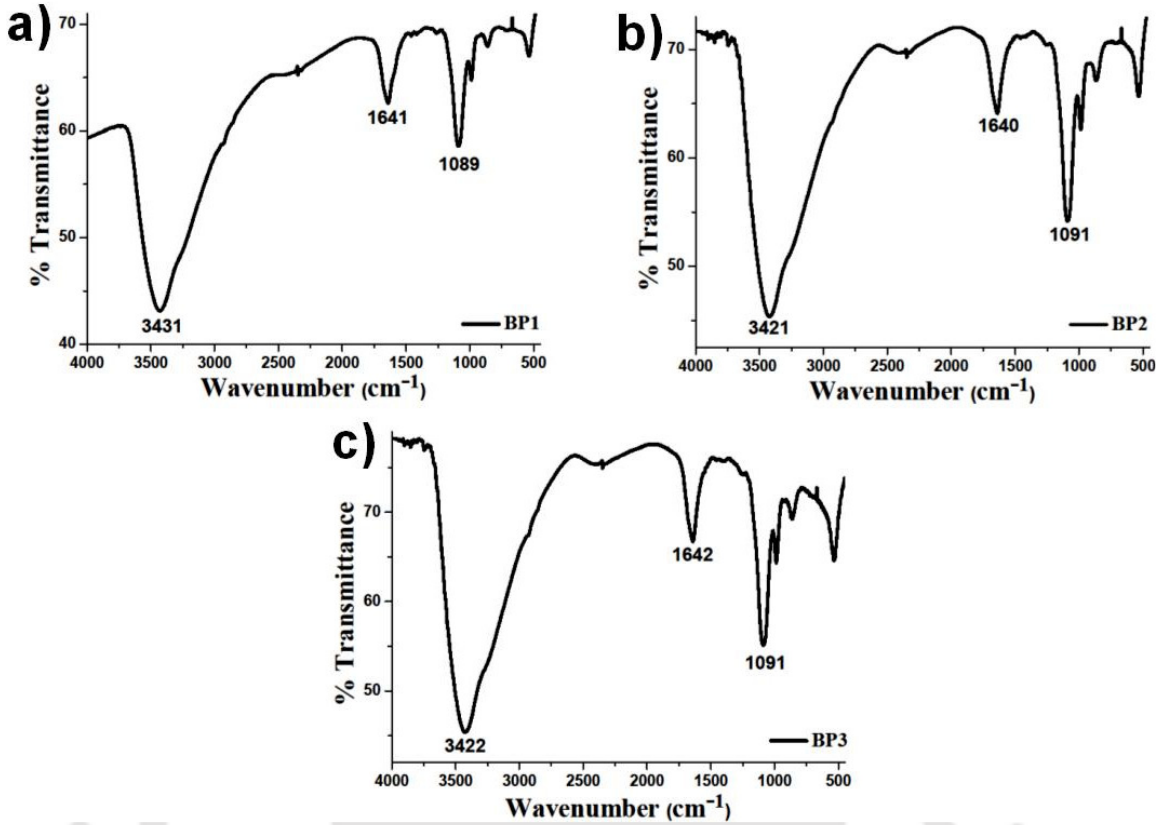

Figure 3.24. FT-IR spectra of of (a) BP1, (b) BP2, and (c) BP3. Spectra were taken after seven days of incubation. All the peptide solutions were incubated in PBS pH 7.4 (50 mM) at 37 °C.

3.2.6.3. Transmission electron microscopy (TEM) and Congo-Red stained Green gold birefringence studies:

TEM is a widely used microscopic technique for structural analysis of fibrils. This technique is used to probe the shape of fibrils formed from any class of aggregating peptides.[11-12,14]

As Congo-Red specifically binds against β-pleated sheet conformation of amyloid, fibrils stained with Congo-Red show green gold birefringence when viewed under a polarisable microscope.[11-12,14]

The fibrillogenicity and amyloidogenicity of the BPs were characterized by TEM and Congo-red stained birefringence (Figure 3.25) studies.

Any fibrillar assembly was not observed from the BPs in TEM, indicating non-fibrillar nature of the BPs. Also, any green gold birefringence was not seen for BPs when viewed under cross-polarized light after staining with Congo-Red dye. Therefore, from the above results, it was confirmed that the BPs were non-aggregating and non-amyloidogenic in nature.

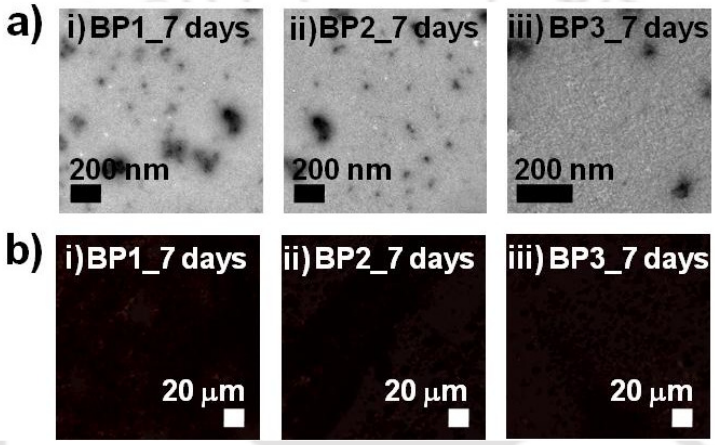

Figure 3.25. (a) TEM images, and (b) Congo-Red stained birefringence images of (i) BP1, (ii) BP2, and (iii) BP3. Images were taken after seven days of incubation in PBS pH 7.4 (50 mM) at 37 °C. Scale bar is indicated as 200 nm for TEM images and 20 μm for Congo red stained birefringence images. All the peptide solutions were incubated in PBS pH 7.4 (50 mM) at 37 °C.

3.2.7. Inhibition of amyloid fibrillar aggregates of $A\beta_{1-40}$ peptide:

To check the inhibition of amyloid fibrillar aggregates of $A\beta_{1-40}$ peptide, BPs were each co-incubated with $A\beta_{1-40}$ in PBS of pH 7.4 at 37 °C on water bath up to seven days in parallel, and the kinetics of the amyloid accumulation was monitored using various biophysical tools.[9-11]

3.2.7.1. Aβ sample preparation:

Dissolving required amount of $A\beta_{1-40}$ in 20 µL of TFA, disaggregated $A\beta_{1-40}$.was obtained. Using nitrogen gas, TFA was evaporated. For complete removal of TFA, HFIP was added, then evaporated using nitrogen gas to get disaggregated $A\beta_{1-40}$ peptide repeating this process twice. 2.0 ml of PBS (50 mM, pH 7.4) was added into the disaggregated material, followed by sonication and vortex to obtain transparent solution. The total solution was divided equally (as required) followed by addition of 800 µL of PBS to each portion and finally soluble $A\beta_{1-40}$ with concentration of 50 µM was obtained.

3.2.7.2. Thioflavin T (ThT) fluorescence assay of $A\beta_{1-40}$:

The kinetics of amyloid formation of $A\beta_{1-40}$ peptide was assessed by ThT fluorescence assay. It is reported that ThT exhibits enhanced fluorescence upon binding to amyloid fibrils, and fluorescence emission intensity is directly proportional to the amount of fibrils present in that solution. Thioflavin T (ThT) stock solution was prepared at a concentration of 50 µM in PBS (50 mM, pH 7.4) and stored at 4 °C with proper protection from light to prevent quenching. Lyophilized solid peptide samples were dissolved in PBS (50 mM, pH 7.4) individually to obtain stock solution of variable concentrations (50 µM of $A\beta_{1-40}$ and different molar ratios of designed peptides) and incubated at 37 °C over water bath. At different time intervals, 40 µL of peptide sample was taken out from the stock solution and

was mixed with 200 µL of ThT solution (50 mM); total volume of was made up to 400 µL with PBS (50 mM, pH 7.4) with which the fluorescence study was performed. Three different replicate solution sets were prepared for study. For ThT fluorescence assay, a slit of 5 nm.was used, emission was measured at 485 nm and excitation at 440 nm. Text file was taken from the instrument and graph was plotted using OriginPro 8 software. Three different replicate solution sets were scanned individually for each data point, from which an average was taken with observed standard deviation.

From the ThT assay, we observed that (Figure 3.26) in the absence of BP1, $A\beta_{1-40}$ peptide (black) was found aggregated with time as indicated by the time-dependent increase of the fluorescence intensity but became static after four days. On the other hand, in the presence of one-fold (red) and five-fold (blue) molar excess of BP1, the fluorescence intensity was suppressed significantly with time indicating the decreased amount of amyloid in the solution probably due to the formation of *in-situ* side-chain peptide cyclization as described earlier. Above mentioned results indicate the dose-dependent inhibiting capability of BP1.

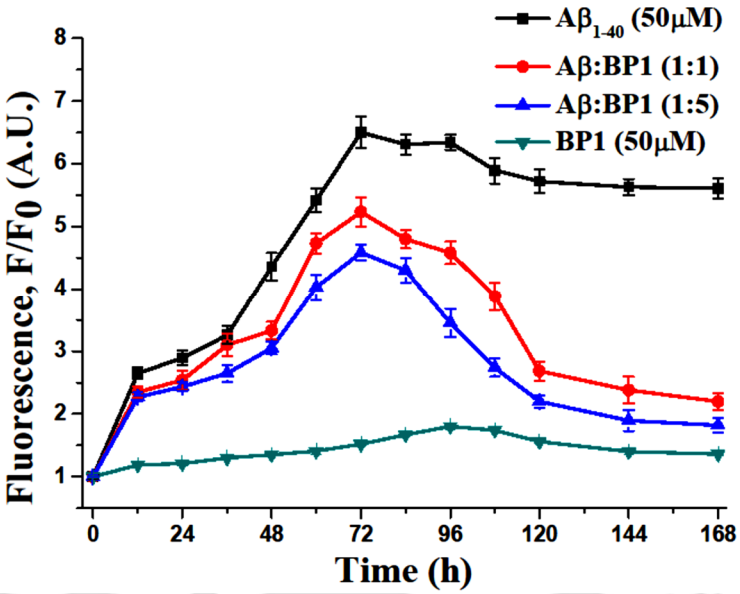

Figure 3.26. Th.T. fluorescence assay of Aβ1-40 in the presence of BP1. The spectra of Aβ1-40 in the absence (black), and presence of one-fold molar excess of BP1 (red), five-fold molar excess of BP1 (blue), and BP1 alone (dark cyan). Error bars represent the standard deviation of measurements from at least three replicate solutions. All the peptide solutions were incubated in PBS pH 7.4 (50 mM) at 37 °C.

At first, the fluorescence intensity increased with time when only Aβ1-40 peptide was present in the solution. But in the presence of one-fold (red) and five-fold (blue) molar excess of BP2 (Figure 3.27), the intensity of fluorescence of the Aβ1-40 solution decreased. The decrease in fluorescence signal indicates the reduction of fibrillary mass. This implied that the inhibition of aggregation of Aβ1-40 occurred probably due to the formation of *in-situ* side-chain peptide cyclization as described earlier. From the above results, it was concluded that BP2 significantly inhibited the amyloid formation of the Aβ1-40 peptide in a dose-dependent manner.

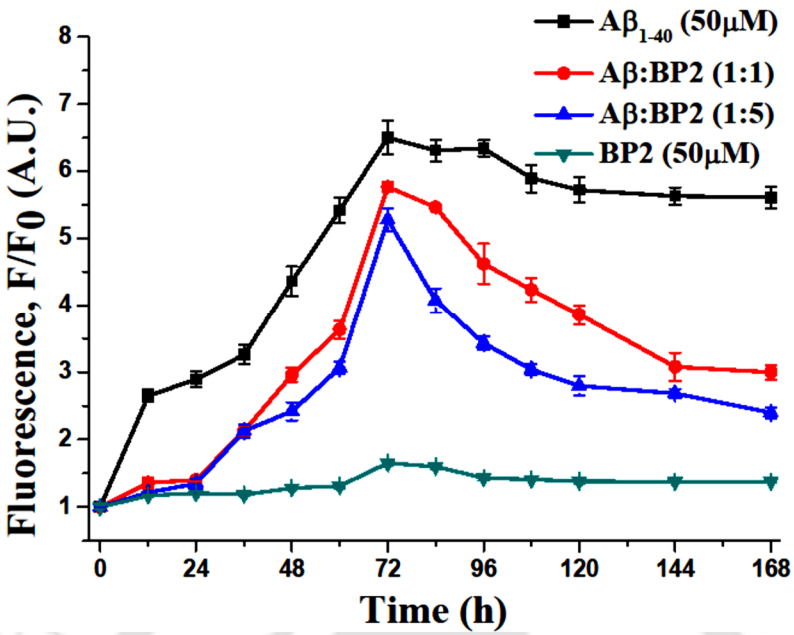

Figure 3.27. Th.T. fluorescence assay of $A\beta_{1-40}$ in the presence of BP2. The spectra of $A\beta_{1-40}$ in the absence (black), and presence of one-fold molar excess of BP2 (red), five-fold molar excess of BP2 (blue), and BP2 alone (dark cyan). Error bars represent the standard deviation of measurements from at least three replicate solutions. All the peptide solutions were incubated in PBS pH 7.4 (50 mM) at 37 °C.

We observed an increment of fluorescence intensity for $A\beta_{1-40}$ peptide when incubated alone. But when one-fold (red) and a five-fold (blue) molar excess of BP3 (Figure 3.28) were added, it was found that fluorescence was suppressed noticeably with time. The decrease in fluorescence signal was due to inhibition of aggregation of $A\beta_{1-40}$ peptide. The formation of *in-situ* side-chain peptide cyclization may be the cause of inhibition. From the above results, the dose-dependent inhibiting capability of BP3 was confirmed.

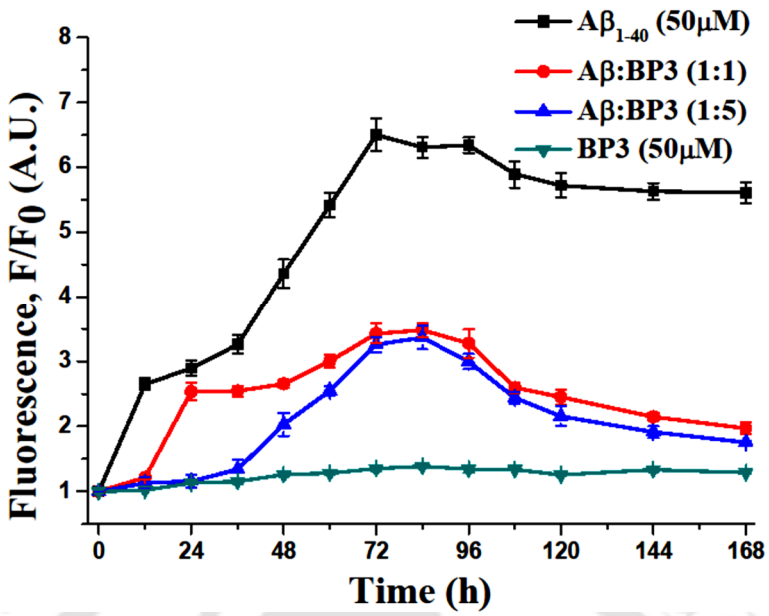

Figure 3.28. Th.T. fluorescence assay of Aβ1-40 in the presence of BP3. The spectra of Aβ1-40 in the absence (black), and presence of one-fold molar excess of BP3 (red), five-fold molar excess of BP3 (blue), and BP3 alone (dark cyan). Error bars represent the standard deviation of measurements from at least three replicate solutions. All the peptide solutions were incubated in PBS pH 7.4 (50 mM) at 37 °C.

3.2.7.3. Comparative Th.T. fluorescence assay of Aβ1-40:

It was found that the fluorescence intensity of Aβ1-40 peptide (black) was increased with time in the absence of BPs and became static after four days. But in the presence of one-fold (Figure 3.29) and five-fold (Figure 3.30) molar excess of BPs, a significant decrease in fluorescence signal of Aβ1-40 peptide was observed probably due to the formation of *in-situ* side-chain peptide cyclization as described earlier. From the results, the dose-dependent inhibiting capability of BPs was confirmed, and five-fold BP3 has shown the best result among all.

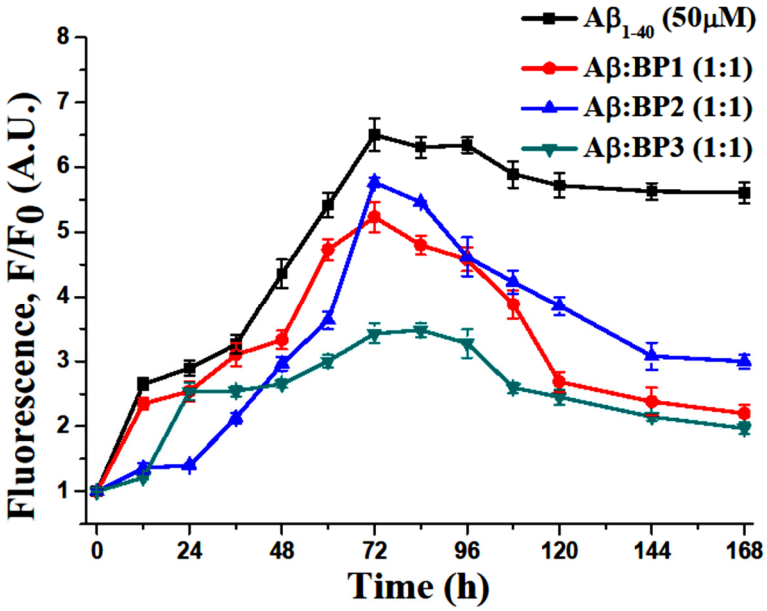

Figure 3.29. Comparative Th.T. fluorescence assay of Aβ1-40 along with one-fold molar excess of BPs. The spectra of Aβ1-40 in the absence (black), and presence of BP1 (red), BP2 (blue), and BP3 (dark cyan). Error bars represent the standard deviation of measurements from at least three replicate solutions. All the peptide solutions were incubated in PBS pH 7.4 (50 mM) at 37 °C.

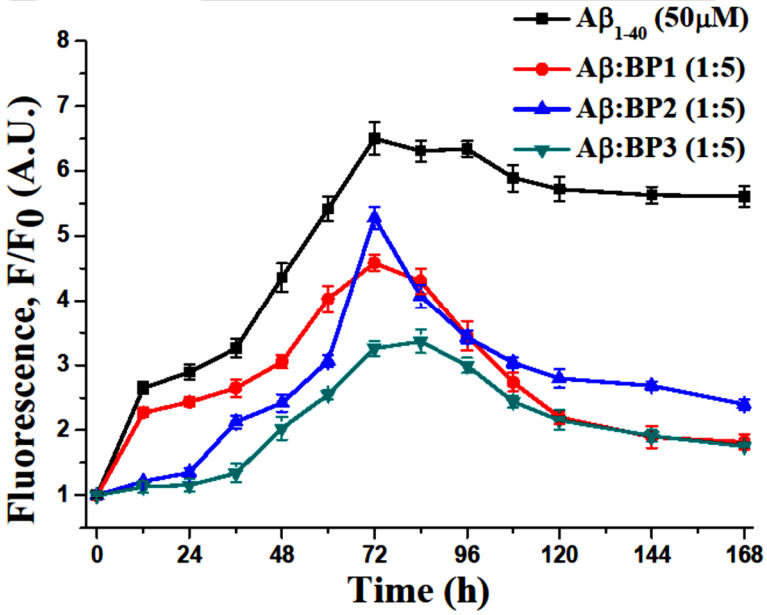

Figure 3.30. Comparative Th.T. fluorescence assay of Aβ1-40 along with five-fold molar excess of BPs. The spectra of Aβ1-40 in the absence (black), and presence of BP1 (red), BP2 (blue), and BP3 (dark cyan). Error bars represent the standard deviation of measurements from at least three replicate solutions. All the peptide solutions were incubated in PBS pH 7.4 (50 mM) at 37 °C.

3.2.7.4. CD spectra of $A\beta_{1-40}$:

The conformation of the peptides was monitored by CD spectroscopy. For CD study, stock solution was diluted with respective buffer solution to obtain final concentration of 100 µM. 200 µL of the sample was taken in a cuvette of 10 mm path length having bandwidth of 1 mm and spectra were recorded as an average of three measurements, from 190 nm to 260 nm. The β-sheet structure of $A\beta_{1-40}$ peptide was confirmed from a negative band at 214 nm and a positive one at 195 nm after seven days of incubation in PBS of pH 7.4 (50 mM) at 37 °C. But when $A\beta_{1-40}$ was incubated with one-fold BP1 (Figure 3.31), a random coil structure (a negative band at 203 nm) was obtained. When $A\beta_{1-40}$ was incubated with five-fold BP1 (Figure 3.31), a mixture of a predominantly random coil and β-turn structure (a negative band at 198 nm and a positive band at 216 nm) was obtained.

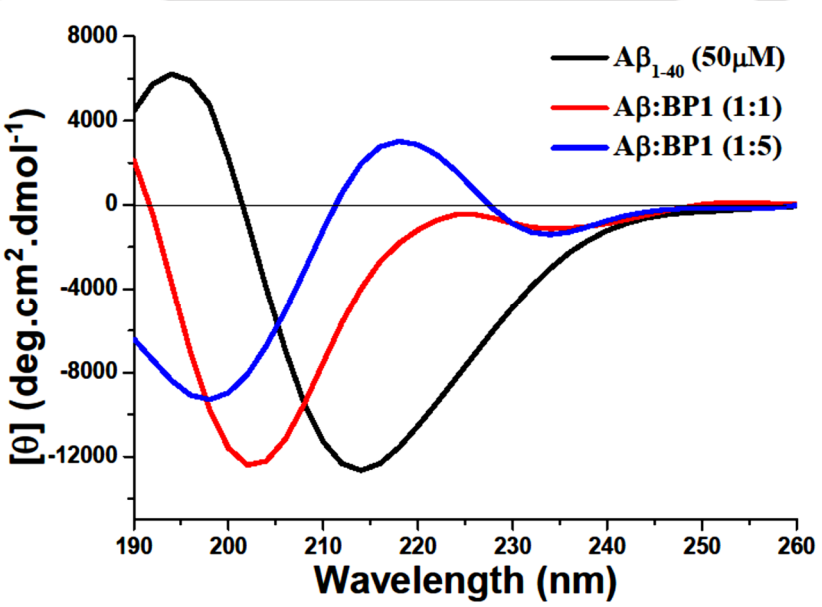

Figure 3.31. CD spectra of $A\beta_{1-40}$ in the presence of BP1. The spectra of $A\beta_{1-40}$ in the absence (black) and the presence of one-fold molar excess of BP1 (red) and five-fold molar excess of BP1 (blue). All the peptide solutions were incubated in PBS pH 7.4 (50 mM) at 37 °C.

The β-sheet structure of $A\beta_{1-40}$ peptide was converted to a random coil structure (a negative band at 206 nm) when co-incubated with one-fold BP2 (Figure 3.32). But when $A\beta_{1-40}$ was

co-incubated with five-fold BP2 (Figure 3.32), a mixture of a predominantly random coil and helix structure (two negative bands at 204 nm and 228 nm) was obtained.

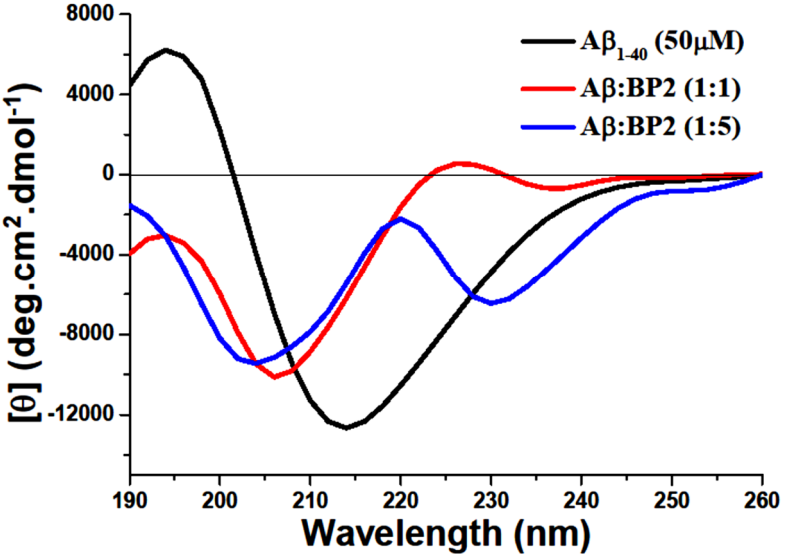

Figure 3.32. CD spectra of $A\beta_{1-40}$ in the presence of BP2. The spectra of $A\beta_{1-40}$ in the absence (black) and the presence of one-fold molar excess of BP2 (red) and five-fold molar excess of BP2 (blue). All the peptide solutions were incubated in PBS pH 7.4 (50 mM) at 37 °C.

When $A\beta_{1-40}$ was co-incubated with (Figure 3.33) one-fold BP3, the β-sheet structure of $A\beta_{1-40}$ peptide was altered to a mixture of α-helix and random coil structure (two negative bands at 205 nm and 226 nm). But when $A\beta_{1-40}$ was co-incubated with five-fold BP3, predominantly a random coil structure (a negative band at 190 nm) was obtained.

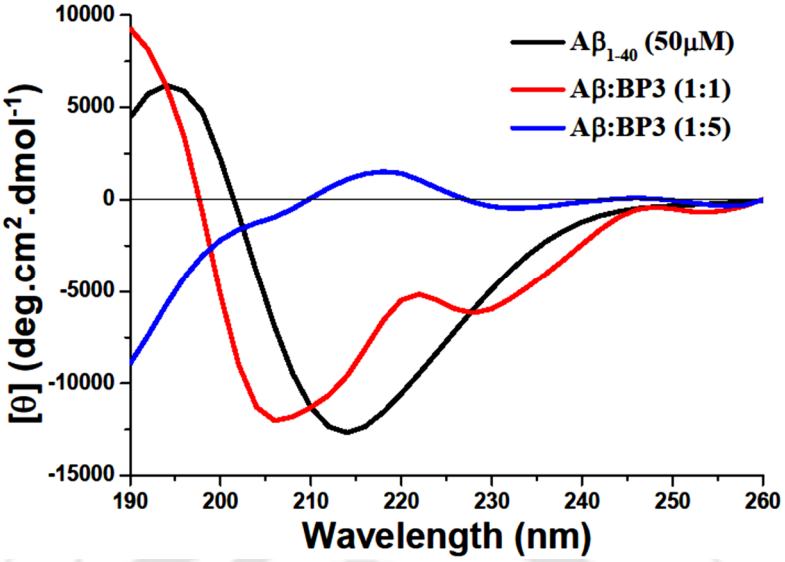

Figure 3.33. CD spectra of Aβ1-40 in the presence of BP3. The spectra of Aβ1-40 in the absence (black) and the presence of one-fold molar excess of BP3 (red) and five-fold molar excess of BP3 (blue). All the peptide solutions were incubated in PBS pH 7.4 (50 mM) at 37 °C.

3.2.7.5. FT-IR spectra of Aβ1-40:

Peptide stock solution prepared for ThT fluorescence assay can be used for FT-IR analysis. To prepare pellets, from the stock 20 µL of the sample was taken after required time of incubation, mixed with KBr and dried completely at 50 ℃. Background scan was subtracted, graphs were plotted from text files using OriginPro 8 software to get final spectra.

Initially, at 0h, a characteristic β-sheet profile was not observed for Aβ1-40 peptide. But after seven days of incubation in PBS of pH 7.4 (50 mM) at 37 °C (Figure 3.34), peak at 1634 cm^{-1} indicated the strong β-sheet structure for Aβ1-40. The peak at 1641 cm^{-1} and 1647 cm^{-1} indicated the random coil structure for Aβ1-40 along with one-fold molar excess of BP1 and five-fold molar excess of BP1, respectively. For BP2 and BP3 (Figure 3.35), the same result as BP1 was noticed when incubated along with Aβ1-40 peptide.

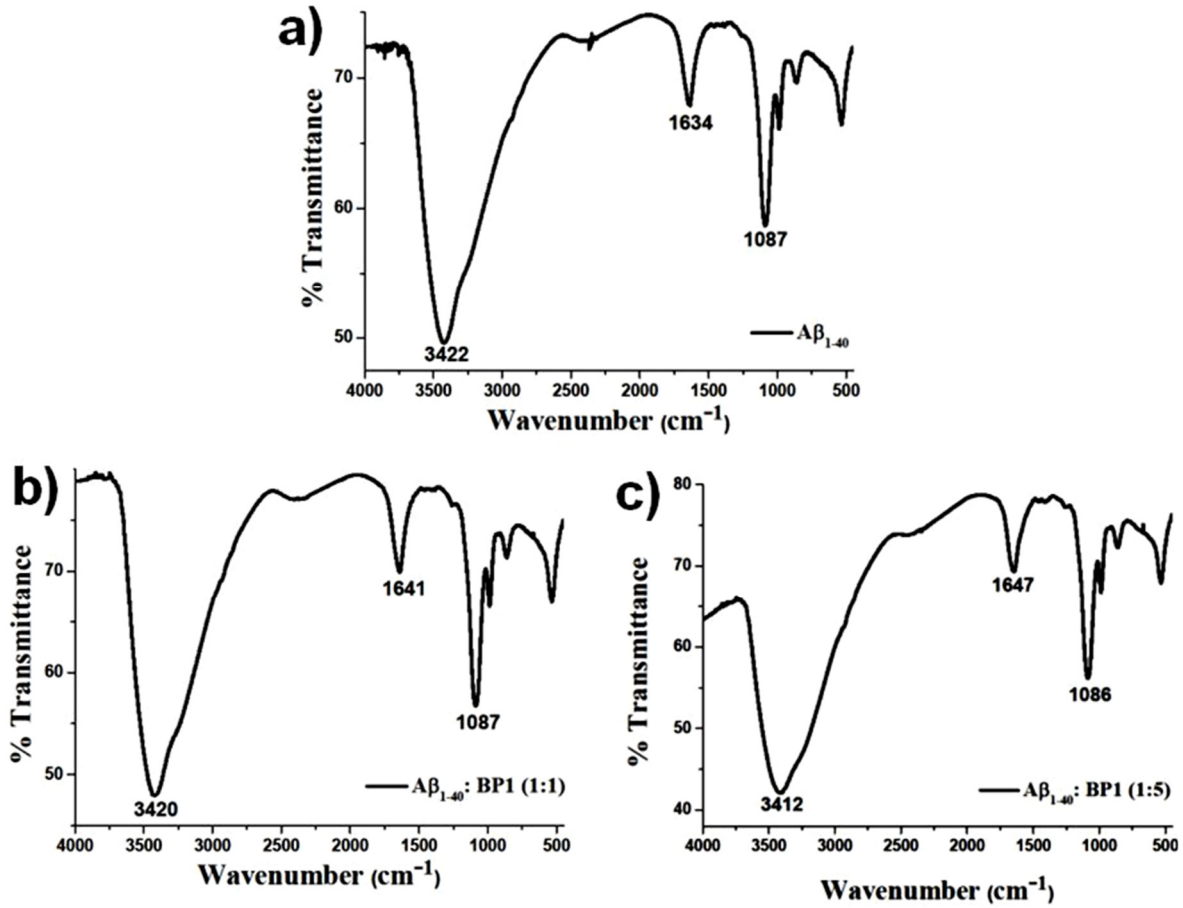

Figure 3.34. FT-IR spectra of (a) Aβ1-40 in absence and presence of (b) 1 fold molar excess of BP1 and (c) 5 fold molar excess of BP1 respectively. Spectra were taken after seven days of incubation in PBS pH 7.4 (50 mM) at 37 °C.

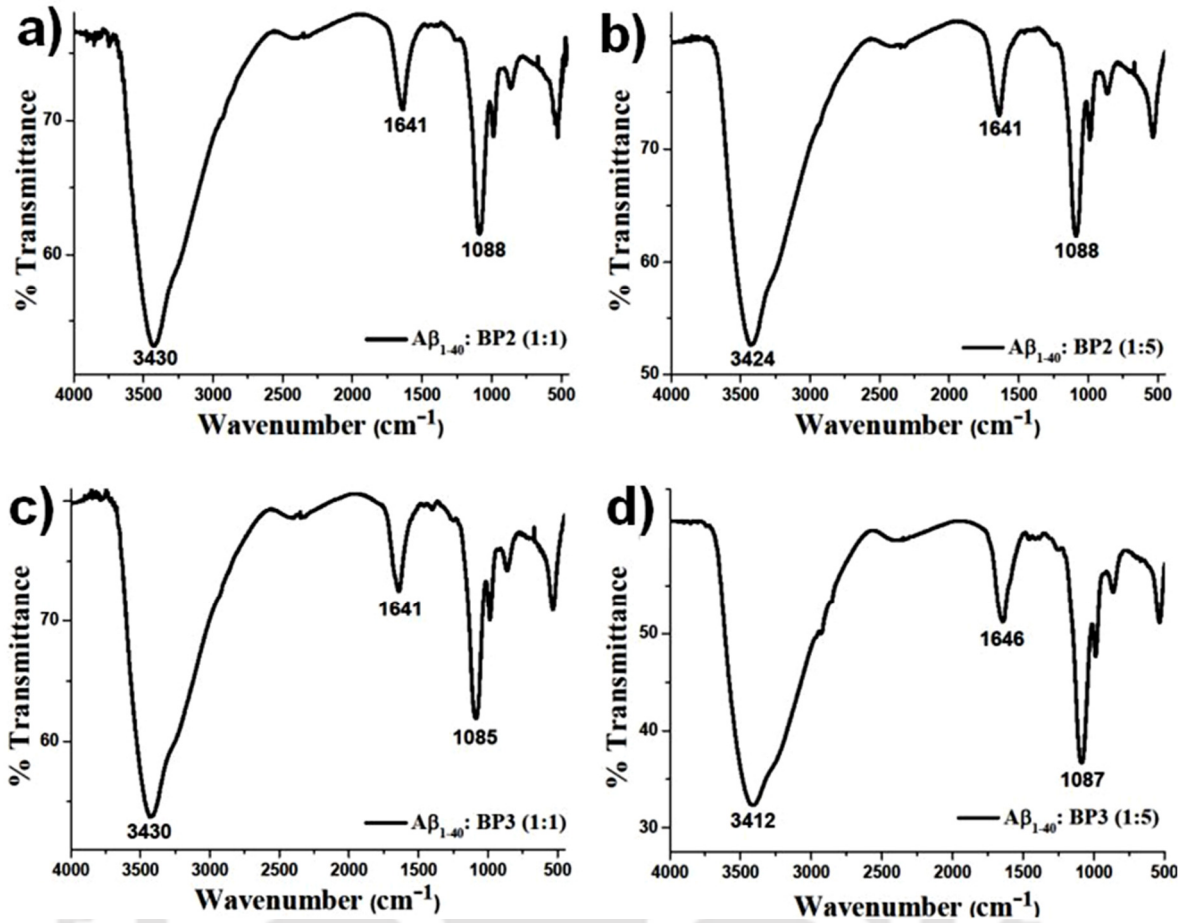

Figure 3.35. FT-IR spectra of $A\beta_{1-40}$ in the presence of (a) one-fold molar excess of BP2, (b) five-fold molar excess of BP2, (c) one-fold molar excess of BP3, and (d) five-fold molar excess of BP3 respectively. Spectra were taken after seven days of incubation.

3.2.7.6. TEM and Green gold birefringence studies:

The presence of fibrillar structure under TEM is a characteristic property of amyloid formed by a peptide. For TEM analyses, 10 µL aliquot was taken out from the seven days incubated stock solution. Over a carbon coated copper grid, aliquot was added, allowed to float for 1 min, then for negative staining 10 µL of 2 % uranyl acetate solution was added. The droplet on grid was allowed to stand for 1 min before removing excess solution by blotting paper and was air-dried at room temperature. Then grid was kept in desiccators and examined at 200 kV under TEM.

It was observed that (Figure 3.36), the $A\beta_{1-40}$ peptide alone exhibited clear fibrillar structure when viewed under TEM after seven days of incubation in PBS of pH 7.4 (50 mM) at 37 °C. But BPs of different molar ratios, along with $A\beta_{1-40}$ peptide, exhibited no such characteristic fibrillar assembly when viewed under TEM at the same time.

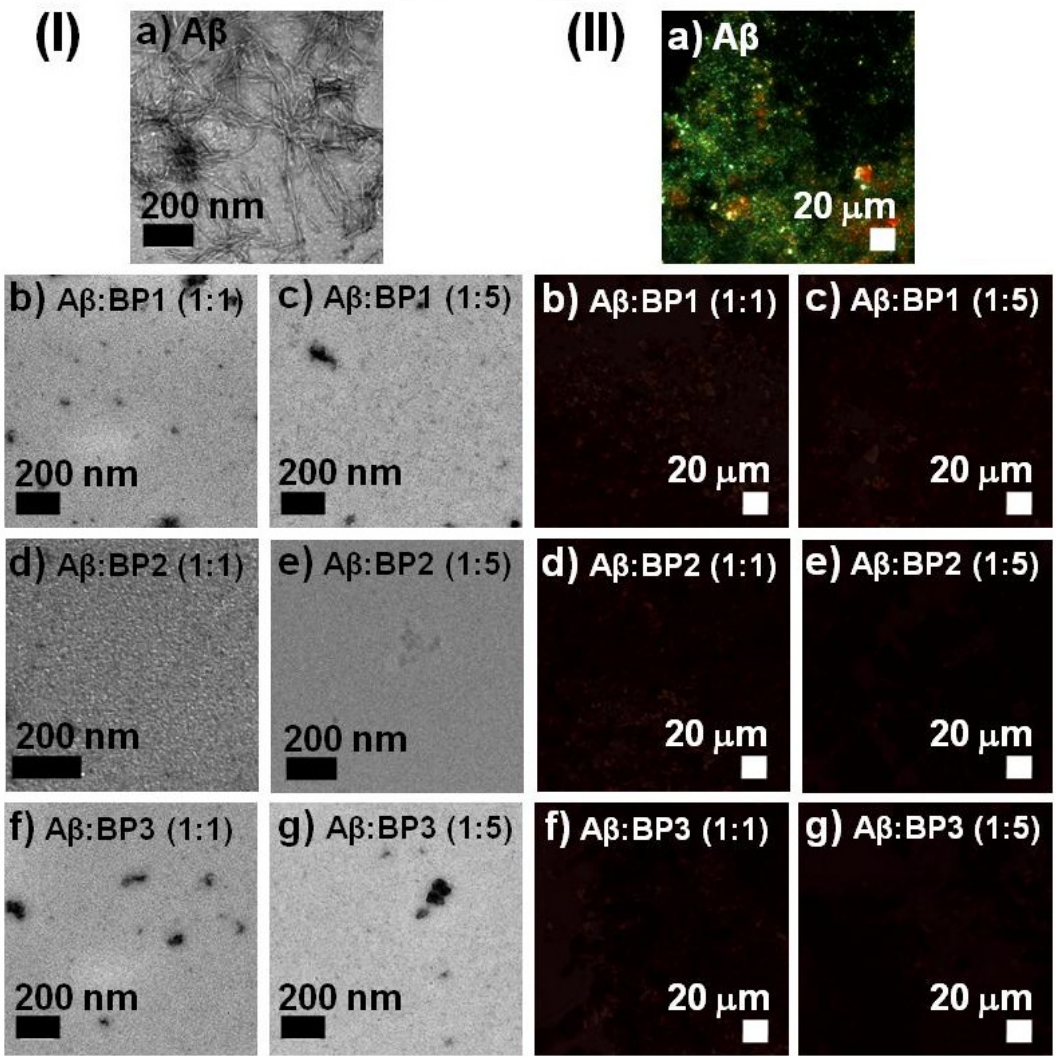

Figure 3.36. (I) TEM images and (II) Congo-Red stained birefringence images of (a) $A\beta_{1-40}$ in the absence, and presence of (b) one-fold molar excess of BP1, (c) five-fold molar excess of BP1, (d) one-fold molar excess of BP2, (e) five-fold molar excess of BP2, (f) one-fold molar excess of BP3, and (g) five-fold molar excess of BP3. Images were taken after 7 days of incubation in PBS pH 7.4 (50 mM) at 37 °C. Scale bar is indicated as 200 nm for TEM images and 20 μm for Congo red stained birefringence images. All the peptide solutions were incubated in PBS pH 7.4 (50 mM) at 37 °C.

Commercially available Congo red was added in 80 % aqueous ethanol until it becomes a saturated solution, then saturated sodium chloride solution was added into it, stirred and filtered to prepare final working solution for analysis. The peptide stock solution prepared for thioflavin T experiment can be used for birefringence studies. Taking 20 µL aliquot of the peptide solution from the stock at different time intervals was added on a glass slide, then 40 µL of the saturated Congo red solution was added over it and was allowed to dry. After removing the excess solution by blotting paper, the sample was dried at room temperature before keeping it in desiccators.

Clear green gold birefringence was observed (Figure 3.36)in the case of $A\beta_{1-40}$ alone under cross-polarized light, but no such birefringence was noticed when incubated along with BPs.

3.2.8. Disruption of preformed amyloid fibrillar aggregates of $A\beta_{1-40}$ peptide:

During optimization (from ThT fluorescence assay during inhibition study), it was observed that the growth phase for fibrillization of $A\beta_{1-40}$ peptide was 72h. Therefore, BPs were added in one-fold, and five-fold molar excess into the preformed fibrillar assembly of $A\beta_{1-40}$ peptide just before 72h (PBS pH 7.4 at 37 °C) in parallel experiments and incubated up to 10 days. The kinetics of the amyloid accumulation was monitored using various biophysical tools.[9-11]

3.2.8.1. ThT Fluorescence assay of $A\beta_{1-40}$:

The kinetics of amyloid accumulation of preformed fibril $A\beta_{1-40}$ was quantified by the ThT fluorescence assay.

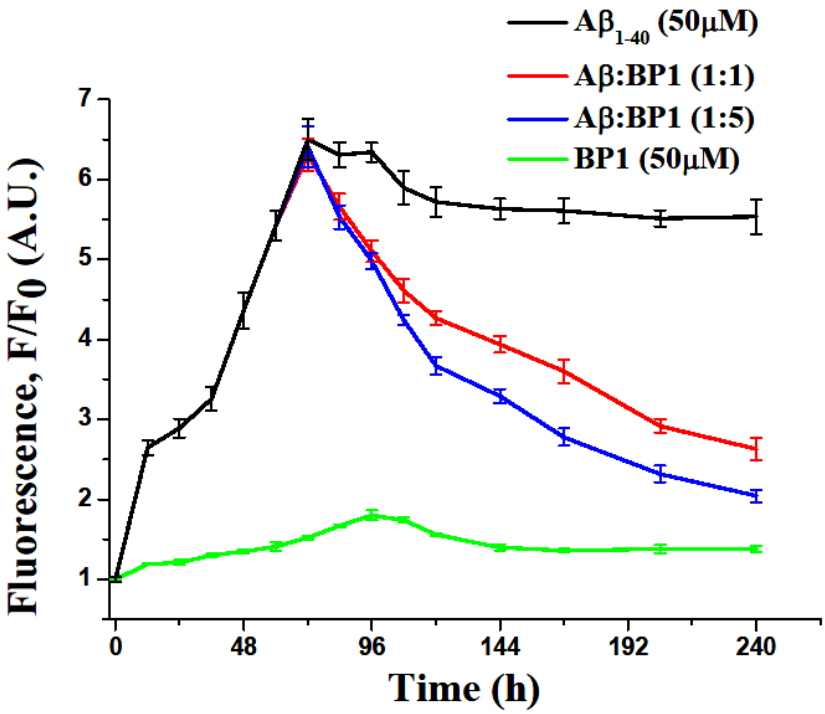

Figure 3.37. ThT Fluorescence assay of $A\beta_{1-40}$ in the presence of BP1. ThT Fluorescence spectra of $A\beta_{1-40}$ in the absence (black), and presence of one-fold molar excess of BP1 (red), five-fold molar excess of BP1 (blue), and BP1 alone(light green). Error bars represent the standard deviation of measurements from at-least three replicate solutions. All the peptide solutions were incubated in PBS pH 7.4 (50 mM) at 37 °C.

From the assay, we noticed (Figure 3.37) that in the absence of BP1, $A\beta_{1-40}$ peptide (black) became aggregated with time as depicted in the inhibition study. But, in the presence of one-fold (red) and five-fold (blue) molar excess of BP1, the fluorescence intensity decreased significantly with time, and it decreased more in the case of five-fold BP1 compare to one-fold BP1. The results confirm the dose-dependent disruption potential of BP1.

From the ThT assay, we observed (Figure 3.38) that in the presence of one-fold (red) and five-fold (blue) molar excess of BP2, the fluorescence intensity of $A\beta_{1-40}$ decreased considerably with time, and also it decreased more in the case of five-fold BP2 compare to one-fold BP2. The results indicate the dose-dependent disruption ability of BP2.

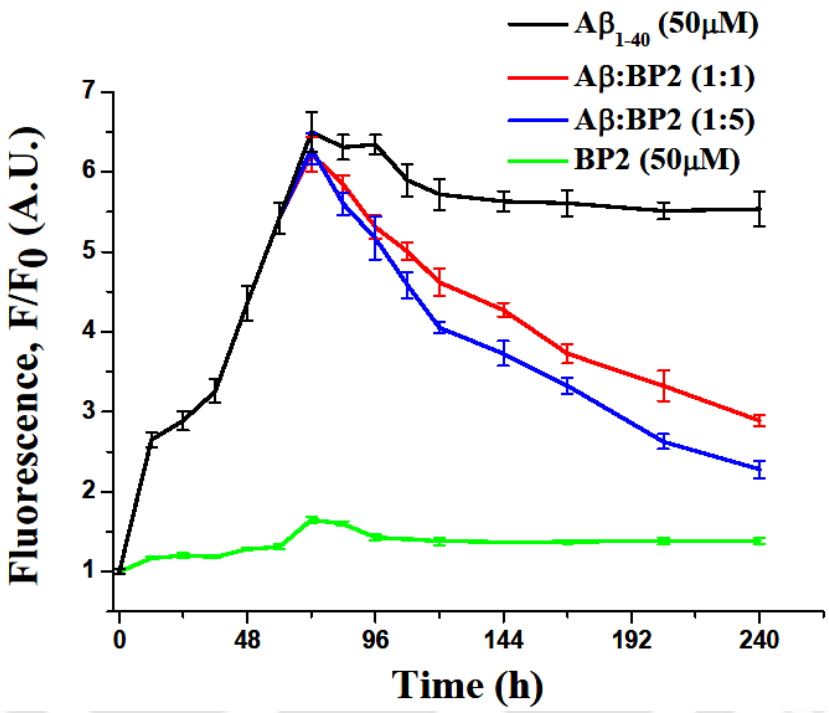

Figure 3.38. ThT Fluorescence assay of $A\beta_{1-40}$ in the presence of BP2. ThT Fluorescence spectra of $A\beta_{1-40}$ in the absence (black), and presence of one-fold molar excess of BP2 (red), five-fold molar excess of BP2 (blue), and BP2 alone(light green). Error bars represent the standard deviation of measurements from at-least three replicate solutions. All the peptide solutions were incubated in PBS pH 7.4 (50 mM) at 37 °C.

From the ThT assay, it was observed (Figure 3.39) that in the presence of one-fold (red) and five-fold (blue) molar excess of BP3, the fluorescence intensity of $A\beta_{1-40}$ decreased with time, but the result was not up to the mark according to the inhibition study. The results indicate the disruption ability of BP3 to some extent.

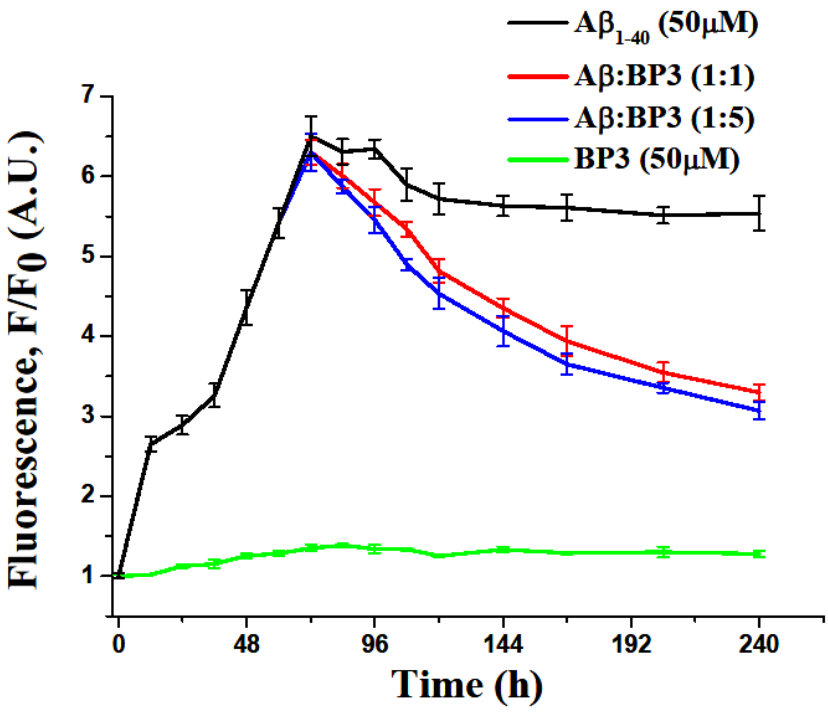

Figure 3.39. ThT Fluorescence assay of $A\beta_{1-40}$ in the presence of BP3. ThT Fluorescence spectra of $A\beta_{1-40}$ in the absence (black), and presence of one-fold molar excess of BP3 (red), five-fold molar excess of BP3 (blue), and BP3 alone(light green). Error bars represent the standard deviation of measurements from at-least three replicate solutions. All the peptide solutions were incubated in PBS pH 7.4 (50 mM) at 37 °C.

3.2.8.2. CD spectra of $A\beta_{1-40}$:

The conformation of the peptides was monitored by CD spectroscopy. After seven days of incubation, in the CD spectrum, a negative band centered at 213 nm and a positive one at 194 nm was recorded, which confirmed the β-sheet conformation of $A\beta_{1-40}$ peptide. But when $A\beta_{1-40}$ was incubated with one-fold BP1 (Figure 3.40), a lower percentage of β-sheet structure was obtained which were confirmed from the decreasing value of negative band at 218 nm. When $A\beta_{1-40}$ was incubated with five-fold BP1, a lower percentage of β-sheet structure along with β-turn structure was obtained which were confirmed from the decreasing value of negative band as well as shifting of the band from 213nm towards 225 nm.

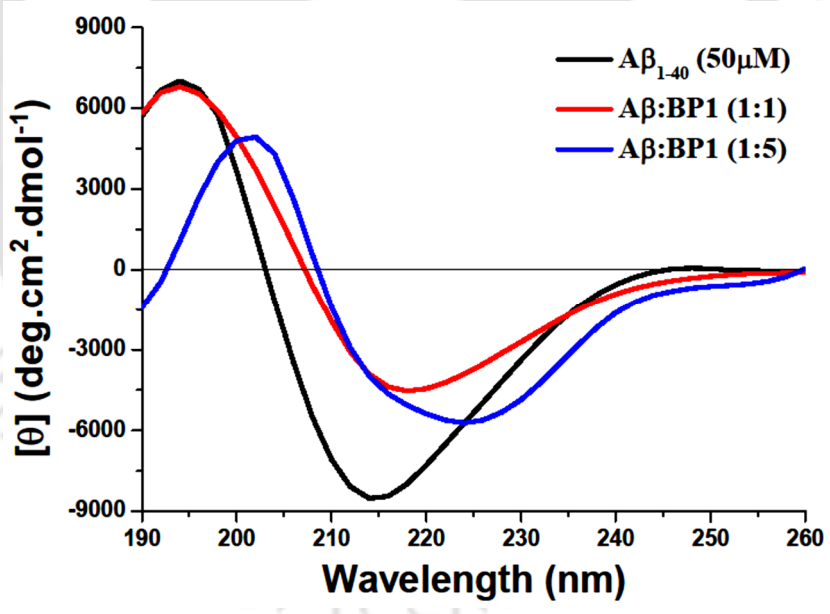

Figure 3.40. CD spectra of $A\beta_{1-40}$ in the presence of BP1. CD spectra of $A\beta_{1-40}$ in the absence (black), and presence of one-fold molar excess of BP1 (red), and five-fold molar excess of BP1 (blue). Spectra were taken after 7 (3+4) days of incubation in PBS pH 7.4 (50 mM) at 37 °C.

When $A\beta_{1-40}$ was incubated along with one-fold and five-fold molar excess of BP2 (Figure 3.41), the β-sheet content of $A\beta_{1-40}$ was reduced noticeably confirmed from the decreasing

value of negative band at 220 nm. This was a clear indication of the breaking of the β-sheet and disruption of preformed fibrillar aggregates.

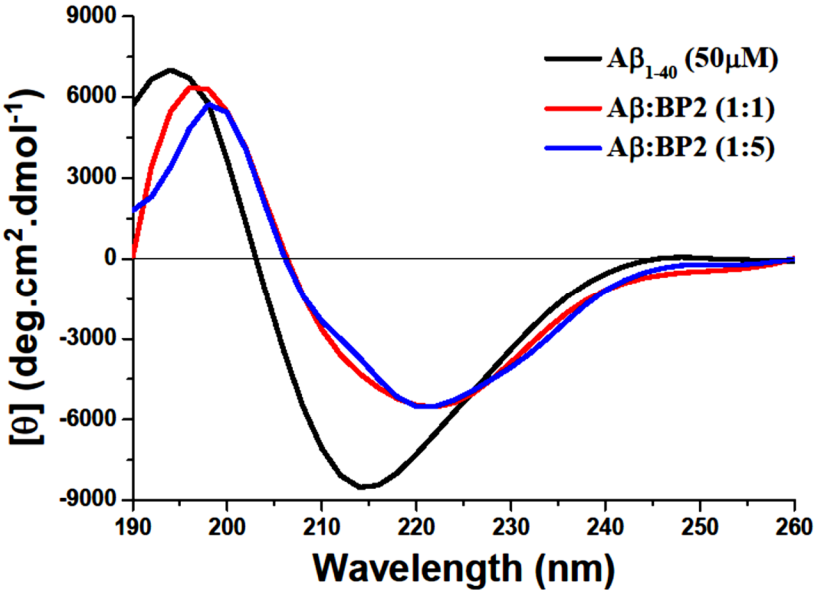

Figure 3.41. CD spectra of Aβ1-40 in the presence of BP2. CD spectra of Aβ1-40 in the absence (black), and presence of one-fold molar excess of BP2 (red), and five-fold molar excess of BP2 (blue). Spectra were taken after 7 (3+4) days of incubation in PBS pH 7.4 (50 mM) at 37 °C.

In the presence of one-fold BP3 (Figure 3.42), β-sheet contents of Aβ1-40 were reduced gradually which were confirmed from the decreasing value of negative band at 220 nm. But when Aβ1-40 was incubated with five-fold BP3, a non-β-sheet structure was obtained which were confirmed from decreasing intensity of the positive band at 195nm and shifting of the negative band from 213nm towards 224 nm. This result was an indication of breaking β-sheet which also supported the disruption of preformed fibrillar aggregation of Aβ1-40 by the BP3.

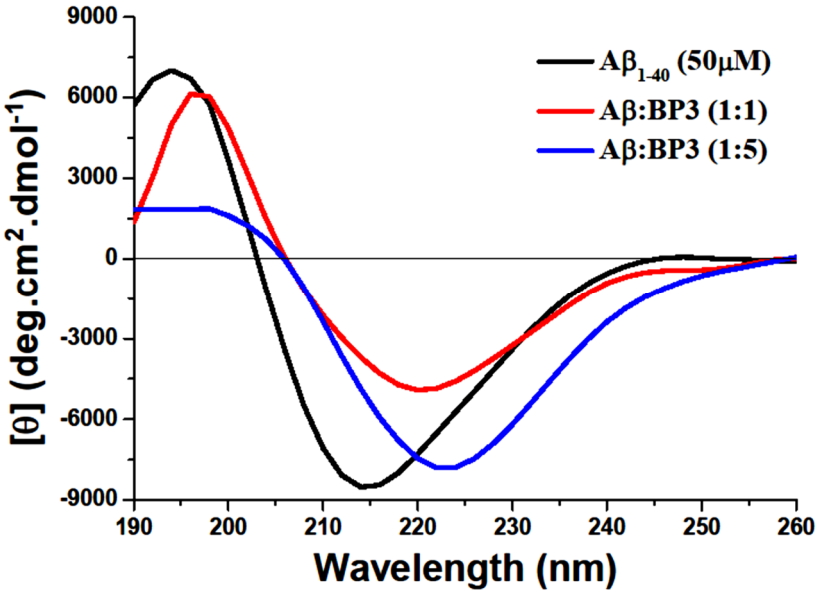

Figure 3.42. CD spectra of Aβ$_{1-40}$ in the presence of BP3. CD spectra of Aβ$_{1-40}$ in the absence (black), and presence of one-fold molar excess of BP3 (red), and a five-fold molar excess of BP3 (blue). Spectra were taken after 7 (3+4) days of incubation in PBS pH 7.4 (50 mM) at 37 °C.

3.2.8.3. FT-IR spectra of Aβ$_{1-40}$:

From the FT-IR result (Figure 3.43) of Aβ$_{1-40}$ alone, a peak at 1633 cm^{-1} was observed after seven days of incubation, indicated the strong β-sheet structure. The peak at 1643 cm^{-1} and 1640 cm^{-1} indicated the random coil structure for Aβ$_{1-40}$ along with one-fold molar excess of BP1 and five-fold molar excess of BP1 respectively.

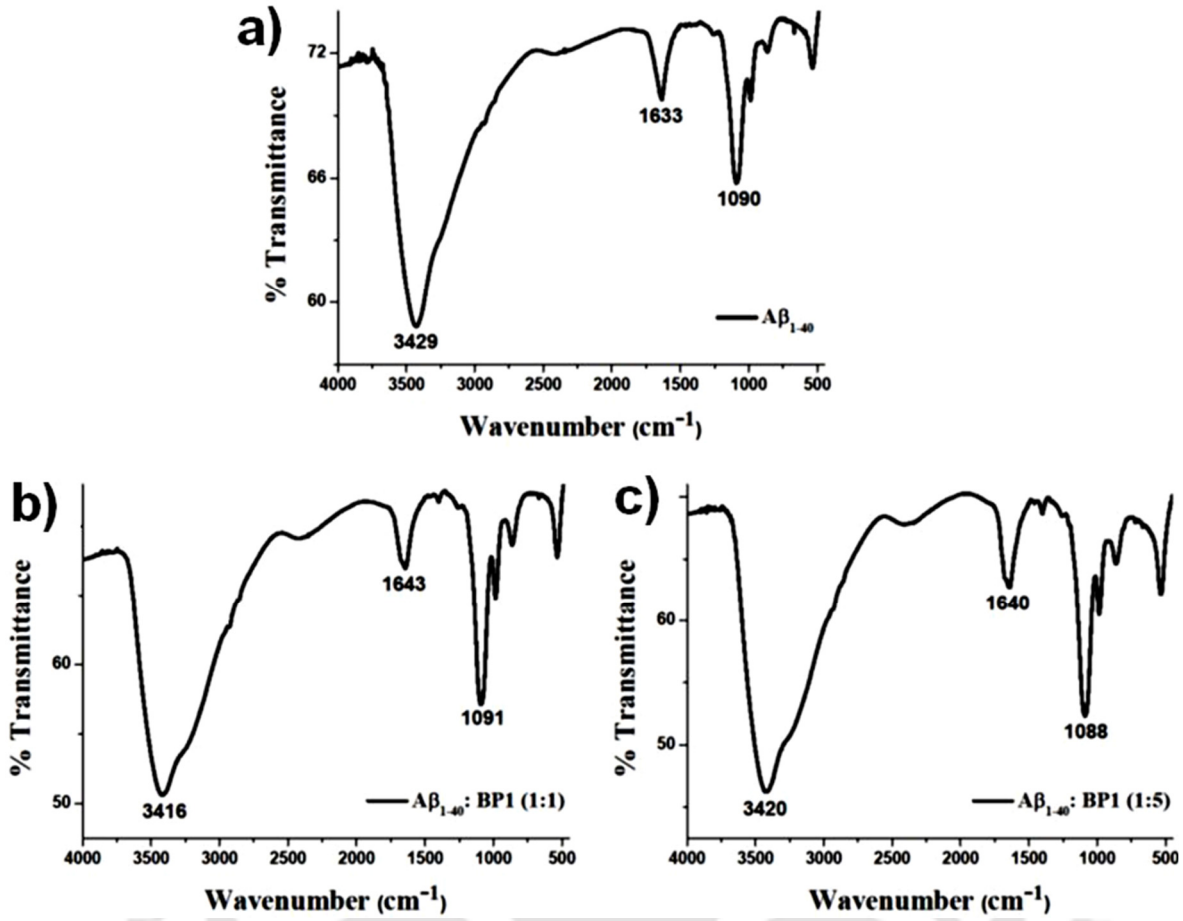

Figure 3.43. FT-IR spectra of (a) Aβ1-40 in absence and presence of (b) 1 fold molar excess of BP1 and (c) 5 fold molar excess of BP1, respectively. Spectra were taken after 7 (3+4) days of incubation in PBS pH 7.4 (50 mM) at 37 °C.

In FT-IR spectra, similar result was observed for BP2 and BP3 (Figure 3.44) as BP1 when incubated along with $A\beta_{1-40}$ peptide. The strong bands at 1640 cm^{-1} and 1642 cm^{-1} in FT-IR indicated the random coil structure for $A\beta_{1-40}$ along with one-fold molar excess of BP2 and five-fold molar excess of BP2 respectively. The peaks at 1651 cm^{-1} and 1646 cm^{-1} correspond to the random coil structure for $A\beta_{1-40}$ incubated with one-fold molar excess of BP3 and five-fold molar excess of BP3 respectively.

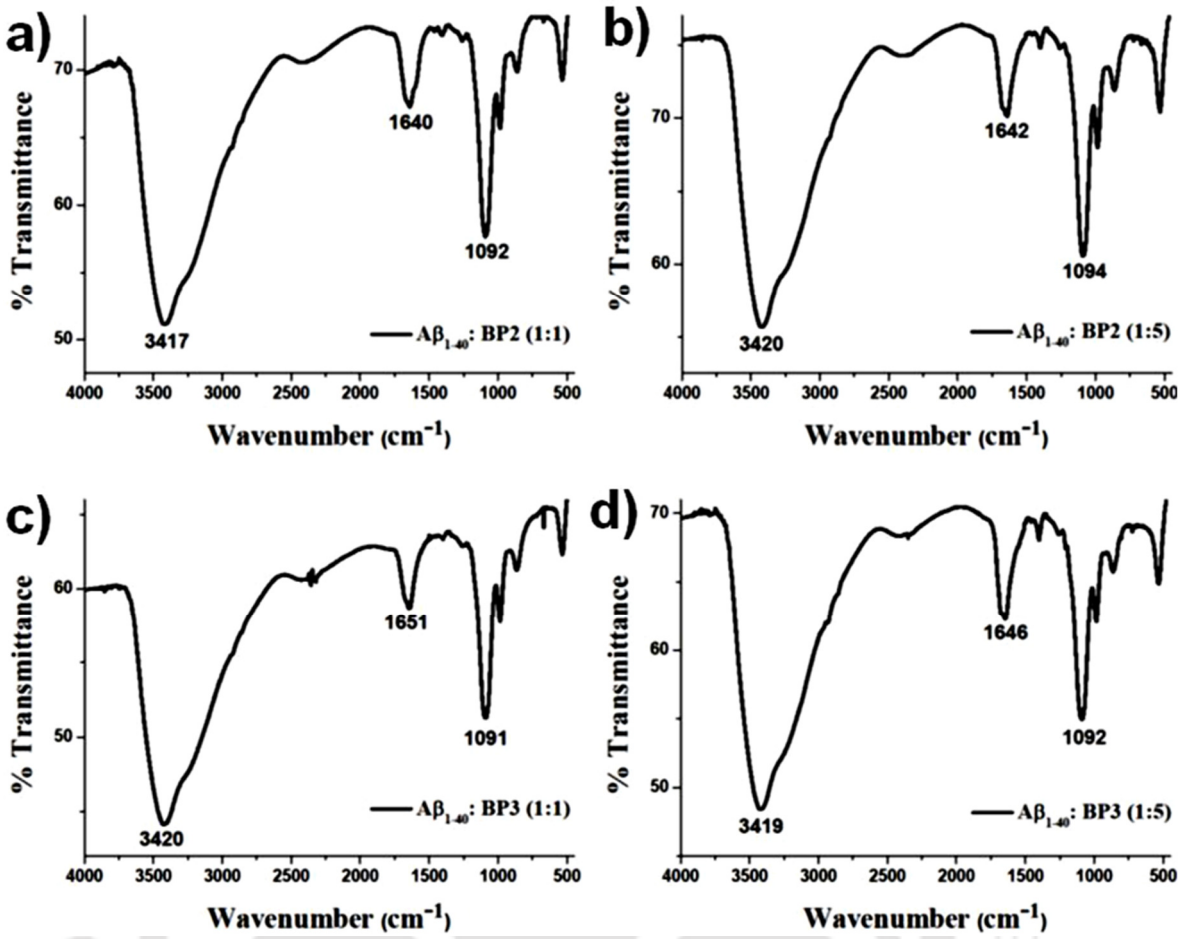

Figure 3.44. FT-IR spectra of Aβ1-40 in the presence of (a) 1 fold molar excess of BP2, (b) 5 fold molar excess of BP2, (c) 1 fold molar excess of BP3, and (d) 5 fold molar excess of BP3 respectively. Spectra were taken after 7 (3+4) days of incubation.

3.2.8.4. TEM and Congo-Red birefringence studies:

The presence of fibrillar structure under transmission electron microscopy (TEM) is a characteristic property of amyloid formed by a peptide. It was cleared that the $A\beta_{1-40}$ peptide alone exhibited clear fibrillar structure when viewed under TEM (Figure 3.45). But BPs of different molar ratios along with $A\beta_{1-40}$ peptide exhibited tiny fibres after 7 (3+4) days of incubation, but no such characteristic fibrillar assembly was observed after 10 (3+7) days when viewed under TEM. The same results were observed in the case of Congo-Red stained birefringence study (Figure 3.45) also. Clear green gold birefringence was observed

in the case of $A\beta_{1-40}$ alone under cross-polarized light, but no such birefringence was noticed when incubated along with BPs.

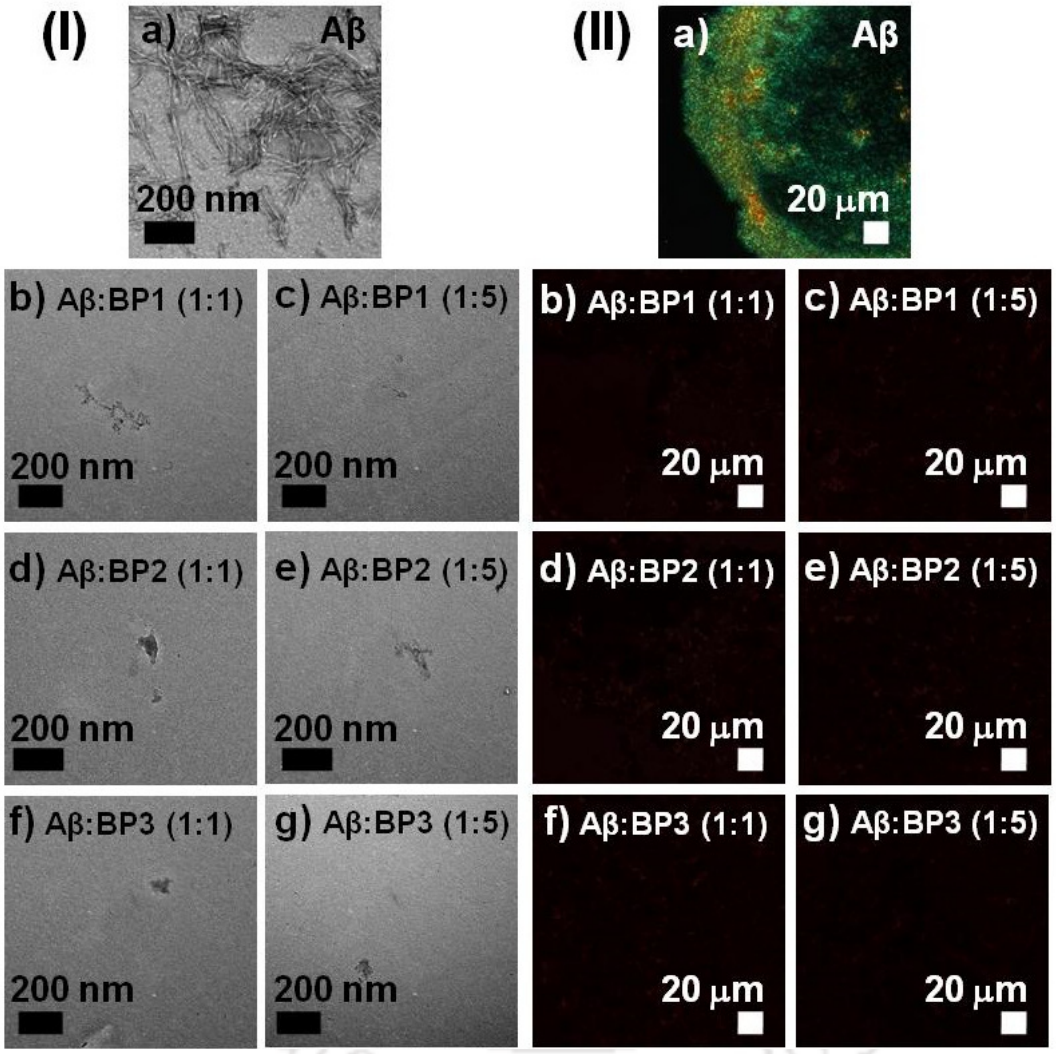

Figure 3.45. TEM images (I) and Congo-Red stained birefringence images (II) of (a) $A\beta_{1-40}$ in the absence, and presence of (b) one-fold molar excess of BP1, (c) five-fold molar excess of BP1, (d) one-fold molar excess of BP2, (e) five-fold molar excess of BP2, (f) one-fold molar excess of BP3, and (g) five-fold molar excess of BP3. Images were taken after 10 (3+7) days of incubation in PBS pH 7.4 (50 mM) at 37 °C. Scale bar is indicated as 200 nm for TEM images and 20 μm for Congo red stained birefringence images.

3.2.9. Large unilamellar vesicle (LUV) studies:

The soluble Aβ oligomers are more toxic species than the mature Aβ fibrils due to its pore formation capability on the membrane. Therfore, Carboxy-fluorescein dye entrapped vesicle leakage studies were performed to check whether our designed BPs inhibited and disrupted such amyloid fibrils to generate toxic or non-toxic metabolites where synthetic LUVs are employed as model membrane system.

3.2.9.1. LUVs preparation and carboxyfluorescein entrapment:

LUVs were prepared by mixing three different lipids, 1,2-dipalmitoyl-*sn-glycero*-3-phosphocholine (DPPC), Cholesterol and ganglioside GM1 with 68:30:2 molar ratios. Lipids were solubilized in chloroform and methanol (2:1) to prepare 2 mM stock solution in a glass vial and was dried completely under a gentle stream of nitrogen. followed by vacuum to make lipid films. The lipid films were hydrated with carboxyfluorescein dye (200 μM, 500 μL) in 50 mM HEPES buffer of pH 7.4 with vigorous vortexing for a period of 30 min to form emulsification. Following this, the glass vial was dipped into liquid nitrogen for 5 min, then frozen solution was dipped into water bath at 50-60 °C, and this entire thawing process was repeated for five times. Ultracentrifugation was done at 20000 rpm for 30 min at 10ºC to remove excess dye. Discarding supernatant dye solution, the lipid pellet was re-hydrated with 50 mM HEPES buffer of pH 7.4 with repeating twice and the final lipid pellet was obtained. After that, 500 μL of HEPES buffer of pH 7.4 was added to the lipid pellet, vortexed to obtain homogenous suspension, filtered through 0.45 μm polycarbonate membrane to get dye loaded LUVs (2 mM).

The formation of LUV was characterized by TEM (Figure 3.46. (a)) taking negatively stained sample over carbon coated copper grid using 2% uranyl acetate solution.

3.2.9.2. Vesicle leakage study:

Four sets of peptide solutions were taken for the vesicle leakage studies (Figure 3.46) along with untreated LUVs: (A) $A\beta_{1-40}$ peptide (incubated for 24 h), (B) $A\beta_{1-40}$ peptide (incubated for 10 days), (C) $A\beta_{1-40}$ peptide and BP1 (1:5, BP1 was added to the Aβ monomer and incubated for 10 days), and (D) $A\beta_{1-40}$ peptide and BP1 (1:5, BP1 was added to the preformed fibrillary aggregates after 72h and incubated for 10 days). Taking peptides and lipid in 1:20 molar ratios, the entrapped carboxyfluorescein dye release was monitored by fluorescence emission. Emission for each sample was recorded at 20 min interval up to 120 min, following 12h interval up to 72h. Emission and excitation were measured at 516 nm and 485 nm respectively, using 5 nm of band width. For complete dye release from the vesicle, 10 µL of Triton X-100 was added and the final fluorescence was measured. Untreated LUVs (natural dye leakage) were taken as control and studied.

The % dye release was calculated as,

% Leakage = {(Observed fluorescence −initial fluorescence) / (Total fluorescence –initial fluorescence)} × 100%

The graph was plotted using Origin Pro 8 software from text file, where average was taken with observed standard deviation of three independent measurements for each data point.

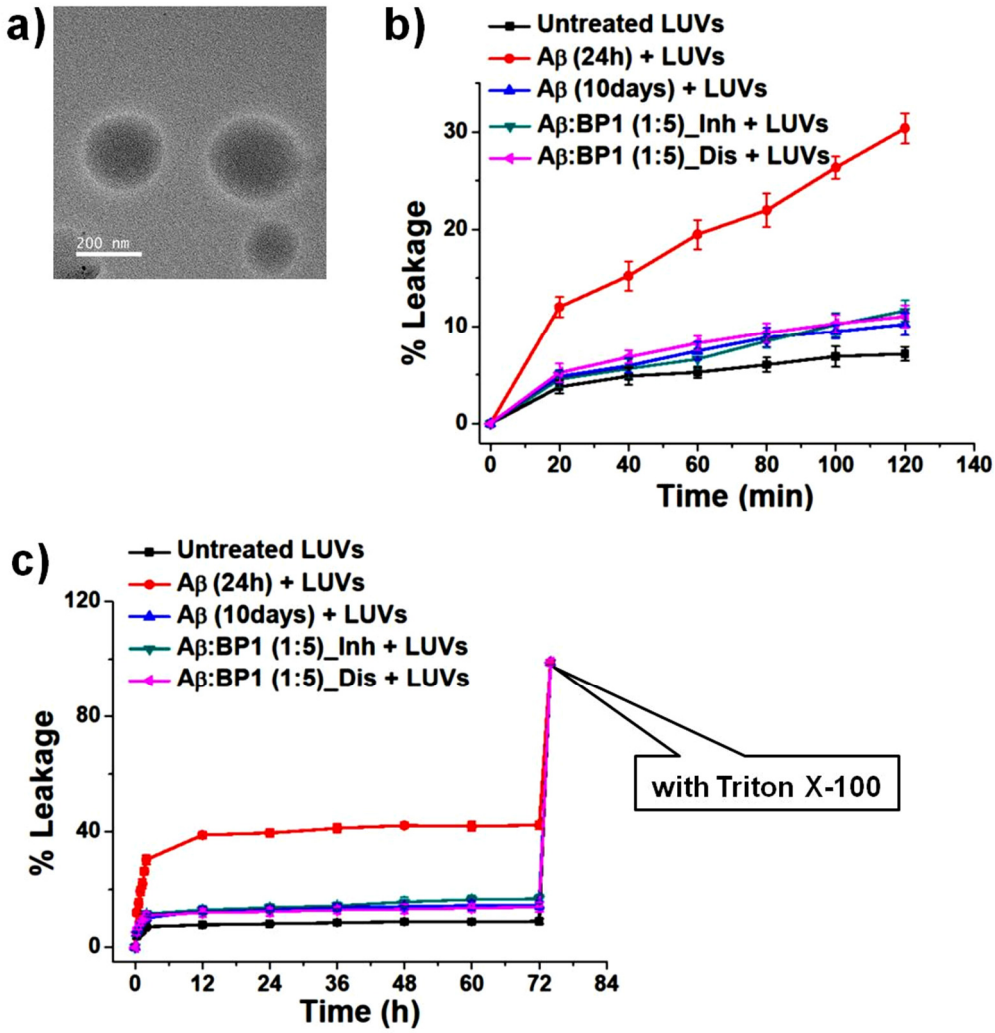

Figure 3.46. (a) TEM images of LUVs (negatively stained). % carboxyfluorescein dye leakage from LUVs (b) up to 120 min and (c) up to 72 h. % of dye leakage by untreated LUVs (black), LUVs treated with Aβ_24 h (oligomer, red), LUVs treated with Aβ_10 days (fibril, blue), LUVs treated with Aβ:BP1 (1:5)_10 days (inhibition study, dark cyan), and LUVs treated with Aβ:BP1 (1:5)_10 days (disruption study, magenta) [in the case of disruption study, BP1 was added after three days of incubation to the preformed Aβ1-40 fibril]. Error bars represent standard deviations of at least three independent measurements.

A negligible percent of dye leakage for $A\beta_{1-40}$ peptide was observed when treated with BP1 in comparison to that of the oligomeric $A\beta_{1-40}$ peptide which was incubated alone for 24h. The results confirmed that BP1 inhibited and disrupted the fibrillar amyloid of $A\beta_{1-40}$ peptide aggregates into non-toxic metabolites.

3.3. Conclusion:

Inhibition and disruption of amyloid is a promising therapeutic approach against AD and related disorders. In this work, we have introduced *in-situ* side-chain peptide cyclization as a β-sheet breaker strategy. We have demonstrated that the breaker peptides (BPs) were non-amyloidogenic in nature at physiological conditions (pH 7.4 and 37 °C). All the results suggest that BPs inhibited the accumulation of $A\beta_{1-40}$ as well as disrupted the preformed fibril of aggregated $A\beta_{1-40}$ peptide significantly. Therefore it can be concluded that the designed BPs may be used as a therapeutic agent against AD and associated disorders after performing the corresponding physiological relevance.

3.4. Characterization Data:

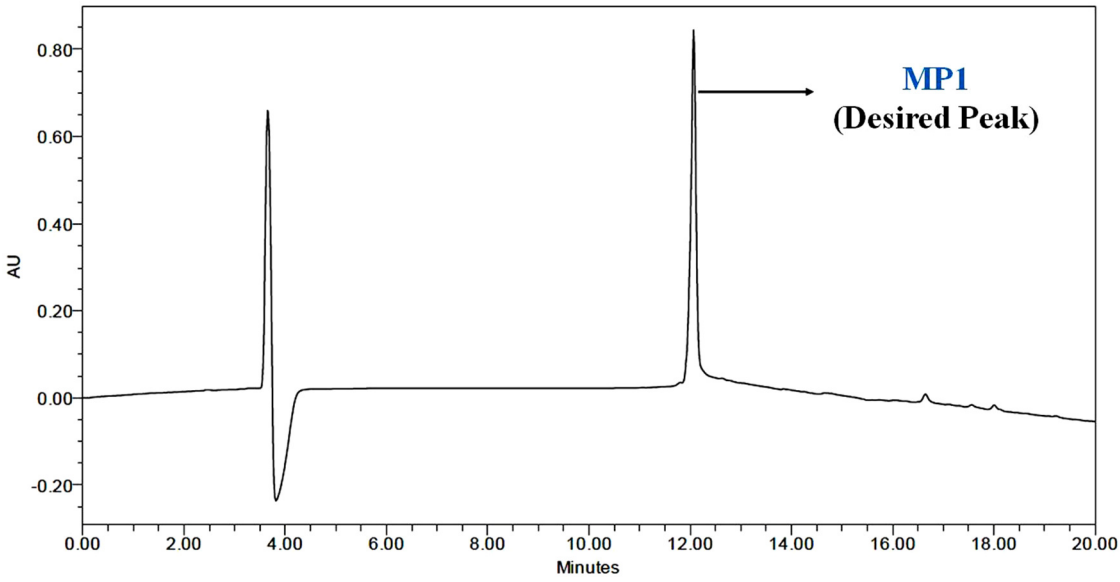

Figure 3.47. HPLC profile picture of the purified peptide MP1.

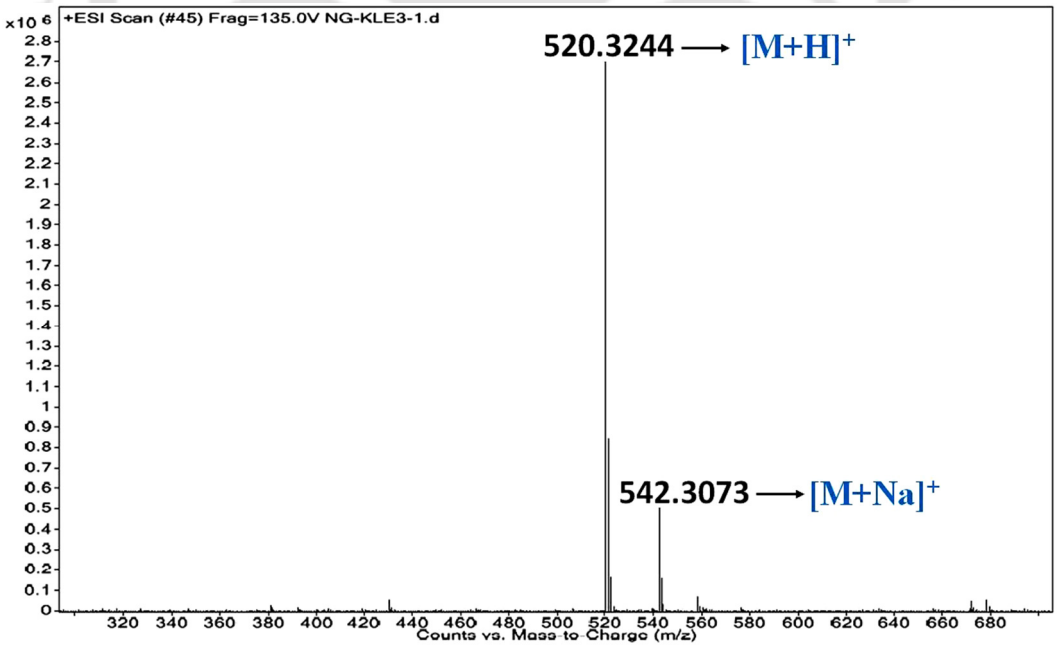

Figure 3.48. ESI-Mass spectrum of the MP1. Calculated m/z for $C_{26}H_{41}N_5O_6$ $[M+H]^+$ is 520.3135, observed 520.3244.

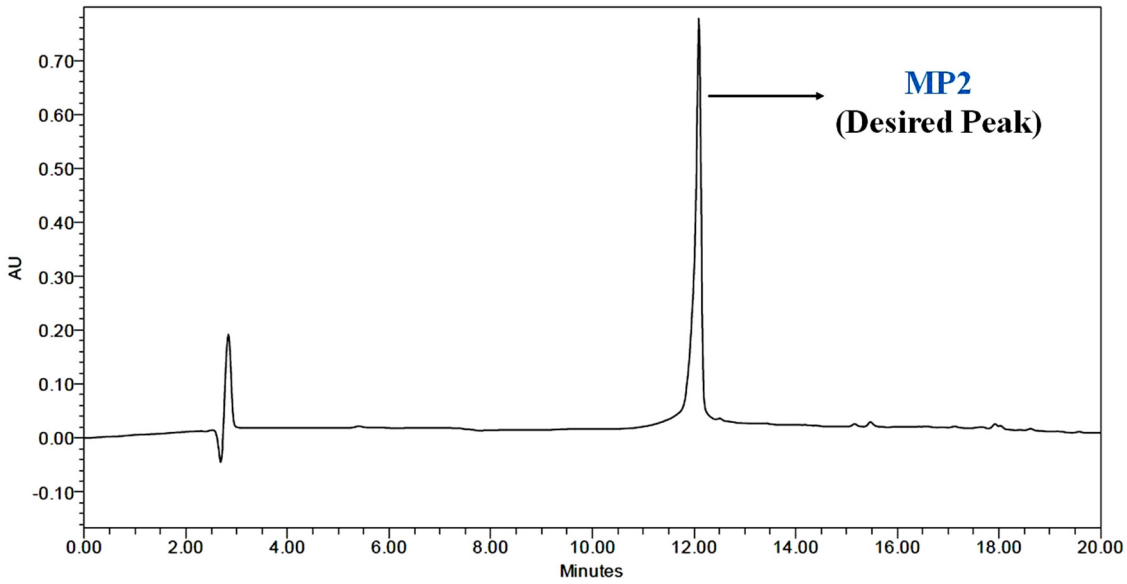

Figure 3.49. HPLC profile picture of the purified peptide MP2.

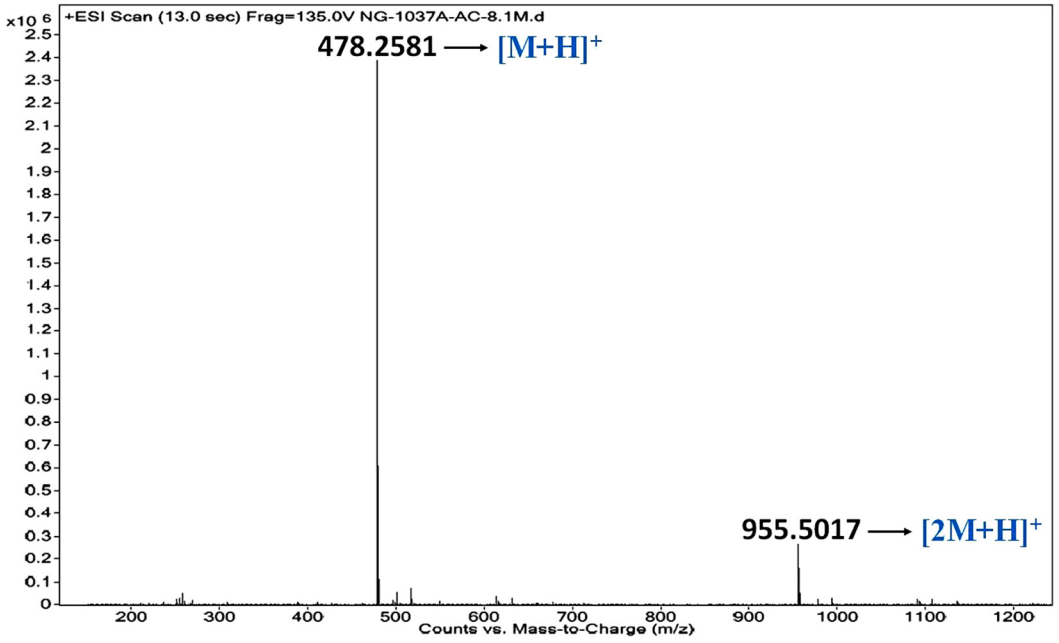

Figure 3.50. ESI-Mass spectrum of the MP2. Calculated m/z for $C_{23}H_{35}N_5O_6$ $[M+H]^+$ is 478.2666, observed 478.2581.

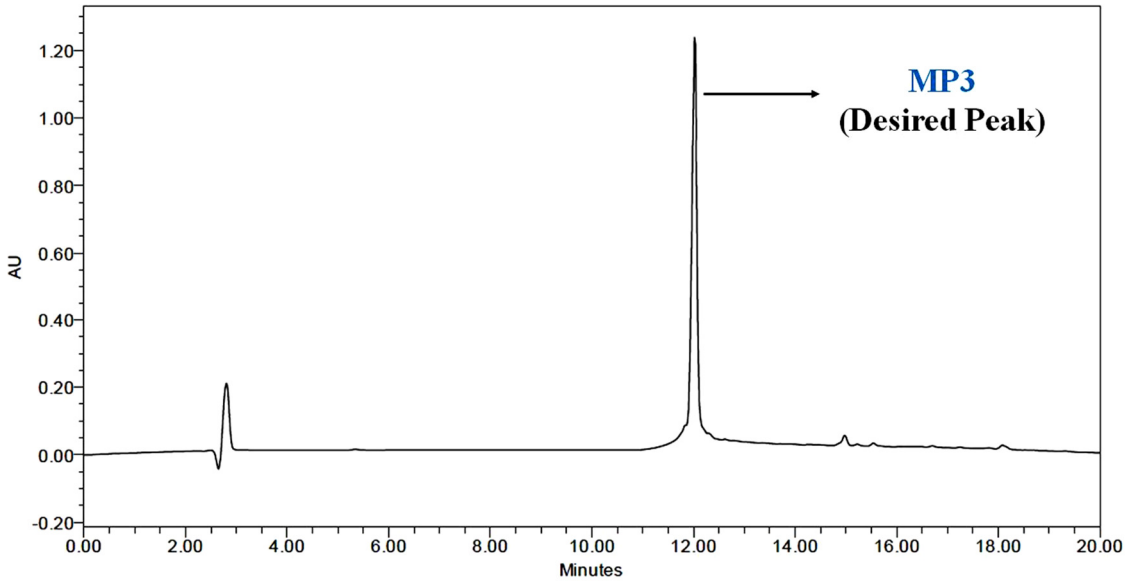

Figure 3.51. HPLC profile picture of the purified peptide MP3.

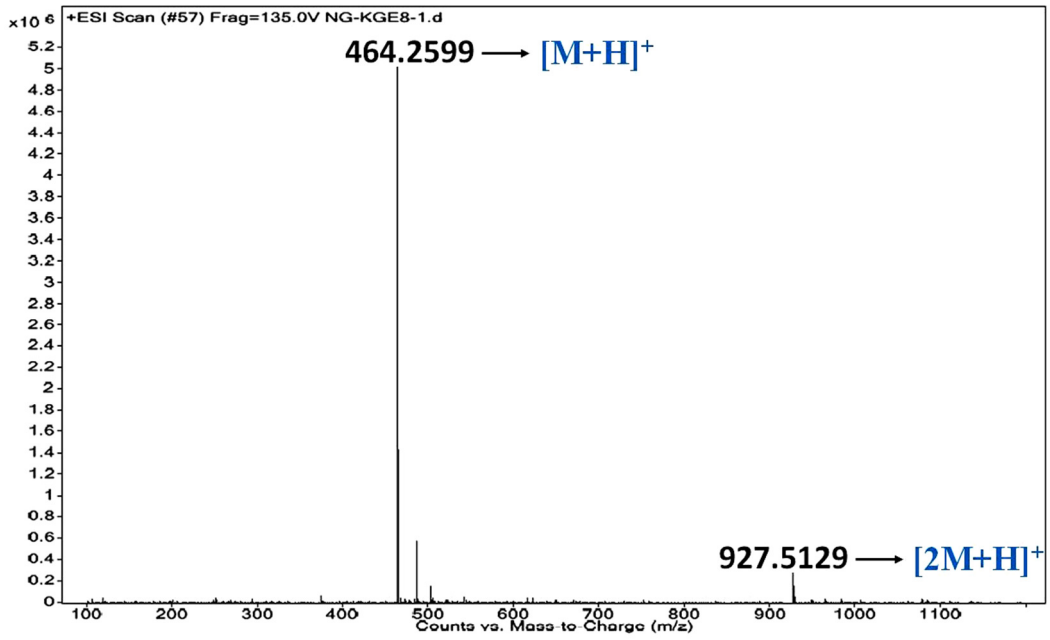

Figure 3.52. ESI-Mass spectrum of the MP3. Calculated m/z for $C_{22}H_{33}N_5O_6$ $[M+H]^+$ is 464.2509, observed 464.2599.

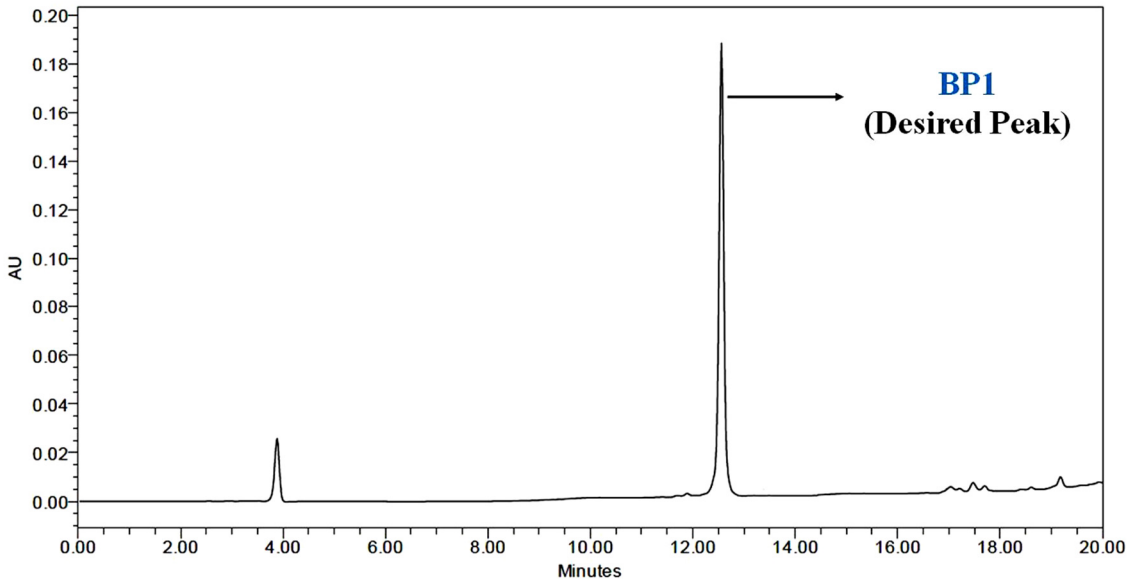

Figure 3.53. HPLC profile picture of the purified peptide BP1.

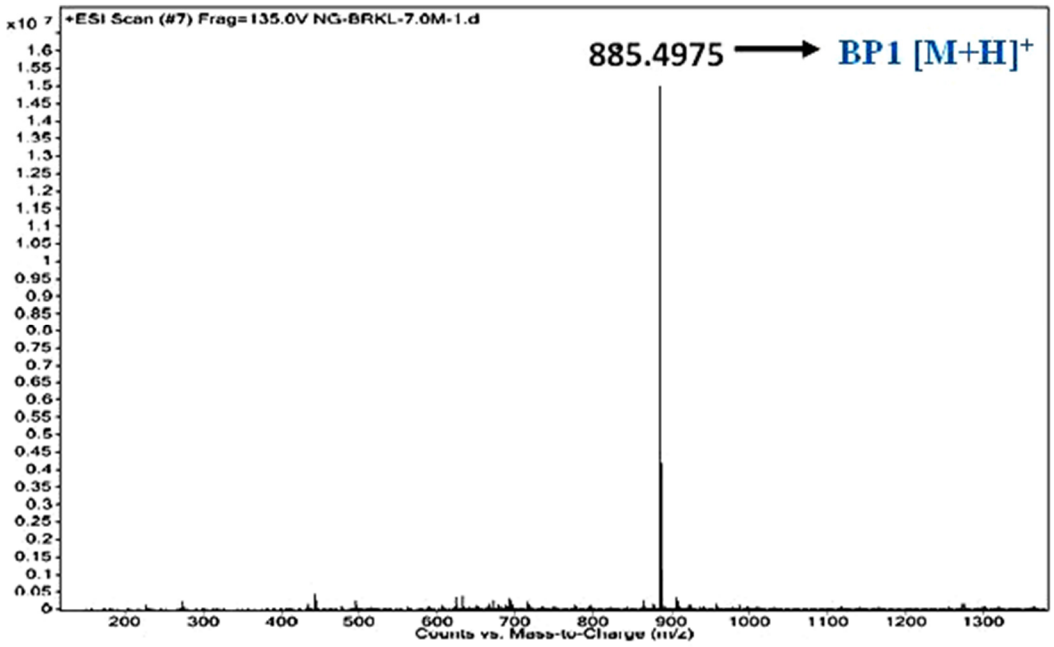

Figure 3.54. ESI-Mass spectrum of the BP1. Calculated m/z for $C_{47}H_{64}N_8O_9$ $[M+H]^+$ is 885.4875, observed 885.4975.

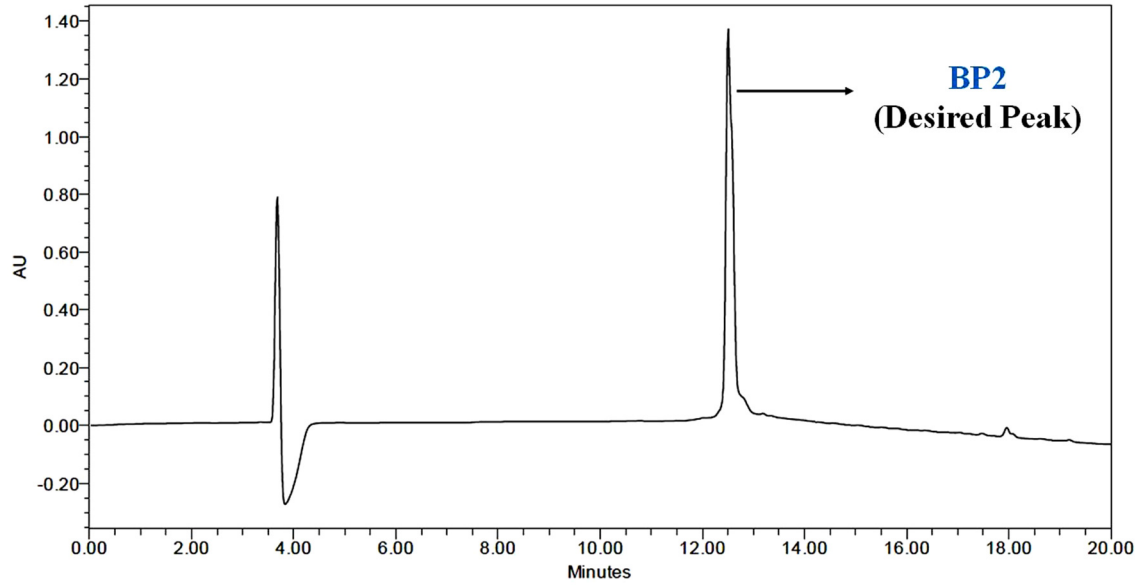

Figure 3.55. HPLC profile picture of the purified peptide BP2.

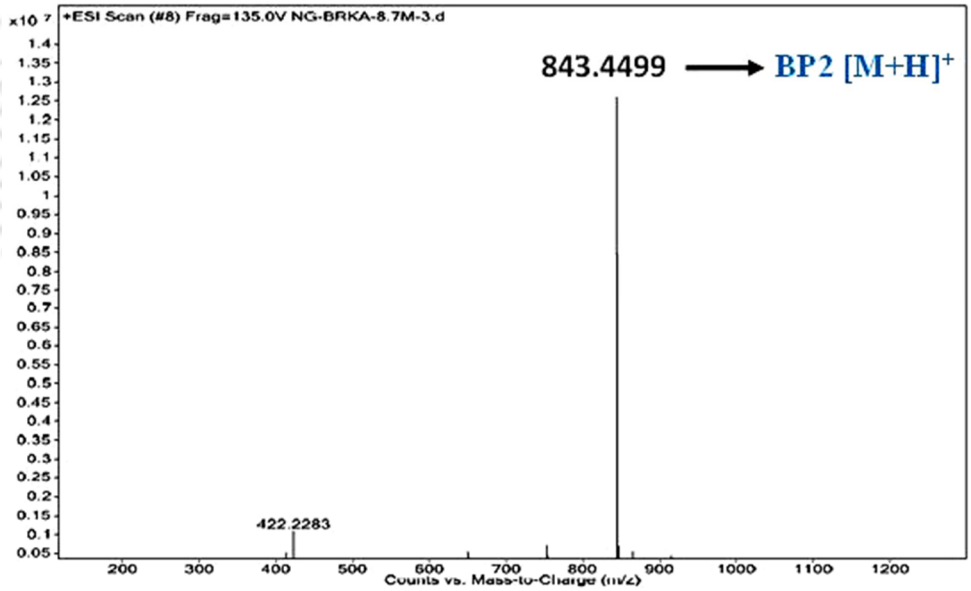

Figure 3.56. ESI-Mass spectrum of the BP2. Calculated m/z for $C_{44}H_{58}N_8O_9$ $[M+H]^+$ is 843.4405, observed 843.4499.

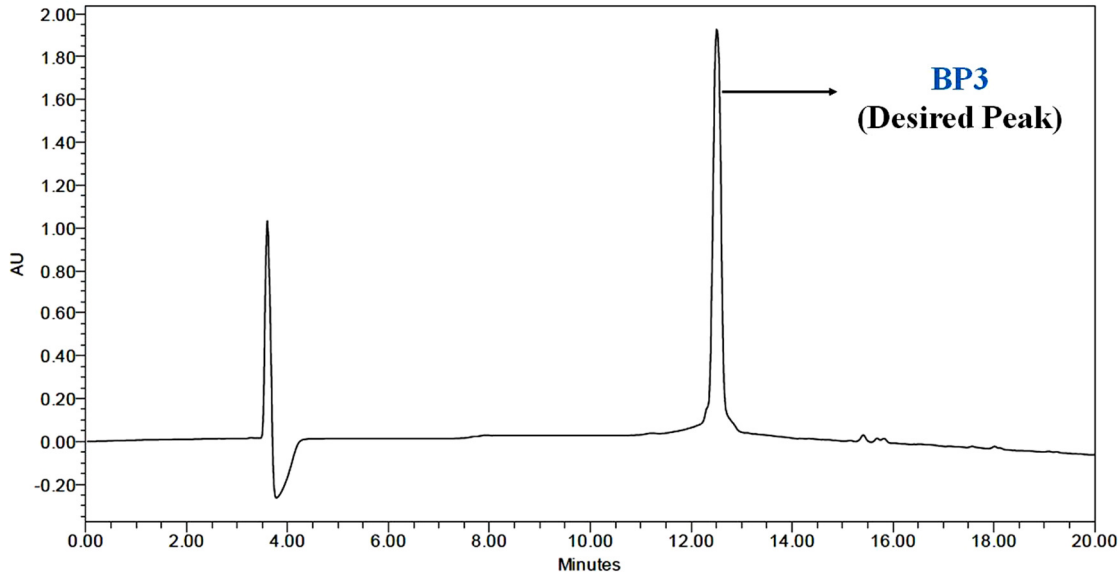

Figure 3.57. HPLC profile picture of the purified peptide BP3.

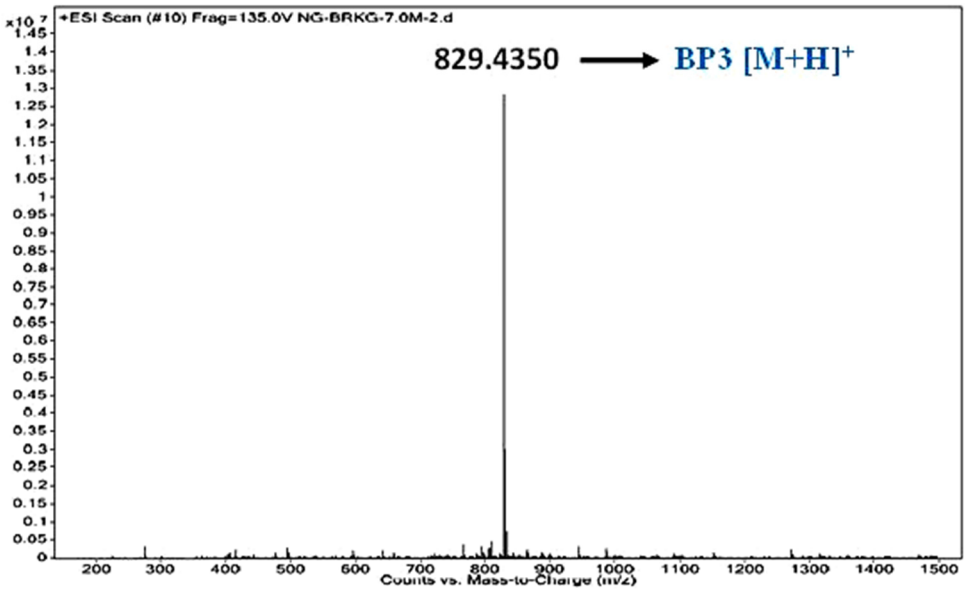

Figure 3.58. ESI-Mass spectrum of the BP3. Calculated m/z for $C_{43}H_{56}N_8O_9$ $[M+H]^+$ is 829.4249, observed 829.4350.

3.5. References:

[1] Chiti, F.; Dobson, C. M. *Annu. Rev. Biochem.* **2006**, *75*, 333-366.

[2] Selkoe, D. J. *J. Neuropathol. Exp. Neurol.* **1994**, *53*, 438-447.

[3] Selkoe, D. J. *Physiol. Rev.* **2001**, *81*, 741-766.

[4] Hard, T.; Lendel, C. *J. Mol. Biol*. **2012**, *421*, 441-465.

[5] Rajasekhar, K.; Chakrabarti, M.; Govindaraju, T. *Chem. Commun.* **2015**, *51*, 13434-13450.

[6] Kapurniotu, A.; Schmauder, A.; Tenidis, K. *J. Mol. Biol*. **2002**, *315*, 339-350.

[7] Gilead, S.; Gazit, E. *Angew. Chem. Int. Ed*. **2004**, *43*, 4041-4044.

[8] Tjernberg, L. O.; Näslund, J.; Lindqvist, F. *J.Biol.Chem*. **1996**, *271*, 8545-8548.

[9] Soto, C.; Sigurdsson, E. M.; Morelli, L.; Kumar, R. A.; Castaño, E. M.; Frangione, B. *Nat. Med.* **1998**, *4*, 822-826.

[10] Scherzer-Attali, R.; Pellarin, R.; Convertino, M. *PLoS ONE* **2010**, *5*, e11101.

[11] Mondal, T.; Mandal, B. *ChemComm.* **2019**, *55*, 4933-4936.

[12] Mondal, T.; Mandal, B. *ChemComm.* **2020**, *56*, 2348-2351.

[13] Trott, O.; Olson, A. J. *J. Comput. Chem.* **2010**, *31*, 455-461.

[14] Nilsson, M. R. *Methods* **2004**, *34*, 151-160.

Chapter 4: Cyclic di-peptide via dual O → N acyl migration inhibited protein-aggregation

4.1. Introduction:

The pathological event behind the neurodegenerative diseases is the misfolding, aggregation, and accumulation of proteins which leads to cellular dysfunction, damage of the network of synaptic connections, destruction of neurons in specific areas of the brain and selective brain mass loss.[1] This misfolded protein forms intermolecular β-sheet-rich structures ranging from small oligomers to large fibrillar aggregates known as amyloid.[1,2] Prevailing neurodegenerative diseases which result from amyloid aggregation are Alzheimer's disease, Parkinson's disease, amyotrophic lateral sclerosis, Huntington's disease, frontotemporal dementia, corticobasal degeneration, progressive supranuclear palsy, dementia with Lewy bodies, and prion diseases. Though these disease-associated proteins differ in sequence, size, structure, expression level, or function but the root of these diseases is the progressive accumulation of misfolded protein aggregates having fibrillar morphology with well-ordered, cross β-sheet structures. The structures formed are highly rigid, often having repetitive hydrophobic and polar interactions along the fibril axis, stabilised by an extensive network of intermolecular main chain hydrogen bonding.[3,4] Small soluble aggregates, referred to as oligomers, formed during the amyloid aggregation are extremely heterogeneous, interconvert into proto fibrils rapidly. It is believed that

oligomers are more toxic than the fibrillar assemblies, also the cause of cell and tissue toxicity, predominantly in neurodegenerative diseases.[1,2,5] The progression of amyloid aggregation occurs via nucleation dependent pathway where soluble proteins transform into insoluble amyloid fibrils after going through a series of conformational changes and self-assembling process. Various strategies have been exploited to reduce the Aβ production, inhibit the Aβ aggregation, enhance the Aβ clearance.[6,7,8,9,10,11] By targeting different conformational species, amyloid aggregation process can be interfered. It include stabilizing monomers by binding with ligands of proteins, small molecules, antibodies, ions, redirecting monomers to nontoxic off-pathway oligomers, accelerating the formation of mature fibril by fibril binders. Beside this, inhibiting fibril growing and disrupting amyloid assembly by β-sheet breaker peptide is another promising strategy for different amyloid related diseases. β-sheet breaker peptides are soluble, small peptides, containing short hydrophobic sequence of amyloidogenic proteins. These peptides can interact and bind with the same sequences within amyloidogenic proteins, thus prevent their aggregation or promoting the disruption of existing fibrils. Several chemical modifications like N-methylation, cyclization, incorporation of unnatural amino acids have done to increase the inhibitory effect of β-sheet breaker peptide against toxic amyloid aggregation. Prof. Soto first introduced β breaker peptide having sequence LPFFD where a turn generating unit proline was incorporated as β breaker element.[12] Another interesting work in this direction is generation of *in situ* kink as breaker element into the peptide backbone when chemically modified aspartic acid residue in a designed β breaker peptide undergo chemical transformation at near physiological pH to form aspartimide.[13] Here we have developed an approach, *in situ* cyclic peptide preparation via dual O → N acyl migration[14,15] to generate a bent unit which may be act as potent inhibitor.

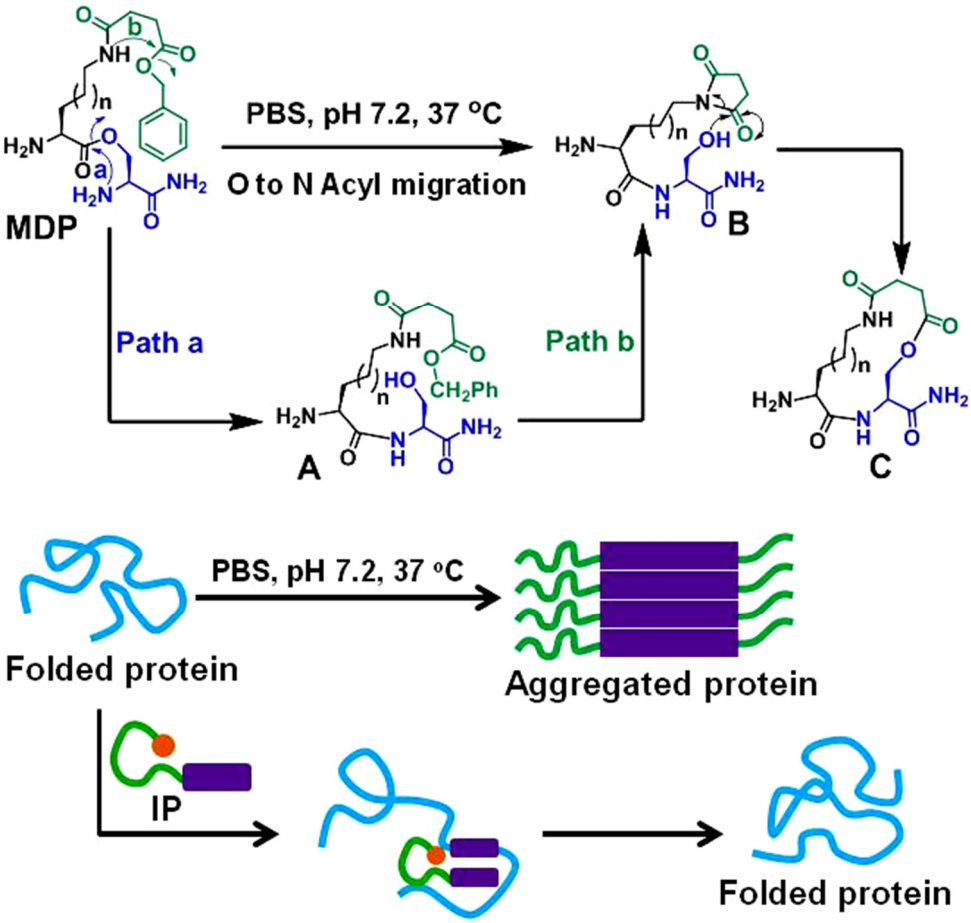

Figure 4.1. Schematic diagram of the inhibition of aggregated protein.

4.2. Results and Discussions:

4.2.1. Design of the Peptides:

From the above discussions, it is cleared that the protein aggregation is responsible for various diseases. So, in this work, our strategy was to inhibit the β-sheet structure of an aggregated protein by the concept of inserting a bent unit. To prove our hypothesis, we have designed a series of small model peptides. First we designed Ser containing modified dipeptide (MDP, Table 1, Figure 4.2) with a variation of Lys and Orn attached with the side-chain of Ser for the desired peptide cyclization. We also prepared a negative control

peptide in which Orn was coupled directly (at the backbone) with Ser. After getting proof of principal from MDP, we have designed the inhibiting peptides (IP) by attaching Phe-Phe unit (for the recognition purpose) with the MDP sequences. We have also designed an aggregated peptide (AP) derived from the amyloid β (Aβ) peptide, and the particular sequence consists of the core hydrophobic region of Aβ for amyloid aggregation.

Table 4.1. List of the designed peptides:

Sl. No.	Name of the Peptides (Short Name)	Peptide Sequence	Functional Activity
1.	Modified di-peptide1 (MDP1)	O(Suc-OBn)-(H^+)S-NH_2	Peptide cyclization
2.	Modified di-peptide2 (MDP2)	K(Suc-OBn)-(H^+)S-NH_2	Peptide cyclization
3.	Negative control (NC)	O(Suc-OBn)-S-NH_2	Control
4.	Inhibiting Peptide1 (IP1)	O(Suc-OBn)-(H^+)S-FF-NH_2	β-sheet inhibitor
5	Inhibiting Peptide2 (IP2)	K(Suc-OBn)-(H^+)S-FF-NH_2	β-sheet inhibitor
6	Aggregating Peptide (AP)	Ac-VHHQKLVFF-NH_2	β-sheet formation

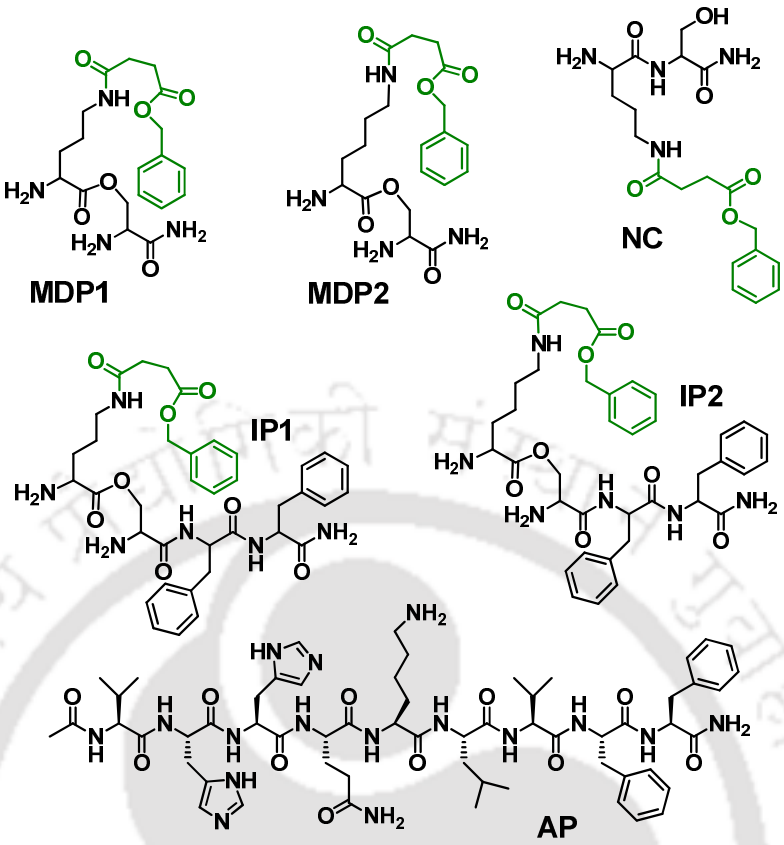

Figure 4.2. Chemical structure of the designed peptides.

4.2.1.1. Synthesis and purification procedure of the designed peptides:

Our designed peptides (Figure 4.2) were synthesized following the standard Fmoc/^{t}Bu solid-phase peptide synthesis (SPPS) method as described in the earlier chapter.[16]

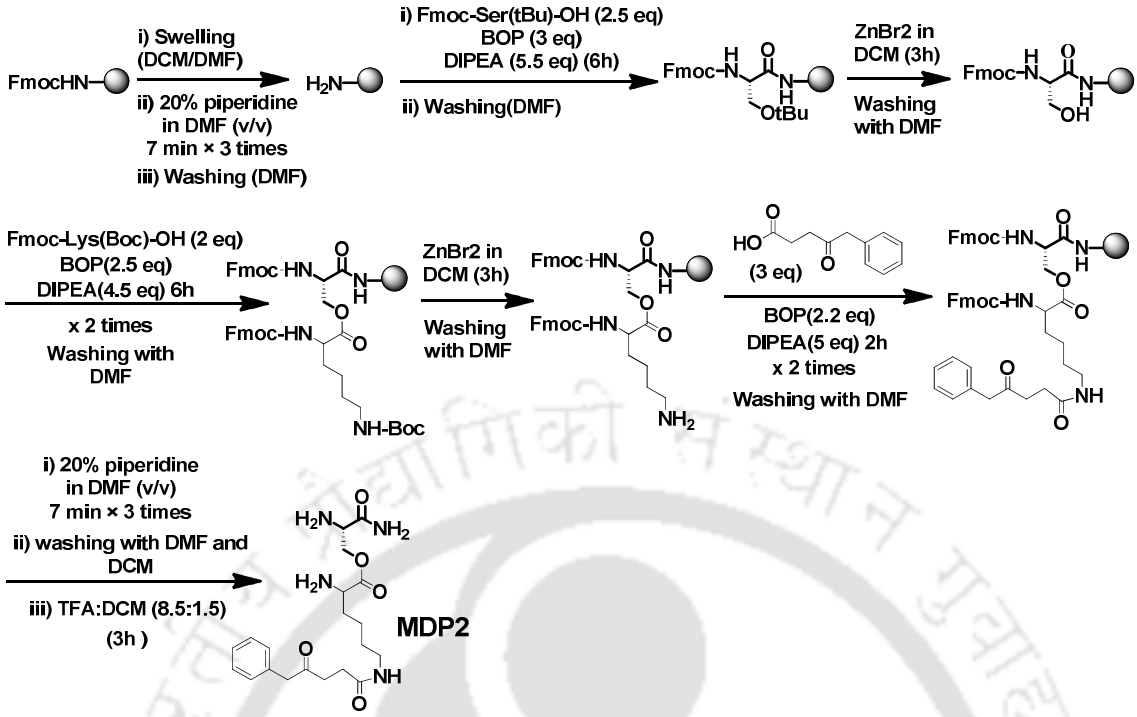

Figure 4.3. Schematic diagram of the synthesis of peptide MDP2 in solid-phase.

Peptide MDP1 was synthesized according to the same protocol (Figure 4.3) with the Orn instead of Lys. For NC peptide, Orn was coupled directly with the free NH2 group of Ser instead of side chain of Ser. IP1 and IP2 were synthesized in same manner where Phe was first coupled with resin and second coupling occurred between two Phe with coupling time 6h for each step.

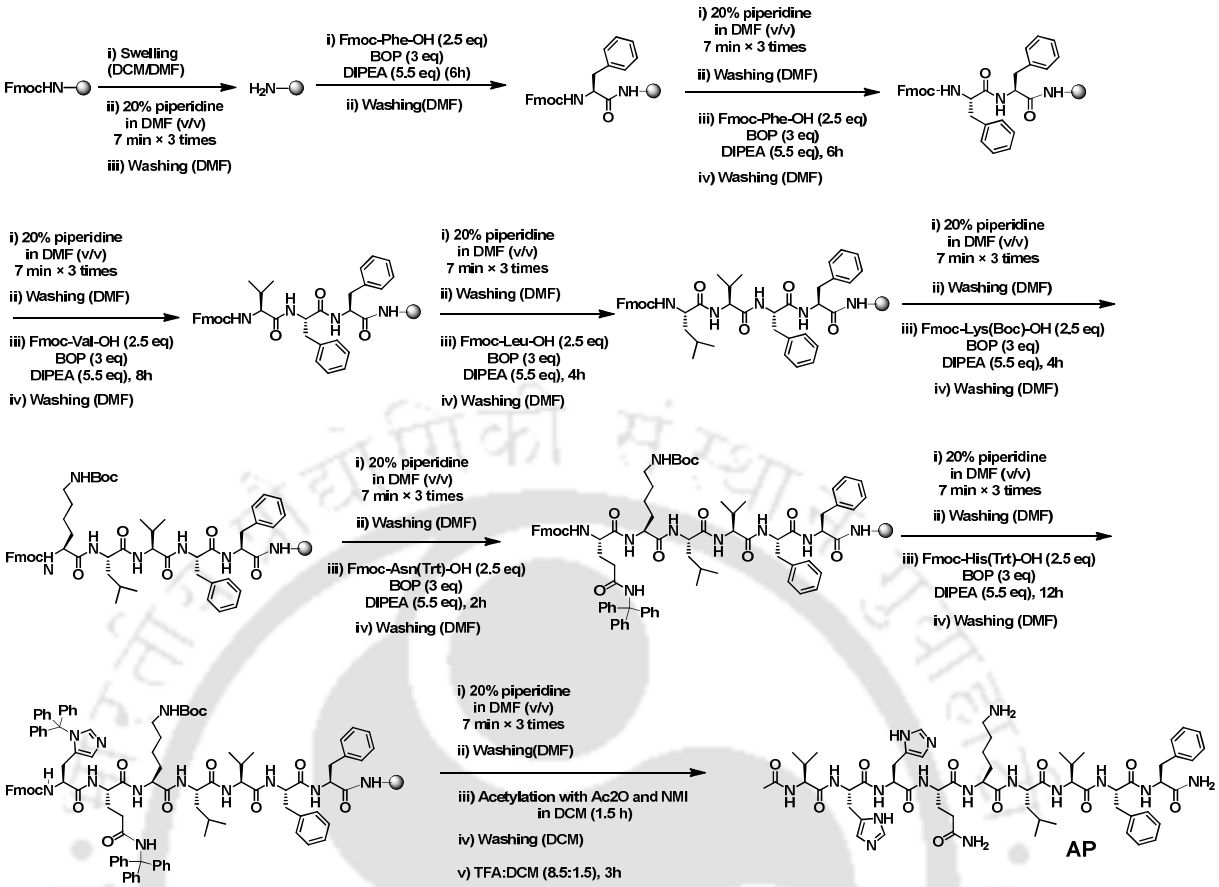

Figure 4.4. Schematic diagram of the synthesis of peptide AP in solid-phase.

Crude peptides were precipitated using cold diethyl ether, centrifuged and washed with ether. Dissolving in CH_3CN/H_2O mixture, peptides were purified by semi preparative RP-HPLC (C18-μ Bondapak column, binary solvents H2O and ACN with gradient 5-100 % CH_3CN for 18 min followed by 100% CH_3CN till 20 min., maintaining flow rate of 4 mL/ min) and lyophilized.

The purity of the peptides was confirmed by analytical HPLC (using Ascentis C18 analytical column, flow rate of 1 ml/min, linear gradient of 5-100% CH_3CN over 18 min in a total run time of 20 min) and ESI-Mass.

4.2.2. Plausible mechanism of the side chain cyclization:

The mechanism of side chain cyclization (Figure 4.5) was hypothesized from the results of time-dependent ESI-MS kinetics and related Circular Dichroism (CD) studies *in vitro*.

At first, in MDP, the free amine of Ser attacks to the carbonyl group of its side chain ester (O → N acyl migration) as depicted in the Path-a to form the compound A. Then another O → N acyl migration (depicted in the Path-b) takes place at the Lys side chain which was modified by attaching benzyl succinamate with it. Finally, nucleophilic attack of Ser to the carbonyl group of succinimide unit takes place to form the cyclic compound C. Also, from the beginning, hydrolysed product D (Figure 4.6) was obtained in-parallel. The conversion of MDP to cyclic compound C was hypothesized to inhibit the protein aggregation of a folded protein which converts to the aggregated state in PBS, pH 7.2, at 37 °C.

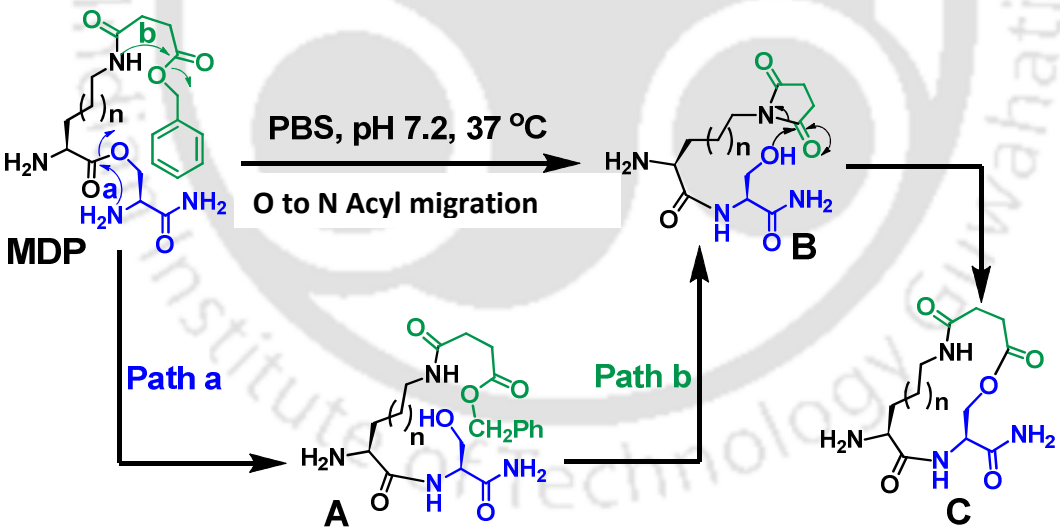

Figure 4.5. A plausible mechanism of formation of cyclic di-peptide via dual O → N acyl migration.

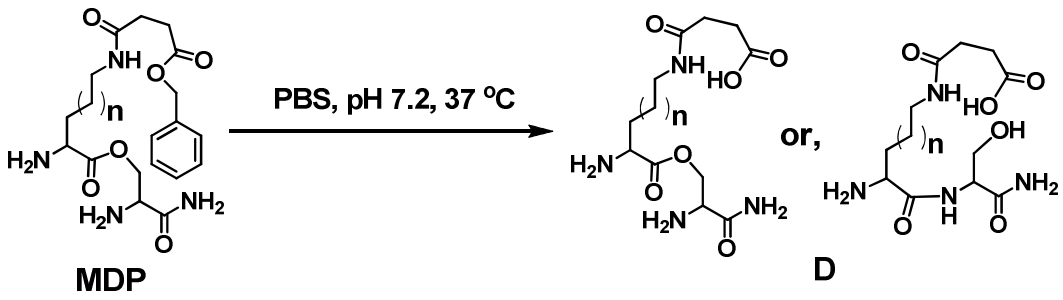

Figure 4.6. The formation of hydrolysed product in PBS of pH 7.2 at 37 °C.

4.2.3. Proof of hypothesis of the side chain cyclization:

To establish our hypothesis, we have performed ESI-MS kinetic studies with the designed MDPs *in vitro*. After analysing all the ESI-MS data, the plausible mechanism was drawn. The mechanism was further supported by CD kinetics in terms of conformation alteration of the peptides. All the biophysical studies were carried out in PBS of pH 7.2 at 37 °C to maintain similarity with the physiological condition.

4.2.3.1. Sample preparation:

Each lyophilised peptide samples were dissolved in PBS (50 mM, pH 7.2) to obtain stock solutions and were sonicated and vortexed. Then the total solution was divided into different Eppendorf tubes equally maintaining a final concentration of 500 µM and incubated at 37 °C over water bath. We collected the required amount of aliquot from vials at different time intervals for kinetic studies *in vitro.* But before collecting the sample for analyses, the stock solutions were sonicated and vortexed for 1 min each.

4.2.3.2. Detection of various fragments of MDP1 by ESI-Mass kinetics study:

All the samples used for the ESI-MS kinetic studies (Figure 4.7 - 4.12) of MDP1 were diluted properly (after quenching with 20% HCl followed by filtration) before injecting in the mass instrument. A^1 is the product obtained from MDP1 after 1st O → N acyl migration following path-a. B^1 is the succinimide containing product after releasing the benzyl alcohol by 2nd O → N acyl migration following path-b. C^1 is the desired cyclic product. D^1 is the un-controlled hydrolysed product obtained in PBS of pH 7.2. Though the mass values were same, the conversion of MDP1 to A^1 was confirmed for the facile O → N acyl migration of Ser which was properly explained in the literature.

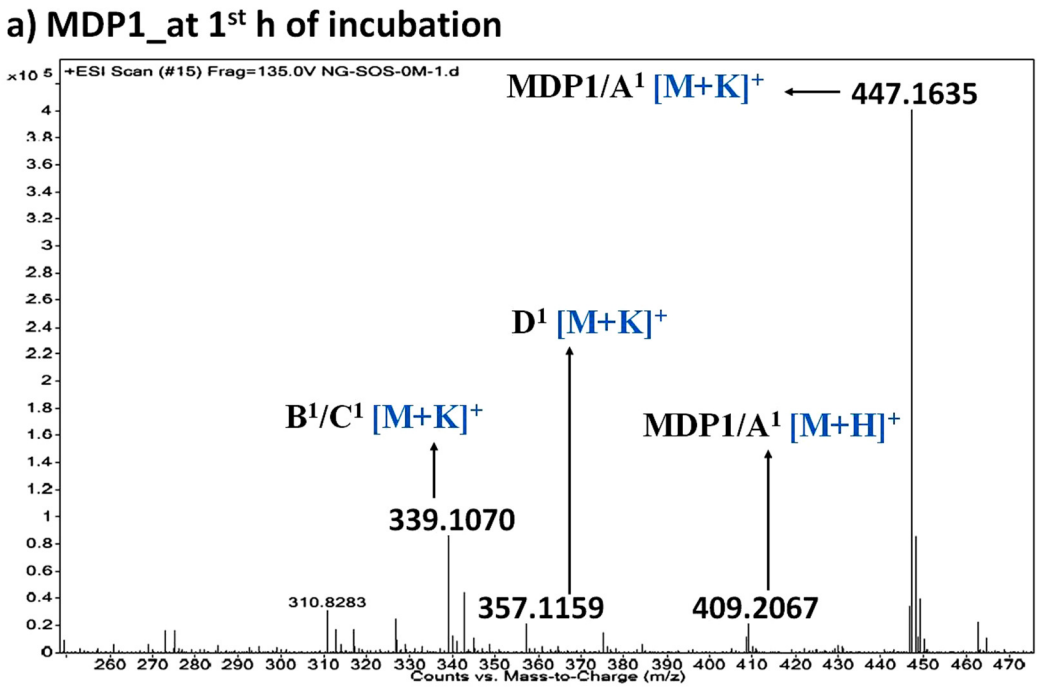

Figure 4.7. ESI-Mass spectrum of MDP1 at the 1st h of incubation in PBS of pH 7.2 at 37 °C.

b) MDP1_after 3 h of incubation

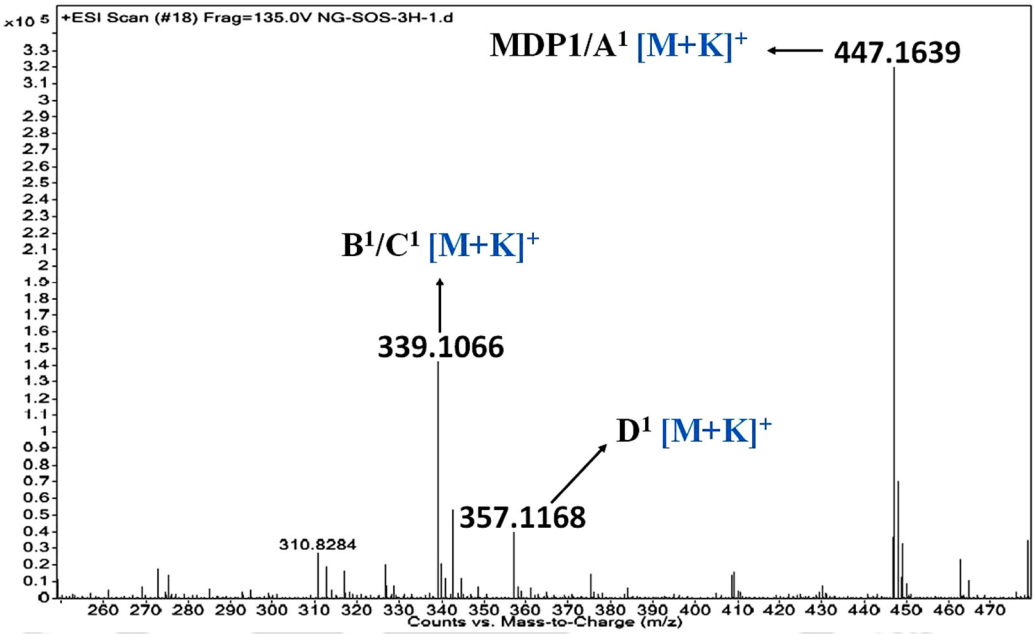

Figure 4.8. ESI-Mass spectrum of MDP1 after 3 h of incubation in PBS of pH 7.2 at 37 °C.

c) MDP1_after 6 h of incubation

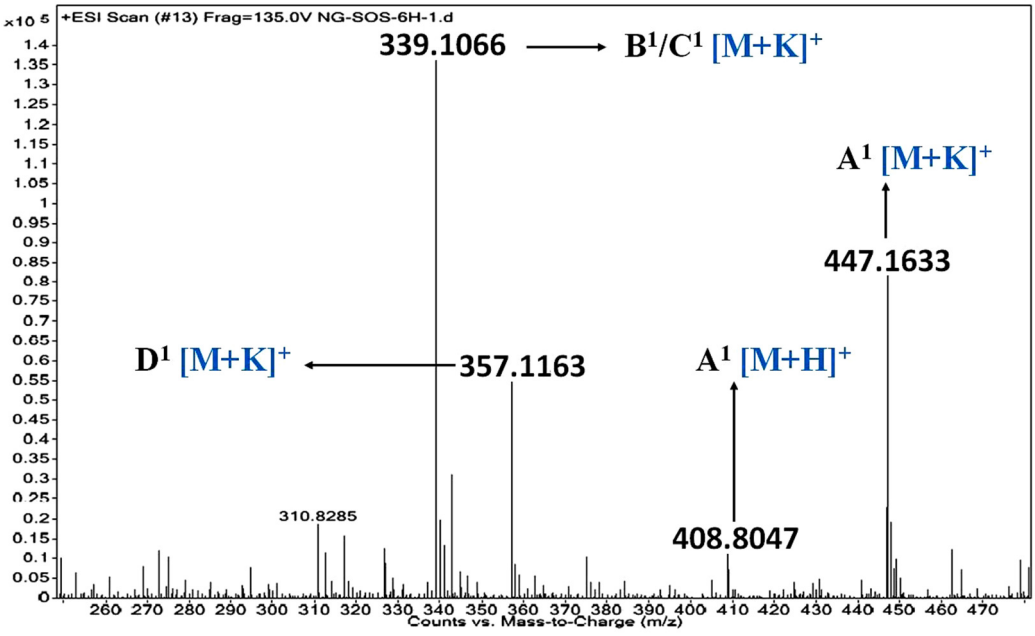

Figure 4.9. ESI-Mass spectrum of MDP1 after 6 h of incubation in PBS of pH 7.2 at 37 °C.

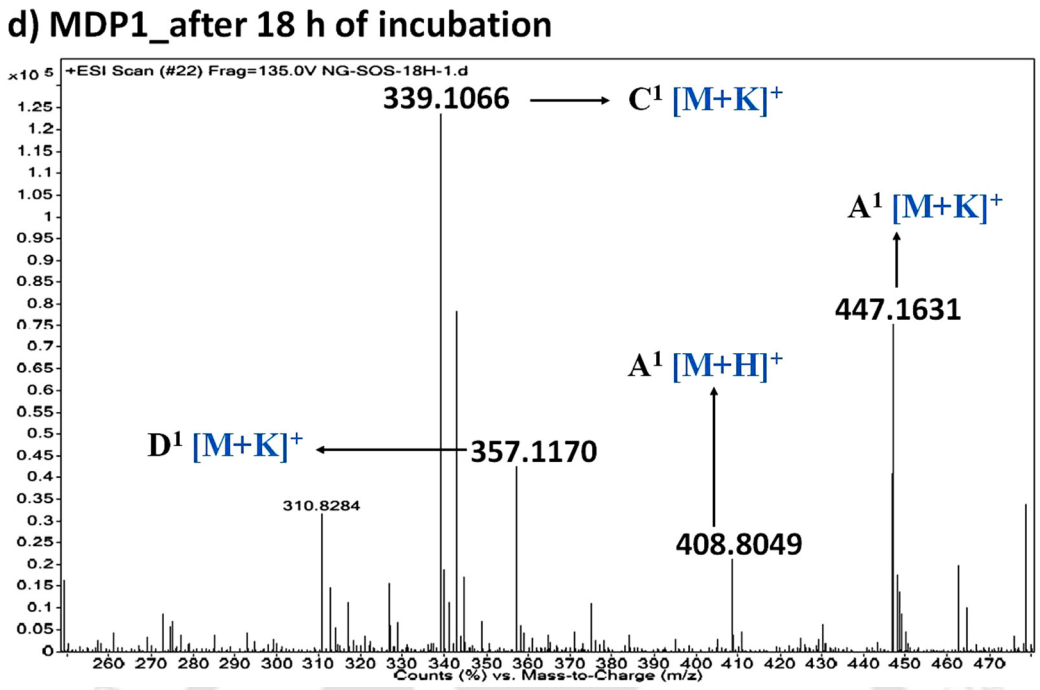

Figure 4.10. ESI-Mass spectrum of MDP1 after 18 h of incubation in PBS of pH 7.2 at 37 ºC.

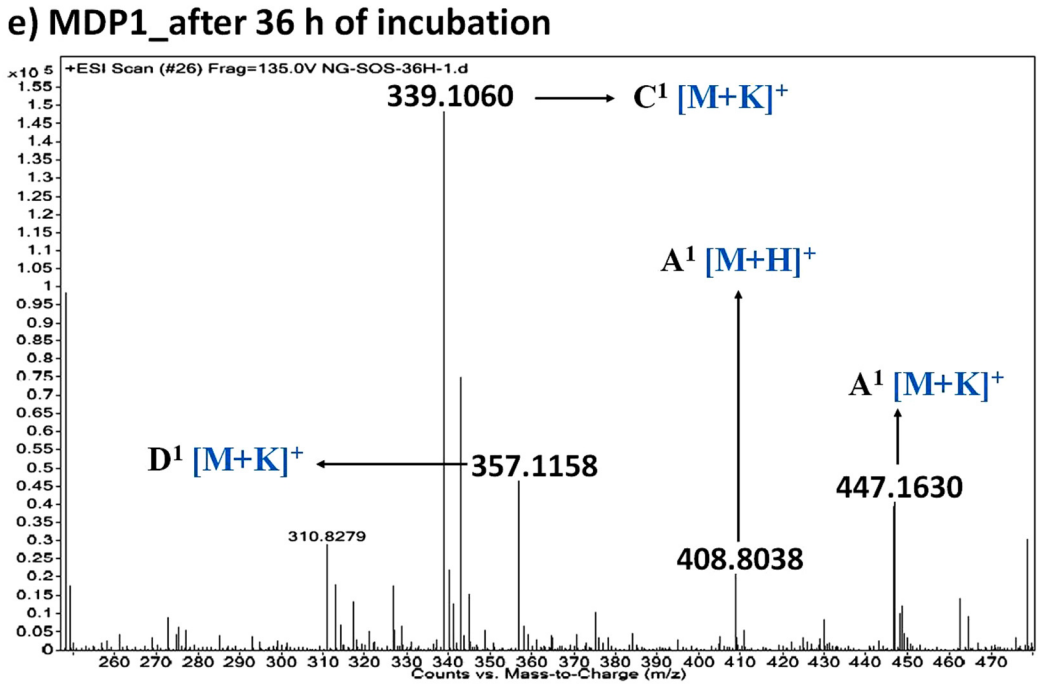

Figure 4.11. ESI-Mass spectrum of MDP1 after 36 h of incubation in PBS of pH 7.2 at 37 ºC.

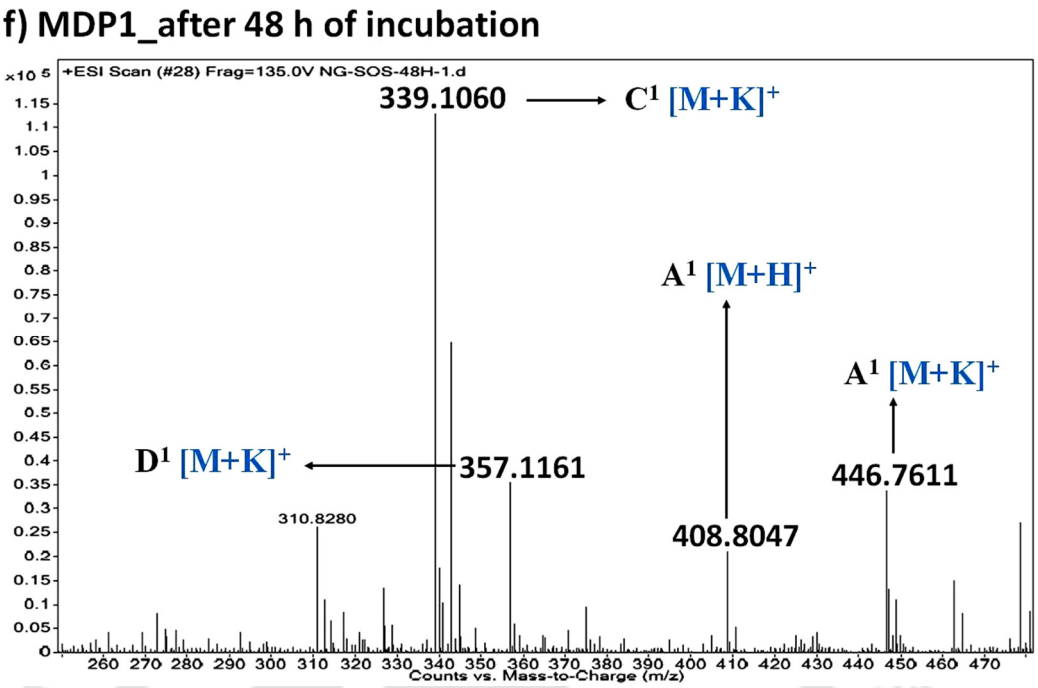

Figure 4.12. ESI-Mass spectrum of MDP1 after 48 h of incubation in PBS of pH 7.2 at 37 ºC.

4.2.3.3. CD kinetics of MDP1 to support the generation of turn unit:

Incubated samples that were taken for the CD alalysis, first treated with 0.1% trifluoroacetic acid to quench any further reaction, and were stored at -20 °C. Before experiment, the samples were diluted with PBS buffer solutions to obtain a final concentration of 100 µM. 200 µL of the sample was taken in a cuvette having pathlength of 1 mm. and samples were measured thrice, spectra was recorded from 190 nm to 260 nm.

From the CD kinetics, the change in conformation of MDP1 (Figure 4.13) was monitored *in vitro*. Initially (black) the random coil of MDP1 was confirmed from the negative band at 195 nm. But with time, the random coil was converted to a mixture of predominantly turn and coil structure, and after 48 h of incubation (magenta) converted to the turn structure

which was confirmed from the positive band at 205 nm. The results confirmed the generation of cyclic peptide C[1].

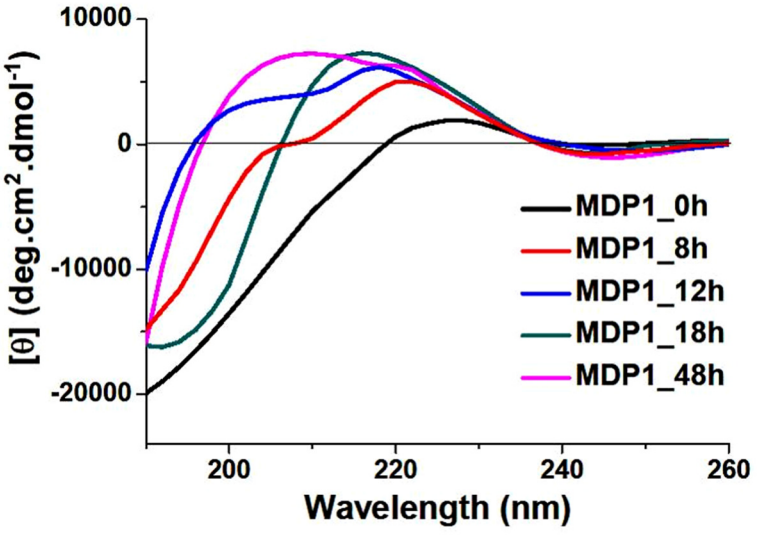

Figure 4.13. The CD spectra of MDP1 at the 1st h (black), after 8 h (red), after 12 h (blue), after 18 h (dark cyan) and after 48 h (magenta) of incubation. The peptide solution (200 µM) was incubated in PBS pH 7.2 (50 mM) at 37 °C.

4.2.3.4. Detection of various fragments of MDP2 by ESI-Mass kinetics study:

We collected the required amount of aliquot for ESI-MS, and CD kinetic studies *in vitro* at different time intervals to monitor the conversion of our designed peptides into bent generating units.

Samples taken for ESI-MS kinetic studies (Figure 4.14 - 4.20) were quenched with 20% HCl, then diluted with HPLC grade CH_3CN and Mili-Q water and filtered through 0.2-micron filter paper before analysis. ESI positive mode was used to analyse mass of the peptide samples. All the samples used for the ESI-MS kinetic studies of MDP2 were diluted properly before injecting in the mass instrument.

A^2 is the product obtained from MDP2 after 1st O → N acyl migration following path-a. B^2 is the succinimide containing product after releasing the benzyl alcohol by 2nd O → N acyl migration following path-b. C^2 is the desired cyclic product. D^2 is the un-controlled hydrolysed product obtained in PBS of pH 7.2. Though the mass values were same, the conversion of MDP2 to A^2 was confirmed for the facile O → N acyl migration of Ser which was explained in the literature.

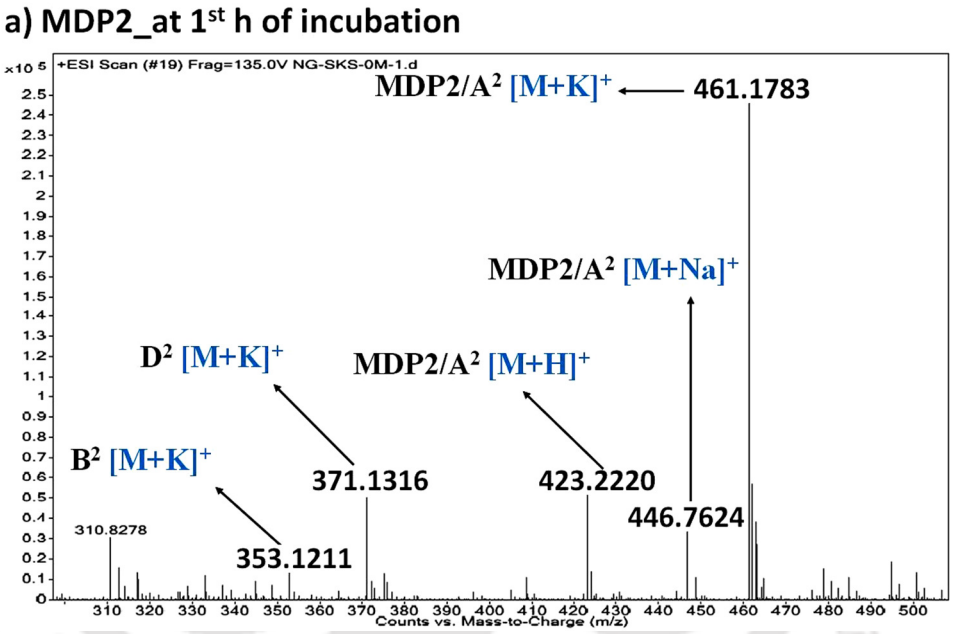

Figure 4.14. ESI-Mass spectrum of MDP2 after starting of incubation in PBS of pH 7.2 at 37 °C.

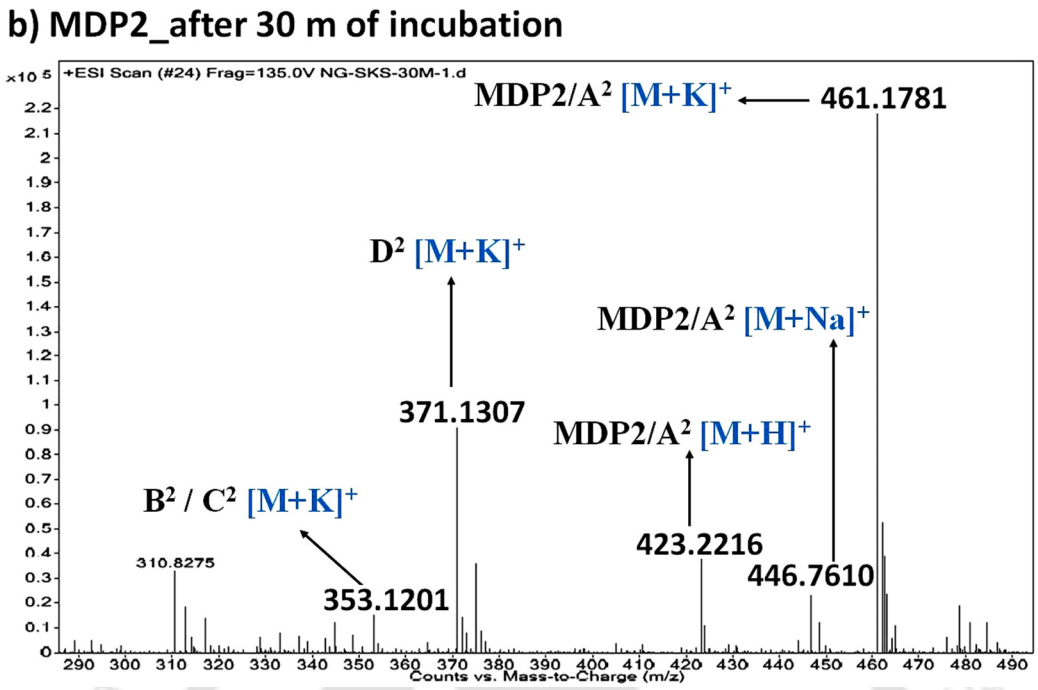

Figure 4.15. ESI-Mass spectrum of MDP2 after 30 m of incubation in PBS of pH 7.2 at 37 °C.

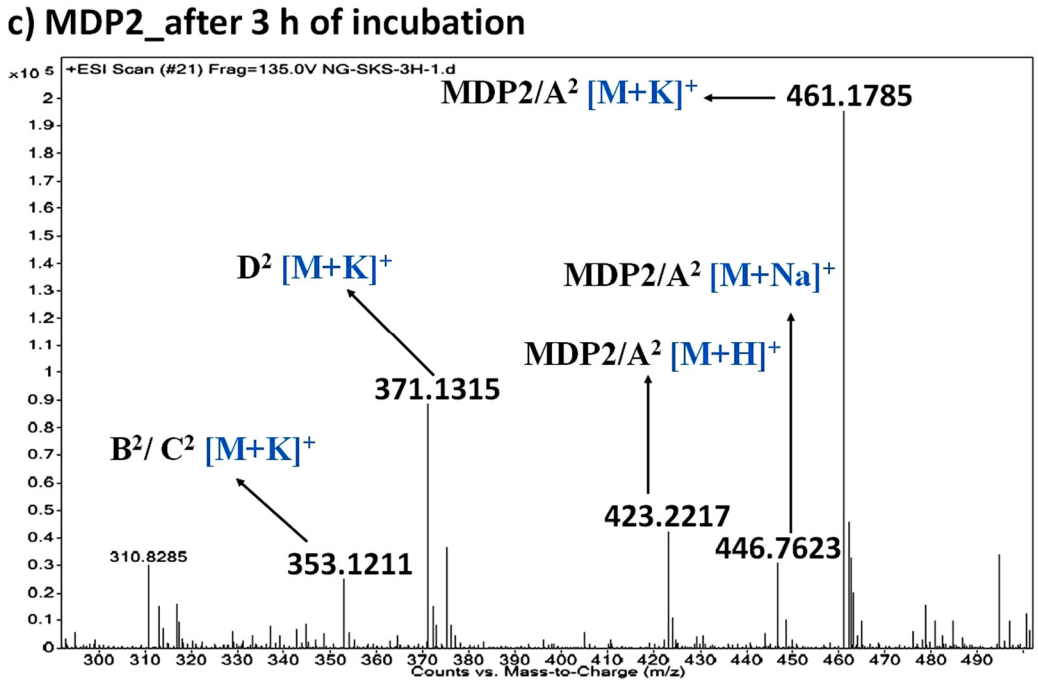

Figure 4.16. ESI-Mass spectrum of MDP2 after 3 h of incubation in PBS of pH 7.2 at 37 °C.

d) MDP2_after 9 h of incubation

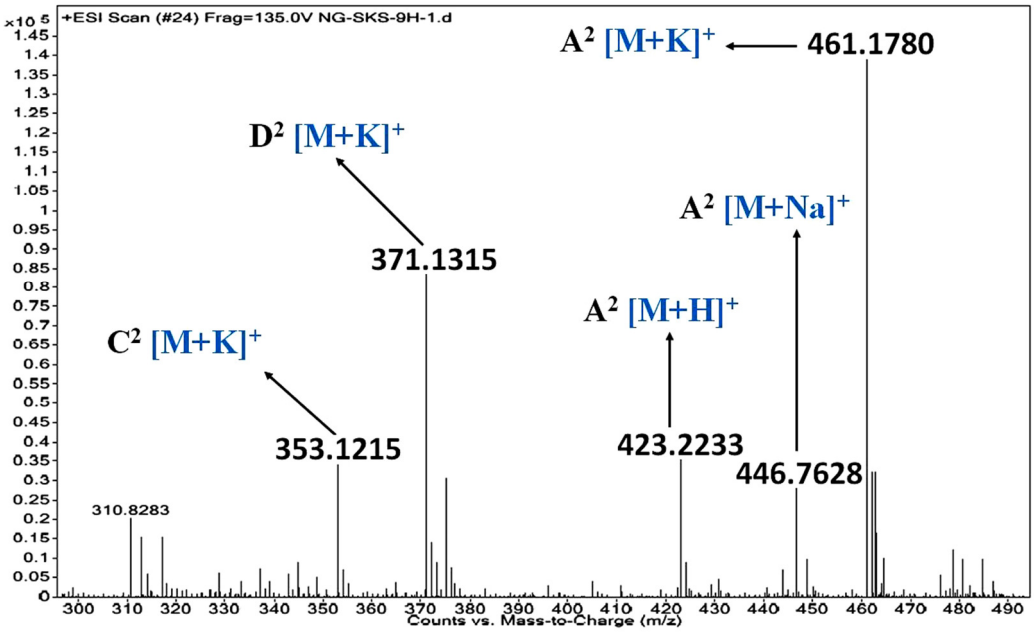

Figure 4.17. ESI-Mass spectrum of MDP2 after 9 h of incubation in PBS of pH 7.2 at 37 °C.

e) MDP2_after 24 h of incubation

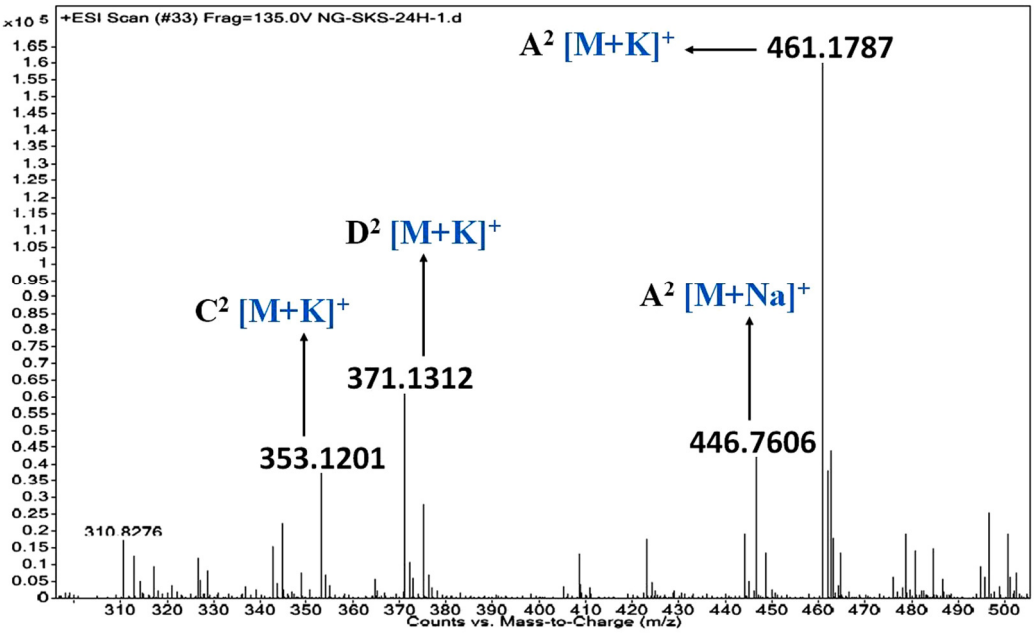

Figure 4.18. ESI-Mass spectrum of MDP2 after 24 h of incubation in PBS of pH 7.2 at 37 °C.

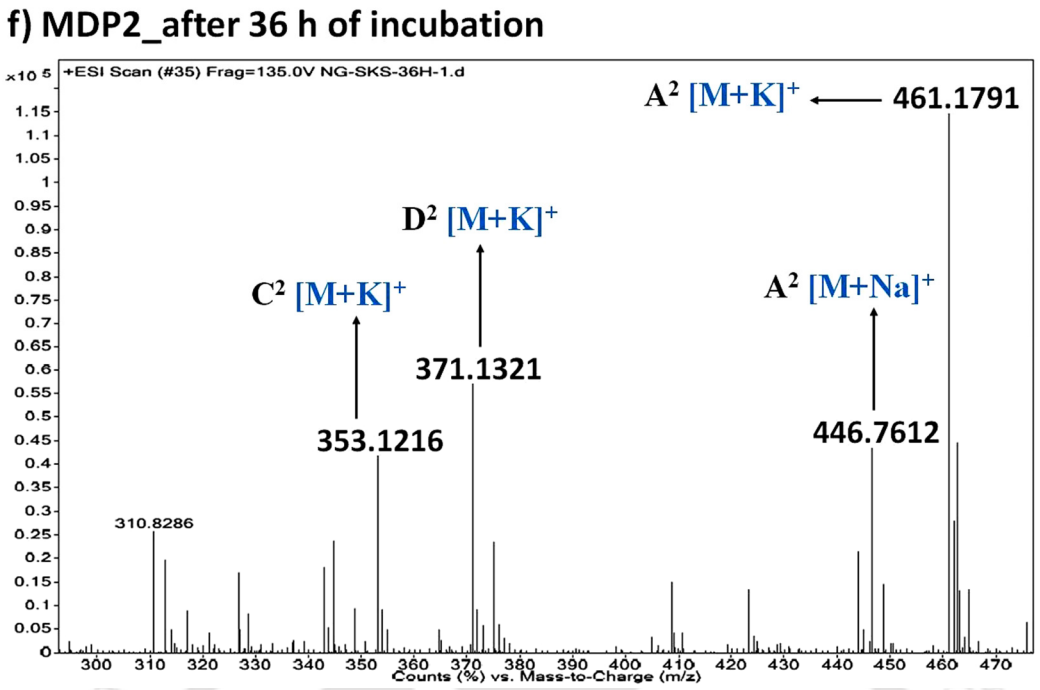

Figure 4.19. ESI-Mass spectrum of MDP2 after 36 h of incubation in PBS of pH 7.2 at 37 °C.

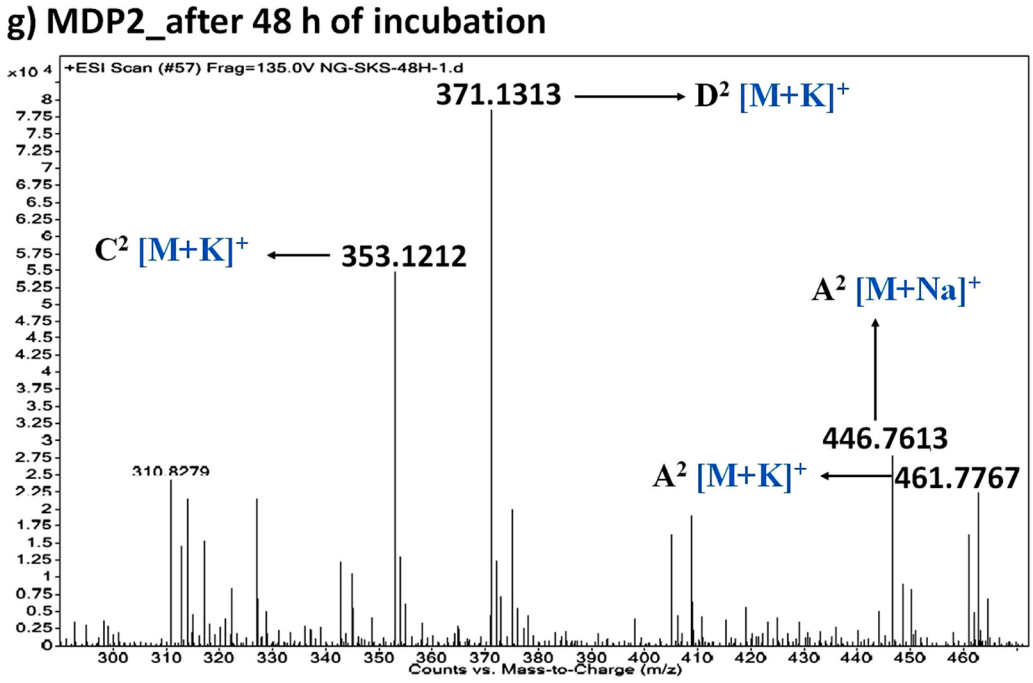

Figure 4.20. ESI-Mass spectrum of MDP2 after 48 h of incubation in PBS of pH 7.2 at 37 °C.

4.2.3.5. CD kinetics of MDP2 to support the generation of turn unit:

From the CD kinetics, the change in conformation of MDP2 (Figure 4.21) was monitored *in vitro*. Initially (black) the random coil of MDP2 was confirmed from the negative band at 200 nm. But with time, the random coil was converted to a mixture of predominantly turn and coil structure, and after 48 h of incubation (magenta) converted to the turn structure which was confirmed from the positive band at 215 nm. The results confirmed the generation of cyclic peptide C^2.

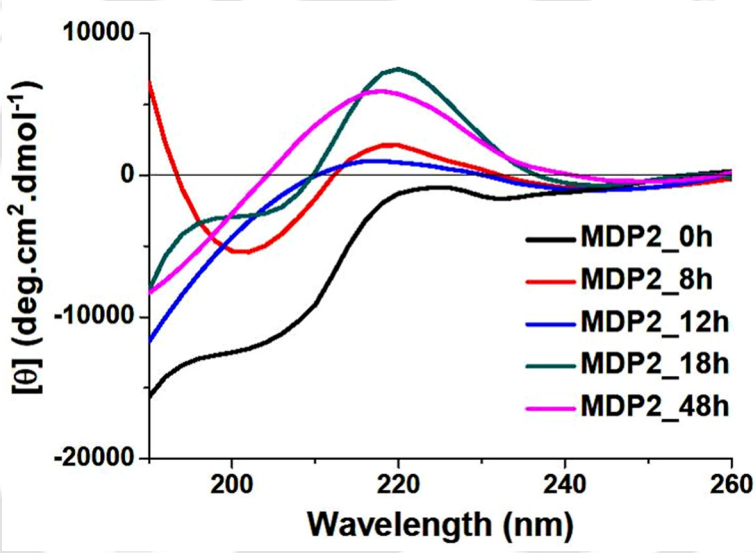

Figure 4.21. The CD spectra of MDP2 at the 1st h (black), after 8 h (red), after 12 h (blue), after 18 h (dark cyan) and after 48 h (magenta) of incubation. The peptide solution (200 μM) was incubated in PBS pH 7.2 (50 mM) at 37 °C.

4.2.4. Inhibition of amyloid aggregates of fibril AP:

To investigate whether our designed inhibiting peptides (IPs) can inhibit the amyloid formation of AP, AP alone was incubated to initiate fibrillization and IPs were co-incubated with AP in PBS of pH 7.2 at 37 °C on a water bath up to seven days. Several biophysical experiments were performed to monitor the kinetics of amyloid accumulation of AP. We have incubated the designed IPs separately in parallel as a control to prove our hypothesis.

4.2.4.1. Thioflavin T (ThT) Fluorescence assay:

ThT-Fluorescence assay is a commonly used quantitative technique to monitor *in vitro* amyloid fibril formation over time. ThT fluorescence originates only from the dye bound to amyloid fibrils, so the kinetics of amyloid formation and its inhibition on the addition of inhibitor can be monitored easily by the ThT assay. Upon binding of fibrils, ThT displays a dramatic shift of the excitation and the emission maxima to higher wavelength whereas on the addition of inhibitor, the fluorescence peak intensity decreases indicating inhibition of fibrillar assembly.[17-19]

ThT stock solution was prepared at a concentration of 50 mM in PBS (50 mM, pH 7.2) and stored at 4 °C with proper protection from light to prevent quenching. Lyophilized peptide samples were dissolved in PBS (50 mM, pH 7.2) to obtain a stock solution of variable concentrations (200 μM of AP and different molar ratios of designed peptides) and incubated at 37 °C over water bath. At different time intervals, 40 μL of peptide sample was taken out from the stock solution and was mixed with 200 μL of ThT solution (50 mM); total volume of was made up to 400 μL with PBS (50 mM, pH 7.4) to perform the fluorescence study. Three different replicate solutions were prepared to get a desired stock

solution. For ThT fluorescence assay, emission was measured at 485 nm and excitation at 440 nm, using a slit of 5 nm. Taking text file from the instrument graph was plotted using OriginPro 8 software. Three different sets of replicate solutions were scanned separately for each data point, from where an average was taken with observed standard deviation.

From the result of ThT assay (Figure 4.22), it was found that the fluorescence intensity increased with time gradually for the aggregating peptide alone (black) due to the presence of hydrophobic segment in it. But in the presence of two-fold (red) and five-fold (blue) molar excess of IP1, the fluorescence intensity of AP was found to be suppressed significantly. In the case of IP1 alone (dark cyan), the fluorescence intensity didn't increase enough confirms its non-aggregating nature. Above mentioned results indicate the inhibiting capability of IP1.

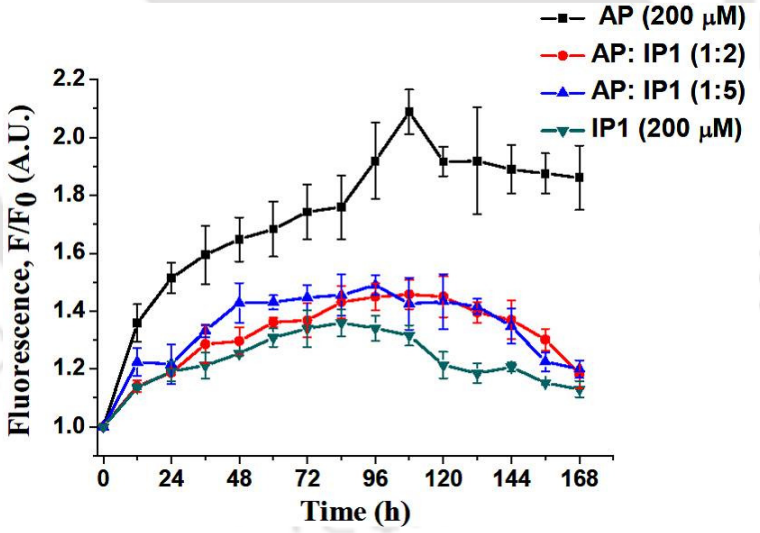

Figure 4.22. ThT Fluorescence assay of AP in the presence of IP1. The fluorescence intensity of AP in the absence (black), and presence of two-fold molar excess of IP1 (red), five-fold molar excess of IP1 (blue), and IP1 alone (dark cyan). Error bars represent the standard deviation of measurements from at least three replicate solutions. All the peptide solutions were incubated in PBS pH 7.4 (50 mM) at 37 °C.

From the ThT assay (Figure 4.23), a time-dependent fluorescence intensity of AP (black) was observed in the absence of IP2, confirms its aggregation. But, in the presence of two-fold (red) and five-fold (blue) molar excess of IP2, the fluorescence intensity was suppressed with time in a dose-dependent manner indicating the decreased amount of amyloid in the solution. The non-aggregating property of IP2 alone was confirmed from its fluorescence intensity which was not increased in a sufficient amount. Above mentioned results indicate the dose-dependent inhibiting potential of IP2.

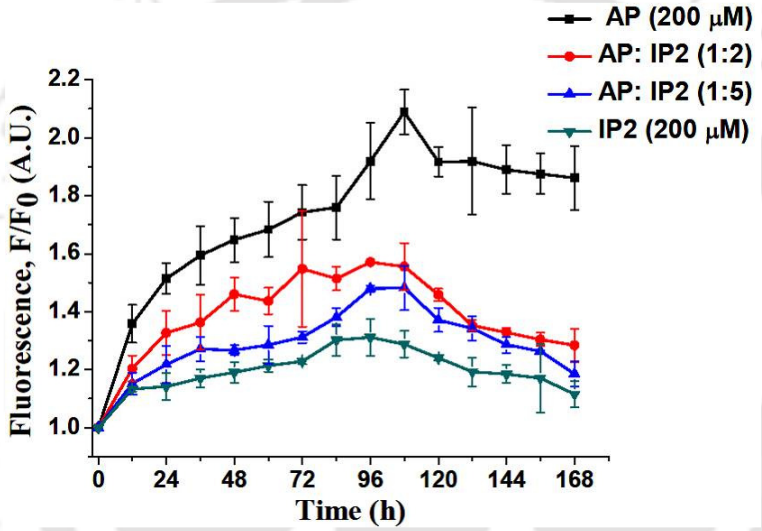

Figure 4.23. ThT Fluorescence assay of AP in the presence of IP2. The fluorescence intensity of AP in the absence (black), and presence of two-fold molar excess of IP2 (red), five-fold molar excess of IP2 (blue), and IP2 alone (dark cyan). Error bars represent the standard deviation of measurements from at least three replicate solutions. All the peptide solutions were incubated in PBS pH 7.4 (50 mM) at 37 °C.

4.2.4.2. Circular Dichroism (CD) spectra:

CD is another spectroscopic technique to study the amyloidogenesis processes by measuring the secondary structural changes during amyloid formation in a solution. The growth of β-sheet conformation can be characterized by CD spectra having positive and negative bands around 195 nm and 220 nm respectively. CD is also an important tool for comparing the structural changes during aggregation. The measurement is usually performed between 190 and 250 nm, as peptide bonds absorb within this wavelength range, 220 nm due to n → π* and 190 nm for π → π* transitions which reveals insights into the secondary structure of proteins.[17-19]

To perform the CD study, stock solution was diluted with respective buffer solution to obtain final concentration of 100 μM. 200 μL of the sample was taken in a cuvette of 10 mm path length having bandwidth of 1 mm. three measurements were accumulated and spectra were recorded from 190 nm to 260 nm.

After seven days of incubation, the conformational changes were studied using CD (Figure 4.24). AP (black) had shown the β-sheet structure which was confirmed from the positive band at around 200 nm and negative band at 225 nm. In the presence of different molar excess (red for 2-fold and blue for 5-fold) of IP1, non-β-sheet structures were obtained which was confirmed from the multiple negative bands ranging from 208 nm to 240 nm. IP1 (dark cyan) itself had shown a mixture of random coil and sheet structure which was confirmed from a positive band at 192 nm and a negative band at 204 nm.

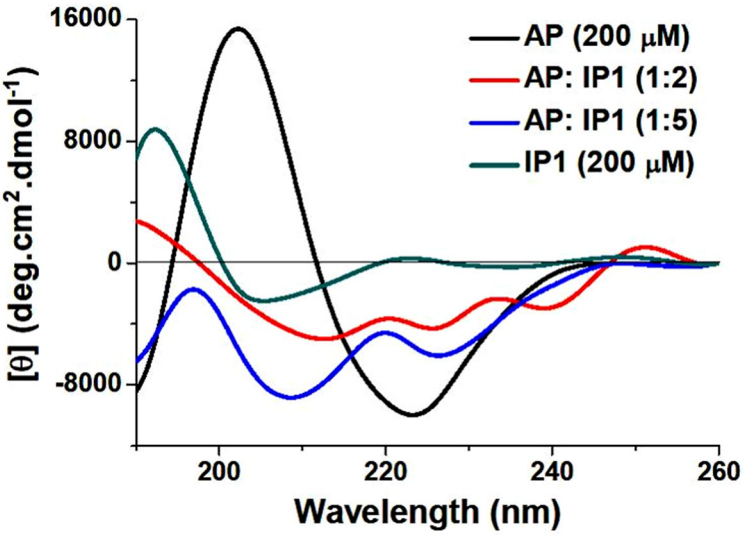

Figure 4.24. CD spectra of AP in the absence (black), and in the presence of 2 fold molar excess of IP1 (red), 5 fold molar excess of IP1 (blue), and IP1 alone (dark cyan). Spectra were taken after 7 days of incubation. All the peptide solutions were incubated in PBS pH 7.2 (50 mM) at 37 °C.

In the presence of two-fold (red) molar excess of IP2 (Figure 4.25), a mixture of helix and minute quantity of β-sheet structure was obtained for AP which was confirmed from a positive band at 196 nm and two negative bands at 212 nm and 225 nm. In the presence of five-fold (blue) molar excess of IP2, a mixture of helix and random coil structure was obtained which was confirmed from a minor positive band at 198 nm and two negative bands at 207 nm and 228 nm. IP2 (dark cyan) itself had shown a mixture of random coil and minute quantity of β-sheet structure which was confirmed from a positive band at 200 nm and a negative band at 209 nm.

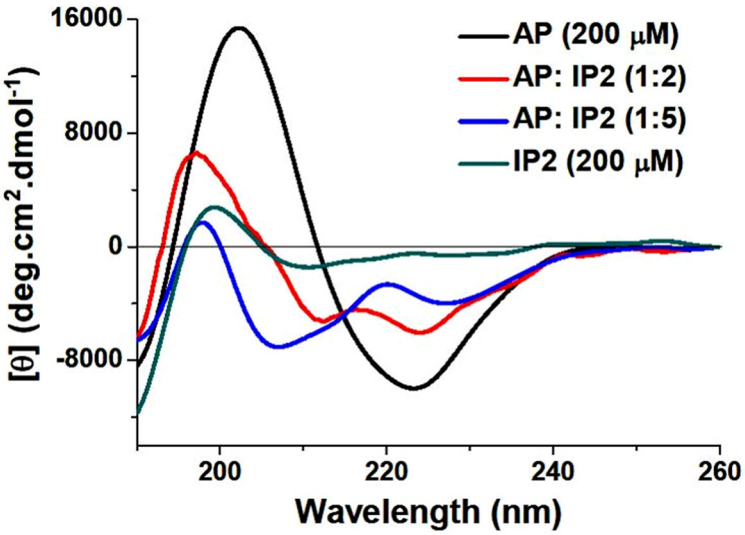

Figure 4.25. CD spectra of AP in the absence (black), and in the presence of 2 fold molar excess of IP2 (red), 5 fold molar excess of IP2 (blue), and IP2 alone (dark cyan). Spectra were taken after 7 days of incubation. All the peptide solutions were incubated in PBS pH 7.2 (50 mM) at 37 ºC.

4.2.4.3. Fourier transformation infrared (FT-IR) spectra:

Protein misfolding is associated with a change in secondary structure and FT-IR being sensitive to the secondary structure of proteins, has become a valuable technique for studying protein aggregation specifically to detect the growth of the β-sheet structure during fibril formation. The amide I band (1700−1600 cm^{-1}) is the most sensitive spectral region to the protein secondary structural components due to almost entirely C=O stretch vibrations of the peptide linkages. The bands in the region of 1625-1640 cm^{-1} are assigned to β-sheet structure and bands arising in between 1640-1660 cm^{-1} indicate random coil or α-helix conformation of peptides or proteins.[17-19]

Peptide stock solution which was prepared for ThT fluorescence assay, was used for FT-IR analysis. 20 μL of the peptide sample was taken from the stock after required time of incubation and mixed with KBr, dried completely at 50 ºC to prepare pellets. To obtain

final spectra, background scan was subtracted and graphs were plotted from text files using OriginPro 8 software.

The conformational changes were also studied using FTIR after seven days in vitro. In the FTIR spectrum of AP (Figure 4.26) alone, the amide I band at 1636 cm^{-1} was observed indicating the β-sheet conformation. But in the FTIR spectra of IPs, the amide I band at 1651 cm^{-1} was observed indicating non-β-sheet conformations of the inhibiting peptides.

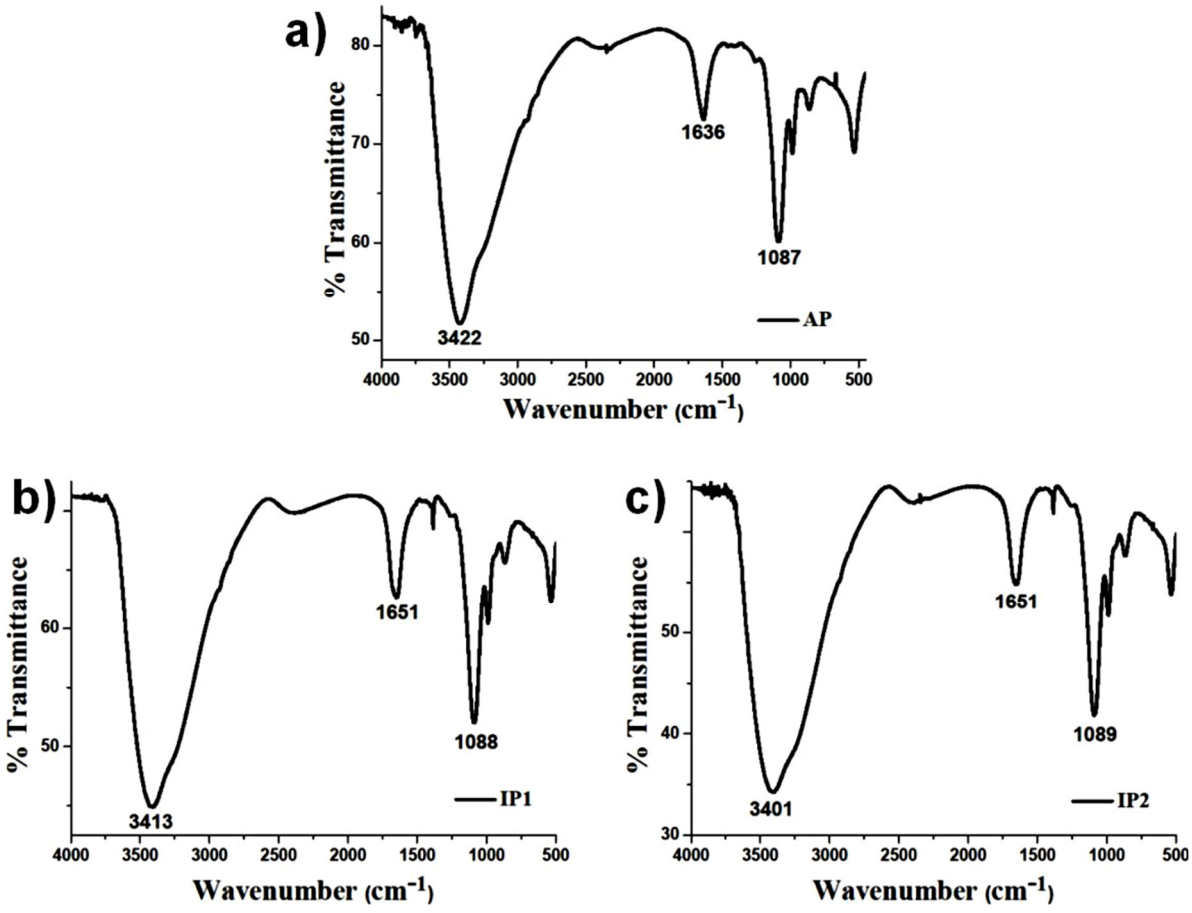

Figure 4.26. (a) FTIR spectra of AP in the absence IP. FTIR spectra of (b) IP1 alone, and (c) IP2 alone. Spectra were taken after 7 days of incubation. All the peptide solutions were incubated in PBS pH 7.2 (50 mM) at 37 ºC.

In the FTIR spectra (Figure 4.27) of AP, the amide I band at 1641 cm^{-1}, 1651 cm^{-1}, 1641 cm^{-1}, and 1652 cm^{-1} were observed in the presence of two-fold IP1, five-fold IP1, two-fold IP2, and five-fold IP2 respectively which indicated the non-β-sheet conformations.

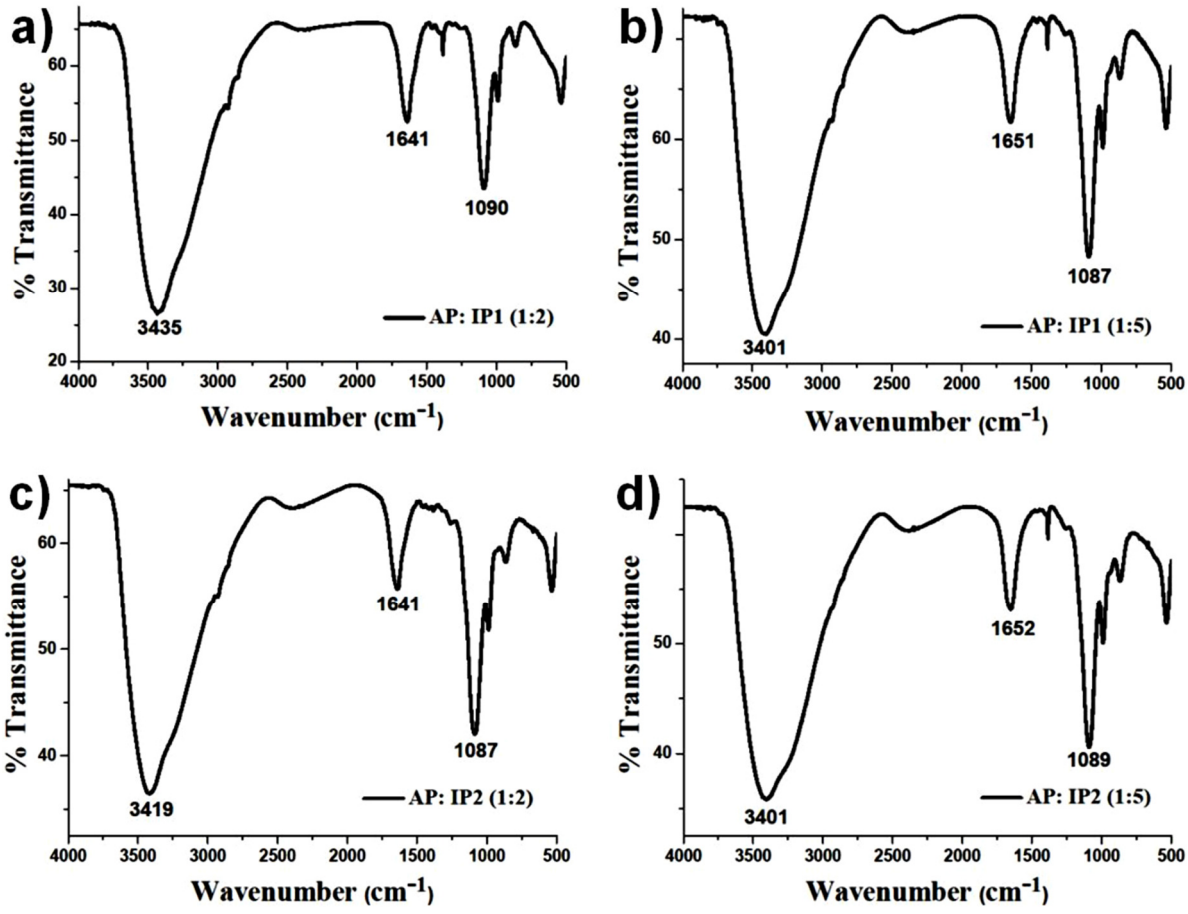

Figure 4.27. FTIR spectra of AP in the presence of (a) 2 fold molar excess of IP1, (b) 5 fold molar excess of IP1, (c) 2 fold molar excess of IP2, and (d) 5 fold molar excess of IP2. Spectra were taken after 7 days of incubation. All the peptide solutions were incubated in PBS pH 7.2 (50 mM) at 37 °C.

4.2.4.4. Transmission electron microscopy (TEM) studies:

TEM is a microscopic technique for qualitatively confirming the presence of amyloid fibers, characterising the morphology of fibrils and pre-fibrillar species in a protein aggregation reaction product.[17-19]

To perform TEM analyses, 10 µL aliquot from the stock peptide solution was taken which were incubated for seven days. Aliquot was added over a carbon coated copper grid allowing to float for 1 min, followed by addition of 10 µL of 2 % uranyl acetate solution over it for negative staining. The droplet was allowed to stand for 1 min and excess solution was removed by blotting paper. Grid was air-dried at room temperature, kept in desiccators and examined at 200 kV under TEM.

The fibrillogenicity of AP in absence and presence of IPs were characterized by TEM studies. A clear fibril structure of AP (a-b) (Figure 4.28) was observed when incubated alone. Any fibrillar assembly was not observed in the case of (c) IP1 and (d) IP2 alone, indicating non-fibrillar character of the IPs. Also, in the presence of (e) two-fold IP1, (f) five-fold IP1, (g) two-fold IP2, and (h) five-fold IP2, no such fibrillar structures of AP were noticed. Therefore, it was confirmed that the IPs significantly inhibited the aggregates of fibril AP.

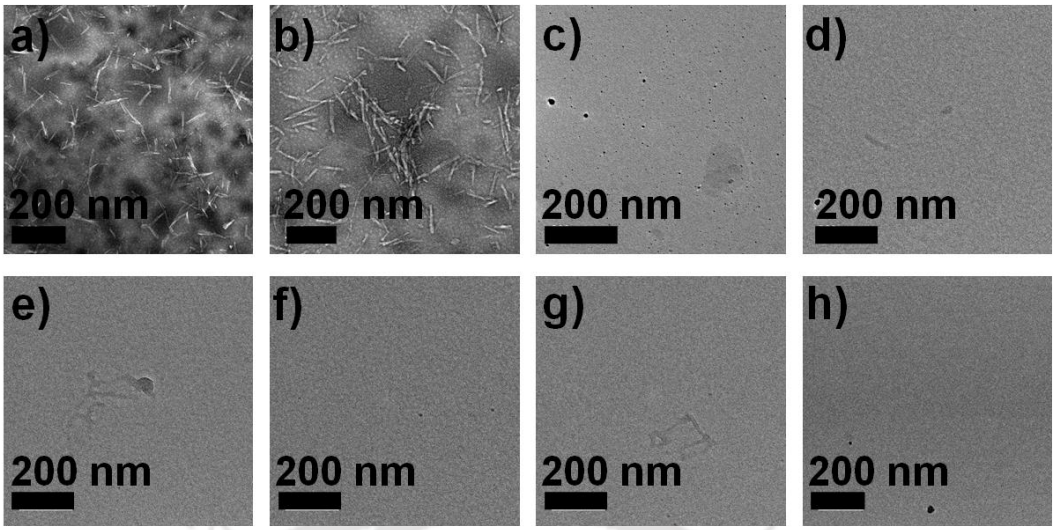

Figure 4.28. TEM images of (a-b) AP in the absence, and in the presence of (e) 2 fold molar excess of IP1, (f) 5 fold molar excess of IP1, (g) 2 fold molar excess of IP2, and (h) 5 fold molar excess of IP2. TEM images of (c) IP1, and (d) IP2. Images were taken after 7 days (5 days for a) of incubation in PBS pH 7.2 (50 mM) at 37 °C. Scale bar is indicated as 200 nm for TEM images.

4.2.4.5. Congo-Red stained Green gold birefringence studies:

Congo-Red preferentially binds to the β-pleated sheet conformation of amyloid fibrils. Fibrils stained with Congo-Red when viewed under a polarisable microscope, it display green gold birefringence, the hallmark of all amyloids, and is therefore used in the diagnosis of amyloidosis.[17-19]

Commercially available Congo red was dissolved in 80 % aqueous ethanol to prepare a saturated solution. Then saturated sodium chloride solution was added into the saturated Congo red solution, stirred and filtered to obtain final working solution for analysis. For birefringence studies, the peptide stock solution which was prepared for thioflavin T experiment can be used.

After required time intervals, 20 mL aliquot of the peptide solution taking from the stock was added on a glass slide followed by 40 mL of the saturated Congo red solution and was allowed to dry. Removing excess solution by blotting paper, the sample was dried at room temperature and kept in desiccators.

The amyloidogenicity of the AP in absence and presence of IPs were characterized by Congo-Red stained birefringence studies. A green gold birefringence of AP (a-b) (Figure 4.29) was observed when viewed under cross-polarized light after staining with Congo-Red dye. Any birefringence in the case of (c) IP1 and (d) IP2 alone were not observed. Also, in the presence of (e) two-fold IP1, (f) five-fold IP1, (g) two-fold IP2, and (h) five-fold IP2, no such birefringence of AP were noticed. From the above results, it was confirmed that the IPs were non-amyloidogenic in nature and inhibited the amyloid aggregates of AP.

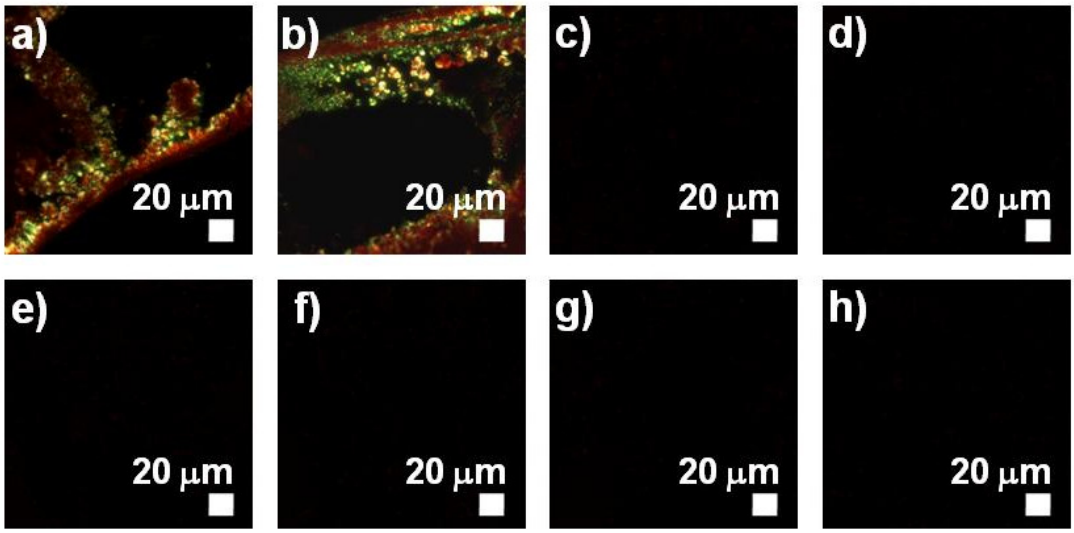

Figure 4.29. Congo-red birefringence images of (a-b) AP in the absence, and in the presence of (e) 2 fold molar excess of IP1, (f) 5 fold molar excess of IP1, (g) 2 fold molar excess of IP2, and (h) 5 fold molar excess of IP2. Birefringence images of (c) IP1, and (d) IP2. Images were taken after 7 days (5 days for a) of incubation in PBS pH 7.2 (50 mM) at 37 °C. Scale bar is indicated as 20 μm.

4.2.5. Molecular docking studies:

Docking studies have been performed with our designed peptides (IP1 and IP2) (Figure 4.30) using AutoDock Vina version 1.1.2 software. [18,19,20] The segment of helical $A\beta_{1-40}$ extracted from RCSB protein data bank (PDB ID: 4NGE) has been used for docking studies. For protein preparation AutoDock 4.2 MGL Tools version 1.5.6 software package was used where removing all water molecules, assigning hydrogen polaraties, calculating Gasteiger charges to protein structures, protein structure was converted to PDBQT format. OpenBabel version 2.4.1 software was used to convert ligand in PDB format after minimizing energy and the PDB file was modified by combining with non-polar hydrogens, addition of Gasteiger charges and rotable bonds, then converted to the PDBQT format of the ligand. The fixable and non-bonded rotation of molecules were assigned by calculating torsion angles. Ligands were docked individually to the receptor (protein molecule) with grid coordinates (grid center) and grid boxes of certain sizes for each receptor which was customized by using Auto Grid version 4.2. The grid size was set at 60×60×60 (x, y, and z) points, and the grid centre was designated at x, y, and z dimensions of 3.130, -3.283, -17.750 respectively, with a grid spacing of 1.000 Å. The output file was generated as ligand_out.pdbqt format which contains ligand-binding affinity predicted as negative Gibbs free energy (ΔG) scores (in kcal/mol) and RMSD lower bound, RMSD upper bound. Post-docking analyses were visualized using PyMOL version 1.7.4.5 software , the best and most energetically favorable conformations of each ligand were selected. From molecular docking studies, it was observed that both the IPs docked with the hydrophobic region as expected and fitted properly in the related binding pocket having a negative binding affinity.

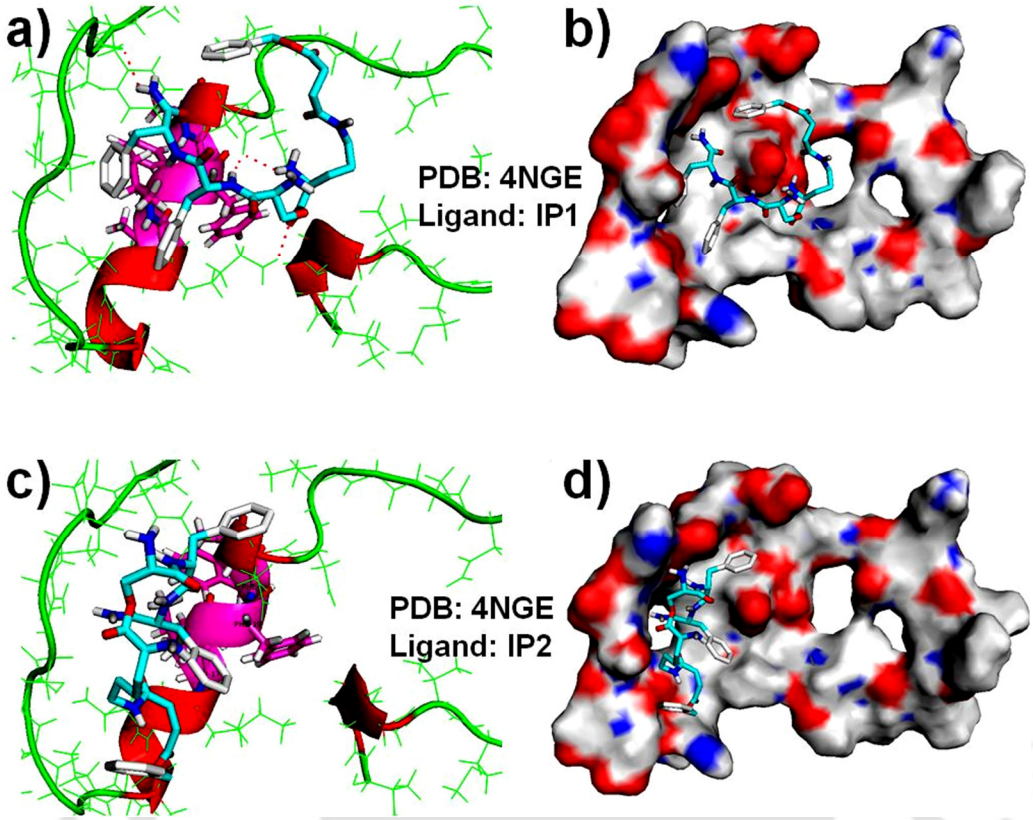

Figure 4.30. Molecular docking images of IP1 (a, b), and IP2 (c, d) into helical Aβ$_{1-40}$ (PDB ID 4NGE) reveals that IPs binds very well with binding affinity -5.6 kcal/mol, and -4.9 kcal/mol respectively. Structures are shown as line and cartoon representation (for a, c), and surface representation (for b, d). The surface of Aβ$_{1-40}$ is coloured according to the charges of the atoms where negatively and positively charged zones are represented in red and blue, respectively.

4.3. Conclusion:

Inhibition strategy is a promising therapeutic approach against protein aggregation diseases like Alzheimer's disease, Prion disease, Huntington's disease, *etc.* In this work, for a representative example, the core hydrophobic segment of amyloid-β was taken and named as the aggregating peptide (AP). The "O → N acyl migration" concept was used here to produce an *in situ* cyclic peptide for the generation of a desirable bent unit. The relevant peptides were designed, synthesized and named as inhibiting peptides (IP). The inhibition mechanism involves the dual "O → N acyl migration" of a side-chain modified dipeptide, followed by the nucleophilic attack of Ser to the carbonyl group of succinamide unit to form a cyclic dipeptide finally. The kinetics of amyloid aggregates of fibril AP was characterized by various biophysical tools (ThT-assay, CD, FTIR, TEM, and Congo-Red stained birefringence studies). Results implied that IPs significantly inhibited the amyloid fibril of AP. Therefore it can be concluded that the designed IPs may be useful to design a drug against Alzheimer's disease and associated disorders.

4.4. Characterization data:

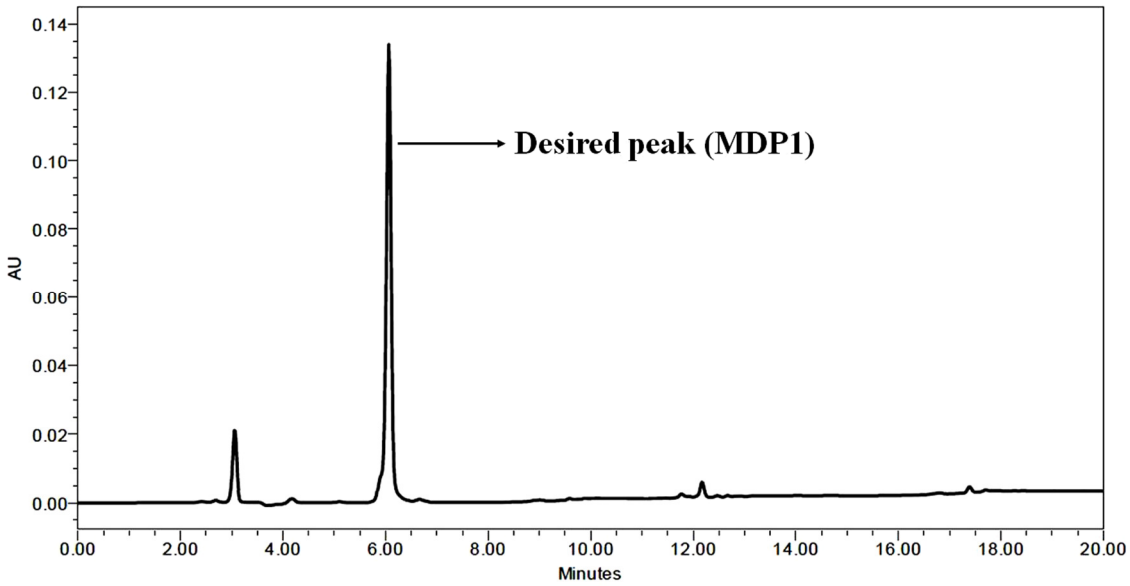

Figure 4.31. HPLC profile picture of the purified MDP1.

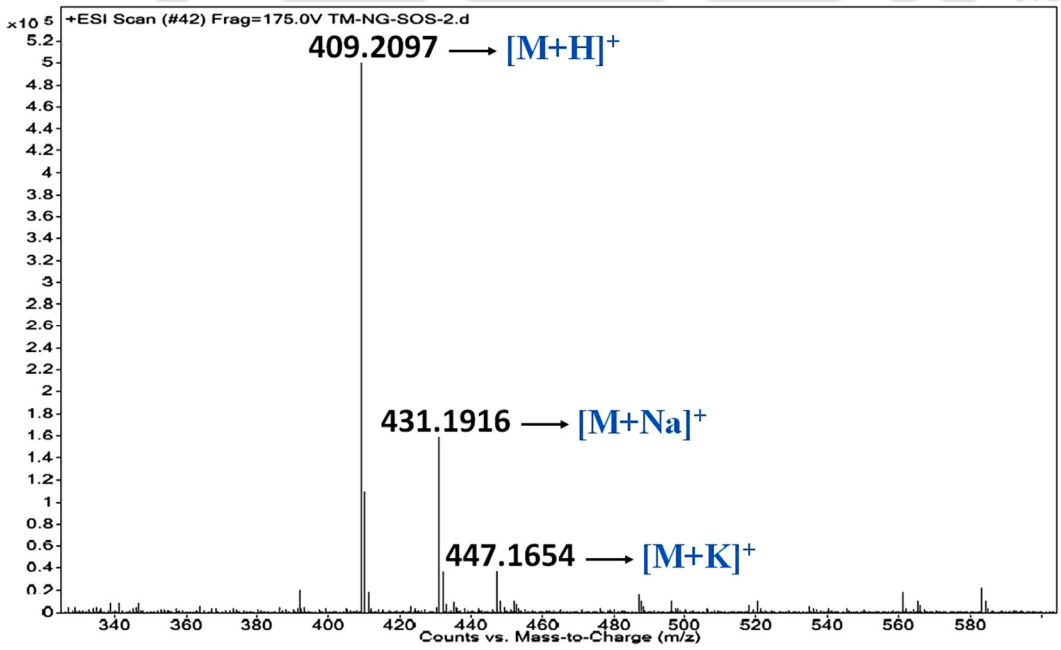

Figure 4.32. ESI-Mass spectrum of the MDP1. Calculated m/z for $C_{19}H_{28}N_4O_6$ $[M+H]^+$ is 409.2087, observed 409.2097.

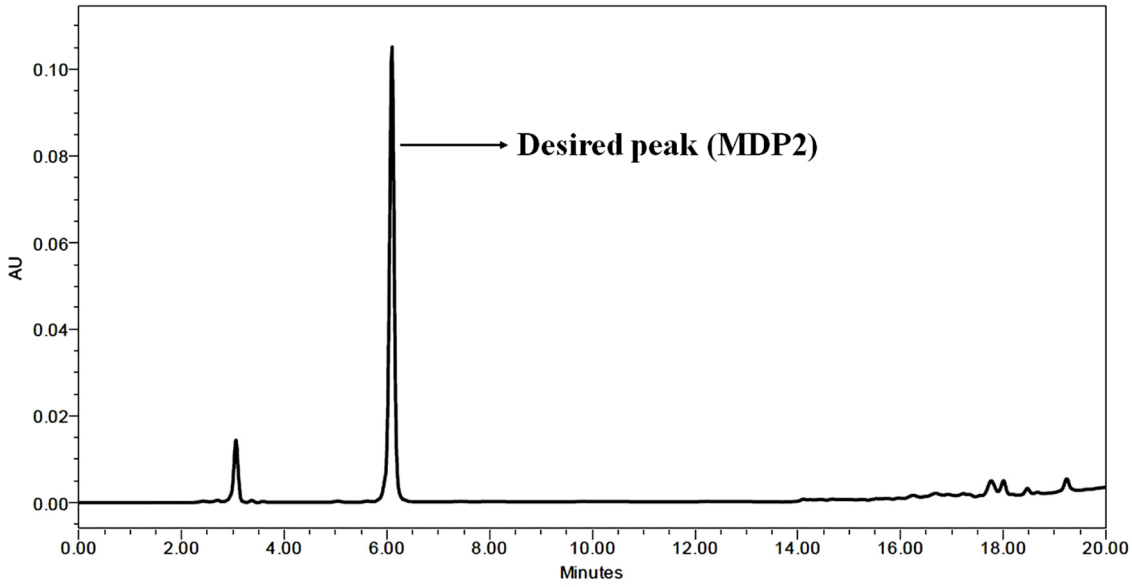

Figure 4.33. HPLC profile picture of the purified MDP2.

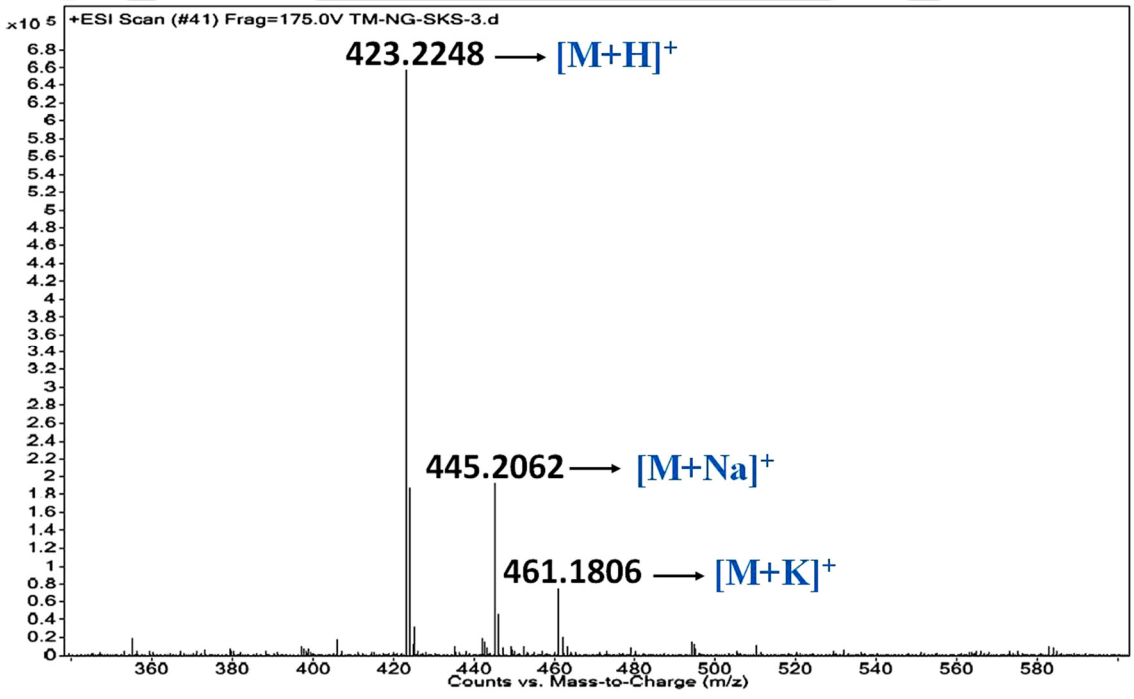

Figure 4.34. ESI-Mass spectrum of the MDP2. Calculated m/z for $C_{20}H_{30}N_4O_6$ $[M+H]^+$ is 423.2243, observed 423.2248.

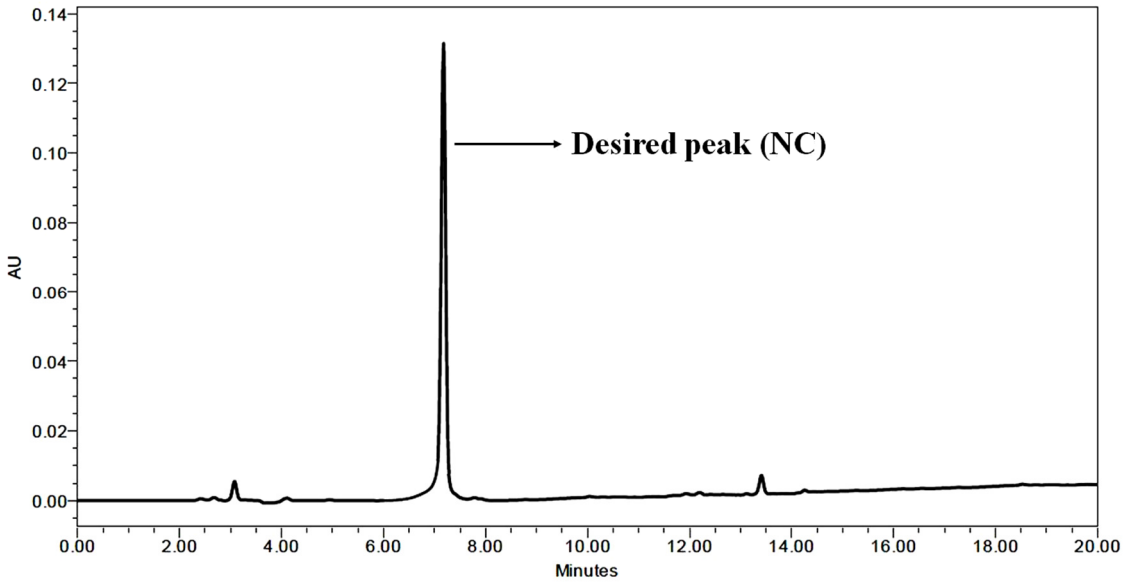

Figure 4.35. HPLC profile picture of the purified NC.

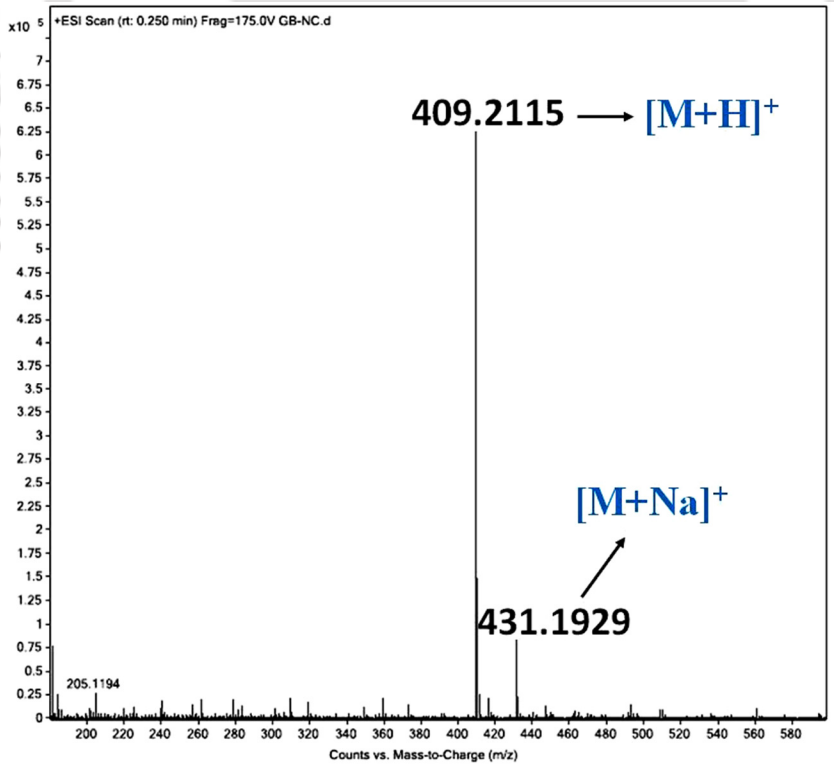

Figure 4.36. ESI-Mass spectrum of the NC. Calculated m/z for $C_{19}H_{28}N_4O_6$ $[M+H]^+$ is 409.2087, observed 409.2115.

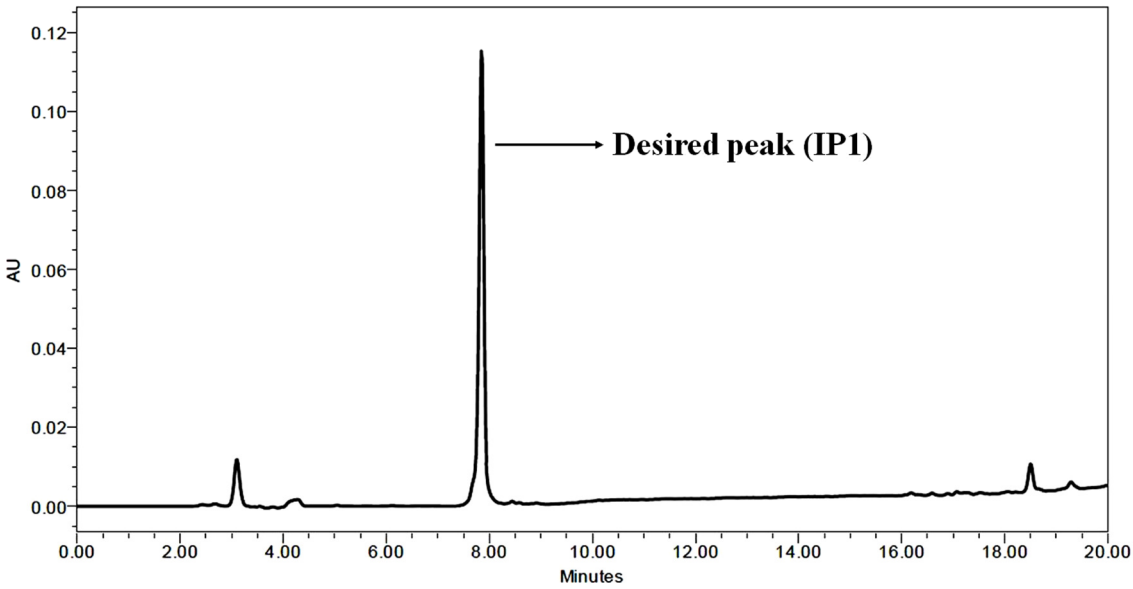

Figure 4.37. HPLC profile picture of the purified IP1.

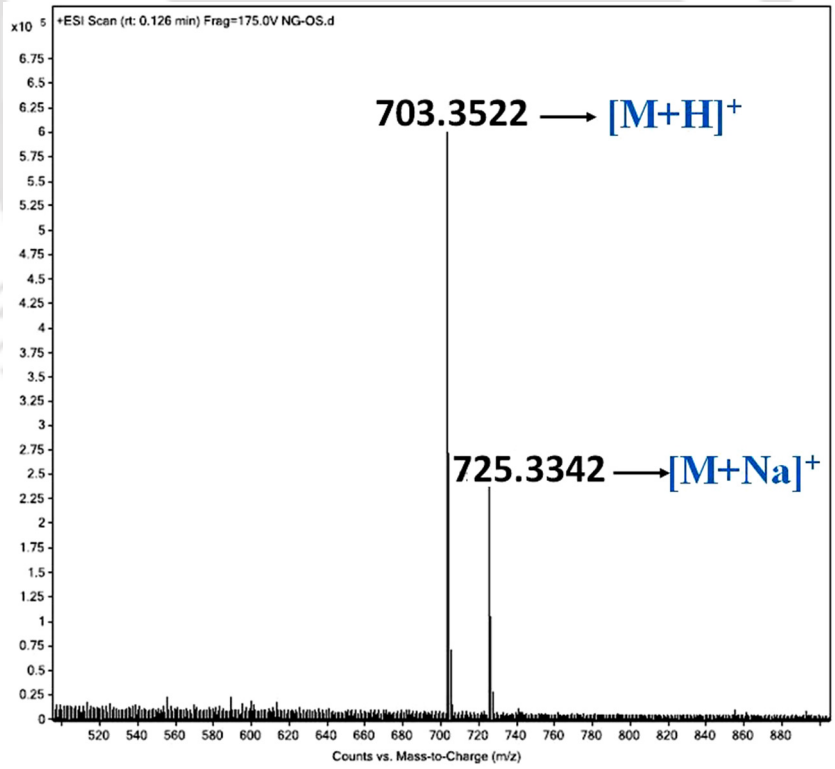

Figure 4.38. ESI-Mass spectrum of the IP1. Calculated m/z for $C_{37}H_{46}N_6O_8$ $[M+H]^+$ is 703.3455, observed 703.3522.

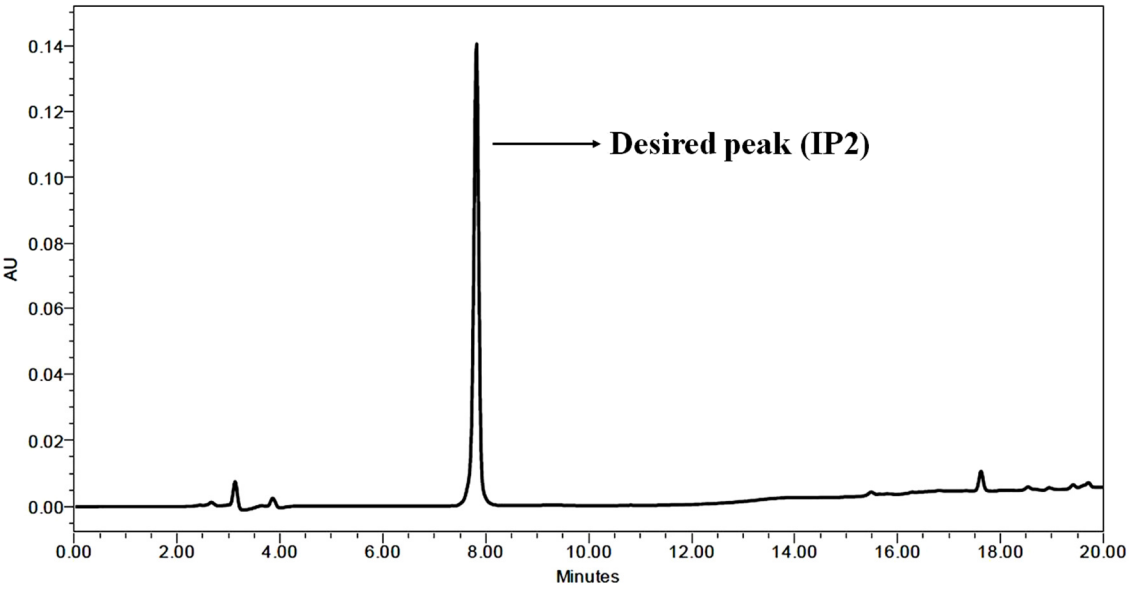

Figure 4.39. HPLC profile picture of the purified IP2.

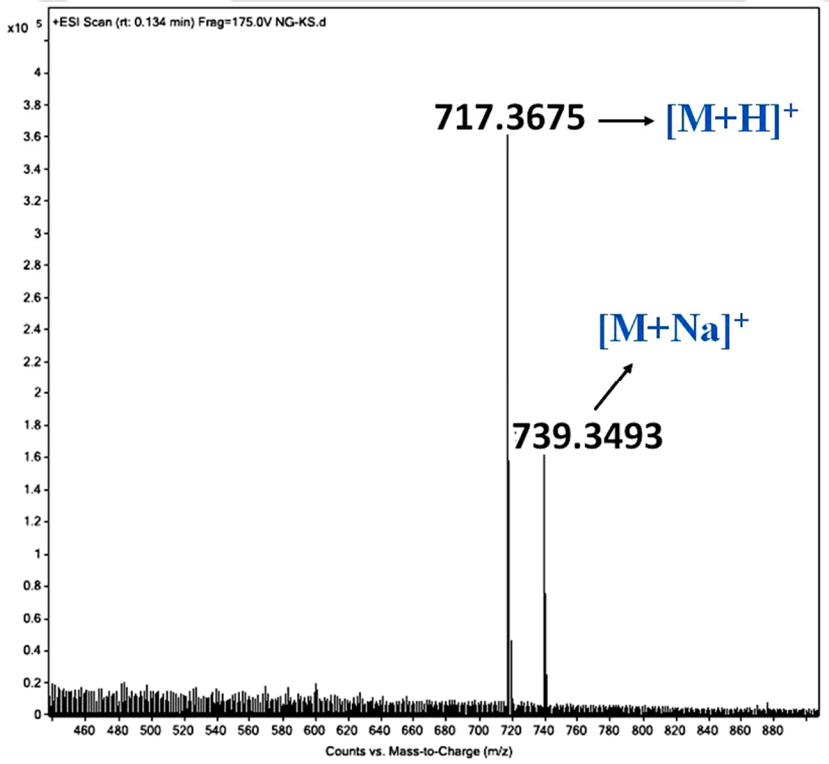

Figure 4.40. ESI-Mass spectrum of the IP2. Calculated m/z for $C_{38}H_{48}N_6O_8$ $[M+H]^+$ is 717.3612, observed 717.3675.

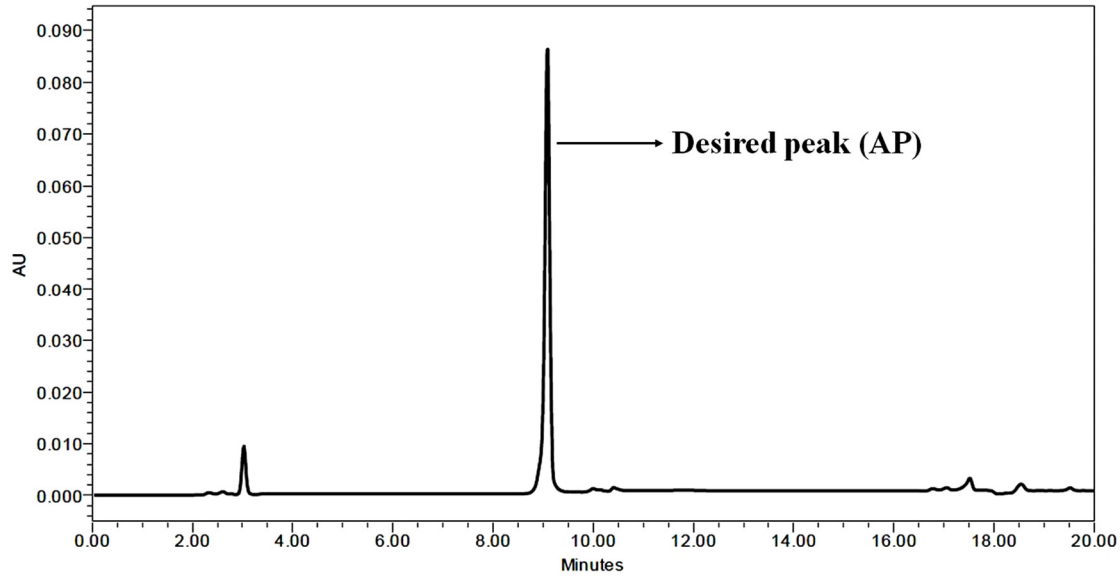

Figure 4.41. HPLC profile picture of the purified AP.

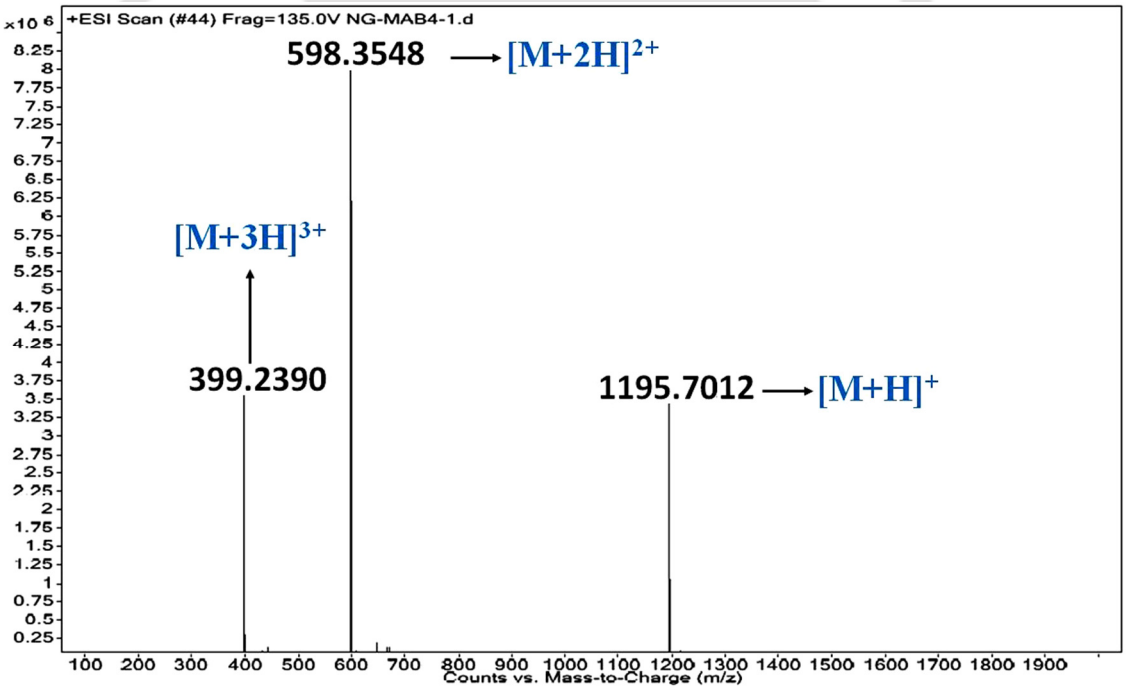

Figure 4.42. ESI-Mass spectrum of the AP. Calculated m/z for $C_{59}H_{86}N_{16}O_{11}$ $[M+H]^+$ is 1195.6740, observed 1195.7012.

4.5. References:

[1] Chiti, F.; Dobson, C. M. *Annu. Rev. Biochem.* **2006**, *75*, 333-366.

[2] Selkoe D. J. *J. Neuropathol. Exp. Neurol.* **1994**, *53*, 438-447.

[3] Abelein, A.; Bolognesi, B.; Dobson, C. M.; Graslund, A.; Lende, C. *Biochemistry* **2012**, *51*, 126-137.

[4] Tracz, S. M.; Abedini, A.; Driscoll, M.; Raleigh, D. P. *Biochemistry* **2004**, *43*, 15901-15908.

[5] Taylor, M.; Moore, S.; Mayes, J.; Parkin, E.; Beeg, M.; Canovi, M.; Gobbi, M.; Mann, D. M.; Allsop, D. *Biochemistry* **2010**, *49*, 3261-3272.

[6] Peretto, I. *et al*. *J. Med.Chem*. **2005**, *48*, 5705-5720.

[7] Tjernberg, L. O.; Näslund, J.; Lindqvist, F.; Johansson, J.; Karlström, A. R.; Thyberg, J.; Terenius, L.; Nordstedt, C. *J.Biol.Chem*. **1996**, *271*, 8545-8548.

[8] Soto, C.; Sigurdsson, E. M.; Morelli, L.; Kumar, R. A.; Castaño, E. M.; Frangione, B. *Nat. Med.* **1998**, *4*, 822-826.

[9] Hard, T.; Lendel, C. *J. Mol. Biol*. **2012**, *421*, 441-465.

[10] Solomon, B.; Koppel, R.; Hanan, E.; Katzav, T. *Proc. Nat. Acad. Sci. USA*. **1996**, *93*, 452-455.

[11] Sehgal, N.; Gupta, A.; Valli, R. K.; Joshi, S. D.; Mills, J. T.; Hamel, E.; Khanna, P.; Jain, S. C.; Thakur, S. S.; Ravindranath, V. *Proc. Nat. Acad. Sci. USA*. **2012**, *109*, 3510-3515

[12] Soto, C.; Sigurdsson, E. M.; Morelli, L.; Kumar, R. A.; Castano, E. M.; Frangione, B. *Nat. Med. 4(7)*, **1998**, 822-826.

[13] Nadimpally, K. C.; Paul, A.; Mandal, B. *ACS Chem Neurosci*. **2014**, *5(5)*, 400-408.

[14] Mutter, M.; Chandravarkar, A.; Boyat, C.; Lopez, J.; Dos Santos, S.; Mandal, B.; Mimna, R.; Murat, K.; Patiny, L.; Saucède, L.; Tuchscherer, G. *Angew. Chem. Int. Ed*. **2004**, *43*, 4172–4178.

[15] Saucede, L.; Santos, S. D.; Chandravarkar, A.; Mandal, B.;Mimna, R.; Murat, K.; Camus, M. S.; Berard, J.; Grouzmann,E.; Adrian, M.; Dubochet, J.; Lopez, J.; Lashuel, H.; Tuchscherer,G.; Mutter, M. C. *Chimia* **2006**, *60*, 199–202.

[16] Coin, I.; Beyermann, M.; Bienert, M. *Nat. Protoc.* **2007**, *2*, 3247-3256.

[17] Nilsson, M. R. *Methods* **2004**, *34*, 151-160.

[18] Mondal, T.; Mandal, B. *ChemComm.* **2019**, *55*, 4933-4936.

[19] Mondal, T.; Mandal, B. *ChemComm.* **2020**, *56*, 2348-2351.

[20] Trott, O.; Olson, A. J. *J. Comput. Chem.* **2010**, *31*, 455-461.

Chapter 5: N → N and O → N acyl migration towards the release of bioactive molecules

5.1. Introduction:

Aspartimide formation[1,2,3] is a particularly nasty side reaction that can occur during fmoc-based solid-phase peptide synthesis.[4,5,6] Aspartimide can spontaneously occur due to the presence of a base like piperidine or DBU during the Fmoc cleavage step. Aspartimide ring closure results due to nucleophilic attack from the amide nitrogen of the preceding residue to the β-carboxyl moiety of Asp with alcohol loss. The β-functional group in the side chain of Asp usually is masked as an ester like ^{t}Bu, Bzl, which acts as a leaving group in this side reaction. Once the five-member cyclic imide formed due to O→N acyl migration, the susceptibility of the two carbonyl carbons to nucleophiles such as H_2O, piperidine, *etc.*, leads to ring-opening. Attack of water to the succinimide moiety produces a mixture of *α*- and *β*-aspartyl peptides, with the latter being the dominant product. Enantiomerization of Asp also results due to treatment of aspartimide peptides with strong bases. Under certain strongly acidic conditions, this unwanted cyclization is also reported to occur on the unprotected β carboxyl group in Boc based SPPS.

Aspartimide formation is highly sequence dependent. [7,8] When glycine, asparagine, aspartic acid, cysteine remain in the preceding position, the highest is the propensity of aspartimide formation. The tendency of aspartimide formation also depends on side-chain ester as

Asp(OBzl) is known to generate aspartimide easily comparing other counterparts. The undesired formation of aspartimide results in low yields with difficulties in purification. To minimize aspartimide formation, three primary approaches are i) increasing the steric bulk of Asp acid ester moiety, aspartimide formation can be decreased. ii) a backbone amide bond protecting acid-labile groups such as dimethoxybenzyl (Dmb), 2-hydroxy-4-methoxy-5-nitrobenzyl (Hmnb) preclude the possibility of aspartimide formation. iii) the addition of HOBt (1-hydroxybenzotriazole) or 2,4-dinitrophenol (Dnp) with the base in DMF during Fmoc deprotection was reported to reduce the amount of aspartimide during SPPS.

Generally, electron-donating and/or sterically hindered *β*-carboxyl protecting groups like cyclohexyl ester in the Boc-based chemistry and *tert*-butyl ester in the Fmoc/Bu*t* approach are well established to minimize the aspartimide formation.

The chemical and structural properties of the 5-membered ring being significantly useful to have been applied from medicinal chemistry to material science. Aspartimide based compounds like bis(*N*-silylalkyl)aspartimides[9] have been used to prepare surfactants, viscosity modifiers, primers, and adhesives. It has been recently observed that the presence of aspartimide moieties supports cell adhesion of peptides *in vivo* and *in vitro*. Poly-aspartimides, due to their biodegradable nature, have become useful solid supports for anchoring sialic acid linkers as inhibitors of viruses like influenza. Aspartimide, like proline and succinimide residue, induces a type II β turn in the peptide backbone conformation due to stabilization by intramolecular hydrogen bonding. Using this concept, Asp acid incorporated Aβ-breaker peptide is reported which converts the native peptide to aspartimide version at the physiological condition to generate a kink *in situ*, subsequent

ring-opening and racemization of Asp completely disrupts the peptide backbone and hence would inhibit the aggregation of Aβ peptide along with β sheet disruption.[10]

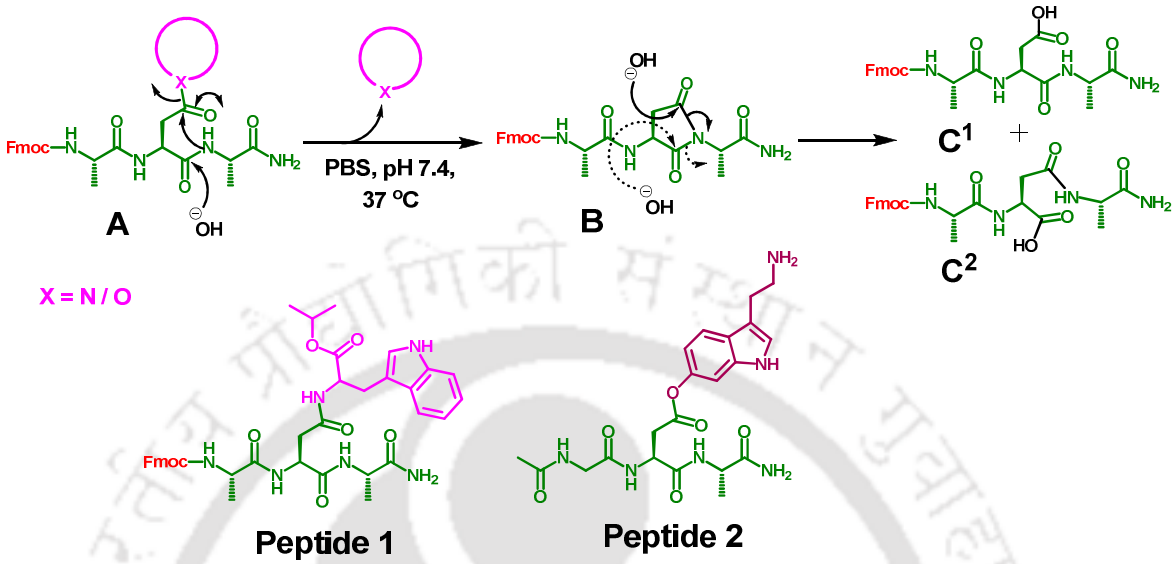

Figure 5.1. A schematic diagram cum plausible mechanism of releasing bioactive molecule from the designed peptide moiety.

5.2. Results and Discussions:

5.2.1. Design of the Peptides:

Though aspartimide formation is an undesirable side reaction in Fmoc based SPPS, taking advantage of *in situ* aspartimide formations almost at physiological conditions without any external reagent, we planned to release covalently attached small, bioactive molecules as leaving group from side-chain modified Asp moiety.

The chemical reaction "O→N acyl migration" is involved in the aspartimide formation, which is a facile process as described earlier. Eventually, it releases the leaving group of the side-chain ester faster than normal ester hydrolysis. Here we have used a small molecule Serotonin (5-hydroxytryptamine) to attach at the side-chain of Asp for the fast release system. Serotonin is mainly found in the brain, bowels, and blood platelets which functions

both as a neurotransmitter in the central nervous system and as a hormone in the periphery. Serotonin is thought to help regulate several physiologic activities, including mood and social behaviour, appetite and digestion, sleep, memory, emotions, motor, cognitive, and autonomic functions.[11]

Besides this, we wanted to develop comparatively a slower release system as the slow, prolonged release of drugs reduce the number and frequency of doses required, taking less frequently of drugs minimize patient noncompliance, a constant lower concentration of the drug release reduces the possibility of toxic levels of drugs hence less adverse effects, more therapeutic effectiveness.[12] Prolonged-release system of the drug also prevents very rapid absorption of the drug, which might result in extremely high peak plasma drug concentration.[13]

On the other hand, trans-amidation (N→N acyl migration) is difficult to happen. But, taking advantage of aspartimide formation, we have planned to release the bioactive molecules slowly *in-vitro* through N→N acyl migration. Here we have used Tryptophan and attached it at the side-chain of Asp. The essential amino acid L-tryptophan serves as the precursor for the synthesis of serotonin. It is a two-step process where the enzyme tryptophan hydroxylase converts tryptophan to 5-hydroxytryptophan at first, which is then decarboxylates to produce serotonin.[14]

5.2.2. Synthesis and purification procedure of the designed peptides:

The main chain of designed peptides was first synthesized following the standard Fmoc/^{t}Bu solid-phase peptide synthesis (SPPS) method (Figure 5.2) taking 200 mg of Rink amide MBHA resin (loading 0.5 mmol/g) in a 5 ml frit-fitted plastic syringe. Then cleaving the peptides from the resin, the side chains of Asp were covalently modified with tryptophan and serotonin in the solution phase.

In solid phase:

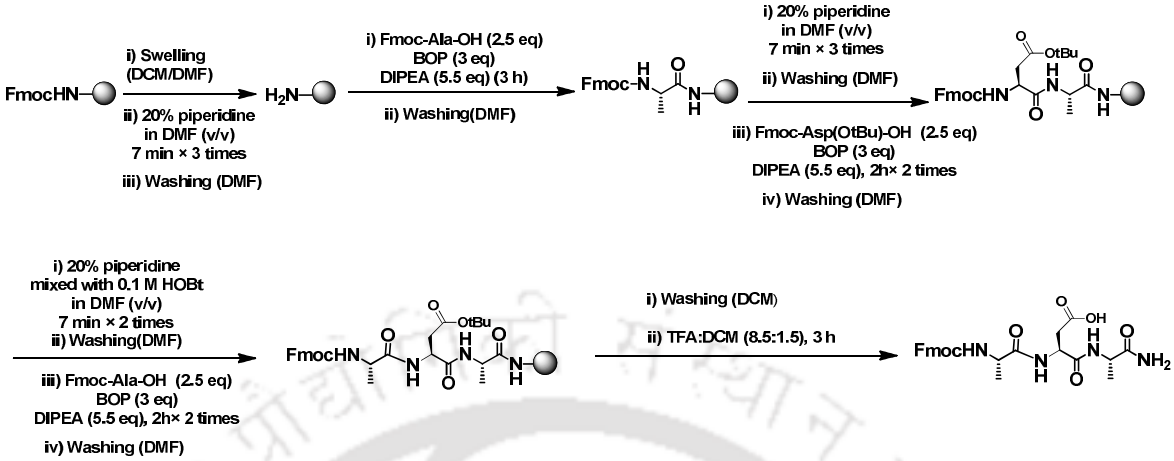

Figure 5.2. Schematic diagram of the synthesis of Fmoc-ADA-NH_2 in solid-phase.

In solution phase:

The side chain of Asp was covalently coupled with isopropyl protected tryptophan for which Fmoc-ADA-NH_2 was treated with W^{ipr} (2.5 eq), coupling reagent BOP (1.2 eq), DIPEA (3.5 eq), and HOBt (0.2 eq) in DCM solvent for 12 h to get Peptide 1 (Figure 5.1).

Peptide 2 (Figure 5.1) was prepared following the same procedure.

In solid-phase:

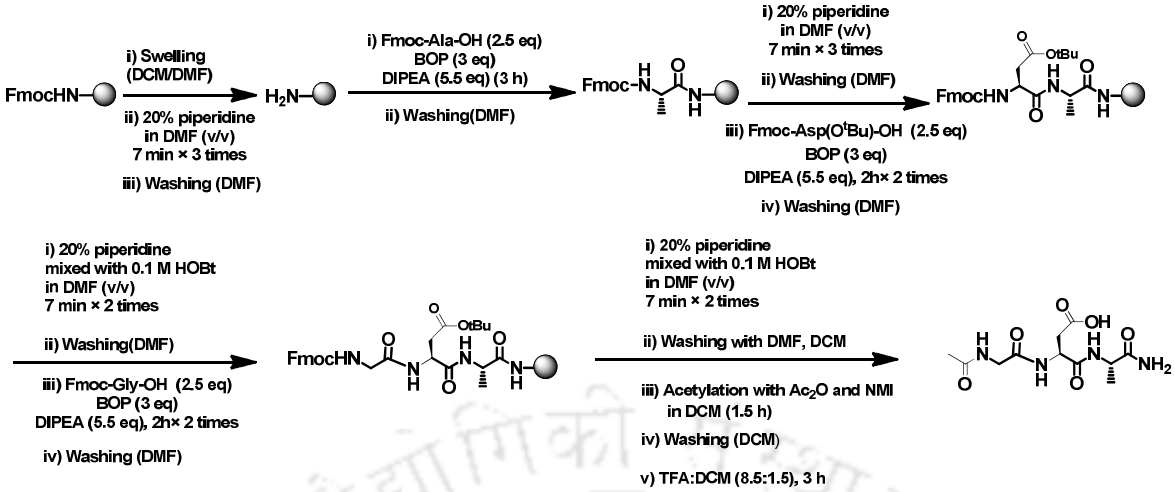

Figure 5.3. Schematic diagram of the synthesis of Ac-GDA-NH_2 in solid-phase.

In solution phase:

The side-chain modification of Asp was carried out by coupling reaction of the crude peptide Ac-GDA-NH_2 (Figure 5.3) with 1.2 eq of Boc-Serotonin, 1.2 eq of BOP (coupling reagent), 3.5 eq of DIPEA (base), and 0.2 eq of HOBt in DCM solvent for 12 h to prepare Peptide 2.

Crude peptides were dissolved in CH_3CN/H_2O mixture and purified by semi-preparative HPLC using C18 reversed-phase column. During purification, binary solvent system [solvent A (0.1 % TFA in H_2O) and solvent B (0.1 % TFA in CH_3CN)], UV detector with dual detection at 214 and 254 nm, the total run time of 20 min. (gradient 5-100 % CH_3CN for 18 min, followed by 100% CH_3CN till 20 min.) with a flow rate of 4 mL/ min was used. Then collected samples were lyophilized.

The purity of the peptides was confirmed by an analytical HPLC system using C18 reversed-phase column with a linear gradient of 5-100% CH_3CN over 18 minutes in a total run time of 20 min selecting dual-wavelength at 214 nm and 254 nm with a flow rate of 1 ml/min. Mass spectrometry of the purified peptide samples was analyzed using positive polarity electrospray ionization (+ESI).

5.2.3. Proof of hypothesis of "N→N acyl migration" and "O→N acyl migration":

Each lyophilized sample was dissolved in a required amount of PBS (50 mM, pH 7.4) followed by sonication and vortex, thus obtained a clear solution. The solution was divided into different Eppendorf tubes equally, maintaining a final concentration of 500 µM, and kept in an incubator at 37 ^{o}C to perform ESI-MS and CD kinetics studies *in vitro*. For kinetic studies, at different time intervals, the required amount of aliquot was collected from Eppendorf tubes after sonicated and vortexed the stock solution for 1 min each.

5.2.3.1. Detection of various fragments of Peptide 1 by Mass spectrometry:

Incubated samples taken at different time intervals for kinetic studies were quenched with 20% HCl, diluted with HPLC grade CH_3CN and Mili-Q water, filtered through 0.2-micron filter paper. Samples were analyzed in ESI positive mode.

From the ESI-MS kinetics studies, it was observed that after three days of incubation (Figure 5.5), Peptide 1 released Tryptophan molecule via aspartimide formation (B) as a result of "N→N acyl migration". The reaction then proceeds to form aspartyl residues (C^1 / C^2). After six days of incubation (Figure 5.6), Peptide 1 was not observed in the solution.

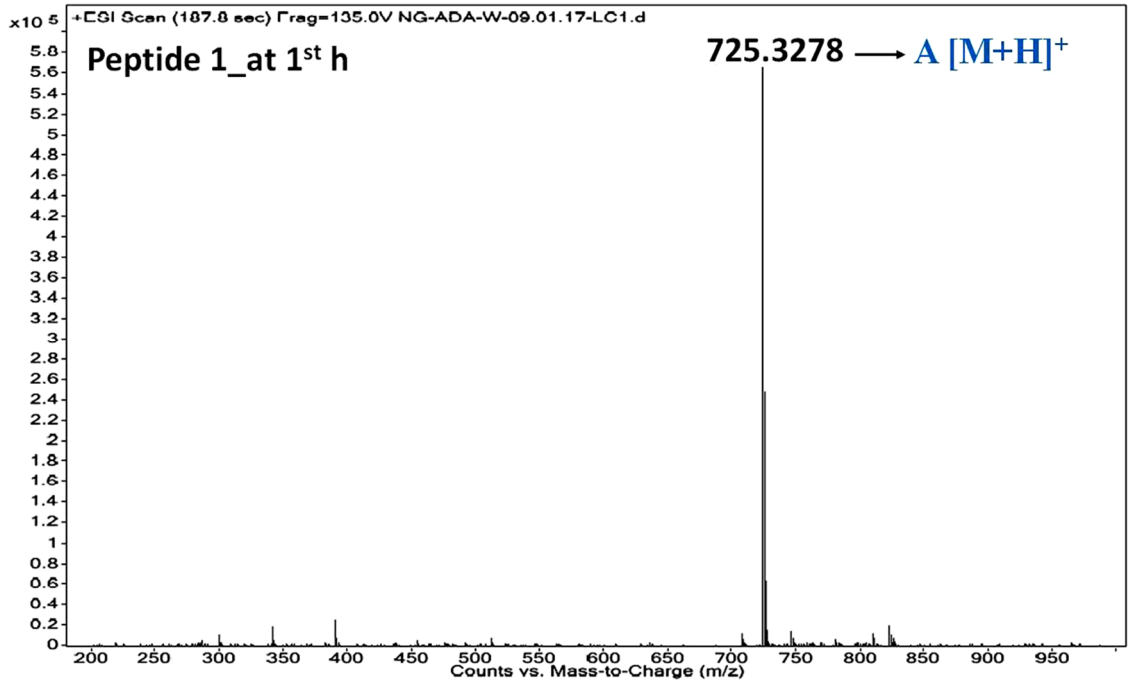

Figure 5.4. The ESI-Mass spectrum of Peptide 1 at the 1st h of incubation in PBS of pH 7.4 at 37 °C.

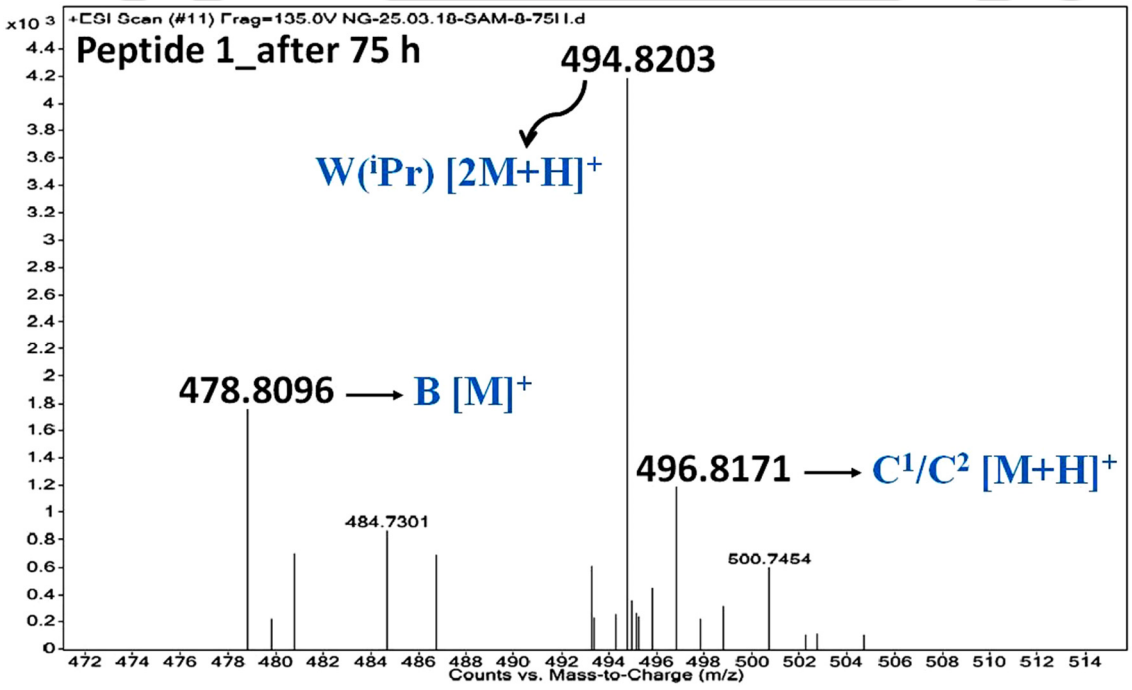

Figure 5.5. The ESI-Mass spectrum of Peptide 1 after 75 h of incubation in PBS of pH 7.4 at 37 °C.

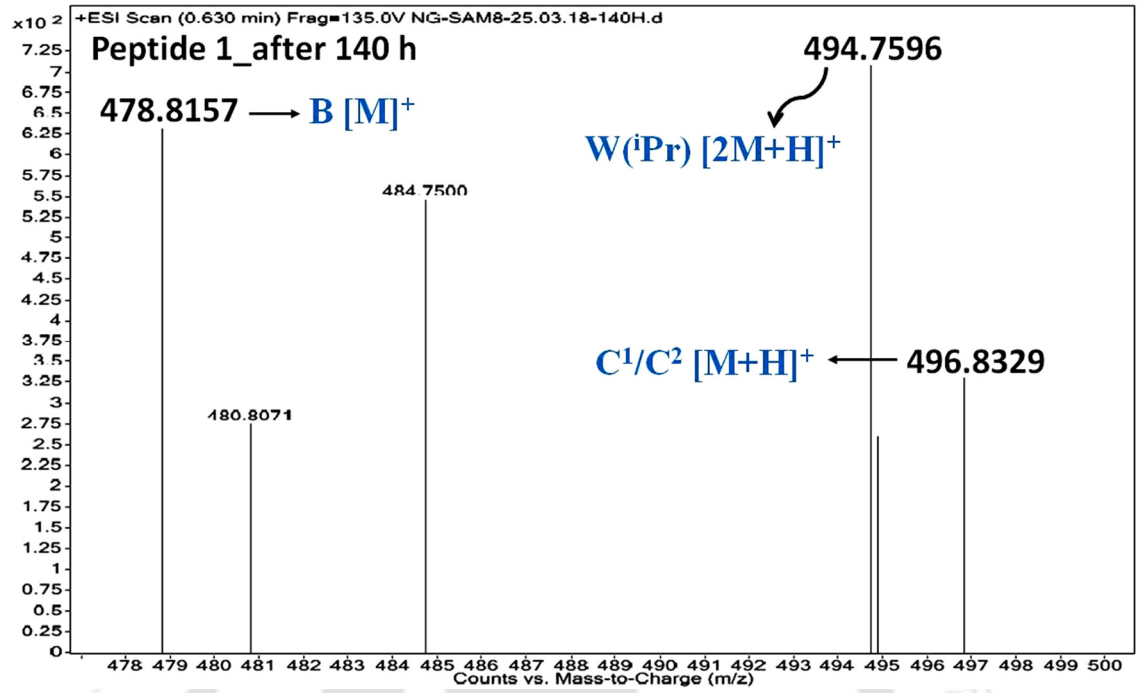

Figure 5.6. The ESI-Mass spectrum of Peptide 1 after 140 h of incubation in PBS of pH 7.4 at 37 ºC.

5.2.3.2. Circular Dichroism (CD) of Peptide 1:

CD spectroscopy is the most useful technique used for estimating the secondary structures of proteins and polypeptides in solution.[15,16] This technique can be used to monitor changes between unordered (random coil) and ordered (alpha-helix or beta-sheet) structures.[17] The CD spectrum of a random coil is usually characterized by a single band below 200 nm, whereas alpha-helical structures usually show two negative bands at 208 and 222 nm along with one positive band at 192 nm; beta-sheet structures typically exhibit a negative band at 217 nm and a positive band at 195 nm.

Incubated samples treating with 0.1% trifluoroacetic acid to quench any further reaction were stored at -20 °C. Before the experiment, the samples were diluted with PBS buffer solutions to obtain a final concentration of 100 µM. For analysis, 200 µL of the sample was taken in a cuvette having a pathlength of 1 mm, samples were measured thrice, and spectra

were recorded from 190 nm to 260 nm. After that, observed ellipticity (mDeg) acquired from Spectra Manager was converted to mean residue molar ellipticity.

From the CD kinetics (Figure 5.7), the alteration in conformation of Peptide 1 was monitored *in vitro*. Initially (black) the random coil of Peptide 1 was confirmed from the negative band at 196 nm. After 75 h of incubation (red), the random coil was converted to the turn structure which was confirmed from the positive band at 198 nm. But with time (blue), the solution retained its random coil structure which was confirmed from the negative band at 205 nm. The results confirmed the generation of aspartyl residues *via* aspartimide formation from the peptide 1.

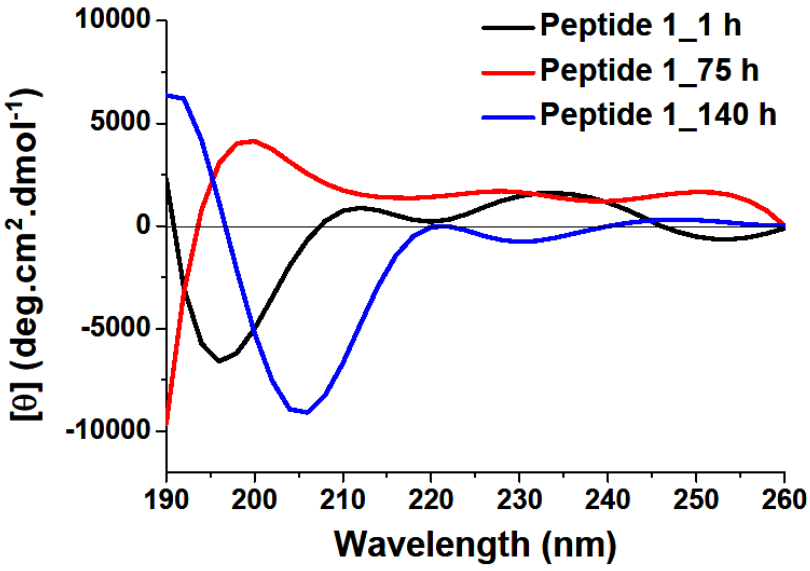

Figure 5.7. CD spectra of Peptide 1 at the 1st h (black), after 75 h (red), and after 140 h (blue) of the reaction. All the peptide solutions were incubated in PBS pH 7.4 (50 mM) at 37 °C.

5.2.3.3. Transmission electron microscopy (TEM) studies of Peptide 1:

TEM, an ultrasensitive technique, facilitate the study of the inner structure and analysis of the features on an atomic scale. In the TEM process, a 10 µL peptide sample was negatively

stained with the 10 µL of 2 % uranyl acetate solution over a carbon-coated copper grid using a micropipette, and the sample was analyzed under TEM at 100 kV.

TEM images of peptide 1 (Figure 5.8) at the 1st h of incubation in PBS of pH 7.4 (50 mM) at 37 °C had shown a well organized (partially aggregated) structure due to the p-p interaction in-between aromatic group of Fmoc and Tryptophan. But with the progression of time, an amorphous structure was obtained due to the release of Tryptophan from Peptide 1.

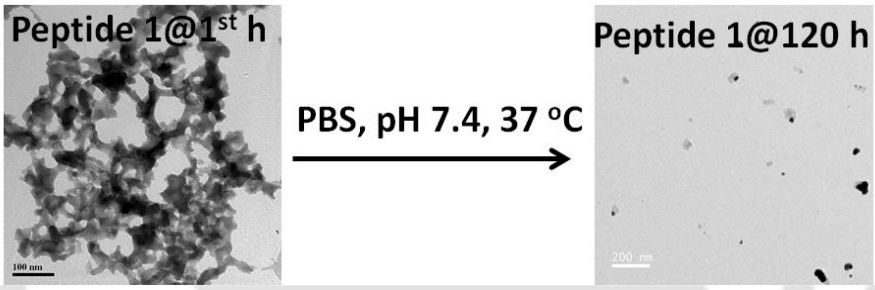

Figure 5.8. TEM images of Peptide 1 at the 1st h (left-side) and after 120 h (right-side) of incubation. All the peptide solutions were incubated in PBS pH 7.4 (50 mM) at 37 °C. Scale bar is indicated as 100 nm (left-side) and 200 nm (right-side) for TEM images.

5.2.3.4. Density functional theory (DFT) calculation of Peptide 1:

The most stable conformation of Fmoc-AD(W)A-NH_2 and Fmoc-GD(W)A-NH_2 were obtained after performing DFT (Figure 5.9) based methods using B3LYP as energy function and 6-31G as the basis set through Gaussian 5.0.9 program. It was noticed that the distance in-between phenyl groups of Fmoc and Tryptophan was very close to p-p interaction in the case of Fmoc-AD(W)A-NH_2, but it was far from the required distance for p-p interaction in the case of Fmoc-GD(W)A-NH_2.

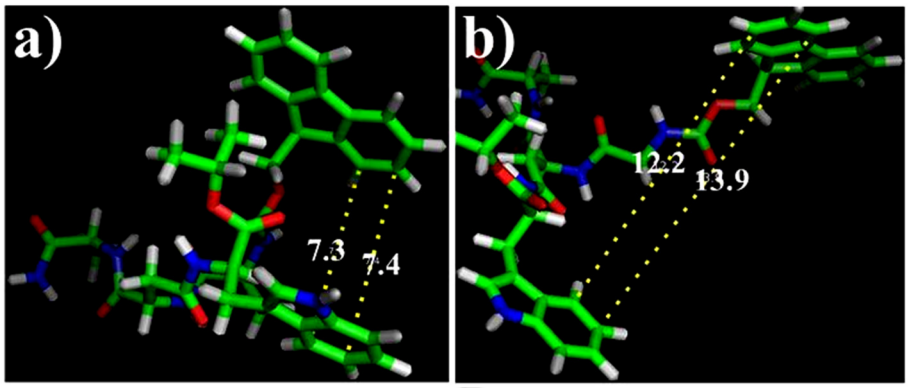

Figure 5.9. Molecular interaction (p-p) between the Fmoc group and Trp of (a) Fmoc-AD(W)A-NH_2 (Peptide 1) and (b) Fmoc-GD(W)A-NH_2.

5.2.3.5. Detection of various fragments of Peptide 2 by Mass spectrometry:

From the ESI-MS kinetics studies (Figure 5.10-5.12), it was observed that after 10 min of incubation, Peptide 2 started to release Serotonin molecule *via* aspartimide formation (B) as a result of "O➔N acyl migration". The reaction then proceeds to form aspartyl residues (C^1 / C^2).

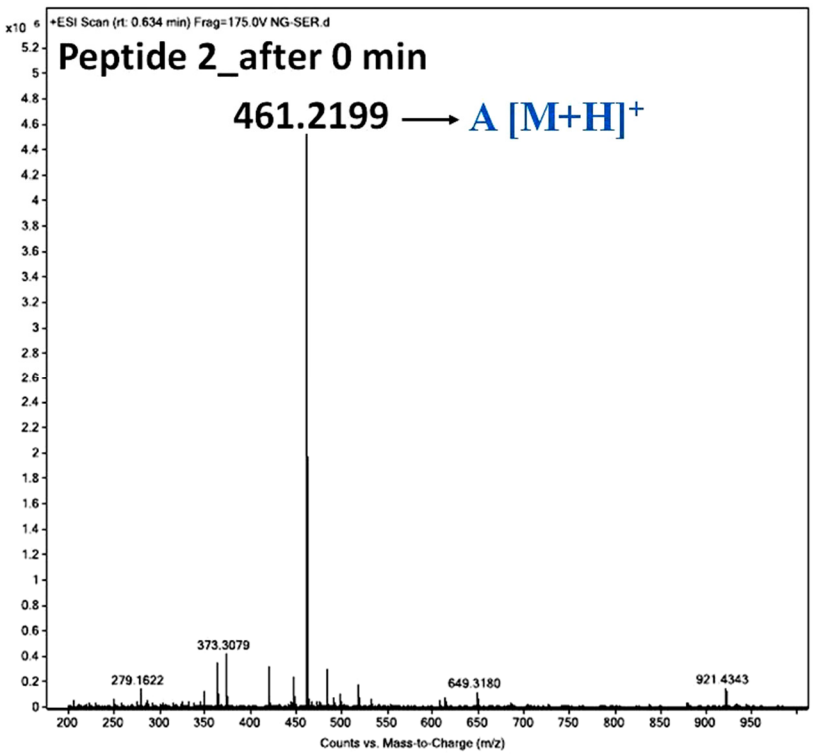

Figure 5.10. ESI-Mass spectrum of Peptide 2 at the 1st min of incubation in PBS of pH 7.4 at 37 °C.

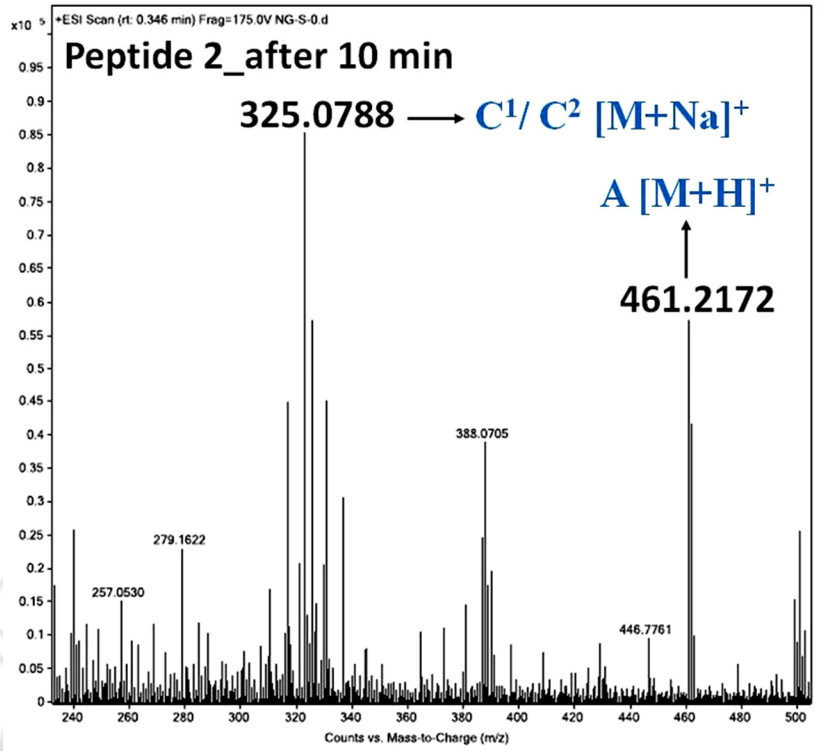

Figure 5.11. The ESI-Mass spectrum of Peptide 2 after 10 min of incubation in PBS.

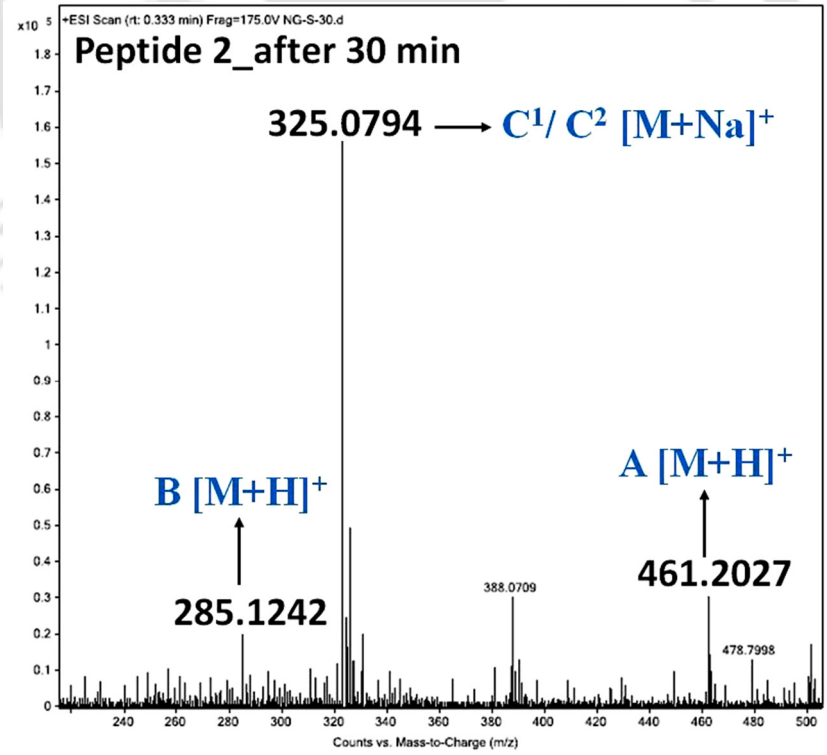

Figure 5.12. ESI-Mass spectrum of Peptide 2 after 30 min of incubation in PBS of pH 7.4 at 37 °C.

5.2.3.6. Circular Dichroism (CD) of Peptide 2:

From the CD kinetics, the conformation alteration of Peptide 2 was checked *in vitro* (Figure 5.13). Initially (black) the random coil of Peptide 2 was confirmed from the negative band at 190 nm. After 10 min of incubation (red), the random coil was converted to the turn structure, which was confirmed from the positive band of lower intensity at 205 nm. But after 30 min of incubation (blue), the turn structure converted to a mixture of predominantly random coil structure along with a helix structure, which was confirmed from two negative bands at 200 nm and 215 nm of weaker intensity. The results confirmed the generation of aspartyl residues *via* aspartimide formation from peptide 2.

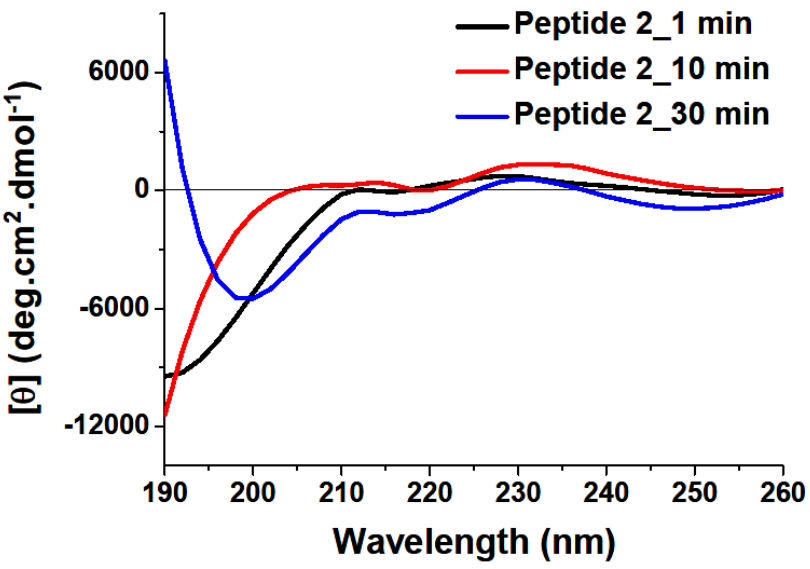

Figure 5.13. CD spectra of Peptide 2 at the 1st min (black), after 10 min (red), and after 30 min (blue) of the reaction. All the peptide solutions were incubated in PBS pH 7.4 (50 mM) at 37 °C.

5.3. Conclusions:

Aspartic acid-containing peptides have a tendency to form aspartimide, a five-membered ring, which could be a useful tool to release therapeutic agents or bioactive molecules. Hence we have designed and synthesized Asp containing peptides having Tryptophan (N

→N acyl migration, slow-release system) and Serotonin (for O→N acyl migration, faster release system) at its side chain. Various biophysical experiments (ESI-Mass, CD, and TEM) were performed to get the proof of principle of our hypothesis. The design could be useful for the controlled release system. Though more studies in-details are needed to validate the concept which is being developed in our Laboratory.

5.4. Characterization data:

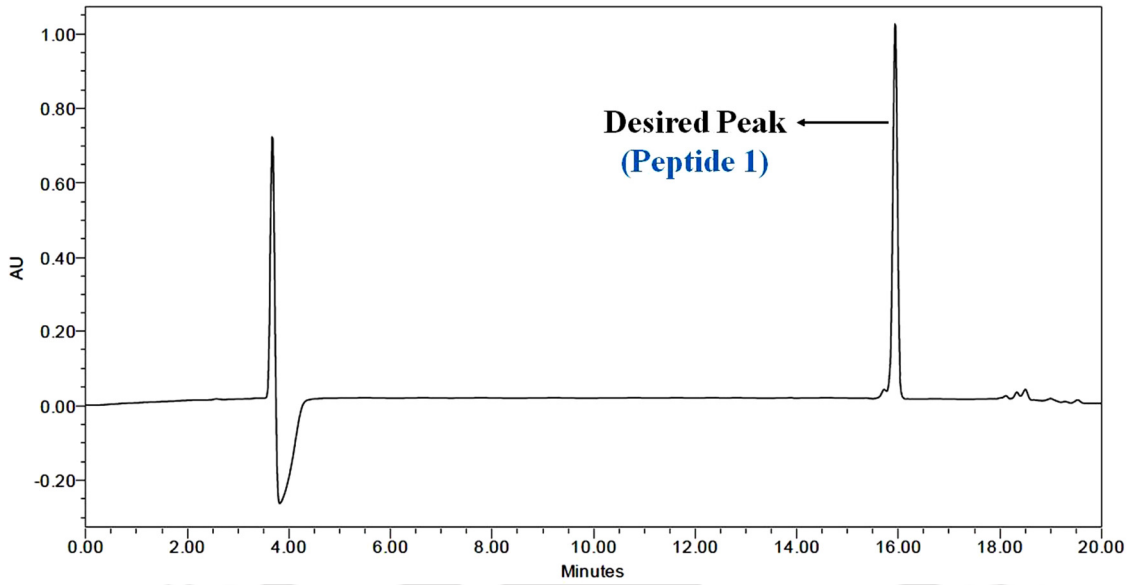

Figure 5.14. HPLC profile picture of the purified Peptide 1.

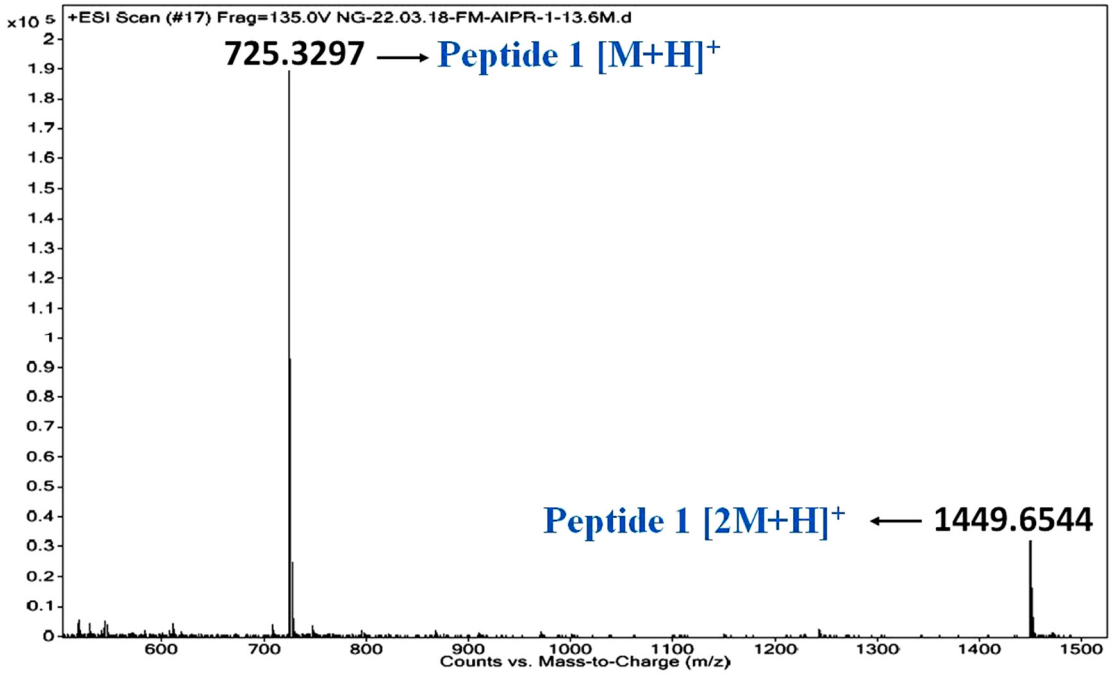

Figure 5.15. The ESI-Mass spectrum of the Peptide 1. Calculated m/z for $C_{39}H_{44}N_6O_8$ $[M+H]^+$ is 725.3221, observed 725.3297.

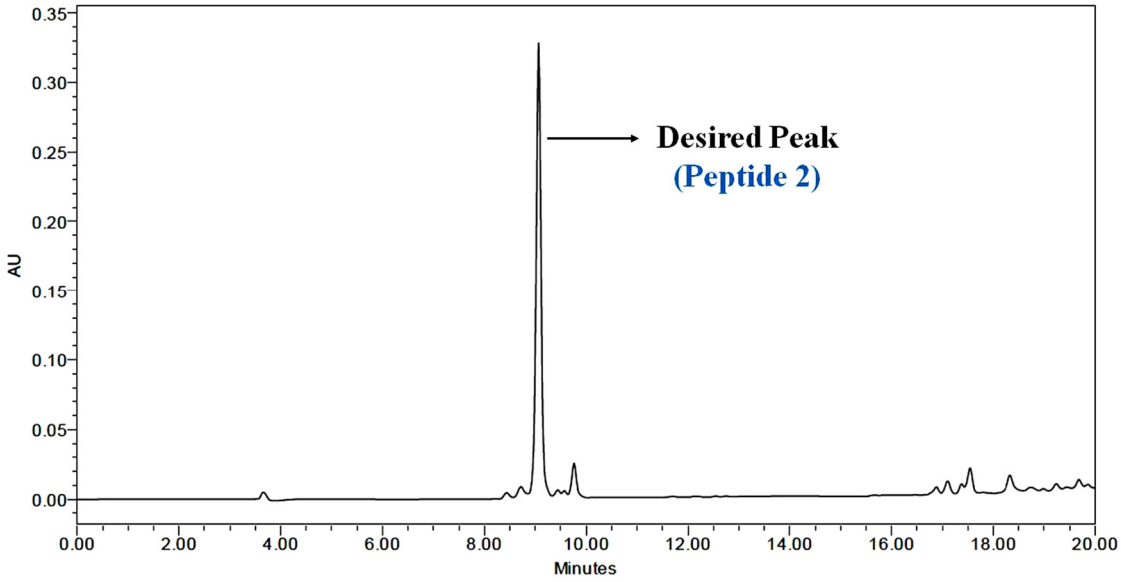

Figure 5.16. HPLC profile picture of the purified Peptide 2.

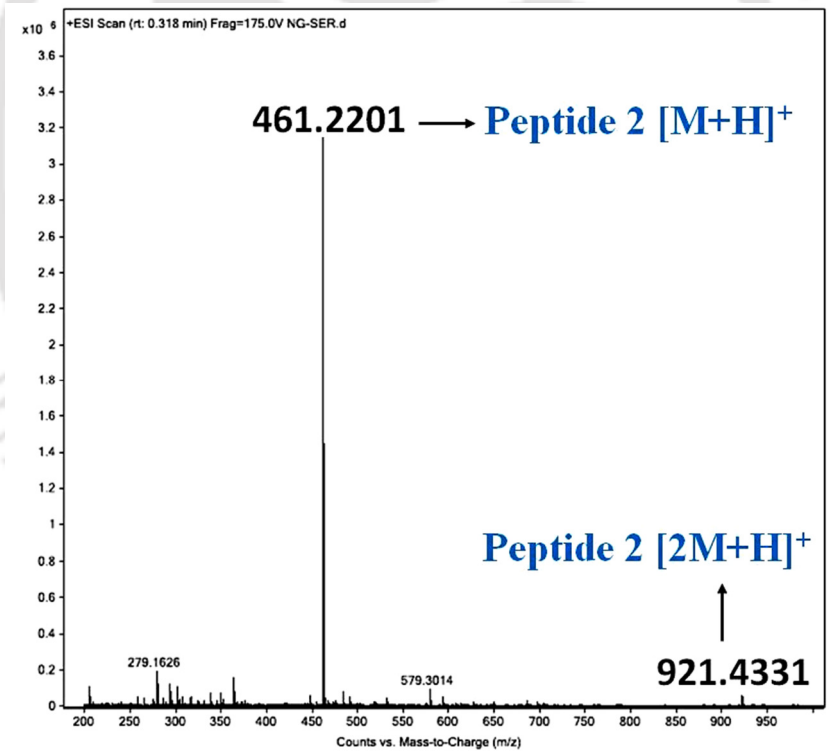

Figure 5.17. The ESI-Mass spectrum of the Peptide 2. Calculated m/z for $C_{21}H_{28}N_6O_6$ $[M+H]^+$ is 461.2070, observed 461.2201.

5.5. References:

[1] Nicolas, E.; Pedroso, E.; Giralt, E. *Tetrahedron. Lett.***1989**, *30*, 497-500.

[2] Dolling, R.; Beyermann, M.; Haenel, J. *et al. Chem. Commun.* **1994**,*7*, 853-854.

[3] Tam, J. P.; Yang, Y.; Sweeney, W. V.; Schneider, K.; Thornqvist, S.; Chait, B. T. *Tetrahedron Lett*. **1994**, *35*, 9689-9692.

[4] Tam, J.; Riemen, M.; Merrifield, R. *Peptide Res*. **1988**, *1*, 6-18.

[5] De Boni, S.; Oberthür, C.; Hamburger, M.; Scriba, C. *J. Chromatogr. A,* **2004**, *1022*, 95-102.

[6] Radkiewicz, J. L.; Zipse, H.; Clarke, S.; Houk, K. N. *J. Am. Chem. Soc*. **1996**, *118*, 9148-9155.

[7] Mergler, M.; Dick, F.; Sax, B.; Weiler, P.; Vorherr, T. *J. Peptide Sci.***2003**, *9*, 36-46.

[8] Clarke, S. *Int. J. Peptide Protein Res.* **1987**, *30*, 808-821.

[9] (a) Ittel, S. D.; Gridnev, A. A. *U.S. Pat. Appl. Publication*, US20,090,165,676, 2009, 14 p; (b) Schon, I.; Kisfaludy, L. *Int J Pept Protein Res* **1979**, *14*, 485–494; (c) Capasso, S.; Mazzarella, L.; Sica, F.; Zagari, A.; Cascarano, G.; Giacovazzo, C. *Acta Crystallogr B* **1992**, *48*, 285–290.

[10] Nadimpally, K. C.; Paul, A.; Mandal, B. *ACS Chem Neurosci*. **2014**, *5(5)*, 400-408.

[11] Frazer, A.; Hensler, J. G. Serotonin Involvement in Physiological Function and Behavior. In: Siegel, G. J.; Agranoff, B. W.; Albers, R. W. *et al.* editors. Basic Neurochemistry: Molecular, Cellular and Medical Aspects. 6th edition. Philadelphia: Lippincott-Raven; **1999**.

[12] The Organic Chemistry of Drug Design and Drug Action, 2nd Edition (Richard B. Silverman) David G. J. Young *Journal of Chemical Education* **2008**, *85 (2)*, 208.

[13] Banker, G. S.; Rhodes, C. T. Sustained and controlled drug delivery system. Modern Pharmaceutics. 4th ed. New York: Marcel Dekker; **2002**.

[14] Richard, D. M.; Dawes, M. A.; Mathias, C. W.; Acheson, A.; Hill-Kapturczak, N.; Dougherty, D. M. *Int J Tryptophan Res***. 2009**, *2*, 45-60.

[15] Martin, S. R.; Schilstra, M. J. *Methods Cell Biol.* **2008**, *84*, 263–293.

[16] Clarke, D. T. *Methods Mol Biol.* **2011**, *752*, 59–72.

[17] Pignataro, M. F.; Herrera, M. G.; Dodero, V. I. *Molecules* **(2020),** *25(20)*, 4854.

Research Publications:

1. Nibedita Ghosh and Lal Mohan Kundu,* "*In-situ* side-chain peptide cyclization as a breaker strategy against the amyloid aggregating peptide", ***Bioorg. Med. Chem.***, 2021, *33*, 116017.

2. Nibedita Ghosh and Lal Mohan Kundu,* "*Breaker peptides against amyloid-β aggregation: a potential therapeutic strategy for Alzheimer's disease*", ***Future Med. Chem.***, 2021, doi: 10.4155/fmc-2021-0184.

3. Nibedita Ghosh and Lal Mohan Kundu* "Sequence-dependent *in-situ* peptide self-cyclization for controlled release of covalently attached biomolecules" (***J. Het. Chem.***, Manuscript ID JHET-21-0095, Under major revision)

4. Nibedita Ghosh and Lal Mohan Kundu*. "Inhibition of protein aggregation by dual O to N acyl migration". (Manuscript submitted)

5. Nibedita Ghosh and Lal Mohan Kundu*. "Aspartimide formation: A technique to release bio-molecules". (Manuscript under preparation)

Conferences attended:

1. Nibedita Ghosh and Dr. Lal Mohan Kundu*, *In-situ* peptide cyclization for controlled release of biomolecules, National Conference on Organic Synthesis (N-COS-2020), 2nd-3rd March 2020, PG Department of Chemistry, Berhampur University, Odisha, Page-48 (P-11) [Flash Poster Presentation].

2. Nibedita Ghosh and Dr. Lal Mohan Kundu*, Green and Novel Approach to Targeted Drug Delivery via Peptide Cyclization, International Conference on Chemistry for Human Development (ICCHD-2018), 8th-10th January 2018, Heritage Institute of Technology, Kolkata, Page-105 (P-059) [Poster Presentation].

Workshops attended:

1. MHRD-GIAN International Workshop on 'Density Functional Theory for Heterogeneous Catalysis, 6th Aug.-11th Aug. 2018, IIT Guwahati, Assam-781039, India.

2. MHRD-GIAN International Workshop on 'Protein Structure and Drug Discovery' (PSDD-2017), 27th Aug.-5th Sep. 2017, School of Life Sciences, University of Hyderabad, Hyderabad-500046, India.

Curriculum Vitae

Name: Nibedita Ghosh

Ph.D. Fellow, IIT Guwahati

Gender: Female; Nationality: Indian; Category: General;

Date of Birth: 03.12.1984

Father's Name: Joydeb Ghosh

Mother's Name: Niyati Ghosh

Husband's Name: Dr. Arindam Das

Children's Name: Auroni

PERMANENT ADDRESS:

3/1 A Pitambar Ghatak Lane, P.O.- Alipore, Dist.- Kolkata,
State**:** West Bengal **,** PIN**:** 700027
E-mail Address: g.nibedita@iitg.ac.in
Mobile No. : +91-7576919641

CURRENT STATUS:

Ph.D. Fellow (December, 2014 - continue)

Ph.D. Supervisor: Dr. Lal Mohan Kundu (IIT Guwahati)

Research Area: Peptide Chemistry, Drug design, and Drug delivery

EDUCATIONAL QUALIFICATION:

Name of Examination	Council/Board/ University	Year of Passing	Key Subjects	Div./ Class
Madhyamik	WBBSE	2001	Beng., Eng., Math., Phy. Sc., Life Sc., Hist., Geo.	1st
Higher Secondary	WBCHSE	2003	Beng., Eng., Phys., Chemistry, Math., Bios.	1st
B.Sc.(Hons.) Chemistry	University of Calcutta, Kolkata	2008	Chemistry (Hons.), Physics, Math.	2nd
M.Sc.(Chemistry)	West Bengal State University	2010	Organic, Inorganic & Physical Chemistry	1st

NATIONAL ACHIEVEMENT:

GATE QUALIFICATION	REGISTRATION NO.	GATE SCORE	AIR
GATE 2014	**CY606401071**	**357**	**1163**
GATE 2015	**CY44001S1283**	**477**	**754**

WORK EXPERIENCE:

- **Assistant Teacher** (**Govt. Service)** (From 10.03.2010 to 30.06.2014)
- **Project Assistant** (From July, 2014 to December, 2014), [Project Guide: Dr. Bhubaneswar Mandal, (Dept. of Chemistry, IIT Guwahati), Project Title: Development of a New Method for Peptide Cyclization and Beckmann Rearrangement using Sulfonate Esters of Oxyma.]